# STRUCTURE-ACTIVITY RELATIONSHIP OF TETRAZOLE DERIVATIVES AS KYNURENINE MONOOXYGENASE INHIBITORS

by

#### WEIHAO MA

(Under the Direction of Robert S. Phillips)

#### **ABSTRACT**

Kynurenine monooxygenase (KMO) is a key enzyme involved in the degradation of tryptophan via the kynurenine pathway (KP). KMO has been implicated in various neurodegenerative and non-neurodegenerative disorders due to its role in regulating levels of several critical metabolites. Inhibition of KMO offers a promising therapeutic strategy. This dissertation focuses on the development of novel KMO inhibitors containing a tetrazole moiety and the investigation of their protein-ligand interactions with KMO. The tetrazole group is a well-established bioisosteric replacement for carboxylic acids. We designed and synthesized a series of tetrazole-containing derivatives and conducted structure–activity relationship (SAR) studies to optimize their potency. KMO crystals were obtained, and the protein structures complexed with our compounds were successfully solved. Additionally, we designed a substrate analog, 5-nitrokynurenine(5-Nkyn), which acts as an uncoupler of KMO activity. We explored the binding mechanisms of both competitive and uncoupling inhibitors. Furthermore, during the synthesis of 5-nitrokynurenine, we developed a novel aromatic nitration method using lithium nitrate under mild conditions. This method is effective for a wide range of deactivated aromatic substrates and heterocyclics and affords moderate to excellent yields. These collective findings

provide a comprehensive framework for rational KMO inhibitor design and offer valuable insights for future therapeutic development targeting the kynurenine pathway.

INDEX WORDS: Kynurenine monooxygenase, kynurenine, tetrazole derivatives, SAR, protein-ligand interactions, 5-Nkyn, aromatic nitration, lithium nitrate.

# STRUCTURE-ACTIVITY RELATIONSHIP OF TETRAZOLE DERIVATIVES AS KYNURENINE MONOOXYGENASE INHIBITORS

by

## WEIHAO MA

B.S. Bioengineering, Nanjing Tech University, China, 2019B.S. Chemistry, Millersville University, 2019

A Dissertation Submitted to the Graduate Faculty of The University of Georgia in Partial

Fulfillment of the Requirements for the Degree

DOCTOR OF PHILOSOPHY

ATHENS, GEORGIA

2025

© 2025

Weihao Ma

All Rights Reserved

# STRUCTURE-ACTIVITY RELATIONSHIP OF TETRAZOLE DERIVATIVES AS KYNURENINE MONOOXYGENASE INHIBITORS

by

WEIHAO MA

Major Professor: Committee: Robert S. Phillips Vladimir Popik Yifan Wang

Electronic Version Approved:

Ron Walcott Vice Provost for Graduate Education and Dean of the Graduate School The University of Georgia August 2025

#### **ACKNOWLEDGEMENTS**

First and foremost, I would like to express my deepest gratitude to my advisor, Dr. Robert Phillips. I truly would not be who I am today without your mentorship. I joined your lab as a master's student, unsure of my path and still finding my footing. When I approached you about staying for a Ph.D., hoping to learn more about chemistry and biology and to grow as a scientist, you welcomed me without hesitation. That moment changed my life. Throughout these years, your unwavering support, patience, and positivity have meant everything. You have always been available to answer questions, offer guidance, or simply listen. You have been a role model not just in science, but in how to live with integrity and passion. I still remember seeing you in the lab over a Christmas holiday, wearing your lab coat and working on experiments. you are the truest example of a scientist for whom research is not just a job, but a way of life. I am honored to have had the opportunity to be your student, and I hope to grow into a scientist like you one day. I am also deeply grateful to my committee members, Dr.Popik and Dr.Wang. Thank you for your thoughtful guidance and support. Your feedback and suggestions have significantly improved my research, and I am grateful for the opportunities you gave me to use your laboratory equipment.

I am deeply thankful to all my friends and lab mates who have been part of this journey. Special thanks to Dr. Emma Carine Iradukunda, who patiently taught me how to express and purify KMO, and helped me begin my research. Olivia, thank you for your guidance and support in protein crystallography. Elijah, who has been with me from the beginning, through both synthesis and crystallography work, your help has meant so much. There are many others whose names I

did not list here, but your kindness, teamwork, and friendship have made this experience more meaningful than I can express.

Lastly, and most importantly, I want to thank my family. To my father—you were the one who encouraged me to come to the United States to pursue graduate school, even when I was unsure. You pushed me forward when I hesitated, and stayed beside me every step of the way. Your strength and selflessness are what allowed me to become the person I am today. To my mother and sister—your love and concern have never wavered. Even from thousands of miles away, you constantly reminded me to take care of myself, to rest, and to never forget that I am not alone. You have been my emotional anchor through it all.

This Ph.D. journey has been filled with challenges and growth, but above all, it has been filled with the unwavering support of the people around me. I could not have done this without you all. Thank everyone from the bottom of my heart.

## TABLE OF CONTENTS

	Page
ACKNOWLEDGEMENTS	iv
LIST OF TABLES	viii
LIST OF FIGURES	ix
LIST OF SCHEMES	xi
CHAPTER	
1 Introduction and Literature Review	1
1.1 Kynurenine pathway	1
1.2 Involvement of KMO in neurodegenerative diseases	2
1.3 Involvement of KMO in non-neurodegenerative diseases	5
1.4 Kynurenine 3-monooxygenase	6
1.5 Reaction mechanism of KMO	6
1.6 KMO structure and species specificity	7
1.7 Development of KMO inhibitors	11
2 Structure-activity relationship of tetrazole derivatives as kynurenine 3-	
monooxygenase inhibitors	17
2.1 Introduction	17
2.2 Rational design and tetrazole replacement	18
2.3 Materials and methods	21
2.4 Results and discussion	23

		2.5 Chemistry	32
		2.6 Conclusion	49
	3	5-Nitrokynurenine as an uncoupler of both <i>Pseudomonas fluorescens</i> and <i>cy</i>	tophaga
		hutchinsonii kynurenine monooxygenase	50
		3.1 Introduction	50
		3.2 Materials and Methods	52
		3.3 Results and discussion	55
		3.4 Chemistry	59
		3.5 Conclusion	62
	4	Nitration of Deactivated Aromatic Compounds Using Lithium Nitrate	63
		4.1 Introduction	63
		4.2 Optimization of reaction condition	65
		4.3 Nitration of mono- and di-substituted aromatics	66
		4.4 Nitration of heterocyclics	69
		4.5 Chemistry	70
		4.6 Conclusion	83
REFE	EREI	NCES	85
APPE	END	ICES	
	A	X-ray diffraction data processing, structure determination and refinement	105
	В	<sup>1</sup> H NMR and <sup>13</sup> C NMR for tetrazole synthesis	108
	C	<sup>1</sup> H NMR and <sup>13</sup> C NMR for 5-nitrokynurenine	148
	D	<sup>1</sup> H NMR and <sup>13</sup> C NMR for nitration	158

## LIST OF TABLES

	Page
Table 2.4.1: Kinetics data of tetrazole derivatives with aromatic modifications	26
Table 4.2.1: screening of the reaction conditions	67
Table 4.5.1: Screening of the reactivity and regioselectivity of different nitrate salts with 2-	
nitrotoluene	71

## LIST OF FIGURES

Page
Figure 1.1.1: Overview of the kynurenine pathway (KP)2
Figure 1.5.1: The proposed catalytic mechanism of KMO
Figure 1.7.1: Published inhibitors for KMO
Figure 2.1.1: Overview of the kynurenine pathway (KP)
Figure 2.2.1: Receptor-based pharmacophoric models of 3,4-dimethoxyhippuric acid aligned
with the conformation of UPF468 as bound to yeast KMO (PDB: 4J36)19
Figure 2.2.2: Chemical structures of L-kyn and some published inhibitors
Figure 2.2.3: Replacement of carboxylic acid group with tetrazole group21
Figure 2.2.4: SAR analysis of the linker length from one to two carbons (one carbon: top row;
two carbons: bottom row)21
Figure 2.4.1: A) Overview of pfKMO with L-kyn bound to one active site (PDB: 6FOX). B)
Interactions of L-kyn with surrounding residues. C) Interactions of compound 4 with
surrounding residues (9B2Y)27
Figure 2.4.2: Co-crystal structure of pfKMO and compound 6 (PDB: 9B07) and 7 (PDB: 9AZ8).
A and B: compound 6 bound to both active sites. C and D: compound 7 bound to both
active sites
Figure 2.4.3: superposition of compound 4 (yellow), 6 (pink), and 7 (gray) within pfKMO active
site at one active site. A: sideview of superposition structures. B: top view of
superposition structures30

Figure 2.4.4: view of compound 7 (yellow) within pfKMO active site overlaid with structure of	f
pfKMO-L-Kyn substrate (pink)	31
Figure 2.4.5: Superposition of compound 7 (yellow) with published tetrazole-containing	
compound (green, PDB:6FPH) bound to pfKMO at both active sites	32
Figure 3.1.1: Schematic overview of kynurenine pathway highlighting metabolites involves in	
neurotoxicity (red labels) and neuroprotection (green label)	52
Figure 3.1.2: Structure of 5-nitrokynurenine, a proposed kynurenine analog binder	52
Figure 3.3.1: Consumption rate of NADPH vs the varied concentrations of 5-Nkyn with chKMC	C
(A) and pfKMO (B)	57
Figure 3.3.2: HPLC analysis of compound F reaction with KMO-orange line; black line: control	1;
blue line reaction of kynurenine with KMO	58
Figure 3.3.3: Active site of yeast KMO (PDB: 4J36) in complex with 5-NKyn	59
Figure 4.3.1: Nitration of mono-substituted aromatic compounds	58
Figure 4.3.2: Nitration of di-substituted aromatic compounds	59
Figure 4.4.1: Nitration of heteroarenes	70

## LIST OF SCHEMES

	Page
Scheme 2.5.1: General synthesis route of tetrazole derivatives	33
Scheme 2.5.2: Preparation of 1-(4-(benzyloxy)-3-chlorophenyl)-2-chloroethan-1-one (12	2b)46
Scheme 3.4.1: Synthesis of 5-NKyn	60
Scheme 4.2.1: Nitration of benzene and nitrobenzene	66

### CHAPTER 1

### INTRODUCTION AND LITERATURE REVIEW

## 1.1 Kynurenine Pathway

Tryptophan is an essential amino acid, and over 95% of tryptophan is metabolized through the Kynurenine Pathway (KP) (figure 1).<sup>1-4</sup> The KP is the primary route for tryptophan catabolism in many organisms, including mammals.<sup>5</sup> The Kynurenine Pathway (KP) starts with the oxygenation of tryptophan, a reaction catalyzed by either tryptophan 2,3-dioxygenase (TDO) or indoleamine 2,3-dioxygenase (IDO), resulting in the formation of N-formyl L-kynurenine.<sup>6,7</sup> This intermediate is then converted into L-kynurenine by the enzyme kynurenine formamidase.8 Lkynurenine can be metabolized through three different pathways: it can be hydroxylated to 3hydroxykynurenine (3-HK) by kynurenine 3-monooxygenase (KMO); it can form kynurenic acid (KynA) via a transamination reaction catalyzed by kynurenine aminotransferase (KAT); or, it can be converted to anthranilic acid by kynureninase, which can subsequently be transformed into 3hydroxyanthranilic acid (3-HANA) by anthranilate 3-monooxygenase. 9-11 Another enzyme, 3hydroxy-anthranilate dioxygenase, acts on 3-hydroxyanthranilic acid to produce 2-amino-3carboxymuconate semialdehyde, which spontaneously cyclizes to form quinolinate (QUIN).<sup>12</sup> Quinolinate is then converted into nicotinic acid mononucleotide (NaMN), and ultimately NAD(P)<sup>+</sup>, by the action of quinolinate phosphoribosyltransferase.<sup>13</sup> Notably, the Kynurenine Pathway produces several neuroactive metabolites, including KynA, 3-HK, 3-HANA, and QUIN.<sup>5</sup>, <sup>14</sup> KynA is considered a neuroprotective agent due to its role as an antagonist of the N-methyl Daspartate (NMDA) receptor.<sup>15</sup> In contrast, other metabolites in the pathway, such as 3-HK, 3HANA, and QUIN, exhibit neurotoxic properties.<sup>1</sup> 3-HK and 3-HANA act as free-radical generators, while QUIN functions as an excitotoxic NMDA agonist.<sup>16, 17</sup> Since KMO has the highest binding affinity for L-kynurenine, the KMO branch is considered the most crucial metabolic route and an optimal drug target within the Kynurenine Pathway.<sup>18</sup> Regulating KMO activity could potentially increase levels of the neuroprotective metabolite KynA while reducing the neurotoxic metabolites 3-HK, 3-HANA, and QUIN. Therefore, inhibiting KMO is expected to shift the pathway away from producing toxic metabolites toward the formation of protective KynA.

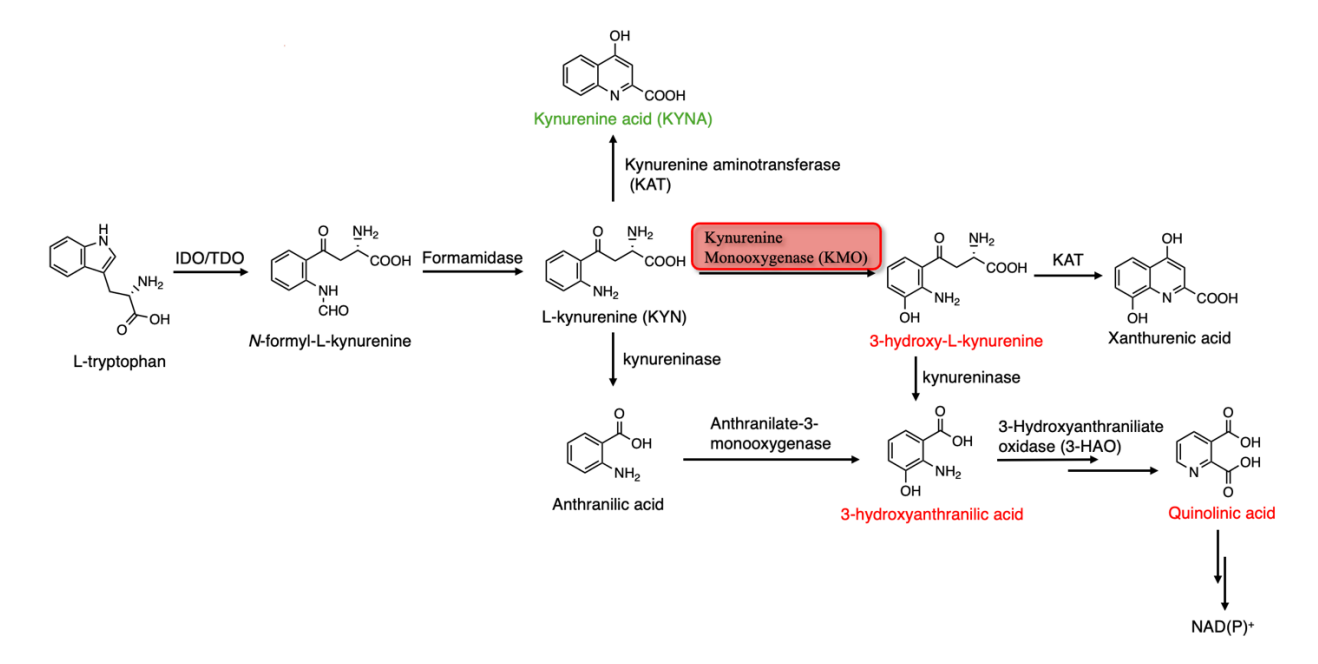


**Figure 1.1.1** Overview of the kynurenine pathway (KP).

## 1.2 Involvement of KMO in neurodegenerative diseases

Kynurenine 3-monooxygenase (KMO) is a crucial enzyme in the kynurenine pathway (KP), responsible for catalyzing the production of neuroactive metabolites. Notably, intermediates such as 3-HK, 3-HANA, and QUIN significantly influence neuronal function and have been strongly associated with the progression of neurodegenerative diseases, including Alzheimer's disease, Huntington's disease, and Parkinson's disease. <sup>19-21</sup>

Alzheimer's disease is the leading cause of dementia, and it is rapidly emerging as one of the most burdensome and fatal diseases of the 21st century.<sup>22</sup> Increased tryptophan (TRP) degradation and concurrent alterations in kynurenine levels have been observed in the plasma of Alzheimer's disease (AD) patients.<sup>23</sup> Demented patients exhibited lower TRP and KYNA concentrations. Although there was a non-significant increase in KYN, 3-HK, and anthranilic acid (AA) levels, a marked elevation of QUIN was observed in AD patients. Positive correlations were observed between cognitive function test scores and plasma KYNA levels, whereas inverse correlations were found between these tests and QUIN levels in Alzheimer-type dementia.<sup>22</sup> Additionally, QUIN compromises the integrity of the blood-brain barrier (BBB), induces the generation of reactive oxygen species, depletes endogenous antioxidants, and promotes lipid peroxidation, ultimately leading to oxidative stress and neuronal damage.<sup>24</sup> Furthermore, QUIN stimulates nitric oxide production in neurons and astrocytes by activating neuronal nitric oxide synthase, thereby intensifying oxidative damage.<sup>25</sup> Therefore, the development of kynurenine 3monooxygenase (KMO) inhibitors appears to present novel therapeutic opportunities and holds promise as a strategy for brain neuroprotection.

Huntington's disease (HD) is among the most common inherited neurodegenerative disorders.<sup>26</sup> It is characterized by uncontrolled movements, known as chorea, as well as impaired memory, attention deficits, and psychiatric disturbances.<sup>27</sup> The disease results from an abnormally expanded CAG repeat sequence, which leads to an expanded polyglutamine (polyQ) tract in the huntingtin (Htt) protein.<sup>28</sup> Research has shown that targeting the KP is related to HD through several lines of evidence.<sup>19</sup> Elevated levels of 3-HK and QUIN have been observed in the neostriatum and cortex during the early stages of disease progression.<sup>29</sup> Conversely, KYNA levels are significantly reduced in the brain and cerebrospinal fluid of striatal regions.<sup>30-32</sup> In addition,

increased KMO activity has been implicated in the elevated 3-HK levels in the brain. Reduced KAT activity has also been observed in the striatum of HD patients.<sup>33</sup> Campesan and colleagues have conducted research on the genetic and pharmacological inhibition of KMO and TDO.<sup>30</sup> Reduced activity of KMO and TDO has been shown to increase neuroprotective KYNA levels while decreasing 3-HK and QUIN levels, thereby demonstrating that neurodegeneration is directly modulated by 3-HK and KYNA. Thus, inhibition of KMO has demonstrated neuroprotective effects. Consequently, KMO inhibitors are considered a promising strategy for mitigating neurodegeneration in HD.

Parkinson's disease (PD) is a progressive neurodegenerative disorder characterized by motor symptoms such as tremors, muscle rigidity, postural instability, and cognitive decline.<sup>34, 35</sup> It is an age-related disorder, with onset and progression typically occurring after the age of 60.<sup>35, 36</sup> Symptoms progressively worsen over time, eventually leading to significant disabilities. PD is marked by the loss of dopaminergic neurons and localized neuroinflammation in the midbrain, which often begins years before the clinical manifestation of symptoms.<sup>37, 38</sup> Research has shown that KP metabolites may play a role in the inflammatory response associated with PD.<sup>39,41</sup> QUIN, an agonist of the N-methyl-D-aspartate (NMDA) receptor, contributes to neuronal damage by overactivating NMDA receptors, leading to excitotoxicity and amplifying the inflammatory response.<sup>32</sup> Additionally, 3-HK and 3-HANA generate reactive oxygen species (ROS), promoting oxidative stress and further accelerating dopaminergic neuron degeneration.<sup>20, 42</sup> In contrast, KYNA acts as an antagonist of NMDA receptors, mitigating excitotoxicity and offering potential neuroprotection.<sup>43</sup> Thus, modulating KMO activity in PD could potentially shift KYN metabolism toward the production of the neuroprotective metabolite KYNA and reduce the generation of

neurotoxic compounds, such as 3-HK and QUIN.<sup>44, 45</sup> Therefore, The KMO inhibitors represent a promising therapeutic approach for PD.

## 1.3 Involvement of KMO in non-neurodegenerative diseases

KMO has also been implicated in non-neurodegenerative diseases, such as acute pancreatitis (AP) and hepatocellular carcinoma (HCC).<sup>46, 47</sup> In the case of AP, heightened KMO activity can lead to an excess of 3-HK and downstream toxic metabolites like quinolinic acid, which collectively contribute to tissue injury and amplify inflammatory responses.<sup>48</sup> Experimental models have shown that inhibiting KMO can dampen inflammation by reducing the production of these harmful metabolites. This not only limits immune cell infiltration—particularly of proinflammatory T cells—but also shifts the metabolic balance toward protective compounds.<sup>49</sup> Furthermore, immune cells such as Th17 cells and macrophages express KMO, and its upregulation under inflammatory conditions suggests it acts as a mediator between metabolic stress and immune dysregulation.<sup>50</sup> Thus, targeting KMO may offer therapeutic benefits in acute pancreatitis by curbing the excessive immune response and mitigating oxidative damage, potentially preserving tissue function and improving clinical outcomes.

Another non-neurodegenerative disorder includes hepatocellular carcinoma (HCC). Elevated KMO expression has been observed in HCC tissues compared to adjacent normal liver, and higher levels are linked to worse clinical outcomes, including shorter overall survival and increased recurrence risk. Functionally, KMO enhances tumor cell proliferation, migration, and invasion, which was demonstrated through in vitro assays where silencing KMO expression reduced these malignant behaviors. Additionally, downstream metabolites regulated by KMO, such as quinolinic acid and 3-hydroxyanthranilic acid, may contribute to immune evasion and tumor-promoting inflammation. These bioactive products potentially alter the tumor

microenvironment to favor cancer progression. Therefore, KMO is more than a passive biomarker—it actively drives tumor aggressiveness and may serve as a promising target for therapeutic intervention in HCC.<sup>53, 54</sup>

## 1.4 Kynurenine 3-monooxygenase

Kynurenine 3-monooxygenase (KMO) is primarily expressed in the kidney and liver, with significantly lower levels in the brain.<sup>55</sup> Within the brain, KMO is predominantly expressed in microglial cells, with minimal expression in neurons, underscoring its connection to inflammatory processes.<sup>56, 57</sup> At the cellular level, KMO is located in the outer membrane of mitochondria with a transmembrane domain near its C-terminus.<sup>58-60</sup> KMO belongs to the family of NADPH-dependent flavin monooxygenases and is encoded by a single gene.<sup>61</sup> It contains a flavin adenine dinucleotide (FAD) cofactor and utilizes either NADPH or NADH for flavin reduction, subsequently releasing NADP<sup>+</sup> or NAD<sup>+</sup>. KMO has a Rossmann fold dinucleotide-binding domain, classifying it as a class A flavoprotein aromatic hydroxylase.<sup>62</sup>

## 1.5 Reaction mechanism of KMO

As in the mechanism of many oxidoreductases, the catalytic mechanism of KMO can be divided into two half reactions, including the first reductive half, and the following oxidative half. The mechanism was extensively studied using a stable form of KMO from *Pseudomonas fluorescens*. <sup>63, 64</sup> As shown in Figure 1.5.1, the substrate L-Kyn first binds to KMO, a process that is relatively slow, making the reductive half of the reaction L-Kyn dependent. Next, NADPH binds to the enzyme. Once both the substrate and NADPH are bound to KMO, the FAD cofactor is reduced by a hydride transfer from NADPH. This is followed by the dissociation of NADP<sup>+</sup> from the enzyme, completing the reductive half of the reaction. During the oxidative half of the reaction, the reduced FAD cofactor reacts with molecular oxygen to form a highly reactive C4a-

peroxyflavin intermediate. This intermediate subsequently hydroxylates the aromatic ring of the substrate, resulting in a C4a-hydroxyflavin. The C4a-hydroxyflavin then undergoes rapid dehydration, returning to its oxidized form. The enzyme complex undergoes a conformational change to facilitate the release of the product, 3-HK. This conformational change also leads to a shift in the visible spectrum of the oxidized enzyme upon product release. Finally, the dissociation of 3-HK completes the catalytic cycle and represents the rate-limiting step of this mechanism.

Figure 1.5.1. The proposed catalytic mechanism of KMO.

## 1.6 KMO structure and species specificity

Human KMO (hKMO) is 486 amino acids in length with a molecular weight about 56kDa.<sup>61, 65</sup> It is a mitochondrial outer membrane protein with two transmembrane domains (TMDs) and a mitochondrial signal sequence located in its C-terminal region.<sup>66</sup> Due to these membrane-binding properties, the expression and purification of human KMO (hKMO) present significant challenges, particularly in the crystallization of the protein. It was only recently that the first structure of hKMO was published. As a result, kinetic studies and crystal structures of KMO

in complex with either substrates or inhibitors have primarily been conducted using KMO from other species, which share a similar active site. The following sections will review all published KMO crystal structures across different species.

## 1.6.1 Saccharomyces cerevisiae

The first crystal structure of KMO was derived from Saccharomyces cerevisiae and published in *Nature* in 2013.<sup>67</sup> It shares 38% sequence identity and 51% sequence similarity with human KMO (hKMO). The structures of S. cerevisiae KMO (ScKMO) were solved as a dimer and truncated at residue 394. However, the activity of ScKMO ( $\Delta$ 396) was not affected by this truncation, unlike hKMO. Although a crystal structure of ScKMO with the substrate bound was not successfully obtained, structures were resolved in both the free form (PDB 4J33) and in complex with the tight-binding inhibitor UPF648 (PDB 4J36). In the inhibitor-bound structure, the UPF648 carboxylate interacts with conserved polar residues Arg83 and Tyr97, while the aromatic dichlorobenzene moiety is surrounded by hydrophobic residues (Leu221, Met230, Ile232, Leu234, Phe246, Pro321, Phe322), which are conserved in many other KMOs, as confirmed by mutagenesis and functional assays. The crystal structure of ScKMO has been an important template for advancing drug discovery, offering a high-resolution framework for docking screens with virtual compound libraries. This has also enabled the identification of promising lead compounds while providing valuable insights into structure-activity relationships, thereby guiding the rational design of innovative inhibitor scaffolds.

### 1.6.2 Pseudomonas fluorescens

The most commonly studied crystal structure of KMO is from *Pseudomonas fluorescens* (PfKMO).<sup>67-74</sup> The enzyme from *P. fluorescens* has been shown to exhibit good stability, allowing it to be heterologously expressed in *Escherichia coli*. It can be expressed in high yields as a soluble

protein and efficiently purified.<sup>64</sup> PfKMO contains two domains, with the main domain holding the Rossmann fold, the active site, the FAD cofactor and a C-terminal domain. All the residues in the catalytic site are conserved for PfKMO compared to hKMO. The first structure of PfKMO was published in 2016 and was resolved in complex with the inhibitor GSK180 (PDB 5FN0).<sup>74</sup> The carboxylate moiety of GSK180 forms a salt bridge with Arg84 and establishes hydrogen bonds with the side chains of Tyr98 and Asn369. The oxazolidinone carbonyl group forms a hydrogen bond with the side chain of the C-terminal domain residue Tyr404, while the 5-chlorine atom engages in a van der Waals interaction with Phe238. Although the level of conserved residues is high, the potency of GSK180 against PfKMO is significantly lower compared to hKMO, with IC50 values of 500 nM and 6 nM, respectively. Subsequently, the same team conducted structureactivity relationship (SAR) studies on numerous GSK180 structural analogs and published structures of PfKMO in complex with the substrate and several analogs. 71-73 They then developed a series of 3-(2-oxo-2,3-dihydro-1,3-benzoxazol-3-yl)propanoic acid derivatives and extensively studied the interactions between PfKMO and these inhibitors. The most potent inhibitors, named GSK065 and GSK366, exhibited IC<sub>50</sub> values of 4.5 nM and 2.3 nM against hKMO, respectively.<sup>73</sup> In the crystal structure, the flavin cofactor is tilted due to the presence of pyridine or pyrazidine. This flavin movement creates a solvent-filled channel from the active site to the surface of the protein, allowing hydrogen bonding with the water network. This structural shift significantly increases the binding affinity of inhibitors and explains the potency of these inhibitors against hKMO. Even though the interactions of these inhibitors with hKMO remain unknown, the PfKMO structures have successfully enabled researchers to develop novel inhibitors that exhibit high potency to hKMO.

### 1.6.3 Mammalian

The first human KMO structure was published by Kim and coworkers in 2018.<sup>69</sup> They resolved the crystal structure of hKMO-374, a truncated mutant containing residues 1–374, at a 2.1 Å resolution. This variant was specifically engineered by removing the transmembrane domains (TMDs) to generate a human KMO protein suitable for crystallization. As previously reported by Hirai,<sup>66</sup> hKMO is localized in the outer mitochondrial membrane, containing two transmembrane domains and a C-terminal region responsible for mitochondrial signaling. The hKMO-374 structure revealed a catalytic mechanism consisting of two domains, a characteristic feature of the FAH enzyme class. The first domain housed the FAD-binding region, which was fully occupied at a 1:1 stoichiometric ratio, while the second comprised a small N-terminal domain consisting of alpha helices and an antiparallel beta sheet.

In 2021, the full-length *Rattus norvegicus* (rat) crystal structure of KMO in its membraneembedded form was published, along with its complexes with compounds, named inhibitors 3 and 4, at a resolution of 3.0 Å.<sup>75</sup> Their findings suggest that KMO is actually a single-pass transmembrane protein, with the second predicted domain lying laterally along the membrane and forming part of the ligand-binding pocket, in contrast to previous predictions by Kim and coworkers suggesting that KMO has two transmembrane domains.<sup>69</sup> They found that KMO exists as a dimer. The dimerization is crucial for catalytic activity. The dimer interface is formed via intermolecular β-sheets at residues F183-Y189 (β12). These β-sheets create 10 hydrogen bonds, stabilizing the dimer structure. Mutations in these β-sheet residues significantly reduce dimer formation, with the Y185P mutation nearly abolishing enzyme activity entirely. The ligandbinding pocket comprises residues from both the FAD-binding domain and the C-terminal region. A residue, R380, from the C-terminal region forms a hydrogen bond interaction with the carboxylic acid moiety of the inhibitor but does not affect enzymatic activity when mutated. Based on their findings, they developed compound 5, which features an isostere replacement of the carboxylic acid moiety with quinazolinedione, identifying it as a brain-penetrant inhibitor. This study provides new insights into the ligand-binding mechanism of mammalian KMO and represents significant progress in developing potential treatments for neurodegenerative diseases.

## 1.7 Development of KMO inhibitors

Before the KMO crystal structure was available, inhibitor design was based on the structure of kynurenine (compound 1, fig 1.7.1). A series of kynurenine-based analogs were synthesized, and their SAR were studied. The kynurenine analog, nicotinylalanine (compound 2, fig 1.7.1), was developed to selectively prevent excitotoxic QUIN buildup while enhancing the neuroprotective production of KYNA in the kidneys of Wistar rat models. 76 The first specific KMO inhibitor, mnitrobenzoyl alanine (m-NBA, compound 3, fig 1.7.1), was reported in 1994 and demonstrated an IC<sub>50</sub> of 3 μM against KMO from resuspended, homogenized rat organs.<sup>77, 78</sup> m-NBA later served as a lead compound for the development of more potent inhibitors. Halogen substitutions on aromatic rings significantly improved potency, leading to the development of 3,4-dichlorobenzoyl alanine (compound 4, fig 1.7.1), which exhibited greater potency ( $IC_{50} = 0.2 \mu M$ ), longer-lasting effects, and higher KYNA elevation compared to m-NBA.<sup>79</sup> Ro61-8048 (compound **5**, **fig 1.7.1**) was later developed through SAR optimization of a screening hit that identified a sulfonamide compound. 80 Ro61-8048 was found to be a competitive inhibitor of KMO, with an IC<sub>50</sub> of 37 nM and a K<sub>i</sub> of 4.8 nM, making it the most potent KMO inhibitor developed at the time. It was believed that the sulfonamide group acts as a bioisostere for the carboxyl group, providing strong hydrogen bonding, while the phenylthiazole ring enhances hydrophobic interactions. In vivo validation of Ro61-8048 also demonstrated excellent oral bioavailability and a longer-lasting inhibitory effect

on KMO. In 1999, a series of pyrrolo[3,2-c]quinoline derivatives were synthesized.<sup>81</sup> Among these compounds, 7-chloro-3-methyl-1H-pyrrolo[3,2-c]quinoline-4-carboxylic acid (compound 6, fig 1.7.1) was identified as a lead compound, exhibiting an IC50 of 24 µM against KMO in rat liver and an IC50 of 8.2 µM against KMO in the brain, suggesting potential CNS activity. After determining that the  $\alpha$ -amino group is not required for inhibition, and that the acid moiety is indeed essential for inhibition, one of the most extensively studied compound, UPF 648 (compound 7, fig 1.7.1), was developed in 2003 with IC<sub>50</sub> of 20 nM and was used in the first KMO crystal structure. 67, 82 Both in vivo and in vitro studies indicated that UPF 648 effectively increases brain KYNA levels, reduces QUIN neurotoxicity, and protects neurons from NMDA receptor-mediated excitotoxicity. 82, 83 In 2012, Ianthellamide A (compound 8, fig 1.7.1), isolated from the Australian marine sponge Ianthella quadrangulate, was shown to selectively inhibit KMO with an IC<sub>50</sub> of 1.5 μM.<sup>84</sup> This achievement marked the beginning of structure-based drug design of KMO. The availability of the KMO crystal structure has significantly enhanced the precision of inhibitor design through computational approaches. High-throughput screening of a library of 78000 compounds was conducted, targeting hKMO, using RapidFire mass spectrometry (RF-MS).85 This screening identified two new compounds: 5-(3-nitrobenzyl)-1H-tetrazole (compound 9, fig 1.7.1) and 6-(3,4-dichlorophenyl)pyrimidine-4-carboxylic acid (compound 10, fig 1.7.1), with IC<sub>50</sub> of 6.3 µM and 0.0016 µM respectively. The latter arylpyrimidine compound was further optimized using the structural data, and its SAR was studied.<sup>86</sup> The pyrimidine ring acts as a bioisostere of the carbonyl group in L-kynurenine. Among these arylpyrimidine derivatives, compound 11 (fig 1.7.1), was identified as the most potent inhibitor, with an IC<sub>50</sub> of 0.5 nM in the enzymatic assay and an IC<sub>50</sub> of 33 nM in the cell-based assay. Structural binding analysis of compound 11 revealed that the pyrimidine N3 forms hydrogen bonds with Arg83 and Thr244, mimicking the carboxylate

group of L-kynurenine. Additionally, the carboxylate moiety interacts with Asn369 and Tyr98, while the chlorophenyl substitution stabilizes hydrophobic interactions with Leu221 and Phe238. One of the most potent inhibitors, GSK180 (compound 12, fig 1.7.1), was developed through highthroughput screening followed by structure-based optimization of kynurenine analogs.<sup>74</sup> This compound exhibited high potency against hKMO, with an IC<sub>50</sub> of 6 nM in the enzymatic assay and an IC<sub>50</sub> of 2.0 μM in the cell-based assay. In contrast, its inhibition of rat KMO was weaker, with an IC<sub>50</sub> of 7 µM, indicating potential species differences in binding affinity. Additionally, GSK180 was found not to significantly inhibit other kynurenine pathway enzymes. Further optimization of GSK180 led to the discovery of GSK065 (compound 13, fig 1.7.1) and GSK366 (compound 14, fig 1.7.1).<sup>71-73</sup> The oxazolidinone core was replaced with a benzisoxazole core for compound 13 and 14, and one chlorine was replaced to 1-(pyridin-2-ylethoxy) group for compound 13 and to 1-(6-methylpyridazin-3-ylethoxy) group for compound 14. These improvements not only enhanced potency but also improved cell solubility and pharmacokinetic properties. Compound 13 was found to have an IC<sub>50</sub> of 1.3 nM against hKMO in the enzymatic assay and an IC<sub>50</sub> of 8.5 µM in the cell-based assay. GSK366 (compound 14) exhibited IC<sub>50</sub> values of 2.3 nM for hKMO and 0.7 nM for PfKMO. Both compounds did not stimulate the KMO to produce peroxide, as flavin tilting prevents NADPH oxidation, unlike GSK180.

A pharmacophore model was developed using the first ScKMO structure along with known KMO inhibitors. A virtual screening of a database of commercially available chemicals was then conducted, leading to the identification of a high-fit compound, 3,4-dichlorohippuric acid (compound 15, fig 1.7.1), which demonstrated strong *in vitro* inhibitory potency with a K<sub>i</sub> of 34 μM.<sup>87</sup> A ligand-based molecular similarity method and drug repurposing approach led to the identification of diclofenac (compound 16, fig 1.7.1), an FDA-approved anti-inflammatory drug,

as a KMO binder and inhibitor with an IC50 of 13.6  $\mu M$  and  $K_d$  of 64.8  $\mu M$ .88 A combination of ligand- and structure-based virtual screening was used to evaluate over 1,000 compounds, leading to the identification of 19 new KMO inhibitors through high-throughput assays for PfKMO and HsKMO.<sup>68</sup> Among these, compound 17 (fig 1.7.1) was discovered as the most potent, with an IC<sub>50</sub> of 9.3 µM for PfKMO and 2.6 µM for HsKMO. Additionally, a prodrug was designed by replacing the carboxylic acid with an ethyl carboxylate, enabling it to cross the blood-brain barrier, release the active form in the CNS, and effectively reduce 3-HK levels. Unlike other substrate analogs, this prodrug does not stimulate the production of hydrogen peroxide. The full-length structure of mammalian KMO in its membrane-embedded form was determined, and a high kynureninecontent enzymatic assay was used to evaluate inhibitors for crystal structural analysis. 75 From the optimization of their lead compound, compounds 18 and 19 were discovered (fig 1.7.1). Compound 18 exhibited the highest potency, with an IC<sub>50</sub> of 3.8 nM against hKMO and 9.0 nM against rat KMO. In the cell-based assay, it had an IC<sub>50</sub> of 12 nM in human cells and 0.24 µM in rat cells. Meanwhile, compound 19 demonstrated exceptional brain permeability, showing a 27fold increase in CNS exposure compared to compound 18. More recently, a compound library was screened, leading to the discovery of the pyridazinylsulfonamide scaffold. Through optimization of SAR, brain penetration, and pharmacokinetic properties, compound 20 (fig 1.7.1) was developed, exhibiting high potency and brain permeability. It was identified as the most promising compound, with an IC<sub>50</sub> of 12.8 nM against human KMO (hKMO).<sup>89, 90</sup>

Figure 1.7.1: Published inhibitors for KMO.

### **CHAPTER 2**

# STRUCTURE-ACTIVITY RELATIONSHIP OF TETRAZOLE DERIVATIVES AS KYNURENINE 3-MONOOXYGENASE INHIBITORS

## 2.1 Introduction

The kynurenine pathway (KP) is the dominant route of tryptophan catabolism in mammals, accounting for over 95% of its degradation (figure 2.1.1). Initiated by tryptophan 2,3-dioxygenase (TDO) or indoleamine 2,3-dioxygenase (IDO), the pathway begins with the formation of Nformyl-L-kynurenine, which is then rapidly converted to L-kynurenine. From this branching point, L-kynurenine can be metabolized into several biologically active compounds.<sup>6, 7</sup> One route involves kynurenine aminotransferase (KAT), producing kynurenic acid (KynA), a neuroprotective NMDA receptor antagonist. Alternatively, kynureninase converts L-kynurenine into anthranilic acid, which leads to the formation of 3-hydroxyanthranilic acid (3-HANA) and, eventually, quinolinate (QUIN)—a neurotoxic NMDA agonist and precursor to NAD(P)<sup>+</sup>. A third and critical route is mediated by kynurenine 3-monooxygenase (KMO), which hydroxylates Lkynurenine to form 3-hydroxykynurenine (3-HK), a known generator of reactive oxygen species.<sup>9-</sup> <sup>11</sup> The neuroactive profile of these metabolites underscores the importance of pathway regulation: while KynA offers protective effects, 3-HK, 3-HANA, and QUIN contribute to neurotoxicity. Among the metabolic branches, KMO plays a central role due to its high affinity for L-kynurenine, making it a strategic target for therapeutic intervention. Inhibiting KMO shifts the metabolic flux toward KynA, reducing the accumulation of toxic intermediates and presenting a promising approach for treating neurodegenerative diseases.<sup>5, 14</sup>

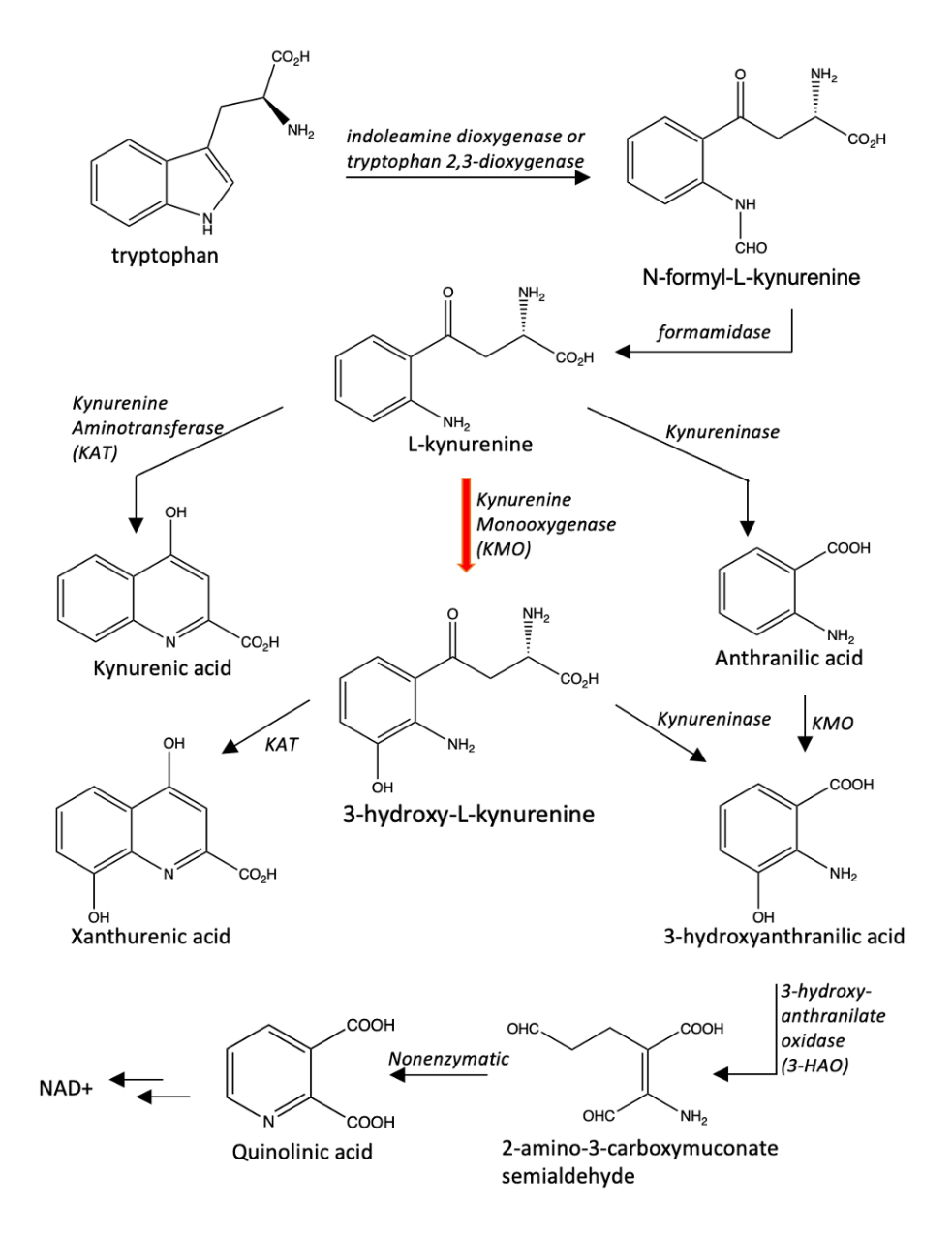
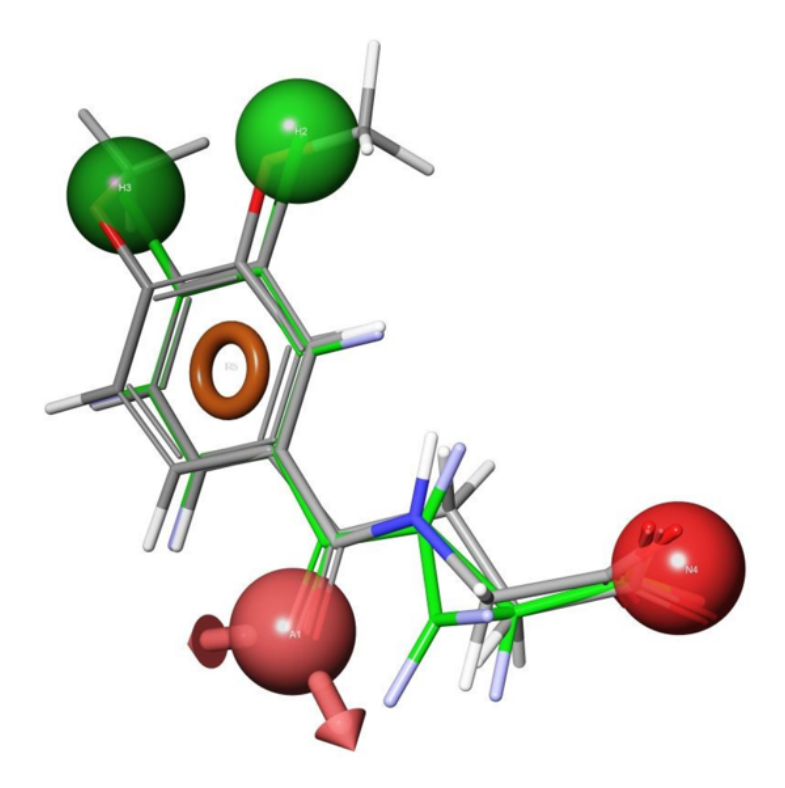


Figure 2.1.1. Overview of the kynurenine pathway (KP).

## 2.2 Rational design and tetrazole replacement

A number of KMO inhibitors have been developed,<sup>68, 71-75, 86-88</sup> most of which share a similar pharmacophore model, including the natural substrate L-kynurenine (1), with four critical features identified (**Figure 2.2.1**): (a) two hydrophobic centers, (b) a core aromatic ring, (c) an electron-rich hydrogen bond acceptor, and (d) an acidic moiety.<sup>87</sup> The receptor-based pharmacophore model was built using a known biologically active molecule, UPF648 (2, figure

**2.2.2**), bound to yeast KMO. This model was later applied in virtual screening to identify potential inhibitors. Two recently developed compounds, 6-(3,4-dichlorophenyl)pyrimidine-4-carboxylic acid (**3, figure 2.2.2**) and GSK180 (**4, figure 2.2.2**), have shown exceptional potency against human KMO.<sup>74, 86</sup> These two compounds align with the pharmacophore model. 6-(3,4-dichlorophenyl)pyrimidine-4-carboxylic acid features a replacement of the pyrimidine group with the carbonyl group of the natural substrate, while GSK180 replaces the benzoyl moiety with oxazolidinone core. Both modifications have significantly improved potency and pharmacokinetic properties. Additional structure–activity relationship (SAR) studies were carried out to refine substitutions on the phenyl ring of the core scaffold, aiming to develop more potent compounds.



**Figure 2.2.1.** Receptor-based pharmacophoric models of 3,4-dimethoxyhippuric acid aligned with the conformation of UPF468 as bound to yeast KMO (PDB: 4J36).

**Figure 2.2.2.** Chemical structures of L-kyn and some published inhibitors.

Most research has focused on optimizing the carbonyl group in the substrate, whereas little attention has been given to modifying the acidic moiety of the natural substrate. Since the  $\alpha$ -amino group is not essential for inhibition, it is typically omitted in the design of most KMO inhibitors.<sup>79,</sup>

Here, we report a replacement of the carboxylic acid with a bio-isosteric tetrazole group (figure 2.2.3). The first example of a tetrazole-containing KMO inhibitor was identified through high-throughput screening of a library of 78,000 compounds targeting KMO using RapidFire mass spectrometry (RF-MS).<sup>85</sup> This screening led to the discovery of a new compound, 5-(3-nitrobenzyl)-1H-tetrazole (5, figure 2.2.2), with an IC<sub>50</sub> of 6.3 μM. The tetrazole group shares many common properties with carboxylic acid. For example, both have a similar size and comparable pK<sub>a</sub> values, often resulting in similar electrostatic potentials in protein-ligand interactions.<sup>92,93</sup>

**Figure 2.2.3.** Replacement of carboxylic acid group with tetrazole group.

The initial modifications began with simplification of the L-kynurenine structure by removing both amino groups. The  $\alpha$ -amino group was found to be non-essential for KMO inhibition. The aromatic amino group was also removed and further optimized through SAR studies to enhance hydrophobic interactions. This led to a simplified core structure. Subsequently, the carboxylate group was replaced with a tetrazole moiety. From this point, the linker length between the carbonyl and the tetrazole group was optimized. We synthesized three derivatives featuring either a one-carbon or two-carbon linker and compared their inhibitory potencies (**Figure 2.2.4**). SAR analysis indicated that compounds with a one-carbon linker exhibited lower  $K_i$  values than those with two-carbon linkers. For derivatives containing two chlorine substituents on the aromatic ring, the  $K_i$  values were nearly identical regardless of linker length. Based on these results, we decided to proceed with the one-carbon linker design.

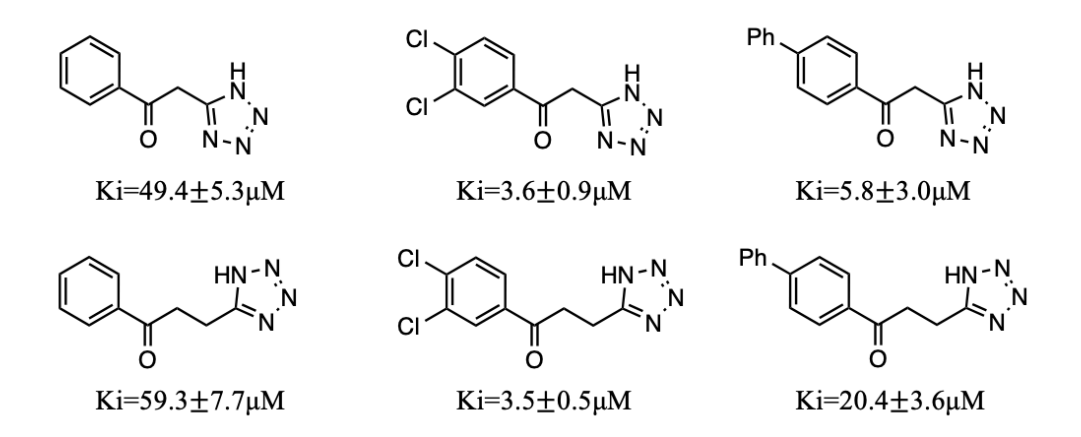


**Figure 2.2.4.** SAR analysis of the linker length from one to two carbons (one carbon: top row; two carbons: bottom row).

### 2.3 Materials and Methods

**Enzyme expression and purification**: The expression, isolation and purification of *Pseudomonas fluorescens* KMO (pfKMO) are carried out as previously reported.<sup>68,94</sup> The gene for

pfKMO is first transformed into *E.coli* BL21(DE3) competent cells for expression. Protein is expressed by growing transformed cells in auto induction LB medium containing 100 mg/L ampicillin for 24h at 23°C. Cells are harvested by centrifugation at 4000 rpm for 15min at 4°C, suspended in lysis buffer (20 mM HEPES buffer pH7.5, 10 mM NaCl, 1 mM DTT, 10  $\mu$ M FAD), lysed by sonication (15x15s). The cell lysate is centrifuged at 4000 rpm for 90min at 4°C to remove cell debris. The soluble cell lysate is loaded onto a prepared diethylaminoethyl Sepharose (DEAE) column, and bound protein is eluted with 20 mM HEPES buffer pH 7.0, 100 mM NaCl, and 1 mM DTT. Then fractions containing the protein are collected and precipitated in 50% saturated ammonium sulphate. The precipitated protein is pelleted by centrifugation at 4000 rpm for 90 mins and resuspended in a small volume of size exclusion buffer (20 mM HEPES buffer pH 7.0, 0.15 M sodium acetate, and 1 mM DTT). Then the protein is passed down a Sepharose CL-6B column. Fractions containing the pure pfKMO are collected. Concentration of pure enzyme is measured at 280nm ( $\Delta \varepsilon$ = 12300 M<sup>-1</sup> cm<sup>-1</sup>) on Nanodrop.

Enzyme inhibition assays: As described previously,<sup>87</sup> The absorbance change of NADPH at 340 nm is measured. The assays contained 20 mM HEPES pH 7.5 buffer, 2 mM NaCl, 0.2 mM NADPH, 1 mM DTT, 5 μM FAD, with varying amounts of L-kynurenine (20-160 μM) and/or inhibitors, in a final volume of 0.8 mL at 25 °C. The reactions are followed at 340 nm ( $\Delta \epsilon = -2.8 \times 10^3 \, \text{M}^{-1} \, \text{cm}^{-1}$ ) in a Cary 100 UV/Vis spectrophotometer. The initial NADPH consumptions are calculated as the velocities. Then, the kinetic parameters are determined by fitting to the Michaelis-Menten equation for competitive inhibition.

**Protein Crystallization:** The crystallization condition of pfKMO has been discovered and repeated with small changes.<sup>71,73</sup> All crystals were grown at room temperature by the hanging drop

vapor diffusion method in a 24-well hanging-drop tray with a pfKMO concentration of 12-15 mg/mL and mixed with the precipitant solution at a 1:1 ratio. The reservoir solution is 12%-14% PEG 8000, 0.11 M-0.13 M Ca(OAc)<sub>2</sub>, 14% glycerol, and 0.08 M sodium cacodylate, pH 6.5. The crystallization drops are set with 1 μL of well solution and 1 μL of protein solution. Diffraction-quality crystals are usually obtained within 3 days. To make the crystal soaking solutions, the pfKMO crystals are transferred into 5 uL cryo solution, containing: 10% EDG (DMSO:ethylene glycol:glycerol,1:1:1) and same concentrations of the components from the reservoir solution. The inhibitors are pre-dissolved in the EDG solution with 10-fold excess molar concentration before soaking. The crystal soaking solution is left at room temperature for 5 hours. Crystals were then flash frozen in liquid nitrogen directly from the soaking drops, without any additional cryoprotectant.

X-ray data collection and crystal structure determination: X-ray diffraction data were collected from single cryo-protected crystals of PfKMO at the NSLS2 beamline. The collected data were indexed, integrated, and scaled using standard data processing software XDS.<sup>95</sup> Initial phases were obtained by molecular replacement in Phaser,<sup>96</sup> using the previously solved *Pf*KMO structure (PDB ID: 5NAK) as the search model. Model building and refinement were performed through an iterative process combining automated tools in Phenix<sup>97</sup> and manual adjustments in COOT<sup>98</sup>. The final refined models exhibited excellent stereochemistry and agreement with the electron density maps. Complete data collection and refinement statistics are provided in the Supplementary Materials.

#### 2.4 Results and discussion

Aromatic modifications led to the discovery of derivatives with diverse substitutions, as shown in Table 2.4.1. The non-substituted Compound 1 exhibited a  $K_i$  value of 49.4  $\mu M$  against

pfKMO. Initially, the benzene ring was replaced with a naphthalene ring to investigate whether aromatic ring size influences inhibitory activity. Compound 2 displayed a K<sub>i</sub> of 40.5 μM, representing only a modest improvement, suggesting that increasing aromatic size does not significantly enhance inhibition. Next, a chloro group was introduced at either the R2 or R3 position. Compound 3 exhibited a K<sub>i</sub> of 19.7 µM, while compound 4 had a K<sub>i</sub> of 28.4 µM, suggesting that substitution at the R2 position plays a more significant role in fitting into the hydrophobic pocket. Substitution of both R2 and R3 with chloro groups significantly reduced the K<sub>i</sub> value to 3.6 μM against pfKMO. Subsequently, bulky functional groups were introduced at the R2 position to evaluate the impact of hydrophobicity on overall potency. Kinetic analysis demonstrated that bulky substituents fit well within the hydrophobic site, resulting in low micromolar K<sub>i</sub> values. Compounds 6 and 7, bearing phenyl and cyclohexyl groups at the R2 position, exhibited K<sub>i</sub> values of 5.8 µM and 2.9 µM, respectively. Both groups substantially reduced  $K_i$  values. The difference in potency between compounds 6 and 7 may be attributed to the greater flexibility of the cyclohexyl group compared to the more rigid phenyl group. In contrast, a trifluoromethyl group at the R2 position yielded a poor result, indicating limited interaction with surrounding residues.

Next, a chloro group was introduced at the R3 position, and substitutions at the R2 position were optimized, yielding compounds 9–12. With either a methoxy or methyl group at the R2 position, the compounds exhibited similar potencies, with K<sub>i</sub> values of 5.0 μM and 4.8 μM, respectively. Compound 11, bearing a cyclohexyl group at R2 and a chloro group at R3, was subsequently synthesized. It was initially expected that this compound would be more potent than compound 7. However, compound 11 exhibited a K<sub>i</sub> of 9.4 μM, which is approximately 3-fold higher than that of compound 7. This discrepancy may be attributed to a conformational change in

the cyclohexyl group. In the absence of a chloro group at R3, the cyclohexyl group lies coplanar with the aromatic ring. In the presence of the chloro group, however, the cyclohexyl moiety adopts a tilted conformation relative to the aromatic ring, thereby reducing its interactions with surrounding residues. Finally, an even bulkier group, benzyloxy, was introduced at R2 along with a chloro group at R3, resulting in compound 12, which exhibited a  $K_i$  of 4.5  $\mu$ M—less potent than compound 7, which contains only a cyclohexyl group at R2.

$$R_2$$
 $R_3$ 
 $R_4$ 
 $N$ 
 $N$ 

Comp.	R <sub>1</sub>	R <sub>2</sub>	R <sub>3</sub>	R <sub>4</sub>	Ki(μM)
					pfKMO
1	Н	Н	Н	Н	49±5
2	Н	Naphthyl		Н	40±13
3	Н	Cl	Н	Н	20±5
4	Н	Н	Cl	Н	28±6
5	Н	C1	Cl	Н	4±1
6	Н	Ph	Н	Н	6±3
7	Н	Су	Н	Н	3±0.4
8	Н	CF <sub>3</sub>	Н	Н	59±18
9	Н	OMe	Cl	Н	5±0.7

10	Н	Me	Cl	Н	5±1
11	Н	Су	C1	Н	9±1
12	Н	PhCH <sub>2</sub> O	Cl	Н	5±2

**Table 2.4.1.** Kinetics data of tetrazole derivatives with aromatic modifications.

Crystal structures were successfully obtained for Compounds 4, 6, and 7. Analysis of these structures revealed that all three compounds form similar and essential hydrogen bonds with key residues in the active site (figures 2.4.1 and 2.4.2). Their crystal structures were compared with that of the substrate to investigate protein–ligand interactions. In the crystal structure of the substrate bound to pfKMO (figure 2.4.1B), the L-kyn occupies only one active site. The amino acid moiety forms extensive interactions with polar residues on the right side of the binding pocket, including Asn369, Tyr404, Arg84, and Tyr98. The carbonyl group does not participate in any interactions. The aromatic ring is positioned in a hydrophobic pocket near the FAD cofactor. The amino group on the aromatic ring forms a hydrogen bond with the oxygen atom of FAD. In the crystal structure of compound 4 bound to pfKMO, similar interactions were observed. Upon replacement of the carboxylate moiety with a tetrazole moiety (figure 2.4.1C), the N2 nitrogen of the tetrazole ring forms a hydrogen bond with Arg84, while the carbonyl oxygen interacts with Tyr404, substituting for the α-amino group interactions observed in the substrate. The chlorophenyl moiety occupies the same hydrophobic pocket as the aromatic ring of the substrate.

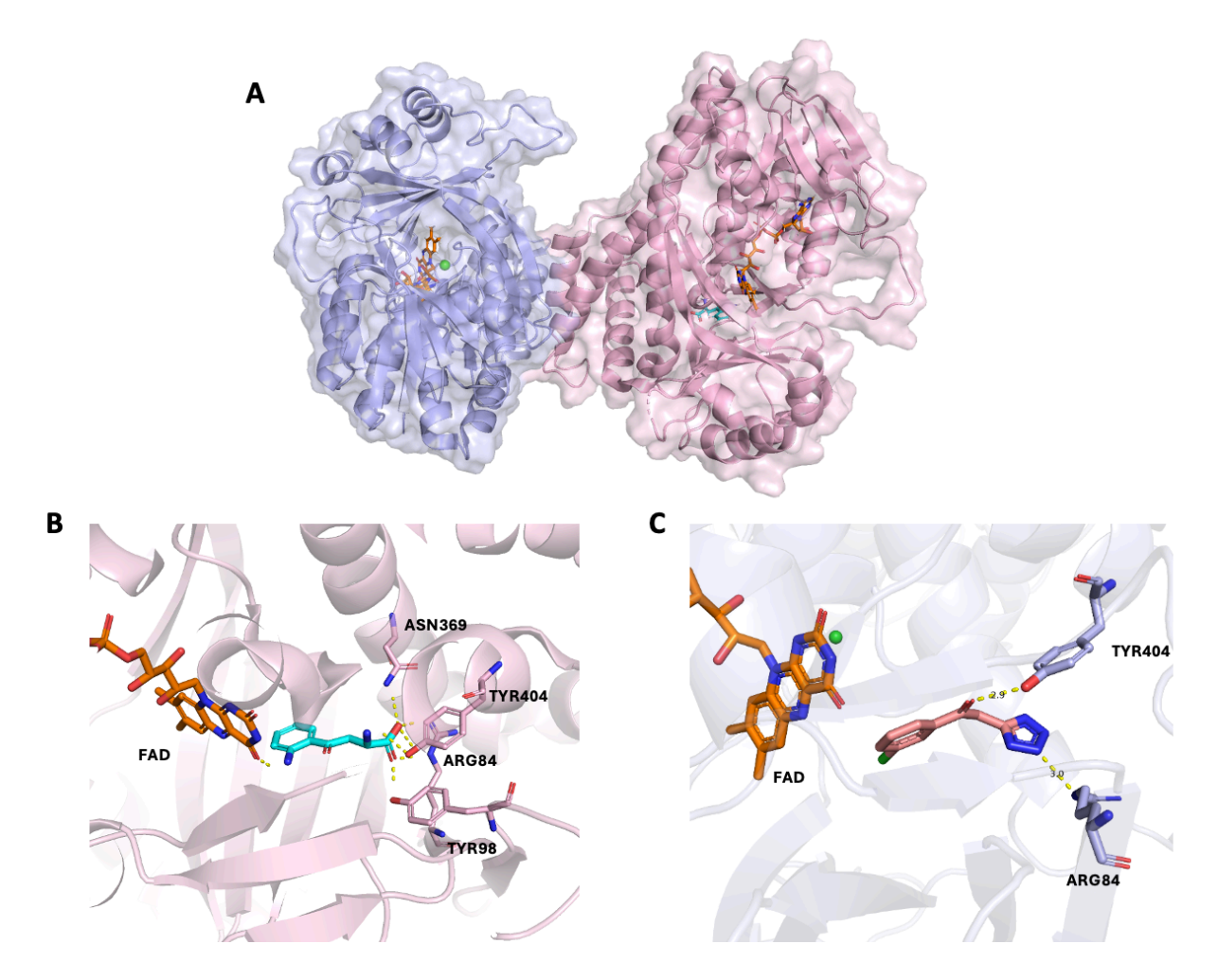


**Figure 2.4.1.** A) Overview of pfKMO with L-kyn bound to one active site (PDB: 6FOX). B) Intereactions of L-kyn with surrounding residues. C) Interactions of compound **4** with surrounding residues (9B2Y).

In contrast, both compounds 6 and 7 bind to both active sites of pfKMO, which may explain their stronger binding affinities compared with compound 4 and the substrate. In one active site of compound 6 bound to pfKMO (Figure 2.4.2B), similar interactions were observed between the carbonyl oxygen and tetrazole moiety and polar residues such as Arg84, Tyr96, and Tyr404 through direct hydrogen bonds and water-mediated interactions. In the other active site (Figure 2.4.2A), extended interactions were observed between the carbonyl group and multiple residues located above the active site via water-mediated hydrogen bonds. These residues include Gly321,

Gln322, His320, Ala56, and Thr408. Similar interactions are observed in the co-crystal structure of compound 7 (Figure 2.4.2C and 2.4.2D). In one active site (Figure 2.4.2D), the carbonyl oxygen and tetrazole moiety form direct hydrogen bonds with Tyr404 and Arg84. In the other active site (Figure 2.4.2C), similar water-mediated interactions are observed with residues located above the active site. The tetrazole group also forms additional interactions with Asn369 through both direct and water-mediated hydrogen bonds. In both active sites, interactions with Tyr96 were not observed. This may be due to the bulky cyclohexyl group, which likely causes the tetrazole moiety to orient away from Tyr96. Overall, the additional hydrogen bonds, particularly the water-mediated interaction networks observed in compounds 6 and 7, may account for their greater potency compared to compound 4. Notably, compound 7 exhibits higher potency than compound 6, which may be attributed to its more extensive hydrogen bonding network, especially through water-mediated interactions, and more favorable accommodation of the cyclohexyl group within the hydrophobic pocket.

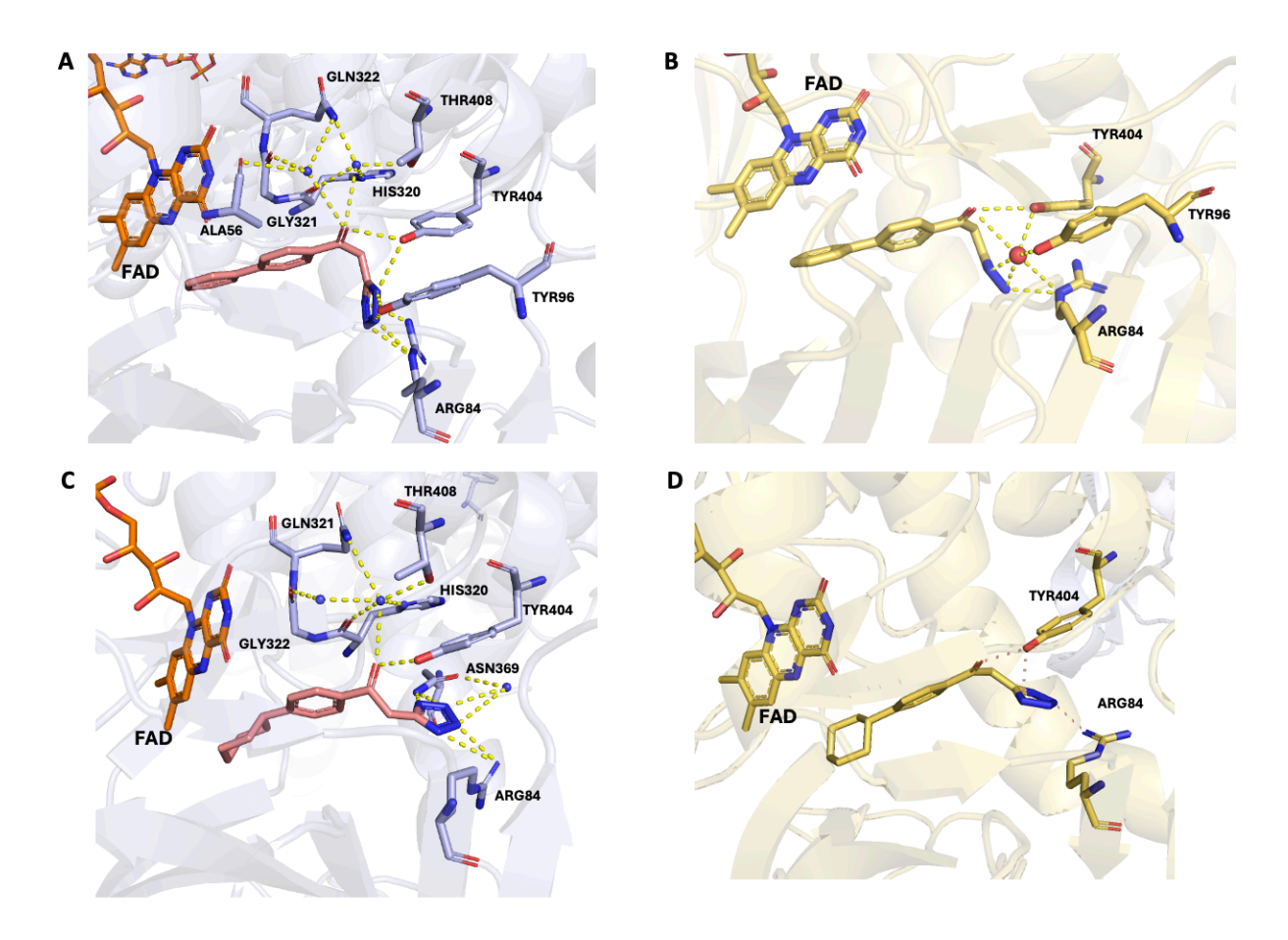


**Figure 2.4.2.** Co-crystal structure of pfKMO and compound 6 (PDB: 9B07) and 7 (PDB: 9AZ8). A and B: compound 6 bound to both active sites. C and D: compound 7 bound to both active sites.

A superposition of the crystal structures of compounds 4, 6, and 7 was performed to compare their structural differences (Figure 2.4.3). The tetrazole moieties of compounds 4 and 7 adopt nearly identical conformations, aligning closely with each other. Tyr404 and Arg84 also exhibit minimal conformational changes in response to these compounds. In contrast, the tetrazole moiety of compound 6 undergoes a significant conformational change, pointing toward the bottom of the active site, with the adjacent methylene group appearing slightly bent. To enable hydrogen bonding with the tetrazole group, Arg84 must rotate to accommodate this altered orientation. This unique conformation of the tetrazole moiety in compound 6 may result from the rigidity and

inflexibility of the phenyl group, which could otherwise lead to steric clashes with Tyr404 and Arg84.

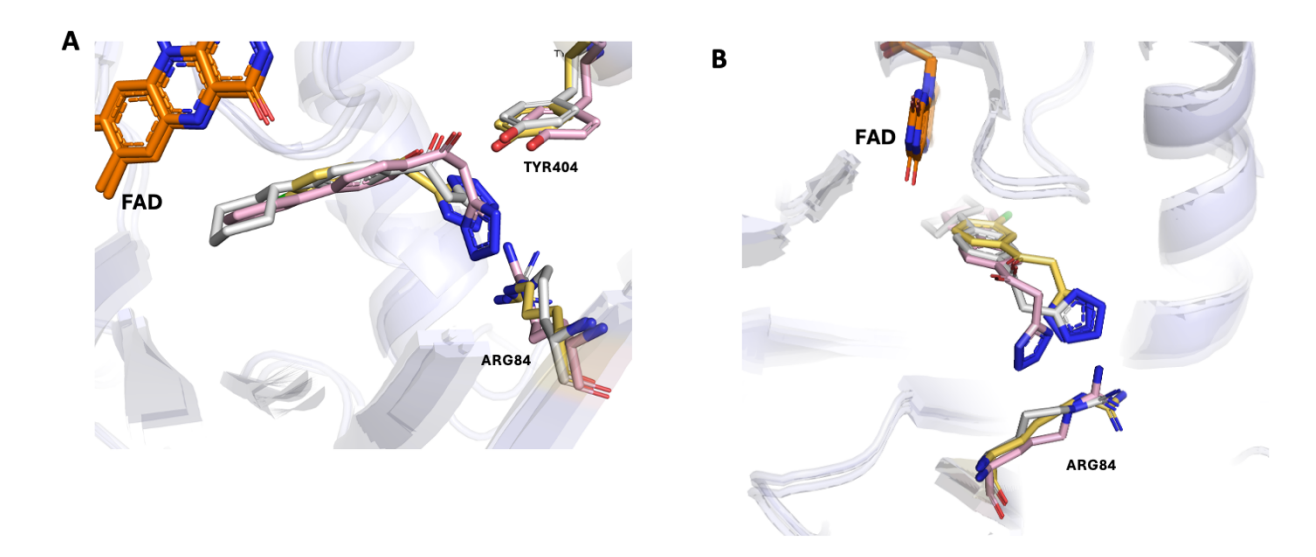


**Figure 2.4.3.** superposition of compound **4** (yellow), **6** (pink), and **7** (gray) within pfKMO active site at one active site. A: sideview of superposition structures. B: top view of superposition structures.

The structural superposition of pfKMO with Compound 7 and the L-kynurenine substrate is studied (**Figure 2.4.4**). The tetrazole moiety of Compound 7 forms the same hydrogen bonds as the carboxylate group of the substrate. However, the interaction between the amino group of the substrate and Tyr404 is replaced by a hydrogen bond between the carbonyl group of Compound 7 and Tyr404. Despite the presence of the bulky cyclohexyl substitution on the aromatic ring, the hydrogen binding distance remains unchanged. Additionally, the presence of the cyclohexyl group in the hydrophobic pocket pushes the tetrazole moiety closer to Arg84, resulting in a 0.2 Å reduction in distance. This enhanced proximity strengthens the interaction and is accompanied by a significant conformational change in Arg84.

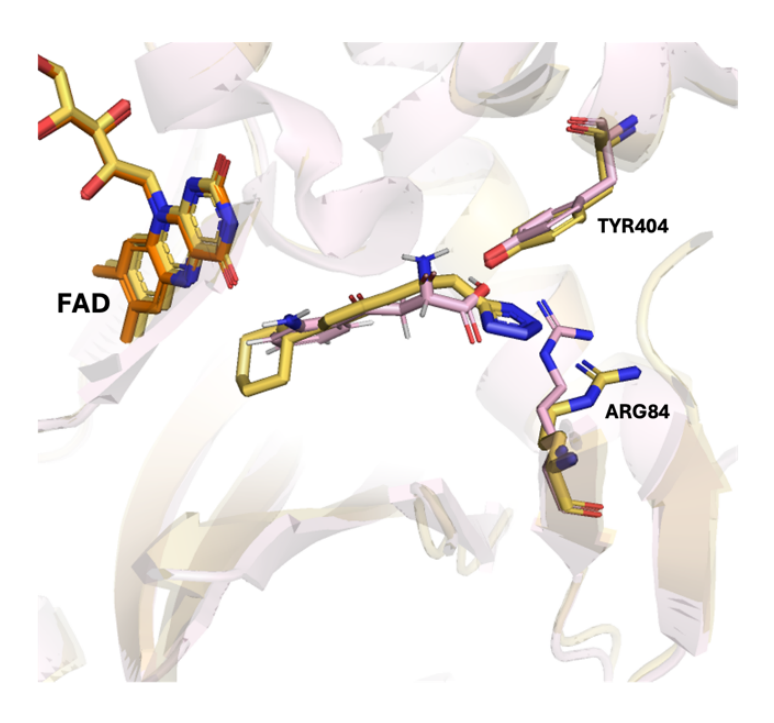


**Figure 2.4.4.** view of compound 7 (yellow) within pfKMO active site overlaid with structure of pfKMO-L-Kyn substrate (pink).

Next, we compared compound 7 with the only published crystal structure containing a structurally analogous tetrazole moiety replacement (Figure 2.4.5). The published tetrazole-containing compound, like compound 7, binds to both active sites of pfKMO. From the crystal structures of both active sites, the tetrazole groups of the two compounds align closely and adopt the same orientation. Additionally, in one of the active sites (Figure 2.4.5A), they form nearly identical interactions with residues located above the active site via water-mediated hydrogen bonding. One major difference between the two structures is the conformation of Arg84, which tilts upward to interact with the tetrazole moiety in the published compound. A similar conformational change was also observed in the crystal structure of compound 6. These findings suggest that Arg84 is highly flexible and can readily adapt to interact with acidic center groups.

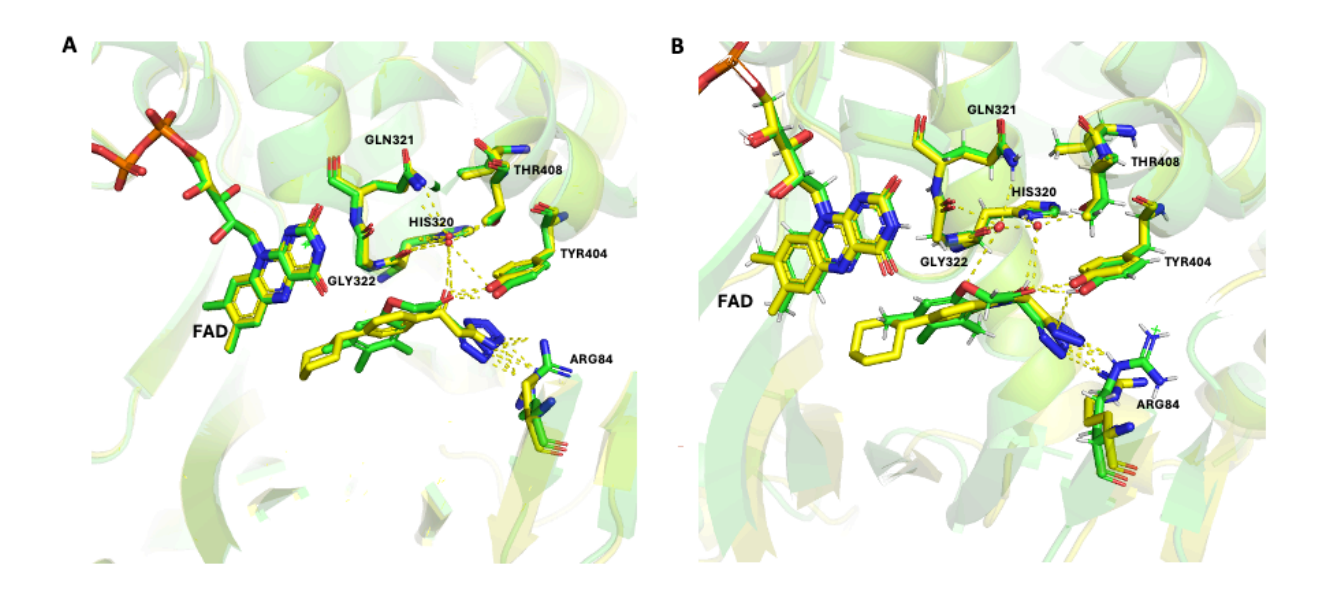


**Figure 2.4.5.** Superposition of compound 7 (yellow) with published tetrazole-containing compound (green, PDB:6FPH) bound to pfKMO at both active sites.

## 2.5 Chemistry

General procedure for Synthesis of substituted 2-chloro-1-phenylethan-1-one derivatives (A) (5c, 6c, 7c, and 9c): To a solution of chloroacetyl chloride (1equiv) and aluminum chloride (1equiv) in 15 mL dichloromethane, substituted benzene (1 equiv) was added. The reaction was stirred at room temperature and monitored by TLC until completion. Then the reaction mixture was slowly poured into cold-ice water with stirring, extracted with DCM (20 mLx3). Organic layer was combined, dried over Na<sub>2</sub>SO<sub>4</sub>, and concentrated under vacuum to give crude acylated product. Flash column chromatography was then performed (hexane: ethyl acetate) to give pure phenacyl chloride products.

General procedure for Synthesis of 3-oxo-3-phenylpropanenitrile (B) (2c-12c): To a solution of substituted phenacyl chloride (1 equiv) in 15 mL ethanol sodium cyanide (2.5 equiv) in 15 mL water was added dropwise at room temperature. Reaction mixture was monitored by TLC until completion. Then the reaction mixture was concentrated to remove ethanol, then

acidified by 6M HCl to pH~5. Precipitations were filtered and purified by flash column chromatography (hexane: ethyl acetate) to yield pure cyanoacetophenone.

General procedure for synthesis of tetrazole derivatives (C) (1d-12d): To a stirring solution of cyanoacetophenone (1 equiv) and aluminum chloride (3 equiv) in anhydrous tetrahydrofuran (THF) was added sodium azide (3 equiv) in one portion. Reaction mixture (RM) was heated and refluxed under nitrogen atmosphere. The reaction was monitored by TLC until completion. Then, the RM was filtered and concentrated under reduced pressure to form yellow residue. Water (30mL) was added to the residue and allowed to stir for 30 mins until precipitate formed, then filtration gave the crude tetrazole product. The crude product was recrystallized from chloroform to give pure product as a white solid.

Scheme 2.5.1. General synthesis route of tetrazole derivatives. (a) chloroacetyl chloride, AlCl<sub>3</sub>, DCM. (b) NaCN, EtOH/H<sub>2</sub>O=1:1, 50°C, 0.5h. (c) NaN<sub>3</sub>, AlCl<sub>3</sub>, anhydrous THF, reflux, 12hrs.

3-Oxo-3-phenylpropanenitrile (1d): To a solution of methyl benzoate (3 mL, 24.11 mmol, 1 equiv) in dry THF (15 mL) was added NaH (2.0 g, 60% in oil, 50.0 mmol, 2 equiv) and CH<sub>3</sub>CN (2.6 mL, 50 mmol, 2 equiv). The reaction mixture was refluxed on oil bath for 6 h. When the reaction was

completed (monitored by TLC), it was cooled to room temperature and H<sub>2</sub>O (60 mL) was added slowly, then the system was neutralized with HCl (12 N). The aqueous phase was extracted with EtOAc (3x30 mL). The combined organic phases were washed water, brine, dried over anhydrous Na<sub>2</sub>SO<sub>4</sub>, filtered, and concentrated in vacuo. A flash column chromatography was performed to yield the **1c** (2.78g, 79%) as light-yellow solid. <sup>1</sup>H NMR (400 MHz, CDCl<sub>3</sub>)  $\delta$  7.92 (d, J = 7.0 Hz, 2H), 7.67 (t, J = 7.5 Hz, 1H), 7.62 – 7.45 (t, 2H), 4.09 (s, 2H). <sup>13</sup>C NMR (101 MHz, CDCl<sub>3</sub>)  $\delta$  187.15, 134.72, 134.34, 129.16, 128.48, 113.79, 29.37.

1-Phenyl-2-(1H-tetrazol-5-yl) ethan-1-one (**1d**): according to general procedure C, NaN<sub>3</sub> (0.67g, 10.31mmol, 3 equiv) was added to a solution of **1c** (0.5g, 3.44 mmol, 1equiv) and AlCl<sub>3</sub> (1.50g, 10.35mmol, 3 equiv) in 15 mL anhydrous THF to give **1d** (0.56g, 87%) as a white solid. <sup>1</sup>H NMR (400 MHz, DMSO)  $\delta$  8.09 (d, J = 6.9 Hz, 2H), 7.72 (t, J = 7.4 Hz, 1H), 7.59 (t, J = 7.6 Hz, 2H), 4.95 (s, 2H). <sup>13</sup>C NMR (101 MHz, DMSO)  $\delta$  194.37, 135.95, 134.48, 129.38, 128.92, 34.52. HRMS: m/z calcd for C<sub>9</sub>H<sub>8</sub>N<sub>4</sub>O [M + H]<sup>+</sup> 189.0771, found 189.0771.

2-Chloro-1-(naphthalen-2-yl)ethan-1-one (**2b**): N-chlorosuccinimide (NCS) (2.36 g, 17.6 mmol, 1 equiv) was added to a stirring solution of 2-Acetonaphthone **2a** (3 g, 17.6 mmol, 1.0 equiv) and p-toluenesulfonic acid monohydrate (3.93g, 17.6 mmol, 1 eq) in anhydrous acetonitrile (20 mL). The mixture was stirred under reflux conditions for 8 hours. When reaction completed (monitored by TLC), the reaction mixture was evaporated under reduced. The resulting residue was dissolved in 40 mL EtOAc, washed with water (3x30 mL), 30 mL brine, dried over Na<sub>2</sub>SO<sub>4</sub>, filtered, concentrated under reduced pressure. The crude product was purified by silica gel column chromatography (Hexane: EtOAc = 18:1 to 15:1) to give **2b** (3.08 g, 85%) as white solid. <sup>1</sup>H NMR (600 MHz, cdcl<sub>3</sub>)  $\delta$  8.47 (s, 1H), 8.05 – 7.81 (m, 4H), 7.61 (dddd, J = 33.5, 8.1, 6.8, 1.3 Hz, 2H),

4.87 (s, 2H). <sup>13</sup>C NMR (101 MHz, CDCl<sub>3</sub>) δ 191.08, 135.93, 132.42, 131.62, 130.48, 129.66, 129.04, 128.88, 127.88, 127.12, 123.87, 45.91.

3-(Naphthalen-2-yl)-3-oxopropanenitrile (**2c**): according to general procedure B, sodium cyanide (1.68 g, 34.3 mmol, 2.5 equiv) in 20mL was added to a solution of **2b** (2.8 g, 13.7 mmol, 1 equiv) in 20mL ethanol. After flash column chromatography (hexane: ethyl acetate = 10:1 to 8:1), **2c** (2.13 g, 80%) was obtained as white solid. <sup>1</sup>H NMR (400 MHz, CDCl<sub>3</sub>)  $\delta$  8.42 (s, 1H), 8.06 – 7.87 (m, 4H), 7.64 (dddd, J = 24.7, 8.1, 6.9, 1.3 Hz, 2H), 4.21 (s, 2H). <sup>13</sup>C NMR (101 MHz, CDCl<sub>3</sub>)  $\delta$  186.92, 136.20, 132.33, 131.70, 130.72, 129.74, 129.53, 129.24, 127.96, 127.44, 123.42, 113.79, 29.39.

1-(Naphthalen-2-yl)-2-(1*H*-tetrazol-5-yl)ethan-1-one (**2d**): according to general procedure C, NaN<sub>3</sub> (0.59 g, 9.0 mmol, 3 equiv) was added to a solution of **2c** (0.59 g, 3.0 mmol, 1 equiv) and AlCl<sub>3</sub> (1.21 g, 9.0 mmol, 3 equiv) in 15 mL anhydrous THF to give **2d** (0.52 g, 72%) as white solid. <sup>1</sup>H NMR (400 MHz, DMSO)  $\delta$  8.87 (s, 1H), 8.16 (d, J = 8.0 Hz, 1H), 8.11 – 8.02 (m, 3H), 7.75 – 7.65 (m, 2H), 5.09 (s, 2H). <sup>13</sup>C NMR (101 MHz, DMSO)  $\delta$  194.29, 135.84, 133.26, 132.61, 131.38, 130.20, 129.57, 129.01, 128.23, 127.66, 123.99, 34.53. HRMS: m/z calcd for C<sub>13</sub>H<sub>10</sub>N<sub>4</sub>O [M + H]+239.0927, found 239.0929.

2-Chloro-1-(4-chlorophenyl) ethan-1-one (**3b**): N-chlorosuccinimide (NCS) (6.17 g, 46 mmol, 1.5 equiv) was added to a stirring solution of 4-chloroacetophenone (4 mL, 30.79 mmol, 1.0 equiv) and p-toluenesulfonic acid monohydrate (8.78 g, 46 mmol, 1.5 eq) in acetonitrile (30 mL). The mixture was stirred under reflux conditions for 8 hours. When reaction completed (monitored by TLC), the reaction mixture was evaporated under reduced. Water (50 mL) was added into the resulting residue, and the solution was stirred for 30 minutes to form precipitate. Filtration gave

the crude product (mixture of mono and di chlorinated products). The crude product was purified by silica gel chromatography (hexane to ethyl acetate = 25:1 to 10:1) to give **3b** (3.49 g, 60%) as white solid. <sup>1</sup>H NMR (400 MHz, CDCl<sub>3</sub>)  $\delta$  7.91 (d, J = 8.7 Hz, 2H), 7.48 (d, J = 8.6 Hz, 2H), 4.66 (s, 2H). <sup>13</sup>C NMR (101 MHz, CDCl<sub>3</sub>)  $\delta$  190.05, 140.59, 132.55, 129.99, 129.27, 45.53.

3-(4-Chlorophenyl)-3-oxopropanenitrile (**3c**): according to general procedure B, sodium cyanide (2.26 g, 46.12 mmol, 2.5 equiv) in 15 mL was added to a solution of **3b** (3.49 g, 18.46 mmol, 1 equiv) in 15 mL ethanol. After flash column chromatography (hexane: ethyl acetate = 10:1 to 6:1), **3c** (2.41 g, 73%) was obtained as a white solid. <sup>1</sup>H NMR (400 MHz, CDCl<sub>3</sub>)  $\delta$  7.87 (d, J = 8.6 Hz, 2H), 7.51 (d, J = 8.6 Hz, 2H), 4.05 (s, 2H). <sup>13</sup>C NMR (101 MHz, CDCl<sub>3</sub>)  $\delta$  185.89, 141.52, 132.61, 129.84, 129.57, 113.36, 29.33.

1-(4-Chlorophenyl)-2-(1*H*-tetrazol-5-yl)ethan-1-one (**3d**): according to general procedure C, NaN<sub>3</sub> (0.87 g, 13.38 mmol, 3 equiv) was added to a solution of **3c** (0.80 g, 4.45 mmol, 1 equiv) and AlCl<sub>3</sub> (1.80 g, 13.50 mmol, 3 equiv) in 15mL anhydrous THF to give **3d** (0.90 g, 91%) as white solid.  $^{1}$ H NMR (400 MHz, DMSO)  $\delta$  8.09 (d, J = 8.6 Hz, 2H), 7.67 (d, J = 8.6 Hz, 2H), 4.95 (s, 2H).  $^{13}$ C NMR (101 MHz, DMSO)  $\delta$  193.49, 139.44, 134.66, 130.84, 129.50, 34.59. HRMS: m/z calcd for C<sub>9</sub>H<sub>7</sub>ClN<sub>4</sub>O [M + H]+223.0381, found 223.0385.

2-Chloro-1-(3-chlorophenyl) ethan-1-one (**4b**): N-chlorosuccinimide (NCS) (2.15g, 16.10 mmol, 1.05equiv) was added to a stirring solution of 3-chloroacetophenone (2mL, 15.39mmol, 1.0equiv) and p-toluenesulfonic acid monohydrate (3.38g, 17.77mmol, 1.1 eq) in acetonitrile (30 mL). The mixture was stirred under reflux conditions for 8 hours. When reaction completed (monitored by TLC), the reaction mixture was evaporated under reduced. The resulting residue was dissolved in 40mL EtOAc, washed with water (3x30mL), 30mL brine, dried over Na<sub>2</sub>SO<sub>4</sub>, filtered,

concentrated under reduced pressure. The crude product was purified by silica gel chromatography to give **4b** (2.11g, 74%) as white solid. <sup>1</sup>H NMR (400 MHz, CDCl<sub>3</sub>)  $\delta$  7.94 (s, 1H), 7.83 (d, J = 7.6 Hz, 1H), 7.59 (d, J = 8.0 Hz, 1H), 7.45 (t, J = 7.9 Hz, 1H), 4.67 (s, 2H). <sup>13</sup>C NMR (101 MHz, CDCl<sub>3</sub>)  $\delta$  189.98, 135.76, 135.33, 133.93, 130.22, 128.66, 126.63, 45.61.

3-(3-Chlorophenyl)-3-oxopropanenitrile (**4c**): according to general procedure B, sodium cyanide (1.10 g, 22.45 mmol, 2.5 equiv) in 15 mL was added to a solution of **4b** (1.70 g, 8.99 mmol, 1 equiv) in 15 mL ethanol. After flash column chromatography (hexane: ethyl acetate = 15:1 to 8:1), **4c** (1.32 g, 82 %) was obtained as light-yellow solid. <sup>1</sup>H NMR (400 MHz, CDCl<sub>3</sub>)  $\delta$  7.90 (s, 1H), 7.80 (d, J = 7.8 Hz, 1H), 7.64 (d, J = 7.9 Hz, 1H), 7.49 (t, J = 7.9 Hz, 1H), 4.06 (s, 2H). <sup>13</sup>C NMR (101 MHz, CDCl<sub>3</sub>)  $\delta$  185.91, 135.75, 135.69, 134.68, 130.48, 128.52, 126.50, 113.19, 29.44.

1-(3-Chlorophenyl)-2-(1*H*-tetrazol-5-yl)ethan-1-one (**4d**): according to general procedure C, NaN<sub>3</sub> (0.48 g, 7.35 mmol, 3 equiv) was added to a solution of **4c** (0.44 g, 2.45 mmol, 1 equiv) and AlCl<sub>3</sub> (0.98 g, 7.35 mmol, 3 equiv) in 15 mL anhydrous THF to give **4d** (0.45 g, 83%) as white solid. <sup>1</sup>H NMR (400 MHz, DMSO)  $\delta$  8.11 (s, 1H), 8.04 (d, J = 7.8 Hz, 1H), 7.80 (d, J = 7.9 Hz, 1H), 7.63 (t, J = 7.9 Hz, 1H), 4.99 (s, 2H). <sup>13</sup>C NMR (101 MHz, DMSO)  $\delta$  193.48, 137.76, 134.32, 134.13, 131.34, 128.62, 127.54, 34.70. HRMS: m/z calcd for C<sub>9</sub>H<sub>7</sub>ClN<sub>4</sub>O [M + H]<sup>+</sup> 223.0381, found 223.0385.

2-Chloro-1-(3,4-dichlorophenyl) ethan-1-one (**5b**): in a dry 250 mL round-bottom flask equipped with a reflux condenser (under nitrogen) and dropping funnel, suspend AlCl<sub>3</sub> (5.02 g, 38 mmol, 1 equiv) in 30 mL of 1,2-dichlorobenzene **5a**. The suspension was cooled in an ice bath to 0 °C, then chloroacetyl chloride (3 mL, 38 mmol, 1 equiv) was added dropwise under vigorous stirring while maintaining the temperature below 5°C. After the addition was complete, the ice bath was

removed, and the mixture was allowed to warm up to room temperature. Then, the reaction mixture was heated to 100-105 °C, observing the color turned to dark red. After 12 hours, the reaction was stopped by cautiously adding 150 mL ice cold water under stirring. the resulting mustard-colored paste was extracted with ethyl acetate (40mL x 3). The organic layer was combined and neutralized with saturated sodium bicarbonate solution and washed with water (50 mL) and brain. The organic layer was dried over sodium sulfate and concentrated under reduced pressure. The remaining 1,2-dichlorobenzene was air dried to give dark oil. The dark oil was purified with silica gel chromatography (hexane: ethyl acetate = 25:1 to 20:1) to yield the **6b** as a white solid (7.35 g, 87%). ¹H NMR (400 MHz, CDCl<sub>3</sub>)  $\delta$  8.03 (d, J = 2.1 Hz, 1H), 7.78 (dd, J = 8.4, 2.1 Hz, 1H), 7.58 (d, J = 8.4 Hz, 1H), 4.65 (s, 2H). ¹³C NMR (101 MHz, DMSO)  $\delta$  184.44, 133.96, 128.95, 128.94, 126.27, 125.77, 122.81, 40.66.

3-(3,4-Dichlorophenyl)-3-oxopropanenitrile (**5c**): according to general procedure B, sodium cyanide (3.66 g, 74.69 mmol, 2.3 equiv) in 20mL was added to a solution of **5b** (7.35 g, 32.89 mmol, 1 equiv) in 20mL ethanol. After flash column chromatography (hexane: ethyl acetate = 15:1 to 10:1), **5c** (6.51 g, 92%) was obtained as a white solid. <sup>1</sup>H NMR (400 MHz, CDCl<sub>3</sub>)  $\delta$  8.01 (d, J = 2.1 Hz, 1H), 7.75 (dd, J = 8.4, 2.1 Hz, 1H), 7.62 (d, J = 8.4 Hz, 1H), 4.05 (s, 2H). <sup>13</sup>C NMR (101 MHz, CDCl<sub>3</sub>)  $\delta$  185.04, 139.75, 134.19, 133.71, 131.33, 130.38, 127.32, 112.96, 29.39.

1-(3,4-Dichlorophenyl)-2-(1*H*-tetrazol-5-yl)ethan-1-one (**5d**): according to general procedure C, NaN<sub>3</sub> (1.98 g, 30.46 mmol, 3 equiv) was added to a solution of **5c** (2.17 g, 10.14 mmol, 1 equiv) and AlCl<sub>3</sub> (4.06 g, 30.46 mmol, 3 equiv) in 20mL anhydrous THF to give **5d** (0.90 g, 91%) as a white solid. <sup>1</sup>H NMR (400 MHz, DMSO)  $\delta$  8.31 (s, 1H), 8.03 (dd, J = 8.4, 2.1 Hz, 1H), 7.88 (d, J = 8.4 Hz, 1H), 4.99 (s, 2H). <sup>13</sup>C NMR (101 MHz, DMSO)  $\delta$  192.79, 137.32, 136.12, 132.46,

131.72, 130.91, 128.87, 34.71. HRMS: m/z calcd for  $C_9H_6Cl_2N_4O$  [M + H]<sup>+</sup> 256.9991, found 256.9993.

1-([1,1'-Biphenyl]-4-yl)-2-chloroethan-1-one (**6b**): according to general procedure A, biphenyl **6a** (4.62 g, 29.96 mmol, 1 equiv) was added to a solution of chloroacetyl chloride (3 mL, 37.64 mmol, 1.25 equiv) and aluminum chloride (5.02 g, 37.65 mmol, 1.26 equiv) in 20 mL dichloromethane. After flash column chromatography (hexane: ethyl acetate = 25:1 to 20:1), **6b** (5.44 g, 79%) was obtained as white solid. <sup>1</sup>H NMR (400 MHz, CDCl<sub>3</sub>)  $\delta$  8.03 (d, J = 8.4 Hz, 2H), 7.71 (d, J = 8.2 Hz, 2H), 7.62 (d, J = 7.6 Hz, 2H), 7.48 (t, J = 7.5 Hz, 2H), 7.41 (t, J = 7.2 Hz, 1H), 4.73 (s, 2H). <sup>13</sup>C NMR (101 MHz, CDCl<sub>3</sub>)  $\delta$  190.74, 146.73, 139.54, 132.92, 129.18, 129.05, 128.54, 127.51, 127.31, 45.95.

3-([1,1'-Biphenyl]-4-yl)-3-oxopropanenitrile (**6c**): according to general procedure B, sodium cyanide (1.45 g, 29.48 mmol, 2.5 equiv) in 15mL was added to a solution of 2b (2.72 g, 11.79 mmol, 1 equiv) in 15 mL ethanol. After flash column chromatography (hexane: ethyl acetate = 10:1 to 5:1), **6c** (1.86 g, 71%) was obtained as a light-yellow solid. <sup>1</sup>H NMR (400 MHz, CDCl<sub>3</sub>)  $\delta$  7.99 (d, J = 8.5 Hz, 2H), 7.74 (d, J = 8.5 Hz, 2H), 7.63 (d, J = 6.9 Hz, 2H), 7.49 (t, J = 7.2 Hz, 2H), 7.43 (t, J = 7.3 Hz, 1H), 4.10 (s, 2H). <sup>13</sup>C NMR (101 MHz, CDCl<sub>3</sub>)  $\delta$  186.58, 147.50, 139.25, 132.97, 129.10, 129.10, 128.74, 127.72, 127.32, 113.76, 29.34.

1-([1,1'-Biphenyl]-4-yl)-2-(1*H*-tetrazol-5-yl)ethan-1-one (**6d**): according to general procedure C, NaN<sub>3</sub> (0.66 g, 10.15 mmol, 3 equiv) was added to a solution of **6c** (0.75 g, 3.39 mmol, 1 equiv) and AlCl<sub>3</sub> (1.36 g, 10.20 mmol, 3 equiv) in 15 mL anhydrous THF to give **6d** (0.89g, 66%) as a white solid. <sup>1</sup>H NMR (400 MHz, DMSO)  $\delta$  8.17 (d, J = 8.1 Hz, 2H), 7.90 (d, J = 8.1 Hz, 2H), 7.79 (d, J = 7.5 Hz, 2H), 7.53 (t, J = 7.5 Hz, 2H), 7.45 (t, J = 7.3 Hz, 1H), 4.98 (s, 2H). <sup>13</sup>C NMR (101

MHz, DMSO)  $\delta$  193.90, 145.79, 139.18, 134.76, 129.69, 129.61, 129.05, 127.55, 127.52, 34.57. HRMS: m/z calcd for  $C_{15}H_{12}N_4O$  [M + H]+265.1084, found 265.1085.

2-Chloro-1-(4-cyclohexylphenyl) ethan-1-one (**7b**): according to general procedure A, cyclohexylbenzene **7a** (4 mL, 24.51 mmol, 1 equiv) was added to a solution of chloroacetyl chloride (2.15 mL, 26.97 mmol, 1.1 equiv) and aluminum chloride (3.6 g, 27 mmol, 1.1 equiv) in 15 mL dichloromethane. After flash column chromatography (hexane: ethyl acetate = 30:1 to 20:1), **7b** (4.7 g, 81%) was obtained as a white solid. <sup>1</sup>H NMR (400 MHz, CDCl<sub>3</sub>) δ 7.89 (d, J = 8.4 Hz, 2H), 7.32 (d, J = 8.3 Hz, 2H), 4.69 (s, 2H), 2.65 – 2.51 (m, 1H), 1.98 – 1.69 (m, 5H), 1.50 – 1.18 (m, 5H). <sup>13</sup>C NMR (101 MHz, CDCl<sub>3</sub>) δ 190.71, 154.88, 132.09, 128.77, 127.40, 45.95, 44.77, 34.04, 26.68, 26.00.

3-(4-Cyclohexylphenyl)-3-oxopropanenitrile (**7c**): according to general procedure B, sodium cyanide (2.43 g, 49.63 mmol, 2.5 equiv) in 15 mL water was added to a solution of **7b** (4.7 g, 19.85 mmol, 1 equiv) in 15mL ethanol. After flash column chromatography (hexane: ethyl acetate = 20:1 to 15:1), **7c** (3.72 g, 80%) was obtained as light-yellow solid. <sup>1</sup>H NMR (400 MHz, CDCl<sub>3</sub>)  $\delta$  7.85 (d, J = 8.4 Hz, 2H), 7.35 (d, J = 8.5 Hz, 2H), 4.04 (s, 2H), 2.58 (s, 1H), 1.97 – 1.69 (m, 5H), 1.52 – 1.17 (m, 5H). <sup>13</sup>C NMR (101 MHz, CDCl<sub>3</sub>)  $\delta$  186.60, 155.77, 132.15, 128.75, 127.66, 113.93, 44.80, 33.99, 29.24, 26.63, 25.96.

1-(4-Cyclohexylphenyl)-2-(1H-tetrazol-5-yl) ethan-1-one (**7d**): according to general procedure C, NaN<sub>3</sub> (0.77 g, 11.22 mmol, 3 equiv) was added to a solution of **7c** (0.85 g, 3.74 mmol, 1 equiv) and AlCl<sub>3</sub> (1.50 g, 11.22 mmol, 3 equiv) in 15 mL anhydrous THF to give **7d** (0.72g, 71%) as a white solid. <sup>1</sup>H NMR (400 MHz, DMSO)  $\delta$  8.01 (d, J = 8.0 Hz, 2H), 7.44 (d, J = 8.0 Hz, 2H), 4.90 (s, 2H), 2.62 (t, J = 11.2 Hz, 1H), 1.76 (dd, J = 35.1, 12.1 Hz, 5H), 1.53 – 1.21 (m, 5H). <sup>13</sup>C NMR

(101 MHz, DMSO)  $\delta$  193.81, 154.60, 151.34, 133.86, 129.19, 127.69, 44.31, 34.38, 33.96, 26.65, 25.94. HRMS: m/z calcd for  $C_{15}H_{18}N_4O$  [M + H]+271.1553, found 271.1554.

2-Bromo-1-(4-(trifluoromethyl)phenyl)ethan-1-one (**8b**): cupric bromide (4.25 g, 19 mmol, 2 equiv) was added to a stirring solution of 4-trifluoromethylacetophenone (1.79 mL, 9.5 mmol, 1.0 equiv) in ethyl acetate and chloroform (10 mL/10 mL). The mixture was stirred under reflux conditions for 10 hours. When reaction completed (monitored by TLC), the reaction mixture was filtered and evaporated under reduced. The resulting residue was dissolved in 30mL EtOAc, washed with water (3x20 mL), 20 mL brine, dried over Na<sub>2</sub>SO<sub>4</sub>, filtered, concentrated under reduced pressure. The crude product was purified by silica gel chromatography to give **8b** (2.12g, 83%) as a pale-yellow solid. <sup>1</sup>H NMR (400 MHz, CDCl<sub>3</sub>)  $\delta$  8.10 (d, J = 8.1 Hz, 2H), 7.77 (d, J = 8.2 Hz, 2H), 4.45 (s, 2H). <sup>13</sup>C NMR (101 MHz, CDCl<sub>3</sub>)  $\delta$  190.40, 129.33, 128.62, 125.92, 125.71, 30.20.

3-Oxo-3-(4-(trifluoromethyl)phenyl)propanenitrile (**8c**): according to general procedure B, sodium cyanide (0.97 g, 19.9 mmol, 2.5 equiv) in 15 mL water was added to a solution of **8b** (2.12 g, 7.9 mmol, 1 equiv) in 15 mL ethanol. After flash column chromatography **8c** (0.4 g, 31%) was obtained as a yellow solid. <sup>1</sup>H NMR (400 MHz, CDCl<sub>3</sub>)  $\delta$  8.05 (d, J = 8.2 Hz, 2H), 7.81 (d, J = 8.2 Hz, 2H), 4.11 (s, 2H). <sup>13</sup>C NMR (101 MHz, CDCl<sub>3</sub>)  $\delta$  186.26, 136.85, 136.17, 128.88, 126.31, 124.57, 113.06, 29.63.

2-(1*H*-Tetrazol-5-yl)-1-(4-(trifluoromethyl)phenyl)ethan-1-one (**8d**): according to general procedure C, NaN<sub>3</sub> (0.37 g, 5.7 mmol, 3 equiv) was added to a solution of **8c** (0.4 g, 1.9 mmol, 1 equiv) and AlCl<sub>3</sub> (0.77 g, 5.7 mmol, 3 equiv) in 15 mL anhydrous THF to give **8d** (0.28 g, 58%) as a white solid. <sup>1</sup>H NMR (400 MHz, DMSO)  $\delta$  8.28 (d, J = 8.1 Hz, 2H), 7.98 (d, J = 8.2 Hz, 2H),

5.04 (s, 2H).  $^{13}$ C NMR (101 MHz, DMSO)  $\delta$  193.98, 139.12, 133.79, 133.47, 129.77, 126.41, 126.37, 126.34, 126.30, 34.93. HRMS: m/z calcd for  $C_{10}H_7F_3N_4O$  [M + H]+ 257.0645, found 257.0649.

2-Chloro-1-(3-chloro-4-methoxyphenyl)ethan-1-one (9b): according to general procedure A, 2-

chloroanisole **8ab** (2.7 g, 18.94 mmol, 1 equiv) was added to a solution of chloroacetyl chloride (1.5 mL, 18.94 mmol, 1 equiv) and aluminum chloride (3 g, 22.5 mmol, 1.2 equiv) in 20mL anhydrous dichloromethane. After flash column chromatography (hexane: ethyl acetate = 15:1 to 10:1), **9b** (3.55 g, 85%) was obtained as white solid. <sup>1</sup>H NMR (400 MHz, CDCl<sub>3</sub>)  $\delta$  7.99 (d, J = 2.2 Hz, 1H), 7.87 (dd, J = 8.7, 2.2 Hz, 1H), 6.99 (d, J = 8.7 Hz, 1H), 4.63 (s, 2H), 3.98 (s, 3H). <sup>13</sup>C NMR (101 MHz, CDCl<sub>3</sub>)  $\delta$  188.89, 159.47, 130.83, 129.18, 127.68, 123.33, 111.52, 56.48, 45.38. 3-(3-Chloro-4-methoxyphenyl)-3-oxopropanenitrile (**9c**): according to general procedure B, sodium cyanide (2.38 g, 40.5 mmol, 2.5 equiv) in 15 mL water was added to a solution of **9b** (3.55 g, 16.2 mmol, 1 equiv) in 15 mL ethanol. After flash column chromatography (hexane: ethyl acetate = 10:1 to 6:1), **9c** (2.45 g, 72%) was obtained as a white solid. <sup>1</sup>H NMR (400 MHz, CDCl<sub>3</sub>)  $\delta$  7.95 (d, J = 2.3 Hz, 1H), 7.84 (dd, J = 8.7, 2.3 Hz, 1H), 7.02 (d, J = 8.7 Hz, 1H), 4.01 (d, J = 5.0 Hz, 5H). <sup>13</sup>C NMR (101 MHz, CDCl<sub>3</sub>)  $\delta$  184.64, 160.09, 130.73, 129.15, 127.77, 123.75, 113.60,

1-(3-Chloro-4-methoxyphenyl)-2-(1*H*-tetrazol-5-yl)ethan-1-one (**9d**): according to general procedure C, NaN<sub>3</sub> (2.28 g, 35.06 mmol, 3 equiv) was added to a solution of **9c** (2.45 g, 11.69 mmol, 1 equiv) and AlCl<sub>3</sub> (4.78 g, 35.06 mmol, 3 equiv) in 15 mL anhydrous THF to give **9d** (2.09 g, 71%). <sup>1</sup>H NMR (400 MHz, DMSO)  $\delta$  8.12 (s, 1H), 8.08 (dd, J = 8.7, 2.1 Hz, 1H), 7.34 (d, J = 8.7 Hz, 1H), 4.91 (s, 2H), 3.98 (s, 3H). <sup>13</sup>C NMR (101 MHz, DMSO)  $\delta$  192.09, 159.35, 130.61,

111.66, 56.58, 29.04.

130.14, 129.46, 122.07, 113.15, 57.24, 34.25. HRMS: m/z calcd for  $C_{10}H_9ClN_4O_2$  [M + H]<sup>+</sup> 253.0487, found 253.0488.

2-Bromo-1-(3-chloro-4-methylphenyl)ethan-1-one (10b): 4-methylacetophenone (5 mL, 37.4 mmol) was added dropwise to a mixture of 8 mL sulfuric acid and 8 mL nitric acid under ice bath while maintaining the temperature below 5°C. The reaction was monitored by TLC until completion. The reaction mixture was poured into 100 mL ice-water mix, followed by vacuum filtration to yield 4-methyl-3-nitroacetophenone (6.5g, 97%) as a yellow solid without further purifications. Iron powder (4.68 g, 5 equivalent) was added to a solution of 4-methyl-3nitroacetophenone (6.5 g, 36.28 mmol, 1 equivalent) in 40 mL MeOH/ AcOH (1:1). the reaction was heated to 50 °C for 1 hour under N<sub>2</sub>. The reaction mixture was concentrated in vacuo. EtOAc (100 mL) and 1 M NaOH (50 mL) were then added to the residue. Precipitate was removed by centrifugation. The aqueous layer was extracted with EtOAc (3 × 50 mL). All organic layers were combined, dried over NaSO<sub>4</sub>, and concentrated under reduced pressure. The crude product was purified by silica gel column chromatography (Hexane: EtOAc = 8:1 to 5:1) to yield 3-amino-4methylacetopenhone (3.5g, 64.7%) as an orange solid. the Sandmeyer reaction was performed using standard reagents, sodium nitrite and cuprous chloride, to give 3-chloro-4methylacetophenone (3.0 g, 75.6%) as a precursor of **10b**. Cupric bromide (7.7 g, 35.4 mmol, 2 equiv) was added to a stirring solution of 3-chloro-4-methylacetophenone (3.0 g, 17.7 mmol, 1.0 equiv) in ethyl acetate and chloroform (20 mL/20 mL). The mixture was stirred under reflux conditions for 10 hours. When reaction was complete (monitored by TLC), the reaction mixture was filtered and evaporated under reduced. The resulting residue was dissolved in 50 mL EtOAc, washed with water (3x30 mL), 30 mL brine, dried over Na<sub>2</sub>SO<sub>4</sub>, filtered, concentrated under reduced pressure. The crude product was purified by silica gel chromatography to give 10b (3.0 g,

70%) as an orange solid. <sup>1</sup>H NMR (600 MHz, cdcl<sub>3</sub>)  $\delta$  7.96 (d, J = 1.8 Hz, 1H), 7.76 (dd, J = 7.9, 1.9 Hz, 1H), 7.35 (d, J = 7.9 Hz, 1H), 4.40 (s, 2H), 2.45 (s, 3H). <sup>13</sup>C NMR (101 MHz, CDCl<sub>3</sub>)  $\delta$  189.94, 142.85, 135.29, 133.27, 131.34, 129.57, 127.11, 30.41, 20.45.

3-(3-Chloro-4-methylphenyl)-3-oxopropanenitrile( $\mathbf{10c}$ ): according to general procedure B, sodium cyanide (1.51 g, 30.8 mmol, 2.5 equiv) in 15 mL water was added to a solution of  $\mathbf{10b}$  (3.0 g, 12.4 mmol, 1 equiv) in 15 mL ethanol. After flash column chromatography (hexane: ethyl acetate = 10:1 to 6:1),  $\mathbf{10c}$  (2.4 g, 99%) was obtained as a yellow solid. <sup>1</sup>H NMR (400 MHz, CDCl<sub>3</sub>)  $\delta$  7.90 (d, J = 1.9 Hz, 1H), 7.70 (dd, J = 8.0, 1.9 Hz, 1H), 7.40 (s, 1H), 4.04 (s, 2H), 2.47 (s, 3H). <sup>13</sup>C NMR (101 MHz, CDCl<sub>3</sub>)  $\delta$  185.64, 143.85, 135.64, 133.53, 131.59, 129.08, 126.56, 113.38, 29.28, 20.51.

1-(3-Chloro-4-methylphenyl)-2-(1H-tetrazol-5-yl)ethan-1-one(**10d**): according to general procedure C, NaN<sub>3</sub> (2.42 g, 37.2 mmol, 3 equiv) was added to a solution of **10c** (2.4 g, 12.3 mmol, 1 equiv) and AlCl<sub>3</sub> (4.96 g, 37.2 mmol, 3 equiv) in 25 mL anhydrous THF to give **10d** (2.1 g, 71%) as a white solid. <sup>1</sup>H NMR (400 MHz, DMSO)  $\delta$  8.09 (d, J = 1.8 Hz, 1H), 7.95 (dd, J = 8.0, 1.9 Hz, 1H), 7.58 (d, J = 8.0 Hz, 1H), 4.95 (s, 2H), 2.43 (s, 3H). <sup>13</sup>C NMR (101 MHz, DMSO)  $\delta$  193.11, 142.56, 135.51, 134.44, 132.19, 129.15, 127.58, 34.56, 20.34. HRMS: m/z calcd for C<sub>10</sub>H<sub>9</sub>ClN<sub>4</sub>O [M + H]<sup>+</sup> 237.0538, found 237.0535.

2-Chloro-1-(3-chloro-4-cyclohexylphenyl)ethan-1-one (11b): similar to the synthesis of 10b, acetyl chloride (4.5 mL, 63 mmol) was first added to a mixture of 7a (10 mL, 61.3 mmol) and aluminum chloride (8.4 g, 63 mmol) in 30 mL DCM to yield 1-(4-cyclohexylphenyl)ethan-1-one (12.4g, 90%), followed by aromatic nitration using sulfuric acid and nitric acid, reduction of the nitro group to amino group using iron powder in methanol and acetic acid (1:1), and conversion of the amino group to chloride by a Sandmeyer reaction to yield 1-(3-chloro-4-

cyclohexylphenyl)ethan-1-one (2.8 g, 20.0%) as a precursor of **11b**. N-Chlorosuccinimide (NCS) (1.58 g, 11.8 mmol, 1 equiv) was added to a stirring solution of 1-(3-chloro-4-cyclohexylphenyl)ethan-1-one (2.8 g, 11.8 mmol, 1.0 equiv) and p-toluenesulfonic acid monohydrate (2.25 g, 11.8 mmol, 1 equiv) in anhydrous acetonitrile (15 mL). The mixture was stirred under reflux conditions for 4 hours. When reaction was complete (monitored by TLC), the reaction mixture was evaporated under reduced. The resulting residue was dissolved in 40 mL EtOAc, washed with water (3x30 mL), 30 mL brine, dried over Na<sub>2</sub>SO<sub>4</sub>, filtered, concentrated under reduced pressure. The crude product was purified by silica gel column chromatography (Hexane: EtOAc = 30:1 to 20:1) to give **11b** (2.31g, 72%) as white solid. <sup>1</sup>H NMR (400 MHz, CDCl<sub>3</sub>)  $\delta$  7.94 (d, J = 1.9 Hz, 1H), 7.80 (dd, J = 8.2, 1.9 Hz, 1H), 7.39 (d, J = 8.1 Hz, 1H), 4.64 (s, 2H), 3.06 (ddd, J = 11.5, 8.5, 3.0 Hz, 1H), 1.94 – 1.79 (m, 5H), 1.51 – 1.31 (m, 5H). <sup>13</sup>C NMR (101 MHz, CDCl<sub>3</sub>)  $\delta$  189.77, 151.34, 134.46, 133.00, 129.65, 127.66, 127.03, 45.57, 40.95, 32.75, 26.66, 26.06.

3-(3-Chloro-4-cyclohexylphenyl)-3-oxopropanenitrile (**11c**): according to general procedure B, sodium cyanide (0.36 g, 7.35 mmol, 2.5 equiv) in 10 mL water was added to a solution of **11b** (0.79 g, 2.9 mmol, 1 equiv) in 10 mL ethanol. After flash column chromatography (hexane: ethyl acetate = 12:1 to 6:1), **11c** (0.45 g, 59%) was obtained as a yellow solid. <sup>1</sup>H NMR (400 MHz, CDCl<sub>3</sub>)  $\delta$  7.89 (d, J = 2.0 Hz, 1H), 7.76 (dd, J = 8.2, 2.0 Hz, 1H), 7.42 (d, J = 8.2 Hz, 1H), 4.02 (s, 2H), 3.07 (t, J = 11.5 Hz, 1H), 1.85 (dd, J = 33.5, 12.6 Hz, 5H), 1.49 – 1.21 (m, 5H). <sup>13</sup>C NMR (101 MHz, CDCl<sub>3</sub>)  $\delta$  134.78, 134.75, 133.72, 129.53, 127.92, 126.91, 118.23, 41.02, 32.71, 29.25, 26.61, 26.02.

1-(3-Chloro-4-cyclohexylphenyl)-2-(1*H*-tetrazol-5-yl)ethan-1-one (**11d**): according to general procedure C, NaN<sub>3</sub> (0.30 g, 4.6 mmol, 3 equiv) was added to a solution of **11c** (0.40 g, 1.5 mmol,

1 equiv) and AlCl<sub>3</sub> (0.61 g, 4.6 mmol, 3 equiv) in 15 mL anhydrous THF to give **11d** (0.30 g, 64%) as a white solid.  $^{1}$ H NMR (400 MHz, DMSO)  $\delta$  8.08 (d, J = 1.9 Hz, 1H), 7.99 (dd, J = 8.2, 1.9 Hz, 1H), 7.60 (d, J = 8.2 Hz, 1H), 4.94 (s, 2H), 3.01 (ddd, J = 12.2, 8.5, 3.0 Hz, 1H), 1.93 – 1.69 (m, 5H), 1.56 – 1.18 (m, 5H).  $^{13}$ C NMR (101 MHz, DMSO)  $\delta$  193.11, 150.57, 135.19, 133.53, 129.62, 128.55, 127.98, 40.96, 34.54, 32.61, 26.70, 25.93. HRMS: m/z calcd for C<sub>15</sub>H<sub>17</sub>ClN<sub>4</sub>O [M + H]<sup>+</sup> 305.1164, found 305.1160.

Scheme 2.5.2. Preparation of 1-(4-(benzyloxy)-3-chlorophenyl)-2-chloroethan-1-one (12b). (a) MeI, K<sub>2</sub>CO<sub>3</sub>, acetone, reflux, 8hrs. (b) acetyl chloride, AlCl<sub>3</sub>, DCM, 0°C-rt, 5hrs. (c)AlCl<sub>3</sub>, anhydrous benzene, reflux, 6hrs. (d) PhCH<sub>2</sub>Br, K<sub>2</sub>CO<sub>3</sub>, acetone, reflux, 2hrs. (e) NCS, TsOH·H<sub>2</sub>O, MeCN, reflux, 8hrs.

2-Chloroanisole (**12ab**): to a stirring solution of 2-chlorophenol (10 mL, 98 mmol, 1 equiv) and potassium carbonate (20.32 g, 147 mmol, 1.5 equiv) in 50 mL acetone, methyl iodide (9.15 mL, 147 mmol, 1.5 equiv) was added. The reaction mixture was heated to reflux. When the reaction was completed (checked by TLC), the reaction mixture was filtered and concentrated under reduced pressure to remove the acetone. Then, the resulting residue was dissolved in ethyl acetate (50 mL), washed with water (30 mL x 3) and brine, dried over sodium sulfate, concentrated under reduced pressure to yield a colorless oil, **12ab** (11.73 g, 84%). No further purification needed. <sup>1</sup>H NMR (400 MHz, CDCl<sub>3</sub>)  $\delta$  7.36 (dd, J = 7.8, 1.6 Hz, 1H), 7.25 – 7.17 (m, 1H), 6.90 (ddd, J = 17.1, 7.9, 1.4 Hz, 2H), 3.89 (s, 3H). <sup>13</sup>C NMR (101 MHz, CDCl<sub>3</sub>)  $\delta$  155.07, 130.27, 127.74, 122.53, 121.30, 112.18, 56.07.

1-(3-Chloro-4-methoxyphenyl)ethan-1-one (**12ac**): To a stirring suspension of acetyl chloride (4.52 mL, 63.33 mmol, 1 equiv) and aluminum chloride (8.44 g, 63.33 mmol, 1 equiv) in 40 mL anhydrous dichloromethane on ice bath, **12ab** (9.03 g, 63.33 mmol, 1 equiv) was slowly added while maintaining the temperature below 5°C. The ice bath was then removed, and the reaction was stirred at room temperature while being monitored by TLC until completion. Then, the reaction mixture was slowly poured into cold-ice water with stirring, extracted with DCM (30 mLx3). Organic layer was combined, washed with water, brine, dried over Na<sub>2</sub>SO<sub>4</sub>, and concentrated under vacuum to give crude acylated product. Flash column chromatography was then performed (hexane: ethyl acetate = 20:1 to 12:1) to give pure **12ac** as a milk-white solid (11.69 g, 100%). <sup>1</sup>H NMR (400 MHz, CDCl<sub>3</sub>)  $\delta$  7.96 (d, J = 2.2 Hz, 1H), 7.84 (dd, J = 8.6, 2.2 Hz, 1H), 6.95 (d, J = 8.6 Hz, 1H), 3.96 (s, 3H), 2.54 (s, 3H). <sup>13</sup>C NMR (101 MHz, DMSO)  $\delta$  190.87, 153.95, 125.98, 125.74, 124.01, 118.00, 106.49, 51.58, 21.45.

1-(3-Chloro-4-hydroxyphenyl)ethan-1-one (**12ad**):**12ac** (11.69 g, 63.32 mmol, 1 equiv) was added to a stirring suspension of aluminum chloride (12.66 g, 94.95 mmol, 1.5 equiv) in 60 mL anhydrous benzene at room temperature. Then the reaction mixture was heated and refluxed for 6 hours (checked by TLC). The reaction mixture was cooled down to room temperature, poured into ice-cold water, extracted with ethyl acetate (50 mL x 3). The organic layers were combined, washed with water, brine, dried over sodium sulfate, concentrated under reduced pressure. The residue was purified by silica gel chromatography to give pure **12ad** as a light-pink solid (8.45g, 82%) <sup>1</sup>H NMR (400 MHz.)  $\delta$  7.99 (d, J = 2.1 Hz, 1H), 7.82 (dd, J = 8.5, 2.1 Hz, 1H), 7.08 (d, J = 8.5 Hz, 1H), 6.15 (s, 1H), 2.55 (s, 3H). <sup>13</sup>C NMR (101 MHz, CDCl<sub>3</sub>)  $\delta$  195.61, 155.50, 131.21, 129.81, 129.27, 120.44, 116.09, 26.24.

1-(4-(Benzyloxy)-3-chlorophenyl)ethan-1-one (**12ae**): benzyl bromide (1.73 mL, 14.10 mmol, 1 equiv) was added to a suspension of **12ad** (2.4 g, 14.0 mmol, 1 equiv) and  $K_2CO_3(1.95 g, 14.1 mmol, 1 equiv)$  in acetone (20 mL). The reaction mixture was refluxed for 2 hours (checked by TLC). Then the reaction mixture was filtered after cooling to room temperature. Acetone was removed under reduced pressure, then water was added to the resulting residue, filtered, washed the filer cake with water, dried under air to give a peach-colored solid (3.6g, 98%). No further purification was needed. <sup>1</sup>H NMR (400 MHz, CDCl<sub>3</sub>)  $\delta$  8.00 (d, J = 2.2 Hz, 1H), 7.81 (dd, J = 8.7, 2.2 Hz, 1H), 7.48 – 7.30 (m, 5H), 6.99 (d, J = 8.6 Hz, 1H), 5.22 (s, 2H), 2.53 (s, 3H). <sup>13</sup>C NMR (101 MHz, CDCl<sub>3</sub>)  $\delta$  195.65, 157.90, 135.70, 131.04, 130.76, 128.73, 128.58, 128.27, 127.03, 123.51, 112.87, 70.88, 26.26.

1-(4-(Benzyloxy)-3-chlorophenyl)-2-chloroethan-1-one (**12b**): N-chlorosuccinimide (NCS) (1.8 g, 13.4 mmol, 1 equiv) was added to a stirring solution of **12ae** (3.48 g, 13.4 mmol, 1.0 equiv) and p-toluenesulfonic acid monohydrate (2.55 g, 13.4 mmol, 1 eq) in acetonitrile (20 mL). The mixture was stirred under reflux conditions for 8 hours. When reaction completed (monitored by TLC), the reaction mixture was evaporated under reduced. The resulting residue was dissolved in 40mL EtOAc, washed with water (3x30mL), 30mL brine, dried over Na<sub>2</sub>SO<sub>4</sub>, filtered, concentrated under reduced pressure. The crude product was purified by silica gel column chromatography to give **12b** (2.44 g, 62%) as white solid. <sup>1</sup>H NMR (400 MHz, CDCl<sub>3</sub>)  $\delta$  8.02 (d, J = 2.2 Hz, 1H), 7.83 (dd, J = 8.6, 2.2 Hz, 1H), 7.49 – 7.30 (m, 5H), 7.03 (d, J = 8.7 Hz, 1H), 5.25 (s, 2H), 4.60 (s, 2H). <sup>13</sup>C NMR (101 MHz, CDCl<sub>3</sub>)  $\delta$  188.89, 158.61, 135.44, 131.01, 129.02, 128.79, 128.38, 127.87, 127.03, 123.96, 113.04, 70.99, 45.30.

3-(4-(Benzyloxy)-3-chlorophenyl)-3-oxopropanenitrile (**12c**): according to general procedure B, sodium cyanide (0.51 g, 10.41 mmol, 2.5 equiv) in 15mL water was added to a solution of **12b** 

(1.22 g, 4.13 mmol, 1 equiv) in 15 mL ethanol. After flash column chromatography (hexane: ethyl acetate = 3:1 to 2:1), **12c** (1.06 g, 90%) was obtained as a white solid. <sup>1</sup>H NMR (600 MHz, cdcl<sub>3</sub>)  $\delta$  7.98 (s, 1H), 7.79 (d, J = 8.6 Hz, 1H), 7.47 – 7.34 (m, 5H), 7.05 (d, J = 8.6 Hz, 1H), 5.26 (s, 2H), 4.02 (s, 2H). <sup>13</sup>C NMR (101 MHz, CDCl<sub>3</sub>)  $\delta$  184.60, 159.20, 135.22, 130.85, 128.97, 128.83, 128.47, 127.91, 127.04, 124.32, 113.55, 113.16, 71.11, 29.02.

1-(4-(Benzyloxy)-3-chlorophenyl)-2-(1*H*-tetrazol-5-yl)ethan-1-one (**12d**): according to general procedure C, NaN<sub>3</sub> (0.18 g, 2.77 mmol, 3 equiv) was added to a solution of **12c** (0.26 g, 0.91 mmol, 1 equiv) and AlCl<sub>3</sub> (0.36 g, 2.7 mmol, 3 equiv) in 15 mL anhydrous THF to give **12d** (0.21 g, 70%) as white solid. <sup>1</sup>H NMR (400 MHz, DMSO)  $\delta$  8.14 (d, J = 2.2 Hz, 1H), 8.06 (dd, J = 8.7, 2.2 Hz, 1H), 7.50 (d, J = 7.0 Hz, 2H), 7.46 – 7.40 (m, 3H), 7.39 – 7.34 (m, 1H), 5.37 (s, 2H), 4.91 (s, 2H). <sup>13</sup>C NMR (101 MHz, DMSO)  $\delta$  192.10, 158.36, 136.41, 130.72, 130.00, 129.63, 129.06, 128.65, 128.04, 122.54, 114.40, 70.96, 34.26. HRMS: m/z calcd for C<sub>16</sub>H<sub>13</sub>ClN<sub>4</sub>O<sub>2</sub> [M + H]<sup>+</sup> 329.0800, found 329.0797.

#### 2.6 Conclusion

Our investigation into the bio-isosteric replacement of the carboxylic acid with a tetrazole group has led to the discovery of a series of novel derivatives. Through extensive SAR analysis, we identified the cyclohexyl group as an optimal substituent for accommodating the hydrophobic region, offering superior fit compared to other functional groups. Crystal structures of compounds 4, 6, and 7 revealed that the tetrazole moiety forms extensive interactions with surrounding residues through both direct hydrogen bonds and water-mediated bridges. These findings provide valuable insights into protein–ligand interactions and will help in the development of more potent and promising KMO inhibitors.

#### **CHAPTER 3**

# 5-NITROKYNURENINE AS AN UNCOUPLER OF BOTH *PSEUDOMONAS FLUORESCENS*AND *CYTOPHAGA HUTCHINSONII* KYNURENINE MONOOXYGENASE

#### 3.1 Introduction

Over the past two decades, kynurenine monooxygenase (KMO) has been of great therapeutic interest because of its involvement in defining the balance between N-Methyl-Daspartic acid (NMDA) receptor agonism and antagonism.<sup>32</sup> Furthermore, the hydroxylation of kynurenine (KYN) by KMO (Figure 3.1.1) is the entry point to the synthesis of two free radical generators: 3-hydroxykynurenine (3-HK) and 3-hydroxyanthranillic acid (3-HAA)<sup>99, 100</sup>, and an NMDA receptor agonist, quinolinic acid (QA)<sup>25, 101-103</sup>. KMO inhibition has therefore emerged as a therapeutic target for neurogenerative disorders such as Alzheimer's (AD) and Huntington (HD) and Parkinson's (PD) diseases 104, 105. KMO inhibition not only eradicates the production of the above neurotoxic metabolites, but it also promotes an increased production of a neuroprotectant NMDA receptor antagonist<sup>106</sup>: Kynurenic acid. Since KMO and KAT share the same substrate, the inhibition of KMO increases the bioavailability of KYN, which, in turn leads to neuroprotection as it increases the levels of KA in the brain. Chronic oral administration of a KMO inhibitor, JM6, in a transgenic mouse model of AD reduced extracellular glutamate owing to the increase of KA levels in the brain. KMO inhibition also results in amelioration of HD symptoms in a mouse model. 105 Brain changes associated with AD, such as high-affinity to choline and a significant decrease in cortical choline acetyltransferase, were observed when QA was introduced

in the nucleus basalis of rats; however, when KA and QA were co-injected, there were no such changes, suggesting that KA protects the brain against damages caused by QA neurotoxicity.<sup>106</sup>

**Figure 3.1.1.** Schematic overview of kynurenine pathway highlighting metabolites involves in neurotoxicity (red labels) and neuroprotection (green label).

**Figure 3.1.2.** Structure of 5-nitrokynurenine, a proposed kynurenine analog binder.

Kynurenine analogs were the first set of KMO binders to be examined for competitive inhibition<sup>80</sup>, <sup>107, 108</sup>. Given their structural similarities with the physiological substrate, they often bind to the active site with greater affinity than KYN and competitively inhibit KMO. Both structure activity relationships (SAR) and crystallographic studies had shown that the key requirement for KMO inhibition are: The aromatic moiety to occupy the hydrophobic region in the active site; and approximately three spacers atoms between the aromatic region and the carboxylic acid moiety in order to keep charge-charge interaction with a conserved Arginine residue in the active site. 67, 79 The SAR studies revealed that the amino group does not involve in binding between ligands and active site. Since KMO is a NADPH dependent flavoenzyme, substrate-like inhibitors can stimulate FAD reduction of dioxygen without going through hydroxylation as expected for monooxygenases, a phenomenon that leads to the accumulation of hydrogen peroxides.<sup>69</sup> The paradoxical importance of these enzymes led us to develop 5-nitrokynurenine (5-Nkyn, Figure **3.1.2**), a kynurenine analog, with the potential to inhibit KMO and thus shift the pathway towards neuroprotection. meta-Nitrobenzoylalanine (m-NBA), the desamino analog of 5-NKyn, was shown previously to inhibit KMO in rats.<sup>77</sup>

#### 3.2 Materials and Methods

Expression and purification of *Cytophaga hutchinsonii* KMO (chKMO). chKMO was expressed in *E. coli* BL21 (DE3). A single colony grown on LB/kanamycin agar plates, was removed, and transferred to 5 ml of sterile LB broth with 5μl kanamycin for overnight at 37 °C with shaking at 180 rpm. That overnight culture was then added to separate 1 L flasks containing 1 L Studier autoinduction<sup>109</sup> medium supplemented with 200 mg/L kanamycin. The cells were grown at 37 °C for 24 hours with shaking (220 rpm). Cells were then collected by centrifugation for 15 minutes at 4000 rpm at 4 °C and stored at -80°C until used for enzyme purification. Cells

were resuspended in 30 ml 0.05M Tris-acetate buffer supplemented with 1 mM DTT, 0.2% Triton X-100, and 5 μM FAD. The yellow suspension was sonicated on ice in 4 20-second bursts with 3 minutes cooling between bursts. Debris were removed by centrifugation for 1 hour 30 minutes at 4000 rpm at 4 °C. The enzyme solution from the previous step was loaded on the Ni-chelate column equilibrated with 0.05 M Tris-acetate buffer (pH 8.0, 5 µM FAD, 0.5 mM DTT), followed by washing with 100 ml 0.05M Tris-acetate buffer (PH 8.0, 5 µM FAD, 0.5 mM DTT, 20 mM imidazole) buffer. The protein was eluted using 0.05 M Tris-acetate buffer (0.2 M mannitol, 0.2% Triton X-100, 5 µM FAD, 1 mM DTT, 200 mM imidazole, pH 8.0). The fractions that possessed a brilliant yellow color and contained significant KMO activity (steady state observations section) were pooled and concentrated using a centrifugal concentrator (30 kDa cutoff) at 4 °C for 1 hour 3 times using the exchange buffer (0.05 M Tris-acetate buffer pH 8.0, 5 µM FAD, 0.5 mM DTT). For further purification, the protein was loaded onto a DEAE-Sepharose column (30 cm · 2.5 cm) pre-equilibrated with the same buffer used for Ni-NTA column, followed by washing with the same buffer with 20 mM NaCl. The protein was eluted overnight using 0.05 M Tris-acetate buffer and 200 mM NaCl. The fractions that possessed a brilliant yellow color and contained significant KMO activity were pooled and concentrated using a centrifugal concentrator (30 kDa cutoff) at 4 °C for 1 hour. The concentrated KMO was then distributed into several Eppendorf tubes, flash frozen with liquid nitrogen, then stored at -80°C. The concentration of KMO was measured at 280 nm ( $\Delta \varepsilon = 12300 \text{ M}^{-1} \text{ cm}^{-1}$ ) by Nanodrop.

Expression and purifications of *Pseudomonas fluorescens* KMO (pfKMO)<sup>68</sup>. pfKMO was expressed in *E. coli* BL21 (DE3). A single colony grown on LB/ampicillin agar plates was transferred to 5 ml of sterile LB broth with 5μg/ml ampicillin for overnight at 37 °C with shaking at 180 rpm. That overnight culture was then added to separate 1 L flasks containing 1 L Studier

autoinduction medium supplemented with 200 mg/L ampicillin. The cells were grown at 25 °C for 24 hours with shaking (220 rpm). Cells were then collected by centrifugation for 15 minutes at 4000 rpm at 4 °C, resuspended in 20 mM HEPES pH 7.5, 10 mM NaCl, 1 mM DTT. The light-yellow suspension was sonicated on ice in 4 20-second bursts with 4 minutes cooling between bursts. Debris were removed by centrifugation for 1 hour 30 minutes at 4000 rpm at 4 °C. The enzyme solution from the previous step was loaded on the DEAE Sepharose column equilibrated with 20 mM HEPES pH7.5, 1 mM DTT with 10 mM NaCl, followed by eluting with 100 ml 20 mM HEPES pH7.5, 1 mM DTT with 100 mM NaCl. Fractions containing KMO were combined and precipitated in 50% saturated ammonium sulphate. The precipitated protein was collected by centrifuge at 4000 rpm at 4 °C, resuspended in 5mL size exclusion buffer (10 mM HEPES pH 7.0, 150 mM sodium acetate, 1 mM DTT) and passed down a Sephacryl S-300 column. Fractions with pure KMO were pooled and distributed into several Eppendorf tubes and stored at -80°C. The concentration of KMO was measured by Nanodrop.

Steady-state kinetics. The enzyme activities were determined by monitoring the NADPH consumption at 340 nm. For KMO the reaction mixture consisted of total 800 μl of buffer (0.05 M Tris-acetate, pH 8.0 for chKMO or 0.02 M HEPES for pfKMO, 1 mM DTT, 5 μM FAD, 0.015M KCl, 0.2 mM NADPH), varied concentrations of kynurenine or 5-Nkyn and 22 μM enzyme. Reaction was initiated by the addition of 10 μl of enzyme sample. Kinetic parameters were determined by initial-velocity measurements at varying concentrations of substrates. the Michaelis constant ,K<sub>m</sub>, was calculated using GraphPad Prism 10.

High-performance liquid chromatography. The reaction of 5-NKyn was measured by following the product formation using a Nucleosil 120-5 C-18 silica gel column from Machery-Nagel. The reaction mixture consisted of 100 μl reaction buffer (0.05 M Tris-acetate pH 8.0 for chKMO or

0.02 M HEPES pH 7.5 for pfKMO, 1 mM DTT, 5  $\mu$ M FAD, 50  $\mu$ M kynurenine) 100  $\mu$ M NADPH, 4  $\mu$ M KMO, (0-100  $\mu$ M) of 5-NKyn. Elution was in 0.1% acetic acid/5% methanol for 5 minutes, then a gradient from 5% methanol to 70% methanol at 25 minutes was applied.

**Synthesis of 5-Nitrokynurenine**. 5-NKyn was prepared from L-tryptophan, starting with esterification to give tryptophan methyl ester hydrochloride **2**, and then acetylation to give intermediate N-acetyl tryptophan methyl ester **3** (**Scheme 3.4.1**). Oxidative ring-opening of indole, and second acetylation gave  $N^{\alpha}$ ,N-diacetyl kynurenine methyl ester **4**, which was followed by electrophilic aromatic nitration to give  $N^{\alpha}$ , N-diacetyl-5-nitro-L-kynurenine methyl ester **5**. Hydrolysis of **5** led to the formation of desired compound 5-NKyn (details see **3.4 Chemistry**).

## 3.3 Results and discussion

In this study, we present the novel synthesis of 5-NKyn and its inhibition potential using biochemical KMO inhibition and binding assays. The nitration of 5-NKyn was unexpectedly challenging. Reaction of protected kynurenine under standard nitration conditions (HNO<sub>3</sub>:H<sub>2</sub>SO<sub>4</sub>, 1:1) resulted in unreacted starting material. This is most likely due to the protonation of the substrate in the strongly acidic medium resulting in deactivation. Under more severe conditions, KNO<sub>3</sub> in H<sub>2</sub>SO<sub>4</sub>, nitration proceeded, but there were a number of products detected by TLC. Hence, we tried a less acidic solvent, trifluoroacetic acid, with LiNO<sub>3</sub> and stoichiometric H<sub>2</sub>SO<sub>4</sub>. This condition resulted in rapid reaction to form two nitrated products by TLC. The 5-nitrated product can be easily separated from the 3-nitro product by column chromatography. Hydrolysis of the protected 5-nitrokynurenine was performed, giving the desired 5-nitrokynurenine isolated in modest yield.

Our interest in 5-nitrokynurenine is based on the reaction mechanism of KMO.<sup>63</sup> Our initial hypothesis was that 5-NKyn may act as inhibitor, substrate, or a non-substrate effector of KMO,

like most other kynurenine analogs.  $^{63,\,87}$  We observed a high blank rate in inhibition assays in the presence of 5-Nkyn for both chKMO and pfKMO, which suggested that it could be either an uncoupler of NADPH oxidation, or a potential KMO substrate as observed in other kynurenine analogs. In order to calculate the Michaelis constant  $K_m$  for 5-NKyn, inhibition assays were then performed without adding substrate kynurenine. As we expected the rate of consumption of NADPH increased as we increased the concentrations of 5-NKyn for both chKMO and pfKMO (figure 3.3.1). The plot was fitted to the Michaelis-Menten equation to give  $K_m$  of  $7 \pm 1 \,\mu\text{M}$  for pfKMO and  $6 \pm 3 \,\mu\text{M}$  for chKMO. They are 10-fold and 12-fold lower than the  $K_m$  of L-kyn (67±15  $\mu\text{M}$ ),  $^{87}$  respectively, suggesting a stronger binding than L-kyn to KMO.

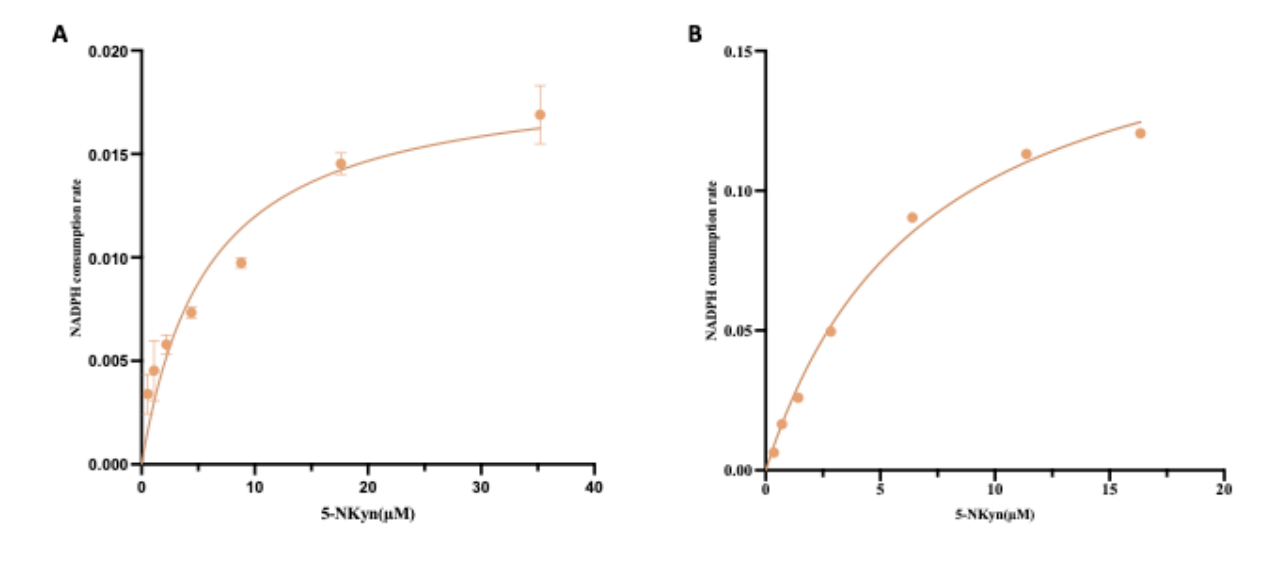


**Figure 3.3.1:** Consumption rate of NADPH vs the varied concentrations of 5-Nkyn with chKMO (A) and pfKMO (B).

Given that the 3-position on the aromatic ring was still open, we thought that 5-NKyn could be also acting as a substrate of KMO. However, using HPLC, we did not observe a new peak with absorbance around 370-400 nm as expected for where hydroxylation of kynurenines occur (**Figure** 

**3.3.2**) which indicated that indeed, 5-NKyn was consuming NADPH without hydroxylation, a phenomenon associated in the accumulation of highly toxic oxygen species<sup>63, 69</sup>.

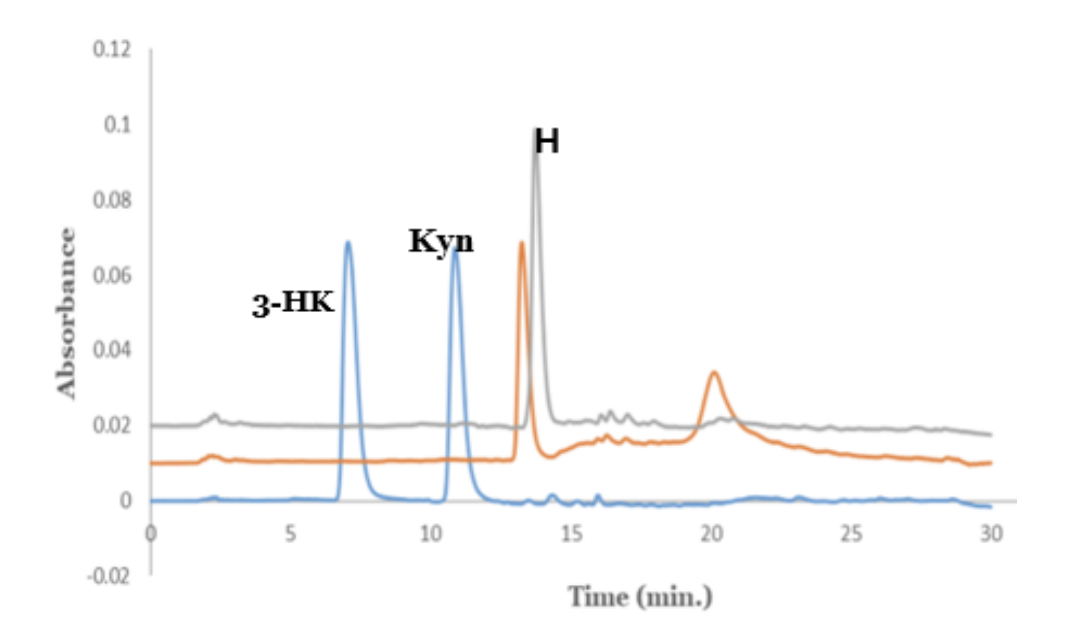


**Figure 3.3.2:** HPLC analysis of 5-Nkyn reaction with KMO-orange line; black line: control; blue line: reaction of kynurenine with KMO.

The structurally similar KMO ligand, *m*-nitrobenzoylalanine (*m*-NBA), had already been shown to function as both an inhibitor or a substrate effector of KMO depending on the enzyme species. <sup>69</sup> Another structurally similar KMO inhibitor, 5-bromo-L-kynurenine, was found to not only oxidize NADPH and reduce FAD but also get hydroxylated to form the 5-bromo-3-hydroxykynurenine product. <sup>69,87</sup> Relative to 5-Nkyn, the enhanced deactivation effect is attributed to the nitro group, which is a more deactivating group compared to the bromo group. The presence of the nitro group significantly reduces the reactivity of the aromatic system, thereby inhibiting the electrophilic aromatic hydroxylation. Consequently, 5-Nkyn is defined as an uncoupler, stimulating oxidation of NADPH to generate H<sub>2</sub>O<sub>2</sub>.

Using Autodock Vina, we followed the protocol proposed and validated by Amaral<sup>67</sup>, Toledo-Sherman<sup>86</sup> and Steven<sup>88</sup> to assess the binding mode of this compound. As expected for KMO binders, 5-NKyn interacted with the conserved Arg 83 residue in the active site via its carboxylate moiety. The benzene ring of 5-NKyn also occupies the hydrophobic pocket close to the FAD binding site where the nitro group forms interactions with FAD and water molecule. This explains the stronger binding for 5-Nkyn that kynurenine doesn't form hydrogen bonds with FAD and water molecule.

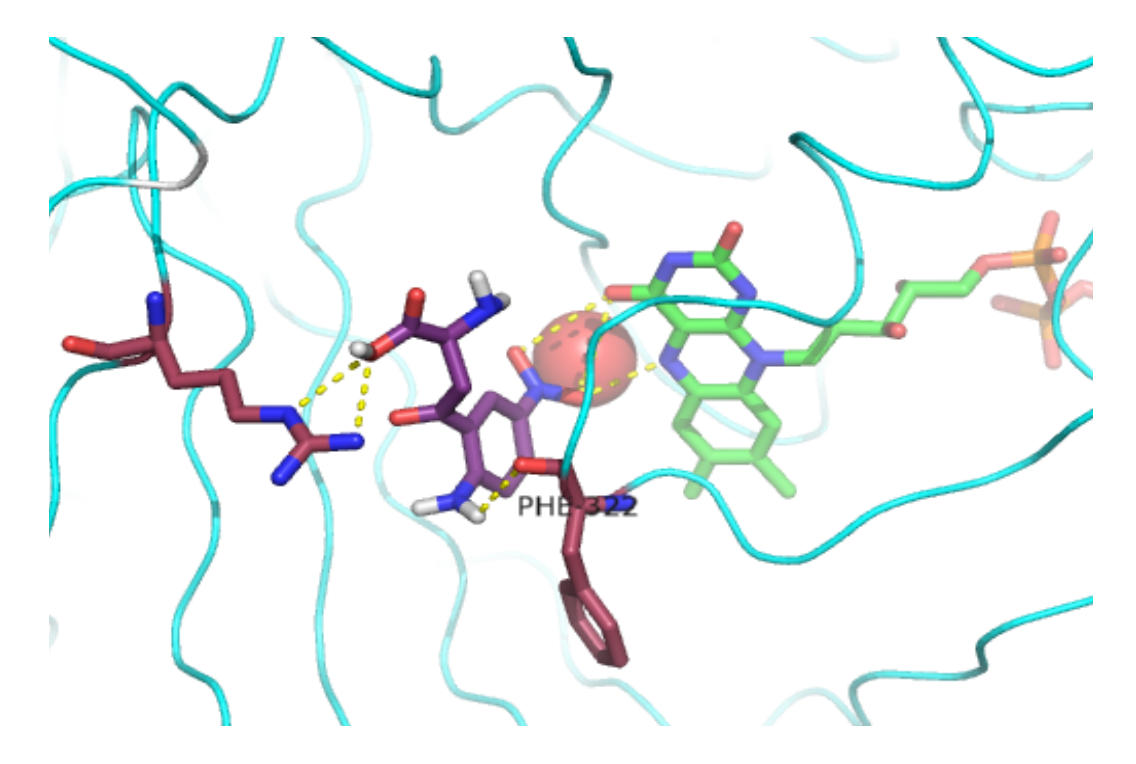


Figure 3.3.3: Active site of yeast KMO (PDB: 4J36) in complex with 5-NKyn.

In conclusion, 5-NKyn functions as an uncoupler of KMO. The introduction of a nitro group on the aromatic ring prevents the formation of hydroxylated product by deactivating the ring. However, adding a nitro group greatly increases the binding affinity to the active site, owing to the hydrogen bond formation between nitro group and FAD and water molecule. We believe this 5-NKyn will offer us better insight into the development of more potent inhibitors of KMO.

# 3.4 Chemistry

Scheme 3.4.1. Synthesis of 5-NKyn.

Tryptophan methyl ester hydrochloride (2): Tryptophan (4.90 g, 24 mmol) 1 was added to a solution of chlorotrimethylsilane (6 mL, 48 mmol) in methanol (45mL). The resulting solution was stirred at room temperature until completion (monitored by TLC). The reaction mixture was concentrated on a rotary evaporator to give the product tryptophan methyl ester hydrochloride 2 (6.13 g, 98%) as a white solid.  $^{1}$ H NMR (400 MHz, Deuterium Oxide)  $\delta$  7.53 (d, J = 8.5 Hz, 1H), 7.45 (d, J = 7.9 Hz, 1H), 7.26 – 7.05 (m, 3H), 4.37 (s, 1H), 3.71 (s, 3H), 3.40 (t, J = 7.0 Hz, 2H).  $^{13}$ C NMR (101 MHz, Deuterium Oxide)  $\delta$  170.44, 136.27, 126.36, 125.37, 122.24, 119.60, 118.02, 112.06, 105.99, 53.55, 53.31, 25.66.

Synthesis of N-acetyl tryptophan methyl ester(3): Tryptophan methyl ester hydrochloride (6.13 g) 2 was dissolved in 100 mL water. 50 mL 2M sodium hydroxide was added to the solution, immediately followed by adding 10 mL acetic anhydride. The solution was allowed to stir for 10 minutes. Precipitates were filtrated and washed with 100 mL water to afford the product N-acetyl

tryptophan methyl ester **3** (4.82g, 77%) as white powder.  $^{1}$ H NMR (400 MHz, Chloroform-d)  $\delta$  8.38 (s, 1H), 7.52 (d, J = 7.9 Hz, 1H), 7.34 (s, 1H), 7.15 (dt, J = 29.0, 7.3 Hz, 2H), 6.95 (s, 1H), 6.07 (d, J = 7.9 Hz, 1H), 4.98 – 4.92 (m, 1H), 3.69 (s, 3H), 3.32 (t, J = 6.2 Hz, 2H), 1.94 (s, 3H).  $^{13}$ C NMR (101 MHz, Chloroform-d)  $\delta$  172.49, 169.90, 136.16, 127.74, 122.78, 122.24, 119.70, 118.50, 111.37, 109.96, 53.12, 52.40, 27.61, 23.23.

#### Synthesis of $N^{\alpha}$ , N-diacetyl-L-kynurenine(4):

4.82 g of N<sup> $\alpha$ </sup>-acetyl tryptophan methyl ester 3 was dissvoled in 60 ml methanol and cooled to -78 °C using a dry ice / acetone bath. Ozone was bubbled through the cold reaction mixture while maintaining temperature below at -70 °C. Reaction was monitored by TLC until completion. The RM was quenched with sodium bisulphite solution (prepared by dissolving 40 gm of sodium bisulfite in 120 ml water) and stirred for about 10 mins as the RM attains RT. Methanol was removed under reduced pressure and 50 ml water was added to the residue. Extract the residue with two 30 ml EtOAc (x3). The EtOAc layers were combined and washed with 50 ml water, followed by 50 ml brine. The organic layer was dried over anhydrous sodium sulfate and concentrated under vacuum to give yellow oil (4.33 g) which is used as it is for the next acylation step. The oil from the previous step was dissolved in 60 ml MeOH. 10 ml trifluoroacetic acid (TFA) was added. The RM was stirred at RT and monitored by TLC until completion. The RM was concentrated under vacuum to remove the solvent MeOH and yielded 6.22 g of a reddishbrown oil. Then the oil was dissolved in 100ml chloroform, added 10 ml acetic anhydride. The RM was stirred at RT for about 3 hrs until completion. The RM was washed with two 50 ml portions of saturated sodium bicarbonate solution followed by 50 ml brine. Dried the organic layer over anhydrous sodium chloride, concentrated under vacuum to remove the solvent completely. The resulting oil was taken in about 20 ml n-hexane. A spatula was used to scratch the inner walls

to induce crystallization. The solid was filtered, washed with n-hexane, and allowed to air dry to afford 4 as light yellow solid (2.78g, 49%). H NMR (400 MHz, Chloroform-d) δ 11.45 (s, 1H), 8.74 (d, 1H), 7.90 (d, 1H), 7.58 (t, 1H), 7.13 (t, 1H), 6.56 (d, 1H), 4.99 (t, 1zH), 3.77 (s, 3H), 3.83-3.66 (m, 2H), 2.24 (s, 3H), 2.04 (s, 3H). <sup>13</sup>C NMR (101 MHz, Chloroform-d) δ 201.94, 171.67, 169.88, 169.47, 141.36, 135.89, 130.94, 122.53, 120.86, 120.61, 52.83, 48.19, 41.78, 25.67, 23.19.  $N^{\alpha}$ , N-diacetyl-4-nitro-L-kynurenine methyl ester (5): Lithium nitrate (0.849 g, 12.31 mmol) and N,N-diacetyl-L-kynurenine methyl ester 4 (0.94 g, 3.07 mmol) was added to 5 mL trifluoroacetic acid, with stirring. Then, 1.36 mL H<sub>2</sub>SO<sub>4</sub> (24.48 mmol) was added, and the orange solution was stirred at room temperature. After 5 hours, TLC (EtOAc) showed that the reaction was complete. The reaction mixture was diluted with 50mL water and extracted with 20mL x3 ethyl acetate. The organic layers were combined and concentrated under reduced pressure. The residue was purified by column chromatography (hexane: ethyl acetate = 3:1 to 1:2) to give 5 as yellow solid (0.52 g, 48%). <sup>1</sup>H NMR (400 MHz, Chloroform-d)  $\delta$  11.74 (s, 1H), 9.00 (d, J = 9.3 Hz, 1H), 8.80 (d, J = 2.4 Hz, 1H), 8.41 (dd, J = 9.3, 2.5 Hz, 1H), 6.50 (d, J = 7.7 Hz, 1H), 5.02 (dd, J = 7.8, 4.1 Hz, 1H), 3.84 (dd, J = 10.6, 3.7 Hz, 2H), 3.79 (s, 3H), 2.31 (d, J = 1.6 Hz, 3H), 2.05 (s, 3H).MHz, Chloroform-d) δ 201.06, 171.30, 169.90, 169.78, 146.30, 141.47, 130.31, 126.68, 121.03, 119.72, 53.02, 48.20, 41.97, 25.81, 23.15.

Synthesis of 5-nitro-L-kynurenine(5-NKyn): 6M HCl (10mL) was added to Nα,N-diacetyl-4-nitro-L-kynurenine 5 (0.18 g, 0.512mmol) and refluxed overnight. The resulting solution was dried under reduced pressure. The residue was dissolved in 5 mL water and passed through a cation exchange column Dowex-50-X8 (H<sup>+</sup>), washed with water until the washings were colorless. The products were then eluted with 8 mL ammonium hydroxide. The orange filtrate was collected and dried under reduced pressure. The residue was triturated with acetone and the precipitates were

filtered to afford 4-nitro-L-kynurenine **6** as red-brown solid (18.3 mg, 15%).  $^{1}$ H NMR (400 MHz, Deuterium Oxide) 8.59 (s, 1H), 7.95 (d, J=8.0Hz, 1H), 6.69 (d, J=8.0 Hz, 1H), 3.62 (s, 1H).  $^{13}$ C NMR (101 MHz, Deuterium Oxide): 201.61, 181.87, 155.69, 135.30, 129.76, 129.33, 117.36, 115.29, 52.64. HRMS: m/z calcd for  $C_{10}H_{11}N_{3}O_{5}$  [M + H]+ 254.0771, found 254.0774.

#### 3.5 Conclusion

In conclusion, 5-NKyn functions as an uncoupler of KMO. The introduction of a nitro group on the aromatic ring prevents the formation of hydroxylated product by deceiving the ring. However, adding a nitro group greatly increases the binding affinity to the active site, owing to the hydrogen bond formation between nitro group and FAD and water molecule. We believe this 5-NKyn will offer us better insight into the development of more potent inhibitors of KMO.

#### **CHAPTER 4**

#### NITRATION OF DEACTIVATED AROMATIC COMPOUNDS USING LITHIUM NITRATE

#### 4.1 Introduction

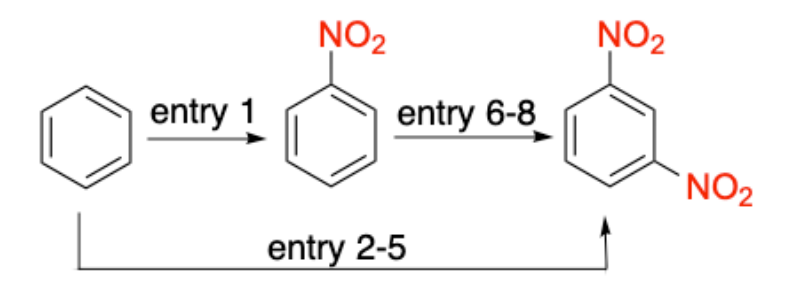
As crucial organic compounds and synthetic precursors, nitroarenes have played a significantly important role in dyes<sup>111</sup>, materials<sup>112</sup>, pesticides<sup>113</sup>, explosives<sup>114</sup>, and pharmaceuticals<sup>115</sup>. Electrophilic nitration is one of the most important chemical reactions in making nitro aromatic compounds<sup>116-118</sup>. Electrophilic nitration involving electron-rich or activated aromatic compounds is comparatively straightforward and feasible, facilitated by the presence of activated functional groups on the aromatics that enhance the attack on the nitronium ion. However, electrophilic nitration on deactivated aromatics continues to have significant challenges. The standard condition for nitration uses large amounts of strong mineral acids, such as nitric acid and sulfuric acid<sup>119, 120</sup>. This method is environmentally unfriendly and costly to manage. In addition, this traditional method has shown challenges for nitration of deactivated aromatic compounds, as well as functional group tolerance. Thus, different methods have been developed for nitration of deactivated aromatic compounds. For example, N-nitro-type reagents, dinitro-5,5-dimethylhydantoin<sup>121</sup>, N-nitropyrazole<sup>122</sup>, N-nitroimidazole<sup>123</sup>, Nsuch nitrosaccharin<sup>124</sup>, N-nitropyridinium salts<sup>125, 126</sup>, N-nitropyrrolidinones<sup>127</sup>, N-Nitrosuccinimide<sup>128</sup> and N-nitrophthalimide<sup>128</sup>, have been developed by different groups for electrophilic nitration. Mixtures of concentrated sulfuric acid and nitrates, such as guanidinium nitrate<sup>129</sup>, urea nitrate<sup>130</sup> 133, nitrourea<sup>130</sup>, nitroguanidine<sup>134</sup>, and nitrate ester<sup>134</sup>, are also reported to nitrate the deactivated aromatic compounds. In addition, nitrate salts, such as Bi(NO<sub>3</sub>)<sub>3</sub>·5H<sub>2</sub>O<sup>135</sup>, Ca(NO<sub>3</sub>)<sub>2</sub><sup>136</sup>,

Ni(NO<sub>3</sub>)<sub>3</sub>·9H<sub>2</sub>O<sup>137</sup>, NaNO<sub>3</sub><sup>138-141</sup>, Fe(NO<sub>3</sub>)<sub>3</sub>·9H<sub>2</sub>O<sup>142-144</sup>, Cu(NO<sub>3</sub>)<sub>2</sub><sup>145-148</sup>, *etc*, have been extensively used for electrophilic aromatic nitration. However, most of those nitration conditions have shown disappointing nitration capabilities, a limited range of applicable substrates, or poor functional group tolerance.

In this chapter, I will discuss our published novel nitration method utilizing LiNO<sub>3</sub> as the source of nitronium ion, in the presence of sulfuric acid and trifluoroacetic acid (TFA). This condition was first developed for the synthesis of 5-nitrokynurenine - an inhibitor of kynurenine monooxygenase (KMO), by nitration of  $N^{\alpha}$ ,  $N^3$ -diacetylkynurenine methyl ester. We found that the standard nitration conditions (98 % H<sub>2</sub>SO<sub>4</sub>/70 % HNO<sub>3</sub>, 1,1) gave recovered starting material in this reaction. Next, KNO<sub>3</sub> in H<sub>2</sub>SO<sub>4</sub> was employed as the nitronium ion source, but the reaction resulted in numerous byproducts and required purification by HPLC with low yield. We thought that the low reactivity of  $N^{\alpha}$ ,  $N^{3}$ -diacetylkynurenine methyl ester is due to protonation of the acetamido group of the substrate in the strongly acidic medium. Hence, we performed the reaction in a weaker acid, TFA, where the amount of TFA did not significantly affect reactivity or yield, using stoichiometric amounts of H<sub>2</sub>SO<sub>4</sub> to generate the nitronium ion. Acetic acid was also tested as a solvent for this reaction, but it failed, likely due to its basicity, which causes it to react with sulfuric acid, reducing the formation of the nitronium ion. Of the common nitrates tested, LiNO<sub>3</sub> gave the best results. LiNO<sub>3</sub> selectively yields only 3-nitrated and 5-nitrated products, with significant improvement in yield, reaching 72 % (Ma and Phillips, in preparation). We reported further investigations on this reaction, with the focus on the reactivity, functional group tolerance, regioselectivity, and position of substitutions.

#### 4.2 Optimization of reaction condition

The electrophilic nitration ability was evaluated and optimized using benzene with varying equivalents of LiNO<sub>3</sub> in sulfuric acid and TFA at either room temperature or heated (table 4.2.1). Initially, one equivalent of LiNO<sub>3</sub> was used. The reaction proceeded quickly and exothermically at room temperature, completing within 30 minutes (entry 1). Two equivalents of LiNO<sub>3</sub> were added, aiming to yield the 1,3-dinitrobenzene in one-pot (entry 2). However, after 24 hours, TLC showed only the presence of nitrobenzene. When the temperature was raised to 55°C for 24 hours (entry 3), TLC showed a mixture of nitrobenzene and 1,3-dinitrobenzene, with <sup>1</sup>H-NMR showing a majority of 1,3-dinitrobenzene (nitrobenzene: 1,3-dinitrobenzene = 1:1.2). Then, three equivalents of LiNO<sub>3</sub> were used with the same reaction temperature and time (entry 4). The reaction resulted in a similar mixture of nitrobenzene and 1,3-dinitrobenzene (with a ratio of 1: 1.5). Four equivalents of LiNO<sub>3</sub> were used to further optimize the nitration reactivity (entry 5). After 24 hrs, TLC indicated a mixture of nitrobenzene and 1,3-dinitrobenzene. However, upon heating to 90°C for 5 hours, TLC displayed only 1,3-dinitrobenzene. Subsequent trials using nitrobenzene as the starting material (entries 6-8) identified optimal conditions at 55°C with four equivalents of LiNO<sub>3</sub> (entry 8). This condition guarantees both a rapid reaction time and high yield. We have tried to use this condition to nitrate 1,3-dinitrobenzene to 1,3,5-trinitrobenzene, but no product was obtained after 3 days under reflex.



Scheme 4.2.1: nitration of benzene and nitrobenzene<sup>a</sup>.

Entry	Equivalents of	Temp	Time(h)	Yield of NB	Yield of DNB
	LiNO <sub>3</sub>			(%)	(%)
1	1	r.t	0.5	96	0
2	2	r.t	24	94	0
3	2	55 °C	24	27	33
4	3	55 °C	24	27	42
$5^b$	4	90 °C	29	0	83
6 °	1	55 °C	24	11	67
7 <sup>c</sup>	2	55 °C	8.5	0	92
8 c	4	55 °C	2.5	0	89

**Table 4.2.1:** screening of the reaction conditions<sup>a</sup>.

#### 4.3 Nitration of mono- and di-substituted aromatics

With the optimized conditions in hand, we began by examining the nitration of a series of monosubstituted aromatic compounds featuring electron-withdrawing groups (EWGs), including nitro, aldehyde, ester, cyano, carboxylic acid, ketone, halides, and trifluoromethyl. They are all well-tolerated under this condition. As expected for inductive effects, the nitro group was added on the *m*-position for arenes with EWGs (2-6,12), except for halobenzenes (9-11). In the case of benzaldehyde, the *o*-nitrated product was also isolated alongside the *m*-product in a 1:3 ratio (3). Nitration of toluene at room temperature produced a mixture of 2,4-dinitrotoluene and 2,6-

<sup>&</sup>lt;sup>a:</sup> conditions: benzene (5 mmol), conc. sulfuric acid (20 mmol), LiNO<sub>3</sub> (20mmol), and TFA (3 mL).

<sup>&</sup>lt;sup>b</sup>: first 24 hrs was done at 55 °C and then 5 hrs was done at 90 °C.

c: nitrobenzene (5 mmol) was used as the starting material.

dinitrotoluene in an 84% yield, with a ratio of 5:1 (7). Nitration of cinnamaldehyde gave the same yield of mixture of p- and o-nitrated products (8). The trifluoromethyl group remained stable under these conditions, resulting in 3-nitrobenzotrifluoride with a yield of 58% (12).

**Figure 4.3.1:** Nitration of mono-substituted aromatic compounds. Reaction conditions: **1-12** (5mmol), conc. LiNO<sub>3</sub> (20mmol) and sulfuric acid (20mmol) in TFA (4mL) at room temperature (**1,3-6,9,10,12**, 0°C for **7** and **8**, and 55°C for **2** and **11**) for overnight. Unless noted otherwise, the yields indicated are the isolated yields.

Disubstituted aromatic compounds were also evaluated. We first examined 1,4-disubstituted aromatic derivatives (13-23). *m*-Nitrated products were obtained for all derivatives, as expected. Notably, when there is a strong electron donating group, amino, the *o*-dinitrated product (16) was obtained at room temperature, and the reaction was complete in 15 minutes with 72% yield. A similar nitrated product was obtained for ethyl 4-aminobenzoate (19), with similar reaction time, but higher yield of 87% at room temperature. When both substituents are deactivating groups, heat is required (14-15, 23). For 4-hydroxybenzonitrile, mixtures of mono- and di-nitrated products were obtained in a ratio of 3 to 2 (18). However, when both substituents were strong deactivating groups, such as in methyl *p*-nitrobenzoate, no products were obtained. In the case of *p*-halobenzonitrile derivatives, no reaction occurred at room temperature; however, upon heating, the nitrile group was hydrolyzed to benzoic acid, yielding 4-halo-3-nitrobenzoic acid derivatives. A similar outcome was observed with 4-nitrobenzyl bromide, where the benzylic carbon was

oxidized to an aldehyde under heating, producing 2,4-dinitrobenzaldehyde. It appears that an electrophilic carbon is highly unstable under these conditions.

1,2-disubstituted aromatic compounds (24-31) were examined to investigate the regioselectivity of this reaction. *o*-Nitrobenzene (24-26) derivatives were tested. Products nitrated at the 3- and 5-position are obtained for all of them, with the 5-nitro product as the major product. When there is a strong electron-donating group (-OMe) at the *o*-position, the dinitration product was isolated (24). Arenes with complex functional groups were also well-tolerated in this condition with moderate yields (28-29). Symmetric aromatic compounds resulted in symmetrically dinitrated products (30-31).

**Figure 4.3.2: Nitration of di-substituted aromatic compounds.** Reaction conditions: **13-31** (5mmol), conc. LiNO<sub>3</sub> (20mmol) and sulfuric acid (20mmol) in TFA (4mL) at room temperature

(13,17,18,24,26-29, 0°C for 16,19-22,30,31, and 55°C for 14,15,23,25) for overnight. Unless noted otherwise, the yields indicated are the isolated yields.

#### 4.4 Nitration of heterocyclics

We then shifted our focus to the nitration of heterocyclic compounds, which are typically considered as highly challenging. Nitration of 2-chlorobenzothiazole gave a mixture of 5-, 6-, and 7- nitrated products in a 58% yield, with a ratio of 3:4:1 (32). 3,5-dimethylpyrazole was nitrated to give 4-nitro-3,5-dimethylpyrazole with 66% yield (33). Thiophene derivatives were examined (34-35). Nitration of thiophene gave mixture of 2-, 2,4-di, and 2,5-dinitro thiophene with total yield of 45%. Nitration of 3-bromothiphene gave only 3-bromo-2-nitrothiophene with good yield. Nitration of 1-methylimidazole gave a mixture of 4-nitro and 5-nitro products (36). This reaction was done under heating and completed after 2 days. We have observed limitations for some heterocyclics, such as 4-methylthiazole, indole, and imidazole. There was no reaction for 4-methylthiazole and imidazole. This could be attributed to the protonation of the heterocyclic compounds, which significantly deactivates the ring. Dimerization of indole occurred in acidic media to give unwanted products. 149

**Figure 4.4.1: Nitration of heteroarenes.** Reaction conditions: **32-36** (5mmol), conc. LiNO<sub>3</sub> (20mmol) and sulfuric acid (20mmol) in TFA (4mL) at 0°C (**32,34,35**, and 55°C for **33,36**) for overnight. Unless noted otherwise, the yields indicated are the isolated yields.

#### 4.5 Chemistry

General Experimental Procedure for Nitration of different substrates: Concentrated sulfuric acid (0.89mL, 20mmol, 4.0 equiv) was added dropwise to reaction mixture of arenes (5 mmol, 1.0 equiv) and LiNO<sub>3</sub> (1.1 gram, 20mmol, 4.0 equiv) in TFA (4mL) on ice bath. The reaction was slowly warmed to room temperature (or 55°C if needed). The reaction was monitored by TLC until completion. Then the reaction mixture was added to cold ice water and extracted with ethyl acetate (3 x 15mL). The combined organic layers were washed with brine and dried over sodium sulfate, filtered, and concentrated under reduced pressure. The crude product was purified by flash column chromatography on silica gel the give the pure nitrated product.

Me 
$$M(NO_3)_n$$
 (4 equiv)  $Me$   $M_2SO_4$  (4 equiv)  $O_2N$   $Me$   $O_2N$   $Me$   $NO_2$   $Me$   $NO_2$   $Me$   $NO_2$   $Me$   $NO_2$   $Me$   $NO_2$   $NO_2$ 

Nitrate salts	Total yield(%)	Ratio of 26a:26b
LiNO <sub>3</sub>	96	1.7:1
NaNO <sub>3</sub>	86	2.4:1
KNO <sub>3</sub>	51 <sup>a</sup>	2.4:1
Fe(NO <sub>3</sub> ) <sub>3</sub> ·9H <sub>2</sub> O	40 <sup>a</sup>	1.9:1
(NH <sub>4</sub> ) <sub>2</sub> Ce(NO <sub>3</sub> ) <sub>6</sub>	84	2.7:1
Bi(NO <sub>3</sub> ) <sub>3</sub> ·5H <sub>2</sub> O	84	2.7:1
Ca(NO <sub>3</sub> ) <sub>2</sub> ·4H <sub>2</sub> O	59 <sup>a</sup>	2.4:1
Cu(NO <sub>3</sub> ) <sub>2</sub> ·2.5H <sub>2</sub> O	92	2.5:1

Table 4.5.1 Screening of the reactivity and regioselectivity of different nitrate salts with 2-nitrotoluene.

<sup>a</sup>: reaction did not go to completion in 3 hours.

### Nitrobenzene (1):150

room temperature (r.t), 96%, colorless oil.  $^{1}$ H NMR (400 MHz, CDCl<sub>3</sub>)  $\delta$  8.23 (d, J = 8.0 Hz, 1H), 7.71 (t, J = 7.5 Hz, 1H), 7.55 (t, J = 7.9 Hz, 1H).  $^{13}$ C NMR (101 MHz, CDCl<sub>3</sub>)  $\delta$  148.23, 134.59, 129.32, 123.49.

### 3-dinitrobenzene (2):151

55°C. 89%, white solid, m.p.= 84-88°C.  $^{1}$ H NMR (400 MHz, CDCl<sub>3</sub>)  $\delta$  9.09 (t, J = 2.1 Hz, 1H), 8.59 (dd, J = 8.2, 2.1 Hz, 2H), 7.83 (t, J = 8.2 Hz, 1H).  $^{13}$ C NMR (101 MHz, CDCl<sub>3</sub>)  $\delta$  119.11, 128.90, 130.75, 148.57.

## 3-nitrobenzaldehyde (3a): 142

r.t, 54%, light yellow solid. m.p.= 54-58°C.  $^{1}$ H NMR (400 MHz, CDCl<sub>3</sub>)  $\delta$  10.13 (s, 1H), 8.73 (s, 1H), 8.50 (d, J = 8.2 Hz, 1H), 8.24 (d, J = 7.6 Hz, 1H), 7.78 (t, J = 7.9 Hz, 1H).  $^{13}$ C NMR (101 MHz,)  $\delta$  189.67, 148.85, 137.45, 134.59, 130.37, 128.57, 124.48.

# 2-nitrobenzaldehyde (3b): 142

r.t, 17%, white solid. m.p.=  $43-45^{\circ}$ C  $^{1}$ H NMR (400 MHz, CDCl<sub>3</sub>)  $\delta$  10.43 (s, 1H), 8.13 (d, J = 7.3 Hz, 1H), 7.96 (d, J = 7.3 Hz, 1H), 7.89 – 7.66 (m, 2H).  $^{13}$ C NMR (101 MHz, CDCl<sub>3</sub>)  $\delta$  188.07, 149.62, 134.04, 133.68, 131.37, 129.62, 124.48.

## Methyl 3-nitrobenoate (4): 152

r.t, 58%, white solid, m.p.= 75-78°C <sup>1</sup>H NMR (400 MHz, CDCl<sub>3</sub>)  $\delta$  8.85 (s, 1H), 8.42 (d, J = 8.1 Hz, 0H), 8.37 (d, J = 7.7 Hz, 1H), 7.68 (t, J = 8.0 Hz, 1H), 4.00 (s, 3H). <sup>13</sup>C NMR (101 MHz, CDCl<sub>3</sub>)  $\delta$  164.91, 148.25, 135.24, 131.84, 129.65, 127.35, 124.54, 52.77.

### 3-nitrobenzonitrile (5):152

r.t, 92%, white solid, m.p.= 115-117°C  $^{1}$ H NMR (400 MHz, CDCl<sub>3</sub>)  $\delta$  8.55 (s, 1H), 8.49 (d, J = 8.4 Hz, 1H), 8.02 (d, J = 7.7 Hz, 1H), 7.76 (t, J = 8.1 Hz, 1H).  $^{13}$ C NMR (101 MHz, CDCl<sub>3</sub>)  $\delta$  148.25, 137.63, 130.70, 127.56, 127.25, 116.55, 114.15.

## 3-nitrobenzoic acid (6):142

r.t, 73%, white solid. m.p.= 129-132°C  $^{1}$ H NMR (400 MHz, CDCl<sub>3</sub>)  $\delta$  8.97 (t, J = 1.9 Hz, 1H), 8.58 – 8.41 (m, 2H), 7.73 (t, J = 8.0 Hz, 1H).  $^{13}$ C NMR (101 MHz, CDCl<sub>3</sub>)  $\delta$  169.72, 148.43, 135.80, 130.90, 129.91, 128.37, 125.30.

### **2,4-dinitrotoluene** (7a and 26a): 152

Ice-bath (0°C) to r.t, 70%, white solid. m.p.= 69-73°C. <sup>1</sup>H NMR (400 MHz, CDCl<sub>3</sub>)  $\delta$  8.83 (d, J = 2.4 Hz, 1H), 8.36 (dd, J = 8.5, 2.4 Hz, 1H), 7.59 (d, J = 8.4 Hz, 1H), 2.74 (s, 3H). <sup>13</sup>C NMR (101 MHz, CDCl<sub>3</sub>)  $\delta$  149.07, 146.43, 140.73, 134.02, 127.01, 120.25, 20.73.

### trans-4-Nitrocinnamaldehyde (8a):153

Ice-bath (0°C), 48%, pale yellow solid. m.p.= 148-151°C.  $^{1}$ H NMR (400 MHz, )  $\delta$  9.77 (d, J = 2.8 Hz, 1H), 8.30 (d, J = 8.8 Hz, 2H), 7.74 (d, J = 8.8 Hz, 2H), 7.53 (d, J = 16.0 Hz, 1H), 6.82 (dd, J = 16.1, 7.4 Hz, 1H).  $^{13}$ C NMR (101 MHz, )  $\delta$  192.77, 149.05, 148.78, 139.94, 131.74, 129.07, 124.33.

#### trans-2-Nitrocinnamaldehyde (8b): 153

Ice-bath (0°C), 47%, pale yellow solid. m.p.= 124-128°C <sup>1</sup>H NMR (400 MHz, CDCl<sub>3</sub>)  $\delta$  9.79 (d, J = 7.6 Hz, 1H), 8.18 - 7.97 (m, 2H), 7.80 - 7.55 (m, 3H), 6.64 (dd, J = 15.8, 7.6 Hz, 1H). <sup>13</sup>C NMR (101 MHz, CDCl<sub>3</sub>)  $\delta$  193.00, 148.11, 147.15, 133.76, 132.70, 131.10, 130.05, 129.06, 125.21.

### **4-fluoro-nitrobenzene** (9): <sup>150</sup>

F NO<sub>2</sub>

r.t, 66%, light yellow oil. <sup>1</sup>H NMR (400 MHz, CDCl<sub>3</sub>)  $\delta$  8.28 (dd, J = 9.2, 4.6 Hz, 2H), 7.22 (dd, J = 9.3, 7.7 Hz, 2H). <sup>13</sup>C NMR (101 MHz, CDCl<sub>3</sub>)  $\delta$  167.55, 144.44, 126.35, 116.51.

4-chloro-nitrobenzene (10a): 150

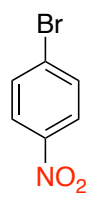


r.t, 72%, pale yellow solid. m.p.=84-86°C . <sup>1</sup>H NMR (400 MHz, CDCl<sub>3</sub>)  $\delta$  8.19 (d, J = 9.0 Hz, 1H), 7.52 (d, J = 9.0 Hz, 1H). <sup>13</sup>C NMR (101 MHz, CDCl<sub>3</sub>)  $\delta$  146.58, 141.38, 129.58, 124.93.

2-chloro-nitrobenzene (10b): 150

r.t, 10%, pale yellow solid. m.p.=34-35°C.  $^{1}$ H NMR (400 MHz, CDCl<sub>3</sub>)  $\delta$  7.87 (dd, J = 8.1, 1.6 Hz, 1H), 7.62 – 7.49 (m, 2H), 7.42 (ddd, J = 8.1, 7.0, 1.8 Hz, 1H).  $^{13}$ C NMR (101 MHz, CDCl<sub>3</sub>)  $\delta$  148.12, 133.14, 131.90, 127.58, 127.09, 125.56.

**4-bromo-nitrobenzene** (11):  $^{150}$ 



55°C, 63%, pale yellow solid. m.p.=126-130°C.  $^{1}$ H NMR (400 MHz, CDCl<sub>3</sub>)  $\delta$  8.11 (d, J = 9.0 Hz, 1H), 7.69 (d, J = 9.0 Hz, 1H).  $^{13}$ C NMR (101 MHz, CDCl<sub>3</sub>)  $\delta$  147.08, 132.63, 129.96, 125.01.

# 3-nitrobenzotrifluoride (12): 150

r.t, 58%, yellow oil.  $^{1}$ H NMR (400 MHz, CDCl<sub>3</sub>)  $\delta$  8.52 (s, 1H), 8.45 (d, J = 8.2 Hz, 1H), 7.98 (d, J = 7.8 Hz, 1H), 7.74 (t, J = 8.1 Hz, 1H).  $^{13}$ C NMR (101 MHz, CDCl<sub>3</sub>)  $\delta$  148.35, 132.23, 131.13, 130.31, 126.65, 121.49, 120.90.

### **2,4-dinitrophenol** (13): 154

r.t, 63%, pale yellow solid. m.p.=120-124°C.  $^{1}$ H NMR (400 MHz, CDCl<sub>3</sub>)  $\delta$  11.03 (s, 1H), 9.08 (d, J = 2.7 Hz, 1H), 8.47 (dd, J = 9.3, 2.7 Hz, 1H), 7.34 (d, J = 9.2 Hz, 1H).  $^{13}$ C NMR (101 MHz, CDCl<sub>3</sub>)  $\delta$  159.07, 140.34, 132.64, 131.65, 121.91, 121.26.

## 4-fluoro-1,3-dinitrobenzene (14): 155

55°C, 72%, pale yellow oil.  $^{1}$ H NMR (400 MHz, CDCl<sub>3</sub>)  $\delta$  8.99 (dd, J = 6.4, 2.7 Hz, 1H), 8.56 (dt, J = 9.2, 3.2 Hz, 1H), 7.55 (t, J = 9.3 Hz, 1H).  $^{13}$ C NMR (101 MHz, CDCl<sub>3</sub>)  $\delta$  160.13, 157.39, 143.69, 130.34, 122.51, 120.06.

## **4-chloro-1,3-dinitrobenzene** (**15**): <sup>152</sup>

55°C, 85%, light yellow solid. m.p.=48-50°C.  $^{1}$ H NMR (400 MHz, CDCl<sub>3</sub>)  $\delta$  8.76 (d, J = 2.6 Hz, 1H), 8.40 (dd, J = 8.8, 2.6 Hz, 1H), 7.80 (d, J = 8.8 Hz, 1H).  $^{13}$ C NMR (101 MHz, CDCl<sub>3</sub>)  $\delta$  121.14, 127.29, 133.23, 133.98, 146.34, 147.83.

## **2,4,6-trinitroaniline** (**16**): <sup>156</sup>

0°C to r.t, 72%, brown solid. m.p.=200-205°C.  $^{1}$ H NMR (400 MHz, DMSO) δ 9.05 (s, 2H), 8.98 (s, 2H).  $^{13}$ C NMR (101 MHz, DMSO) δ 144.02, 134.71, 133.07, 128.51.

### 4-isopropyl-3-nitrobenzonitrile (17):

r.t, 67%, yellow solid.  $^{1}$ H NMR (400 MHz, CDCl<sub>3</sub>)  $\delta$  8.00 (s, 1H), 7.81 (d, J = 7.9 Hz, 1H), 7.63 (d, J = 8.4 Hz, 1H), 3.45 (p, J = 6.4 Hz, 1H), 1.32 (d, J = 6.8 Hz, 6H).  $^{13}$ C NMR (101 MHz, CDCl<sub>3</sub>)  $\delta$  149.77, 147.84, 135.35, 129.07, 127.51, 116.65, 111.08, 29.07, 23.25.

## 4-Cyano-2-nitrophenol (18): $^{154}$

r.t, , 51%, orange solid.  $^{1}$ H NMR (400 MHz, )  $\delta$  10.90 (s, 1H), 8.48 (d, J = 2.1 Hz, 1H), 7.83 (dd, J = 8.7, 2.1 Hz, 1H), 7.30 (d, J = 8.8 Hz, 1H).  $^{13}$ C NMR (101 MHz, )  $\delta$  157.81, 139.55, 134.37, 130.11, 121.77, 116.58, 104.57.

#### Ethyl 4-amino-3,5-dinitrobenzoate (19):

0°C to r.t, 87%, orange solid.  $^{1}$ H NMR (400 MHz, CDCl<sub>3</sub>) δ 9.15 (s, 2H), 8.80 (s, 2H), 4.43 (q, J = 7.1 Hz, 2H), 1.43 (t, J = 7.1 Hz, 3H).  $^{13}$ C NMR (101 MHz, CDCl<sub>3</sub>) δ 163.20, 143.54, 134.76, 134.71, 116.70, 62.08, 14.33.

#### 4-Methoxy-3-nitrobenzoic acid (20): 157

Ice-bath (0°C) to r.t, 88%, white solid. m.p.=198-200°C. <sup>1</sup>H NMR (400 MHz, CDCl<sub>3</sub>)  $\delta$  8.57 (d, J = 2.2 Hz, 1H), 8.28 (dd, J = 8.8, 2.2 Hz, 1H), 7.17 (d, J = 8.9 Hz, 1H), 4.05 (s, 3H). <sup>13</sup>C NMR (101 MHz, CDCl<sub>3</sub>)  $\delta$  168.56, 156.68, 139.54, 135.82, 127.89, 121.71, 113.25, 56.93.

## 4-(dimethylamino)-3-nitrobenzaldehyde (21):158

Ice-bath (0°C) to r.t, 80%, white solid. m.p.=101-103°C. <sup>1</sup>H NMR (400 MHz, CDCl<sub>3</sub>)  $\delta$  9.80 (s, 1H), 8.25 (d, J = 2.0 Hz, 1H), 7.89 (dd, J = 8.9, 2.0 Hz, 1H), 7.06 (d, J = 8.9 Hz, 1H), 3.04 (s, 6H). <sup>13</sup>C NMR (101 MHz, CDCl<sub>3</sub>)  $\delta$  188.67, 149.37, 137.17, 132.33, 130.89, 125.47, 117.31, 42.25.

#### 4-Methoxy-3-nitrobenzaldehyde (22):157

Ice-bath (0°C) to r.t, 82%, white solid. m.p.=105-108°C <sup>1</sup>H NMR (400 MHz, CDCl<sub>3</sub>)  $\delta$  9.94 (s, 1H), 8.35 (t, J = 1.5 Hz, 1H), 8.10 (dd, J = 8.7, 2.1 Hz, 1H), 7.24 (s, 1H), 4.07 (s, 3H). <sup>13</sup>C NMR (101 MHz, CDCl<sub>3</sub>)  $\delta$  188.72, 157.16, 139.96, 134.68, 129.11, 127.39, 113.84, 57.07.

### 4-chloro-3-nitrobenzaldehyde (23): 159

55°C, 72%, white solid. m.p.=57-60°C <sup>1</sup>H NMR (400 MHz, CDCl<sub>3</sub>)  $\delta$  10.05 (s, 1H), 8.37 (d, J = 1.9 Hz, 1H), 8.04 (dd, J = 8.2, 1.9 Hz, 1H), 7.76 (d, J = 8.3 Hz, 1H). <sup>13</sup>C NMR (101 MHz, CDCl<sub>3</sub>)  $\delta$  188.39, 148.59, 135.48, 133.10, 133.01, 132.70, 126.33.

### **2,4-dinitroanisole** (**24a**):<sup>122</sup>

$$O_2$$
N

r.t, 46%, white solid. m.p.=89-93°C.  $^{1}$ H NMR (400 MHz, CDCl<sub>3</sub>)  $\delta$  8.76 (d, J = 2.7 Hz, 1H), 8.46 (dd, J = 9.2, 2.6 Hz, 1H), 7.23 (s, 1H), 4.11 (s, 3H).  $^{13}$ C NMR (101 MHz, CDCl<sub>3</sub>)  $\delta$  157.32, 140.19, 138.89, 129.17, 121.94, 113.63, 57.50.

# **2,4,6-trinitroanisole** (**24b**):<sup>160</sup>

r.t, 32%, pale yellow solid. m.p.=73-75. °C ¹H NMR (400 MHz, CDCl<sub>3</sub>) δ 8.89 (s, 2H), 4.18 (s, 3H). ¹³C NMR (101 MHz, CDCl<sub>3</sub>) δ 152.12, 144.76, 141.46, 124.16, 65.36.

### 2,4-dinitrochlorobenzene (25a):152

55°C, 72%, yellow solid. m.p.=55-58. °C 1H NMR (400 MHz, DMSO)  $\delta$  8.91 (d, J = 2.1 Hz, 1H), 8.51 (dd, J = 8.9, 2.2 Hz, 1H), 8.09 (d, J = 8.8 Hz, 1H). <sup>13</sup>C NMR (101 MHz, DMSO)  $\delta$  147.93, 146.80, 133.59, 132.18, 128.47, 121.48.

# 2,6-dinitrochlorbenzene (25b):152

55°C, 13%, pale yellow solid. m.p.=89-90°C. 1H NMR (400 MHz, DMSO)  $\delta$  8.40 (d, J = 8.2 Hz, 2H), 7.87 (t, J = 8.2 Hz, 1H). <sup>13</sup>C NMR (101 MHz, DMSO)  $\delta$  149.35, 130.40, 129.24, 118.70.

# 2,6-dinitrotoluene (26b):161

r.t, 80%, white solid. m.p.=58-60°C.  $^{1}$ H NMR (400 MHz, CDCl<sub>3</sub>)  $\delta$  8.34 (s, 1H), 8.09 (d, J = 8.9 Hz, 1H), 7.65 (d, J = 8.7 Hz, 1H).  $^{13}$ C NMR (101 MHz, CDCl<sub>3</sub>)  $\delta$  146.71, 139.87, 133.94, 131.09, 125.62, 122.58.

## 4-nitro-1,2-dichlorobenzne (27):150

r.t, 80%, white solid. m.p.=46-47°C.  $^{1}$ H NMR (400 MHz, CDCl<sub>3</sub>)  $\delta$  8.34 (s, 1H), 8.09 (d, J = 8.9 Hz, 1H), 7.65 (d, J = 8.7 Hz, 1H).  $^{13}$ C NMR (101 MHz, CDCl<sub>3</sub>)  $\delta$  146.71, 139.87, 133.94, 131.09, 125.62, 122.58.

#### N-(2-acetyl-4-nitrophenyl) acetamide (28):

r.t, 57%, light yellow solid.  $^{1}$ H NMR (400 MHz, CDCl<sub>3</sub>)  $\delta$  12.01 (s, 1H), 8.98 (d, J = 9.4 Hz, 1H), 8.81 (d, J = 2.6 Hz, 1H), 8.40 (dd, J = 9.4, 2.6 Hz, 1H), 2.78 (s, 3H), 2.30 (s, 3H).  $^{13}$ C NMR (101 MHz, CDCl<sub>3</sub>)  $\delta$  201.65, 170.02, 146.09, 141.45, 134.25, 129.84, 127.32, 120.90, 28.67, 25.69.

#### Methyl (S)-2-acetamido-4-(2-acetamido-5-nitrophenyl)-4-oxobutanoate (29):

r.t, 48%, yellow solid. m.p.=152-155°C.  $^{1}$ H NMR (600 MHz, CDCl<sub>3</sub>)  $\delta$  11.77 (s, 1H), 9.00 (d, J = 9.4 Hz, 1H), 8.80 (d, J = 2.6 Hz, 1H), 8.41 (dd, J = 9.3, 2.6 Hz, 1H), 6.53 (d, J = 7.6 Hz, 1H), 5.09 – 4.89 (m, 1H), 3.93 – 3.76 (m, 5H), 2.31 (s, 3H), 2.06 (s, 3H).  $^{13}$ C NMR (101 MHz, CDCl<sub>3</sub>)  $\delta$  201.06, 171.30, 169.90, 169.78, 146.30, 141.47, 130.31, 126.68, 121.03, 119.72, 53.02, 48.20, 41.97, 25.81, 23.15.

### 2,7-dinitro-9-fluorenone (30):

$$O_2N$$
  $NO_2$ 

0°C, 92%, yellow solid. <sup>1</sup>H NMR (400 MHz, DMSO) δ 8.60 (dd, J = 8.2, 2.2 Hz, 1H), 8.38 – 8.28 (m, 2H). <sup>13</sup>C NMR (101 MHz, DMSO) δ 188.96, 149.78, 147.66, 135.81, 131.31, 124.49, 119.42.

#### 2,7-Dinitro-9H-xanthen-9-one (31):

$$O_2N$$
  $O_2$   $NO_2$ 

 $0^{\circ}$ C, 93%, white solid.  $^{1}$ H NMR (400 MHz, CDCl<sub>3</sub>)  $\delta$  9.24 (d, J = 2.6 Hz, 1H), 8.65 (dd, J = 9.2, 2.8 Hz, 1H), 7.74 (d, J = 9.4 Hz, 1H).  $^{13}$ C NMR (101 MHz, CDCl<sub>3</sub>)  $\delta$  174.38, 158.73, 144.75, 130.05, 123.65, 121.42, 120.02.

#### 2-chloro-6-nitrobenzothiazole (32a):<sup>162</sup>

0°C, 1.34g, 93%, white solid. <sup>1</sup>H NMR (400 MHz, CDCl<sub>3</sub>) δ 8.75 (d, J = 2.3 Hz, 1H), 8.38 (dd, J = 9.0, 2.3 Hz, 1H), 8.07 (d, J = 9.0 Hz, 1H). <sup>13</sup>C NMR (101 MHz, CDCl<sub>3</sub>) δ 158.75, 154.78, 145.48, 136.48, 123.36, 122.24, 117.66.

## **2-chloro-5-nitrobenzothiazole** (32b):<sup>162</sup>

$$O_2N$$
  $N$   $C$ 

0°C, 1.34g, 93%, white solid. <sup>1</sup>H NMR (400 MHz, CDCl<sub>3</sub>)  $\delta$  8.81 (d, J = 2.2 Hz, 1H), 8.32 (dd, J = 8.8, 2.2 Hz, 1H), 7.95 (d, J = 8.9 Hz, 1H). <sup>13</sup>C NMR (101 MHz, CDCl<sub>3</sub>)  $\delta$  156.78, 150.87, 142.49, 123.36, 121.70, 120.35, 118.41.

### 3,5-dimethyl-4-nitropyrazole (33):163

55°C, 1.34g, 93%, white solid. m.p.=120-124°C. <sup>1</sup>H NMR (400 MHz, CDCl<sub>3</sub>) δ 10.05 (s, 1H), 2.61 (s, 6H). <sup>13</sup>C NMR (101 MHz, CDCl<sub>3</sub>) δ 144.46, 131.16, 13.11.

### 3-bromo-2-nitrothiophene (34):163

0°C, 1.34g, 93%, white solid. m.p.=80-82°C. <sup>1</sup>H NMR (400 MHz, CDCl<sub>3</sub>)  $\delta$  7.50 (d, J = 5.6 Hz, 1H), 7.12 (d, J = 5.7 Hz, 1H). <sup>13</sup>C NMR (101 MHz, CDCl<sub>3</sub>)  $\delta$  146.72, 132.64, 130.75, 112.98.

## **2-nitrothiophene** (35a):<sup>163</sup>

$$NO_2$$

0°C, 1.34g, 93%, white solid. m.p.=42-43°C. <sup>1</sup>H NMR (400 MHz, CDCl<sub>3</sub>) δ 7.93 (dd, J = 4.1, 1.6 Hz, 1H), 7.55 (dd, J = 5.4, 1.6 Hz, 1H), 7.07 (dd, J = 5.3, 4.1 Hz, 1H). <sup>13</sup>C NMR (101 MHz, CDCl<sub>3</sub>) δ 152.69, 132.41, 128.50, 126.95.

## 2,4-dinitrothiophene (35b):164

$$O_2N$$
 $S$ 
 $NO_2$ 

0°C, 1.34g, 93%, white solid. m.p.=56-58°C. <sup>1</sup>H NMR (400 MHz, CDCl<sub>3</sub>)  $\delta$  8.45 (d, J = 2.0 Hz, 1H), 8.41 (d, J = 2.0 Hz, 1H). <sup>13</sup>C NMR (101 MHz, CDCl<sub>3</sub>)  $\delta$  146.52, 130.65, 122.36.

#### 1-methyl-5-nitroimidazole (36a):<sup>163</sup>

55°C, 1.34g, 93%, white solid. m.p.=58-59°C. <sup>1</sup>H NMR (400 MHz, CDCl<sub>3</sub>) δ 8.02 (s, 1H), 7.70 (s, 1H), 4.04 (s, 3H). <sup>13</sup>C NMR (101 MHz, CDCl<sub>3</sub>) δ 141.08, 139.04, 131.64, 35.46.

### 1-methyl-4-nitroimidazole (36b):<sup>163</sup>

55°C, 1.34g, 93%, white solid. m.p.=133-135°C. <sup>1</sup>H NMR (400 MHz, CDCl<sub>3</sub>)  $\delta$  7.76 (d, J = 1.6 Hz, 1H), 7.42 (d, J = 1.5 Hz, 1H), 3.82 (s, 3H). <sup>13</sup>C NMR (101 MHz, CDCl<sub>3</sub>)  $\delta$  148.24, 136.62, 120.09, 34.58.

#### 4.6 Conclusion

In summary, we explored the electrophilic nitration of various substituted aromatic compounds and heterocyclic compounds employing lithium nitrate in the presence of sulfuric acid and trifluoroacetic acid. We believe that the reaction does not proceed with TFA or sulfuric acid alone for deactivated compounds but may be effective for activated compounds. Additionally, for weakly basic compounds such as kynurenine, sulfuric acid presents challenges as it induces strong deactivation, requiring more severe reaction conditions that may result in decomposition and side product formation. This method demonstrated exceptional capability in nitration of deactivated

arenes, high rate of reactivity, great functional group tolerance, and moderate to high yield, which distinguish this method for nitration of highly deactivated aromatic and heterocyclic compounds.

#### REFERENCE

- (1) Phillips, R. S.; Iradukunda, E. C.; Hughes, T.; Bowen, J. P. Modulation of Enzyme Activity in the Kynurenine Pathway by Kynurenine Monooxygenase Inhibition. *Front Mol Biosci* **2019**, *6*.
- (2) Vécsei, L.; Szalárdy, L.; Fülöp, F.; Toldi, J. Kynurenines in the CNS: recent advances and new questions. *Nat Rev Drug Discov* **2013**, *12* (1), 64-82.
- (3) Chen, Y. Q.; Guillemin, G. J. Kynurenine Pathway Metabolites in Humans: Disease and Healthy States. *Int J Tryptophan Res* **2009**, *2*, 1-19.
- (4) Botting, N. P. Chemistry and neurochemistry of the kynurenine pathway of tryptophan metabolism. *Chem Soc Rev* **1995**, *24* (6), 401-&.
- (5) Dounay, A. B.; Tuttle, J. B.; Verhoestt, P. R. Challenges and Opportunities in the Discovery of New Therapeutics Targeting the Kynurenine Pathway. *J Med Chem* **2015**, *58* (22), 8762-8782.
- (6) Batabyal, D.; Yeh, S. R. Human tryptophan dioxygenase: A comparison to indoleamine 2,3-dioxygenase. *J Am Chem Soc* **2007**, *129* (50), 15690-15701.
- (7) Ball, H. J.; Sanchez-Perez, A.; Weiser, S.; Austin, C. J. D.; Astelbauer, F.; Miu, J.; McQuillan, J. A.; Stocker, R.; Jermiin, L. S.; Hunt, N. H. Characterization of an indoleamine 2,3-dioxygenase-like protein found in humans and mice. *Gene* **2007**, *396* (1), 203-213.
- (8) Wogulis, M.; Chew, E. R.; Donohoue, P. D.; Wilson, D. K. Identification of formyl kynurenine formamidase and kynurenine aminotransferase from using crystallographic, Bioinformatic and biochemical evidence. *Biochemistry-Us* **2008**, *47* (6), 1608-1621.
- (9) Hughes, T. D.; Guner, O. F.; Iradukunda, E. C.; Phillips, R. S.; Bowen, J. P. The Kynurenine Pathway and Kynurenine 3-Monooxygenase Inhibitors. *Molecules* **2022**, *27* (1).
- (10) Phillips, R. S. Structure and mechanism of kynureninase. *Arch Biochem Biophys* **2014**, *544*, 69-74.

- (11) Han, Q.; Cai, T.; Tagle, D. A.; Li, J. Y. Structure, expression, and function of kynurenine aminotransferases in human and rodent brains. *Cell Mol Life Sci* **2010**, *67* (3), 353-368.
- (12) Brkic, H.; Kovacevic, B.; Tomic, S. Human 3-hydroxyanthranilate 3,4-dioxygenase (3HAO) dynamics and reaction, a multilevel computational study. *Mol Biosyst* **2015**, *11* (3), 898-907.
- (13) Liu, H.; Woznica, K.; Catton, G.; Crawford, A.; Botting, N.; Naismith, J. H. Structural and kinetic characterization of quinolinate phosphoribosyltransferase (hQPRTase) from. *J Mol Biol* **2007**, *373* (3), 755-763.
- (14) Schwarcz, R.; Stone, T. W. The kynurenine pathway and the brain: Challenges, controversies and promises. *Neuropharmacology* **2017**, *112*, 237-247.
- (15) Moroni, F.; Cozzi, A.; Sili, M.; Mannaioni, G. Kynurenic acid: a metabolite with multiple actions and multiple targets in brain and periphery. *J Neural Transm* **2012**, *119* (2), 133-139.
- (16) Guillemin, G. J. Quinolinic acid, the inescapable neurotoxin. *Febs J* **2012**, *279* (8), 1356-1365.
- (17) Leipnitz, G.; Schumacher, C.; Dalcin, K. B.; Scussiato, K.; Solano, A.; Funchal, C.; Dutra-Filho, C. S.; Wyse, A. T. S.; Wannmacher, C. M. D.; Latini, A.; Wajner, M. evidence for an antioxidant role of 3-hydroxykynurenine and 3-hydroxyanthranilic acid in the brain. *Neurochem Int* **2007**, *50* (1), 83-94.
- (18) Garrison, A. M.; Parrott, J. M.; Tuñon, A.; Delgado, J.; Redus, L.; O'Connor, J. C. Kynurenine pathway metabolic balance influences microglia activity: Targeting kynurenine monooxygenase to dampen neuroinflammation. *Psychoneuroendocrino* **2018**, *94*, 1-10.
- (19) Maddison, D. C.; Giorgini, F. The kynurenine pathway and neurodegenerative disease. *Semin Cell Dev Biol* **2015**, *40*, 134-141.

- (20) Goldstein, L. E.; Leopold, M. C.; Huang, X. D.; Atwood, C. S.; Saunders, A. J.; Hartshorn, M.; Lim, J. T.; Faget, K. Y.; Muffat, J. A.; Scarpa, R. C.; et al. 3-Hydroxykynurenine and 3-hydroxyanthranilic acid generate hydrogen peroxide and promote α-crystallin cross-linking by metal ion reduction. *Biochemistry-Us* **2000**, *39* (24), 7266-7275.
- (21) Stone, T. W.; Perkins, M. N. Quinolinic Acid a Potent Endogenous Excitant at Amino-Acid Receptors in Cns. *Eur J Pharmacol* **1981**, *72* (4), 411-412.
- (22) Gulaj, E.; Pawlak, K.; Bien, B.; Pawlak, D. Kynurenine and its metabolites in Alzheimer's disease patients. *Adv Med Sci-Poland* **2010**, *55* (2), 204-211.
- (23) Widner, B.; Leblhuber, F.; Walli, J.; Tilz, G. P.; Demel, U.; Fuchs, D. Tryptophan degradation and immune activation in Alzheimer's disease. *J Neural Transm* **2000**, *107* (3), 343-353.
- (24) Guillemin, G. J.; Williams, K. R.; Smith, D. G.; Smythe, G. A.; Croitoru-Lamoury, J.; Brew, B. J. Quinolinic acid in the pathogenesis of Alzheimer's disease. *Developments in Tryptophan and Serotonin Metabolism* **2003**, *527*, 167-176.
- (25) Guillemin, G. J.; Brew, B. J. Implications of the kynurenine pathway and quinolinic acid in Alzheimer's disease. *Redox Report* **2002**, *7* (4), 199-206.
- (26) Finkbeiner, S. Huntington's Disease. Csh Perspect Biol 2011, 3 (6).
- (27) Walker, F. O. Huntington's disease. Semin Neurol 2007, 27 (2), 143-150.
- (28) McColgan, P.; Tabrizi, S. J. Huntington's disease: a clinical review. *Eur J Neurol* **2018**, *25* (1), 24-34.
- (29) Guidetti, P.; Luthi-Carter, R. E.; Augood, S. J.; Schwarcz, R. Neostriatal and cortical quinolinate levels are increased in early grade Huntington's disease. *Neurobiol Dis* **2004**, *17* (3), 455-461.

- (30) Campesan, S.; Green, E. W.; Breda, C.; Sathyasaikumar, K. V.; Muchowski, P. J.; Schwarcz, R.; Kyriacou, C. P.; Giorgini, F. The Kynurenine Pathway Modulates Neurodegeneration in a Model of Huntington's Disease. *Curr Biol* **2011**, *21* (11), 961-966.
- (31) Jauch, D.; Urbanska, E. M.; Guidetti, P.; Bird, E. D.; Vonsattel, J. P. G.; Whetsell, W. O.; Schwarcz, R. Dysfunction of Brain Kynurenic Acid Metabolism in Huntingtons-Disease Focus on Kynurenine Aminotransferases. *J Neurol Sci* **1995**, *130* (1), 39-47.
- (32) Heyes, M. P.; Saito, K.; Crowley, J. S.; Davis, L. E.; Demitrack, M. A.; Der, M.; Dilling, L. A.; Elia, J.; Kruesi, M. J. P.; Lackner, A.; et al. Quinolinic Acid and Kynurenine Pathway Metabolism in Inflammatory and Noninflammatory Neurological Disease. *Brain* **1992**, *115*, 1249-1273.
- (33) Sathyasaikumar, K. V.; Breda, C.; Schwarcz, R.; Giorgini, F. Assessing and Modulating Kynurenine Pathway Dynamics in Huntington's Disease: Focus on Kynurenine 3-Monooxygenase. *Methods Mol Biol* **2018**, *1780*, 397-413.
- (34) Bloem, B. R.; Okun, M. S.; Klein, C. Parkinson's disease. *Lancet* **2021**, *397* (10291), 2284-2303.
- (35) Sveinbjornsdottir, S. The clinical symptoms of Parkinson's disease. *J Neurochem* **2016**, *139*, 318-324.
- (36) Braak, H.; Ghebremedhin, E.; Rüb, U.; Bratzke, H.; Del Tredici, K. Stages in the development of Parkinson's disease-related pathology. *Cell Tissue Res* **2004**, *318* (1), 121-134.
- (37) Segura-Aguilar, J.; Paris, I.; Muñoz, P.; Ferrari, E.; Zecca, L.; Zucca, F. A. Protective and toxic roles of dopamine in Parkinson's disease. *J Neurochem* **2014**, *129* (6), 898-915.
- (38) Lees, A. J.; Hardy, J.; Revesz, T. Parkinson's disease. Lancet 2009, 373 (9680), 2055-2066.

- (39) Chen, P.; Geng, X. F. Research progress on the kynurenine pathway in the prevention and treatment of Parkinson's disease. *J Enzym Inhib Med Ch* **2023**, *38* (1).
- (40) Zinger, A.; Barcia, C.; Herrero, M. T.; Guillemin, G. J. The Involvement of Neuroinflammation and Kynurenine Pathway in Parkinson's Disease. *Parkinsons Dis-Us* **2011**, 2011.
- (41) Ogawa, T.; Matson, W. R.; Beal, M. F.; Myers, R. H.; Bird, E. D.; Milbury, P.; Saso, S. Kynurenine Pathway Abnormalities in Parkinsons-Disease. *Neurology* **1992**, *42* (9), 1702-1706.
- (42) Hiramatsu, R.; Hara, T.; Akimoto, H.; Takikawa, O.; Kawabe, T.; Isobe, K. I.; Nagase, F. Cinnabarinic acid generated from 3-hydroxyanthranilic acid strongly induces apoptosis in thymocytes through the generation of reactive oxygen species and the induction of caspase. *J Cell Biochem* **2008**, *103* (1), 42-53.
- (43) Stone, T. W.; Forrest, C. M.; Darlington, L. G. Kynurenine pathway inhibition as a therapeutic strategy for neuroprotection. *Febs J* **2012**, *279* (8), 1386-1397.
- (44) Havelund, J. F.; Andersen, A. D.; Binzer, M.; Blaabjerg, M.; Heegaard, N. H. H.; Stenager, E.; Faergeman, N. J.; Gramsbergen, J. B. Changes in kynurenine pathway metabolism in Parkinson patients with L-DOPA-induced dyskinesia. *J Neurochem* **2017**, *142* (5), 756-766.
- (45) Bellac, C. L.; Coimbra, R. S.; Christen, S.; Leib, S. L. Inhibition of the Kynurenine-NAD Pathway Leads to Energy Failure and Exacerbates Apoptosis in Pneumococcal Meningitis. *J Neuropath Exp Neur* **2010**, *69* (11), 1096-1104.
- (46) Jakkampudi, A.; Sarkar, P.; Unnisa, M.; Patil, A.; Koutarapu, C.; Jaggaiahgari, S.; Naik, P.; Sarkar, S.; Prasanna, A.; Chintaluri, S.; et al. Kynurenine pathway alteration in acute pancreatitis and its role as a biomarker of infected necrosis. *Pancreatology* **2023**, *23* (6), 589-600.

- (47) Ala, M.; Eftekhar, S. P. The Footprint of Kynurenine Pathway in Cardiovascular Diseases. *Int J Tryptophan Res* **2022**, *15*.
- (48) Chiarugi, A.; Calvani, M.; Meli, E.; Traggiai, E.; Moroni, F. Synthesis and release of neurotoxic kynurenine metabolites by human monocyte-derived macrophages. *J Neuroimmunol* **2001**, *120* (1-2), 190-198.
- (49) Comai, S.; Costa, C. V. L.; Ragazzi, E.; Bertazzo, A.; Allegri, G. The effect of age on the enzyme activities of tryptophan metabolism along the kynurenine pathway in rats. *Clin Chim Acta* **2005**, *360* (1-2), 67-80.
- (50) Stephens, G. L.; Wang, Q.; Swerdlow, B.; Bhat, G.; Kolbeck, R.; Fung, M. Kynurenine 3-monooxygenase mediates inhibition of Th17 differentiation via catabolism of endogenous aryl hydrocarbon receptor ligands. *Eur J Immunol* **2013**, *43* (7), 1727-1734.
- (51) Jin, H. J.; Zhang, Y. R.; You, H. Y.; Tao, X. M.; Wang, C.; Jin, G. Z.; Wang, N.; Ruan, H. Y.; Gu, D. S.; Huo, X. S.; et al. Prognostic significance of kynurenine 3-monooxygenase and effects on proliferation, migration, and invasion of human hepatocellular carcinoma. *Sci Rep-Uk* **2015**, *5*.
- (52) Chiu, Y. H.; Lei, H. J.; Huang, K. C.; Chiang, Y. L.; Lin, C. S. Overexpression of Kynurenine 3-Monooxygenase Correlates with Cancer Malignancy and Predicts Poor Prognosis in Canine Mammary Gland Tumors. *J Oncol* **2019**, *2019*.
- (53) Giménez-Gómez, P.; Pérez-Hernández, M.; Gutiérrez-López, M. D.; Vidal, R.; Abuin-Martínez, C.; O'Shea, E.; Colado, M. I. Increasing kynurenine brain levels reduces ethanol consumption in mice by inhibiting dopamine release in nucleus accumbens. *Neuropharmacology* **2018**, *135*, 581-591.

- (54) Badawy, A. A. B.; Bano, S. Elevation of Kynurenine Metabolites in Rat Liver and Serum: A Potential Additional Mechanism of the Alcohol Aversive and Anti-cancer Effects of Disulfiram? *Alcohol Alcoholism* **2016**, *51* (1), 20-26.
- (55) Guillemin, G. J.; Smythe, G.; Takikawa, O.; Brew, B. J. Expression of indoleamine 2,3-dioxygenase and production of quinolinic acid by human microglia, astrocytes, and neurons. *Glia* **2005**, *49* (1), 15-23.
- (56) Guillemin, G. J.; Cullen, K. M.; Lim, C. K.; Smythe, G. A.; Garner, B.; Kapoor, V.; Takikawa, O.; Brew, B. J. Characterization of the kynurenine pathway in human neurons. *J Neurosci* **2007**, *27* (47), 12884-12892.
- (57) Okuda, S.; Nishiyama, N.; Saito, H.; Katsuki, H. 3-hydroxykynurenine, an endogenous oxidative stress generator, causes neuronal cell death with apoptotic features and region selectivity. *J Neurochem* **1998**, 70 (1), 299-307.
- (58) Uemura, T.; Hirai, K. L-kynurenine 3-monooxygenase from mitochondrial outer membrane of pig liver: Purification, some properties, and monoclonal antibodies directed to the enzyme. *J Biochem* **1998**, *123* (2), 253-262.
- (59) Erickson, J. B.; Flanagan, E. M.; Russo, S.; Reinhard, J. F. A Radiometric Assay for Kynurenine 3-Hydroxylase Based on the Release of (H2o)-H-3 during Hydroxylation of L-[3,5-H-3]Kynurenine. *Anal Biochem* **1992**, *205* (2), 257-262.
- (60) Okamoto, H.; Yamamoto, S.; Nozaki, M.; Hayaishi, O. On Submitochondrial Localization of L-Kynurenine-3-Hydroxylase. *Biochem Bioph Res Co* **1967**, *26* (3), 309-+.
- (61) AlberatiGiani, D.; Cesura, A. M.; Broger, C.; Warren, W. D.; Rover, S.; Malherbe, P. Cloning and functional expression of human kynurenine 3-monooxygenase. *Febs Lett* **1997**, *410* (2-3), 407-412.

- (62) van Berkel, W. J. H.; Kamerbeek, N. M.; Fraaije, M. W. Flavoprotein monooxygenases, a diverse class of oxidative biocatalysts. *J Biotechnol* **2006**, *124* (4), 670-689.
- (63) Crozier-Reabe, K. R.; Phillips, R. S.; Moran, G. R. Kynurenine 3-Monooxygenase from : Substrate-like Inhibitors both Stimulate Flavin Reduction and Stabilize the Flavin-Peroxo Intermediate yet Result in the Production of Hydrogen Peroxide. *Biochemistry-Us* **2008**, *47* (47), 12420-12433.
- (64) Crozier, K. R.; Moran, G. R. Heterologous expression and purification of kynurenine-3-monooxygenase from
- strain 17400. Protein Expres Purif 2007, 51 (2), 324-333.
- (65) Breton, J.; Avanzi, N.; Magagnin, S.; Covini, N.; Magistrelli, G.; Cozzi, L.; Isacchi, A. Functional characterization and mechanism of action of recombinant human kynurenine 3-hydroxylase. *Eur J Biochem* **2000**, *267* (4), 1092-1099.
- (66) Hirai, K.; Kuroyanagi, H.; Tatebayashi, Y.; Hayashi, Y.; Hirabayashi-Takahashi, K.; Saito, K.; Haga, S.; Uemura, T.; Izumi, S. Dual role of the carboxyl-terminal region of pig liver l-kynurenine 3-monooxygenase: mitochondrial-targeting signal and enzymatic activity\*. *J Biochem* **2010**, *148* (6), 639-650.
- (67) Amaral, M.; Levy, C.; Heyes, D. J.; Lafite, P.; Outeiro, T. F.; Giorgini, F.; Leys, D.; Scrutton, N. S. Structural basis of kynurenine 3-monooxygenase inhibition. *Nature* **2013**, *496* (7445), 382-+.
- (68) Zhang, S. W.; Sakuma, M.; Deora, G. S.; Levy, C. W.; Klausing, A.; Breda, C.; Read, K. D.; Edlin, C. D.; Ross, B. P.; Muelas, M. W.; et al. A brain-permeable inhibitor of the neurodegenerative disease target kynurenine 3-monooxygenase prevents accumulation of neurotoxic metabolites. *Commun Biol* **2019**, *2*.

- (69) Kim, H. T.; Na, B. K.; Chung, J.; Kim, S.; Kwon, S. K.; Cha, H.; Son, J.; Cho, J. M.; Hwang, K. Y. Structural Basis for Inhibitor-Induced Hydrogen Peroxide Production by Kynurenine 3-Monooxygenase. *Cell Chem Biol* **2018**, *25* (4), 426-+.
- (70) Gao, J. J.; Yao, L. C.; Xia, T. T.; Liao, X. B.; Zhu, D. Y.; Xiang, Y. Biochemistry and structural studies of kynurenine 3-monooxygenase reveal allosteric inhibition by Ro 61-8048. *Faseb J* **2018**, *32* (4), 2036-2045.
- (71) Walker, A. L.; Ancellin, N.; Beaufils, B.; Bergeal, M.; Binnie, M.; Bouillot, A.; Clapham, D.; Denis, A.; Haslan, C. P.; Holmes, D. S.; et al. Development of a Series of Kynurenine 3-Monooxygenase Inhibitors Leading to a Clinical Candidate for the Treatment of Acute Pancreatitis. *J Med Chem* **2017**, *60* (8), 3383-3404.
- (72) Liddle, J.; Beaufils, B.; Binnie, M.; Bouillot, A.; Denis, A. A.; Hann, M. M.; Haslam, C. P.; Holmes, D. S.; Hutchinson, J. P.; Kranz, M.; et al. The discovery of potent and selective kynurenine 3-monooxygenase inhibitors for the treatment of acute pancreatitis. *Bioorg Med Chem Lett* **2017**, *27* (9), 2023-2028.
- (73) Hutchinson, J. P.; Rowland, P.; Taylor, M. R. D.; Christodoulou, E. M.; Haslam, C.; Hobbs, C. I.; Holmes, D. S.; Homes, P.; Liddle, J.; Mole, D. J.; et al. Structural and mechanistic basis of differentiated inhibitors of the acute pancreatitis target kynurenine-3-monooxygenase. *Nat Commun* **2017**, *8*.
- (74) Mole, D. J.; Webster, S. P.; Uings, I.; Zheng, X. Z.; Binnie, M.; Wilson, K.; Hutchinson, J. P.; Mirguet, O.; Walker, A.; Beaufils, B.; et al. Kynurenine-3-monooxygenase inhibition prevents multiple organ failure in rodent models of acute pancreatitis. *Nat Med* **2016**, *22* (2), 202-209.

- (75) Mimasu, S.; Yamagishi, H.; Kubo, S.; Kiyohara, M.; Matsuda, T.; Yahata, T.; Thomson, H. A.; Hupp, C. D.; Liu, J. L.; Okuda, T.; Kakefuda, K. Full-length structure and mechanism of rat kynurenine 3-monooxygenase inhibition. *Commun Biol* **2021**, *4* (1).
- (76) Moroni, F.; Russi, P.; Gallomezo, M. A.; Moneti, G.; Pellicciari, R. Modulation of Quinolinic and Kynurenic Acid Content in the Rat-Brain Effects of Endotoxins and Nicotinylalanine. *J Neurochem* **1991**, *57* (5), 1630-1635.
- (77) Chiarugi, A.; Carpenedo, R.; Moroni, F. Kynurenine disposition in blood and brain of mice: Effects of selective inhibitors of kynurenine hydroxylase and of kynureninase. *J Neurochem* **1996**, 67 (2), 692-698.
- (78) Pellicciari, R.; Natalini, B.; Costantino, G.; Mahmoud, M. R.; Mattoli, L.; Sadeghpour, B. M.; Moroni, F.; Chiarugi, A.; Carpenedo, R. Modulation of the Kynurenine Pathway in Search for New Neuroprotective Agents Synthesis and Preliminary Evaluation of (M-Nitrobenzoyl)Alanine, a Potent Inhibitor of Kynurenine-3-Hydroxylase. *J Med Chem* **1994**, *37* (5), 647-655.
- (79) Giordani, A.; Pevarello, P.; Cini, M.; Bormetti, R.; Greco, F.; Toma, S.; Speciale, C.; Varasi, M. 4-phenyl-4-oxo-butanoic acid derivatives inhibitors of kynurenine 3-hydroxylase. *Bioorg Med Chem Lett* **1998**, *8* (20), 2907-2912.
- (80) Röver, S.; Cesura, A. M.; Huguenin, P.; Kettler, R.; Szente, A. Synthesis and biochemical evaluation of -(4-phenylthiazol-2-yl)benzenesulfonamides as high-affinity inhibitors of kynurenine 3-hydroxylase. *J Med Chem* **1997**, *40* (26), 4378-4385.
- (81) Heidempergher, F.; Pevarello, P.; Pillan, A.; Pinciroli, V.; Della Torre, A.; Speciale, C.; Marconi, M.; Cini, M.; Toma, S.; Greco, F.; Varasi, M. Pyrrolo[3,2-c]quinoline derivatives: a new class of kynurenine-3-hydroxylase inhibitors. *Farmaco* **1999**, *54* (3), 152-160. From NLM Medline.

- (82) Pellicciari, R.; Amori, L.; Costantino, G.; Giordani, A.; Macchiarulo, A.; Mattoli, L.; Pevarello, P.; Speciale, C.; Varasi, M. Modulation of the kynurine pathway of tryptophan metabolism in search for neuroprotective agents. focus on kynurenine-3-hydroxylase. *Developments in Tryptophan and Serotonin Metabolism* **2003**, *527*, 621-628.
- (83) Sapko, M. T.; Guidetti, P.; Yu, P.; Tagle, D. A.; Pellicciari, R.; Schwarcz, R. Endogenous kynurenate controls the vulnerability of striatal neurons to quinolinate: Implications for Huntington's disease. *Exp Neurol* **2006**, *197* (1), 31-40.
- (84) Feng, Y. J.; Bowden, B. F.; Kapoor, V. Ianthellamide A, a selective kynurenine-3-hydroxylase inhibitor from the Australian marine sponge. *Bioorg Med Chem Lett* **2012**, *22* (10), 3398-3401.
- (85) Lowe, D. M.; Gee, M.; Haslam, C.; Leavens, B.; Christodoulou, E.; Hissey, P.; Hardwicke, P.; Argyrou, A.; Webster, S. P.; Mole, D. J.; et al. Lead Discovery for Human Kynurenine 3-Monooxygenase by High-Throughput RapidFire Mass Spectrometry. *J Biomol Screen* **2014**, *19* (4), 508-515.
- (86) Toledo-Sherman, L. M.; Prime, M. E.; Mrzljak, L.; Beconi, M. G.; Beresford, A.; Brookfield, F. A.; Brown, C. J.; Cardaun, I.; Courtney, S. M.; Dijkman, U.; et al. Development of a Series of Aryl Pyrimidine Kynurenine Monooxygenase Inhibitors as Potential Therapeutic Agents for the Treatment of Huntington's Disease. *J Med Chem* **2015**, *58* (3), 1159-1183.
- (87) Phillips, R. S.; Anderson, A. D.; Gentry, H. G.; Guner, O. F.; Bowen, J. P. Substrate and inhibitor specificity of kynurenine monooxygenase from Cytophaga hutchinsonii. *Bioorg Med Chem Lett* **2017**, *27* (8), 1705-1708. From NLM Medline.

- (88) Shave, S.; McGuire, K.; Pham, N. T.; Mole, D. J.; Webster, S. P.; Auer, M. Diclofenac Identified as a Kynurenine 3-Monooxygenase Binder and Inhibitor by Molecular Similarity Techniques. *Acs Omega* **2018**, *3* (3), 2564-2568.
- (89) Tsuboi, K.; Kimura, H.; Nakatsuji, Y.; Kassai, M.; Deai, Y.; Isobe, Y. Discovery of N-(6-(5-fluoro-2-(piperidin-1-yl)phenyl) pyridazin-3-yl)-1-(tetrahydro-2H-pyran-4-yl)methanesulfonamide as a brain-permeable and metabolically stable kynurenine monooxygenase inhibitor. *Bioorg Med Chem Lett* **2021**, *44*.
- (90) Kimura, H.; Suda, H.; Kassai, M.; Endo, M.; Deai, Y.; Yahata, M.; Miyajima, M.; Isobe, Y. N-(6-phenylpyridazin-3-yl)benzenesulfonamides as highly potent, brain-permeable, and orally active kynurenine monooxygenase inhibitors. *Bioorg Med Chem Lett* **2021**, *33*.
- (91) Smith, J. R.; Jamie, J. F.; Guillemin, G. J. Kynurenine-3-monooxygenase: a review of structure, mechanism, and inhibitors. *Drug Discov Today* **2016**, *21* (2), 315-324.
- (92) Malik, M. A.; Wani, M. Y.; Al-Thabaiti, S. A.; Shiekh, R. A. Tetrazoles as carboxylic acid isosteres: chemistry and biology. *J Incl Phenom Macro* **2014**, 78 (1-4), 15-37.
- (93) Herr, R. J. 5-substituted-1-tetrazoles as carboxylic acid isosteres:: Medicinal chemistry and synthetic methods. *Bioorgan Med Chem* **2002**, *10* (11), 3379-3393.
- (94) Colabroy, K. L.; Begley, T. P. The pyridine ring of NAD is formed by a nonenzymatic pericyclic reaction. *J Am Chem Soc* **2005**, *127* (3), 840-841.
- (95) Kabsch, W. Xds. Acta Crystallogr D 2010, 66, 125-132.
- (96) Mccoy, A. J.; Grosse-Kunstleve, R. W.; Adams, P. D.; Winn, M. D.; Storoni, L. C.; Read, R. J. crystallographic software. *J Appl Crystallogr* **2007**, *40*, 658-674.
- (97) Liebschner, D.; Afonine, P. V.; Baker, M. L.; Bunkóczi, G.; Chen, V. B.; Croll, T. I.; Hintze, B.; Hung, L. W.; Jain, S.; McCoy, A. J.; et al. Macromolecular structure determination using X-

- rays, neutrons and electrons: recent developments in. *Acta Crystallographica Section D-Structural Biology* **2019**, *75*, 861-877.
- (98) Casañal, A.; Lohkamp, B.; Emsley, P. Current developments in for macromolecular model building of Electron Cryo-microscopy and Crystallographic Data. *Protein Sci* **2020**, *29* (4), 1069-1078.
- (99) Dong-Ruyl, L.; Sawada, M.; Nakano, K. Tryptophan and its metabolite, kynurenine, stimulate expression of nerve growth factor in cultured mouse astroglial cells. *Neurosci Lett* **1998**, *244* (1), 17-20. From NLM Medline.
- (100) Nakagami, Y.; Saito, H.; Katsuki, H. 3-Hydroxykynurenine toxicity on the rat striatum in vivo. *Jpn J Pharmacol* **1996**, *71* (2), 183-186. From NLM Medline.
- (101) Giil, L. M.; Midttun, O.; Refsum, H.; Ulvik, A.; Advani, R.; Smith, A. D.; Ueland, P. M. Kynurenine Pathway Metabolites in Alzheimer's Disease. *J Alzheimers Dis* **2017**, *60* (2), 495-504. From NLM Medline.
- (102) Boegman, R. J.; Jhamandas, K.; Beninger, R. J. Neurotoxicity of tryptophan metabolites. *Ann N Y Acad Sci* **1990**, *585*, 261-273. From NLM Medline.
- (103) Beal, M. F.; Kowall, N. W.; Ellison, D. W.; Mazurek, M. F.; Swartz, K. J.; Martin, J. B. Replication of the neurochemical characteristics of Huntington's disease by quinolinic acid. *Nature* **1986**, *321* (6066), 168-171. From NLM Medline.
- (104) Lim, C. K.; Fernández-Gomez, F. J.; Braidy, N.; Estrada, C.; Costa, C.; Costa, S.; Bessede, A.; Fernandez-Villalba, E.; Zinger, A.; Herrero, M. T.; Guillemin, G. J. Involvement of the kynurenine pathway in the pathogenesis of Parkinson's disease. *Prog Neurobiol* **2017**, *155*, 76-95. (105) Zwilling, D.; Huang, S. Y.; Sathyasaikumar, K. V.; Notarangelo, F. M.; Guidetti, P.; Wu, H. Q.; Lee, J.; Truong, J.; Andrews-Zwilling, Y.; Hsieh, E. W.; et al. Kynurenine 3-monooxygenase

- inhibition in blood ameliorates neurodegeneration. *Cell* **2011**, *145* (6), 863-874. From NLM Medline.
- (106) Boegman, R. J.; el-Defrawy, S. R.; Jhamandas, K.; Beninger, R. J.; Ludwin, S. K. Quinolinic acid neurotoxicity in the nucleus basalis antagonized by kynurenic acid. *Neurobiol Aging* **1985**, *6* (4), 331-336. From NLM Medline.
- (107) Natalini, B.; Mattoli, L.; Pellicciari, R.; Carpenedo, R.; Chiarugi, A.; Moroni, F. Synthesis and Activity of Enantiopure (S)(M-Nitrobenzoyl) Alanine, Potent Kynurenine-3-Hydroxylase Inhibitor. *Bioorg Med Chem Lett* **1995**, *5* (14), 1451-1454.
- (108) Speciale, C.; Wu, H. Q.; Cini, M.; Marconi, M. A.; Varasi, M.; Schwarcz, R. (R,S)-3,4-dichlorobenzoylalanine (FCE 28833A) causes a large and persistent increase in brain kynurenic acid levels in rats. *Eur J Pharmacol* **1996**, *315* (3), 263-267.
- (109) Studier, F. W. Protein production by auto-induction in high density shaking cultures. *Protein Expr Purif* **2005**, *41* (1), 207-234. From NLM Medline.
- (110) Ma, W. H.; Mcbride, J. T.; Phillips, R. S. Nitration of deactivated aromatic compounds using Lithium nitrate. *Tetrahedron Lett* **2025**, *159*.
- (111) Haleem, A.; Shafiq, A.; Chen, S. Q.; Nazar, M. A Comprehensive Review on Adsorption, Photocatalytic and Chemical Degradation of Dyes and Nitro-Compounds over Different Kinds of Porous and Composite Materials. *Molecules* **2023**, *28* (3).
- (112) Botvay, A.; Máthé, A.; Pöppl, L. Nitration of polyethersulfone by ammonium nitrate and trifluoroacetic anhydride. *Polymer* **1999**, *40* (17), 4965-4970.
- (113) Ju, K. S.; Parales, R. E. Nitroaromatic Compounds, from Synthesis to Biodegradation. *Microbiol Mol Biol R* **2010**, *74* (2), 250-+.

- (114) Kanekar, P.; Dautpure, P.; Sarnaik, S. Biodegradation of nitro-explosives. *Indian J Exp Biol* **2003**, *41* (9), 991-1001. From NLM Medline.
- (115) Nepali, K.; Lee, H. Y.; Liou, J. P. Nitro-Group-Containing Drugs. *J Med Chem* **2019**, *62* (6), 2851-2893.
- (116) Gillespie, R. J.; Millen, D. J. Aromatic Nitration. *Q Rev Chem Soc* **1948**, *2* (4), 277-306.
- (117) Westheimer, F. H.; Kharasch, M. S. The Kinetics of Nitration of Aromatic Nitro Compounds in Sulfuric Acid. *J Am Chem Soc* **1946**, *68* (10), 1871-1876.
- (118) Hughes, E. D.; Ingold, C. K.; Reed, R. I. Kinetics of Aromatic Nitration the Nitronium Ion. *Nature* **1946**, *158* (4013), 449-449.
- (119) Guggenheim, T. L.; Odle, R. R.; Pace, J. Process Design and Operational Controls To Safeguard Strong Nitric Acid Recovery Systems. *Acs Sym Ser* **2013**, *1155*, 185-202.
- (120) Othmer, D. F.; Jacobs, J. J.; Levy, J. F. Multration of benzene Continuous process, using nitric acid alone. *Ind Eng Chem* **1942**, *34*, 286-291.
- (121) Jia, F. Q.; Li, A.; Hu, X. D. Dinitro-5,5-Dimethylhydantoin: An Arene Nitration Reagent. *Org Lett* **2023**, *25* (25), 4605-4609.
- (122) Yang, T.; Li, X. Q.; Deng, S.; Qi, X. T.; Cong, H. J.; Cheng, H. G.; Shi, L. W.; Zhou, Q. H.; Zhuang, L. From N-H Nitration to Controllable Aromatic Mononitration and Dinitration-The Discovery of a Versatile and Powerful Nitropyrazole Nitrating Reagent. *Jacs Au* **2022**, *2* (9), 2152-2161.
- (123) Long, T. F.; Liu, L.; Tao, Y. Q.; Zhang, W. L.; Quan, J. L.; Zheng, J.; Hegemann, J. D.; Uesugi, M.; Yao, W. B.; Tian, H.; Wang, H. Light-Controlled Tyrosine Nitration of Proteins. Angew Chem Int Edit 2021, 60 (24), 13414-13422.

- (124) Calvo, R.; Zhang, K.; Passera, A.; Katayev, D. Facile access to nitroarenes and nitroheteroarenes using N-nitrosaccharin. *Nat Commun* **2019**, *10*.
- (125) Cupas, C. A.; Pearson, R. L. Transfer Nitration Via N-Nitropyridinium Salts. *J Am Chem Soc* **1968**, *90* (17), 4742-&.
- (126) Olah, G. A.; Olah, J. A.; Overchuk, N. A. Aromatic Substitution .23. Nitration and Nitrosation of Pyridine with Nitronium and Nitrosonium Tetrafluoroborate . Isolation of N-Nitroand N-Nitrosopyridinium Tetrafluoroborates. *J Org Chem* **1965**, *30* (10), 3373-&.
- (127) Coburn, M. D.; Ungnade, H. E. Synthesis and Structure of N-Nitropyrrolidinones. *J Heterocyclic Chem* **1965**, *2* (3), 308-&.
- (128) Kauffman, H. F.; Burger, A. N-Nitrosuccinimide and N-Nitrophthalimide. *J Org Chem* **1954**, *19* (10), 1662-1670.
- (129) Ramana, M. M. V.; Malik, S. S.; Parihar, J. A. Guanidinium nitrate: a novel reagent for aryl nitrations. *Tetrahedron Lett* **2004**, *45* (47), 8681-8683.
- (130) Almog, J.; Klein, A.; Sokol, A.; Sasson, Y.; Sonenfeld, D.; Tamiri, T. Urea nitrate and nitrourea: powerful and regioselective aromatic nitration agents. *Tetrahedron Lett* **2006**, *47* (49), 8651-8652.
- (131) Mundla, S. R. Regioselective synthesis of 4-halo -dinitrobenzene derivatives. *Tetrahedron Lett* **2000**, *41* (22), 4277-4279.
- (132) Sura, T. P.; Ramana, M. M. V.; Kudav, N. A. Urea Nitrate a Reagent for Regioselective Nitration of Aromatic-Amines. *Synthetic Commun* **1988**, *18* (16-17), 2161-2165.
- (133) Majumdar, M. P.; Kudav, N. A. Nitration of Organic-Compounds with Urea Nitrate Sulfuric Acid. *Indian J Chem B* **1976**, *14* (12), 1012-1013.

- (134) Oxley, J. C.; Smith, J. L.; Moran, J. S.; Canino, J. N.; Almog, J. Aromatic nitration using nitroguanidine and EGDN. *Tetrahedron Lett* **2008**, *49* (28), 4449-4451.
- (135) Sun, H. B.; Hua, R. M.; Yin, Y. W. Highly efficient nitration of phenolic compounds in solid phase or solution using Bi(NO<sub>3</sub>)<sub>3</sub>•5H<sub>2</sub>O as nitrating reagent. *J Org Chem* **2005**, 70 (22), 9071-9073.
- (136) Bose, A. K.; Ganguly, S. N.; Manhas, M. S.; Rao, S.; Speck, J.; Pekelny, U.; Pombo-Villars, E. Microwave promoted rapid nitration of phenolic compounds with calcium nitrate. *Tetrahedron Lett* **2006**, *47* (12), 1885-1888.
- (137) Anuradha, V.; Srinivas, P. V.; Aparna, P.; Rao, J. M. -toluenesulfonic acid catalyzed regiospecific nitration of phenols with metal nitrates. *Tetrahedron Lett* **2006**, *47* (28), 4933-4935.
- (138) Patel, S. S.; Patel, D. B.; Poddar, A. K.; Patel, J. B.; Rana, D. N.; Patel, K. P.; Thakar, S. P.; Patel, H. D. Copper phthalocyanine tetrasulfonic acid (CuPcS) as an efficient recyclable catalyst for aromatic nitration using sodium nitrate. *J Mol Struct* **2023**, *1280*.
- (139) Albadi, J.; Shirini, F.; Ghabezi, B.; Seiadatnasab, T. Melamine trisulfonic acid catalyzed regioselective nitration of aromatic compounds with sodium nitrate under solvent-free conditions. *Arab J Chem* **2017**, *10*, S509-S513.
- (140) Tajik, H.; Zolfigol, M. A.; Albadi, J.; Eslami, R. Nitration of some aromatic compounds by sodium nitrate in the presence of benzyltriphenylphosphonium peroxodisulfate. *Synthetic Commun* **2007**, *37* (16), 2771-2776.
- (141) Zolfigol, M. A.; Ghaemi, E.; Madrakian, E. Nitration of phenols under mild and heterogeneous conditions. *Molecules* **2001**, *6* (7), 614-620.
- (142) Wu, J. W.; Zhang, P.; Guo, Z. X. Nitration of deactivated aromatic compounds mechanochemical reaction. *Tetrahedron Lett* **2021**, *72*.

- (143) Wang, C. M.; Tang, K. X.; Gao, T. H.; Chen, L.; Sun, L. P. Cu(II)-Catalyzed
- -C-H Nitration of Aryl Ureas By C-H Functionalization. J Org Chem 2018, 83 (15), 8315-8321.
- (144) Rajagopal, R.; Srinivasan, K. V. Regio-selective mono nitration of phenols with ferric nitrate in room temperature ionic liquid. *Synthetic Commun* **2003**, *33* (6), 961-966.
- (145) Liu, D. M.; Luo, P. Y.; Ge, J. Y.; Jiang, Z. L.; Peng, Y. Y.; Ding, Q. P. Synthesis of 2-Arylbenzothiazole and 2-Arylthiazole Derivatives via a Ru Catalyzed Selective C-H Nitration Reaction. *J Org Chem* **2019**, *84* (20), 12784-12791.
- (146) Gao, S. S.; Ma, Y. R.; Tang, H.; Luo, J. F.; Wang, K. Cu-Catalyzed C5 Nitration of Indolines under Mild Conditions. *Chemistryselect* **2019**, *4* (29), 8705-8708.
- (147) Dou, Y. D.; Yin, B.; Zhang, P. F.; Zhu, Q. Copper-Catalyzed Regioselective Nitration and Azidation of 1-Naphthylamine Derivatives via Remote C-H Activation. *Eur J Org Chem* **2018**, *2018* (33), 4571-4576.
- (148) Bose, A.; Mal, P. Using weak interactions to control C-H mono-nitration of indolines. *Chem Commun* **2017**, *53* (82), 11368-11371.
- (149) Bergman, J.; Koch, E.; Pelcman, B. Reactions of Indole-3-Acetic-Acid Derivatives in Trifluoroacetic-Acid. *Tetrahedron Lett* **1995**, *36* (22), 3945-3948.
- (150) Li, S. Y.; Zhao, W.; Wang, L. L.; Jia, Y. X.; Cui, Q. Y.; Wen, B.; Chen, X. Q. Controllable Selective Oxidation of Anilines to Azoxybenzenes and Nitrobenzenes by Regulating the Base. *Acs Omega* **2024**, *9* (38), 39715-39723.
- (151) Wu, Y. X.; Lu, W.; Ma, Y. N.; Chen, F. J.; Ren, W.; Chen, X. N. Trifluoromethanesulfonic Acid Promoted Controllable Electrophilic Aromatic Nitration. *J Org Chem* **2023**, *88* (15), 11322-11327.

- (152) Aridoss, G.; Laali, K. K. Ethylammonium Nitrate (EAN)/TfO and EAN/TFAA: Ionic Liquid Based Systems for Aromatic Nitration. *J Org Chem* **2011**, *76* (19), 8088-8094.
- (153) Hayashi, Y.; Sakamoto, D.; Okamura, D. One-Pot Synthesis of (S)-Baclofen via Aldol Condensation of Acetaldehyde with Diphenylprolinol Silyl Ether Mediated Asymmetric Michael Reaction as a Key Step. *Org Lett* **2016**, *18* (1), 4-7.
- (154) Zheng, Y. Z.; Hu, Q. Q.; Huang, Q.; Xie, Y. W. Late-Stage C-H Nitration of Unactivated Arenes by Fe(NO<sub>3</sub>)<sub>3</sub>.9H<sub>2</sub>O in Hexafluoroisopropanol. *Org Lett* **2024**, *26* (15), 3316-3320.
- (155) Bradlow, H. L.; Vanderwerf, C. A. The Effect of Fluorine Substitution on Chemotherapeutic Agents .1. Synthesis of Some Fluorine-Containing Medicinals. *J Am Chem Soc* **1948**, 70 (2), 654-657.
- (156) Dou, J. H.; Sun, L.; Ge, Y. C.; Li, W.; Hendon, C. H.; Li, J.; Gul, S.; Yano, J. K.; Stach, E. A.; Dinca, M. Signature of Metallic Behavior in the Metal-Organic Frameworks M (hexaiminobenzene)(M = Ni, Cu). *J Am Chem Soc* **2017**, *139* (39), 13608-13611.
- (157) Jia, Z.; Zhang, P.; Guo, Z. X. The oxidation of 2-phenylethanols by Fe(NO<sub>3</sub>)<sub>3</sub>•9H<sub>2</sub>O in CF<sub>3</sub>COOH: The dramatic substituent effect. *J Organomet Chem* **2024**, *1018*.
- (158) Wang, K.; Chen, L. G.; Dai, X. Y.; Zhou, C.; Zhang, C. J.; Feng, Z. Q. Synthesis and structure-activity relationships of N-(3-(1H-imidazol-2-yl) phenyl)-3-phenylpropionamide derivatives as a novel class of covalent inhibitors of p97/VCP ATPase. *Eur J Med Chem* **2023**, 248.
- (159) Saaidin, A. S.; Murai, Y.; Ishikawa, T.; Monde, K. Design and Synthesis of Ligand-Tag Exchangeable Photoaffinity Probe Utilizing Nosyl Chemistry. *Eur J Org Chem* **2019**, *2019* (46), 7563-7567.

- (160) Gallardo, I.; Guirado, G.; Marquet, J. Nucleophilic aromatic substitution for heteroatoms: An oxidative electrochemical approach. *J Org Chem* **2002**, *67* (8), 2548-2555.
- (161) Mathias, A.; Taylor, D. Analysis of Dinitrotoluene Isomer Mixtures by Nuclear Magnetic Resonance. *Anal Chim Acta* **1966**, *35* (3), 376-&.
- (162) Lv, F. P.; Li, Z. F.; Hu, W. H.; Wu, X. H. Small molecules enhance functional -mannosylation of Alpha-dystroglycan. *Bioorgan Med Chem* **2015**, *23* (24), 7661-7670.
- (163) Katritzky, A. R.; Scriven, E. F. V.; Majumder, S.; Akhmedova, R. G.; Akhmedov, N. G.; Vakulenko, A. V. Direct nitration of five membered heterocycles. *Arkivoc* **2005**, 179-191.
- (164) Morley, J. O.; Matthews, T. P. Studies on the biological activity of some nitrothiophenes. *Org Biomol Chem* **2006**, *4* (2), 359-366.

#### **APPENDICES**

### A. X-ray diffraction data processing, structure determination and refinement

Table A1. Data collection and refinement statistics.

	9AZ8	9B07	9B2Y
	KMO-	KMO-	КМО-3-
	cyclohexylphenyl-	biphenylacetyl-	Chlorophenylacetylt
	acetyltetrazole (7d)	tetrazole (6d)	etrazole (4d)
Wavelength, Å	1.0000	1.0000	1.0000
Resolution range, Å	41.9 - 1.95	55.38 - 1.88	43.68 - 2.05
	(2 - 1.95)	(1.93 - 1.88)	(2.1 - 2.05)
Space group	P 1 21 1	P 1 21 1	P 1 21 1
Unit cell	69.54 52.54 136.51 90	70.05 52.19 135.88 90	69.41 51.66 134.98 90
	104.11 90	103.7 90	103.86 90
<b>Total reflections</b>	225870 (14399)	243685 (17778)	238514 (17748)
Unique reflections	129564 (8707)	142993 (10121)	104865 (7765)
Multiplicity	1.7 (1.7)	1.7 (1.8)	2.3 (2.3)
Completeness (%)	97.16 (93.63)	98.08 (96.70)	93.68 (90.88)
Mean I/sigma(I)	5.39 (0.44)	6.59 (0.34)	6.09 (0.37)
Wilson B-factor	41.58	43.95	50.67
R-merge	0.06663 (1.519)	0.04834 (1.859)	0.06949 (2.023)
R-meas	0.09202 (2.06)	0.06782 (2.588)	0.08806 (2.541)
R-pim	0.06321 (1.383)	0.0475 (1.795)	0.05325 (1.516)
CC1/2	0.997 (0.258)	0.998 (0.195)	0.998 (0.176)

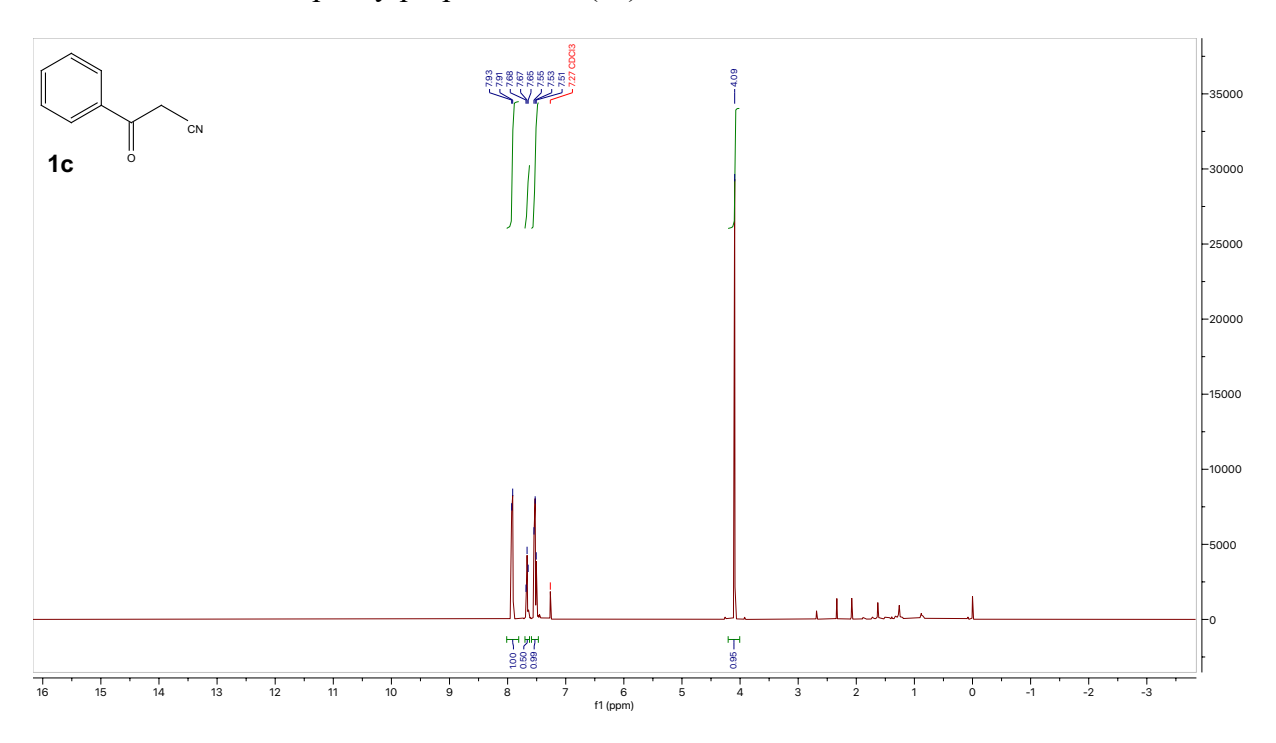
CC*	0.999 (0.64)	1 (0.572)	1 (0.547)
Reflections used in	68209 (4630)	76624 (5369)	55104 (3797)
refinement			
Reflections used for	2015 (133)	2003 (143)	2022 (138)
R-free			
R-work	0.1699 (0.3130)	0.1943 (0.3974)	0.2060 (0.4163)
R-free	0.2111 (0.3295)	0.2290 (0.3786)	0.2417 (0.4578)
Number of non-	7673	7782	7436
hydrogen atoms			
macromolecules	7103	7155	7055
ligands	153	152	122
solvent	417	475	259
Protein residues	902	902	899
RMS(bonds)	0.012	0.004	0.006
RMS(angles)	1.16	0.65	0.83
Ramachandran	98.00	98.55	98.66
favored (%)			
Ramachandran	2.00	1.34	1.12
allowed (%)			
Ramachandran	0.00	0.11	0.22
outliers (%)			
Rotamer outliers	1.07	0.80	0.68
(%)			

Clashscore	5.27	3.99	3.72
Average B-factor	55.38	66.55	67.46
macromolecules	55.50	67.28	68.02
ligands	47.77	53.30	50.16
solvent	56.10	59.70	60.56

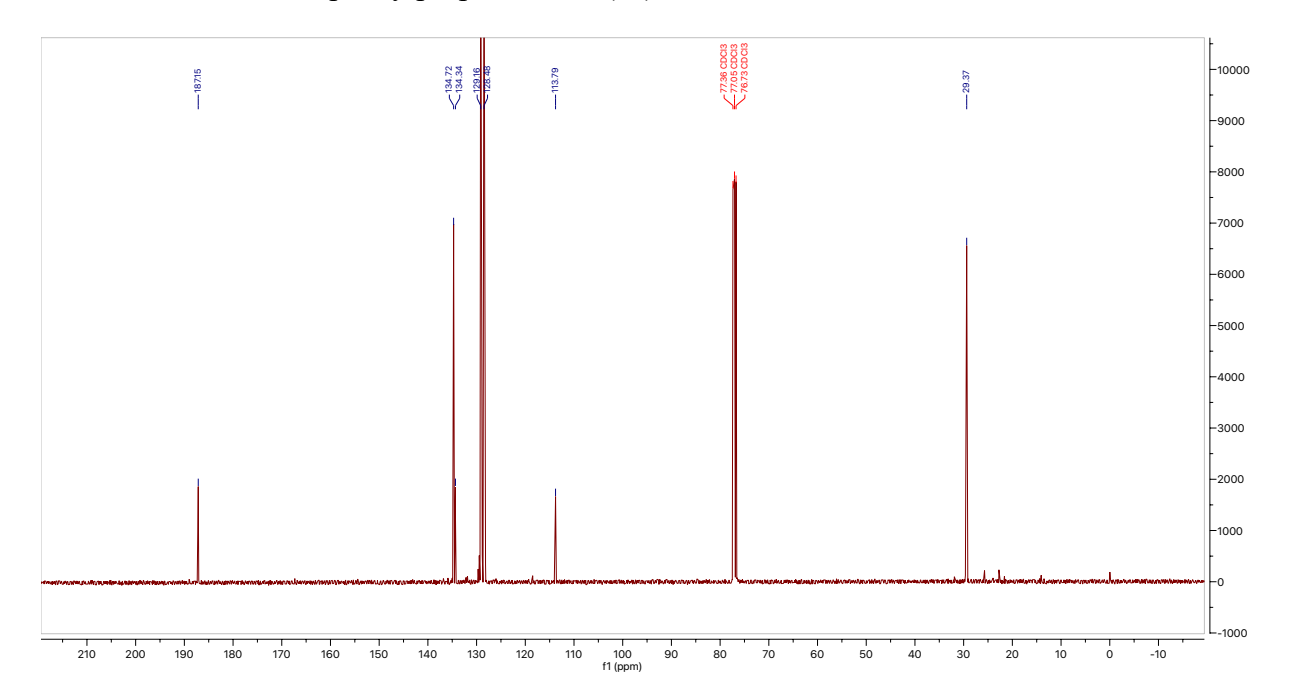
Statistics for the highest-resolution shell are shown in parentheses.

# B. $^{1}\mathrm{H}$ and $^{13}\mathrm{C}$ NMR for tetrazole synthesis

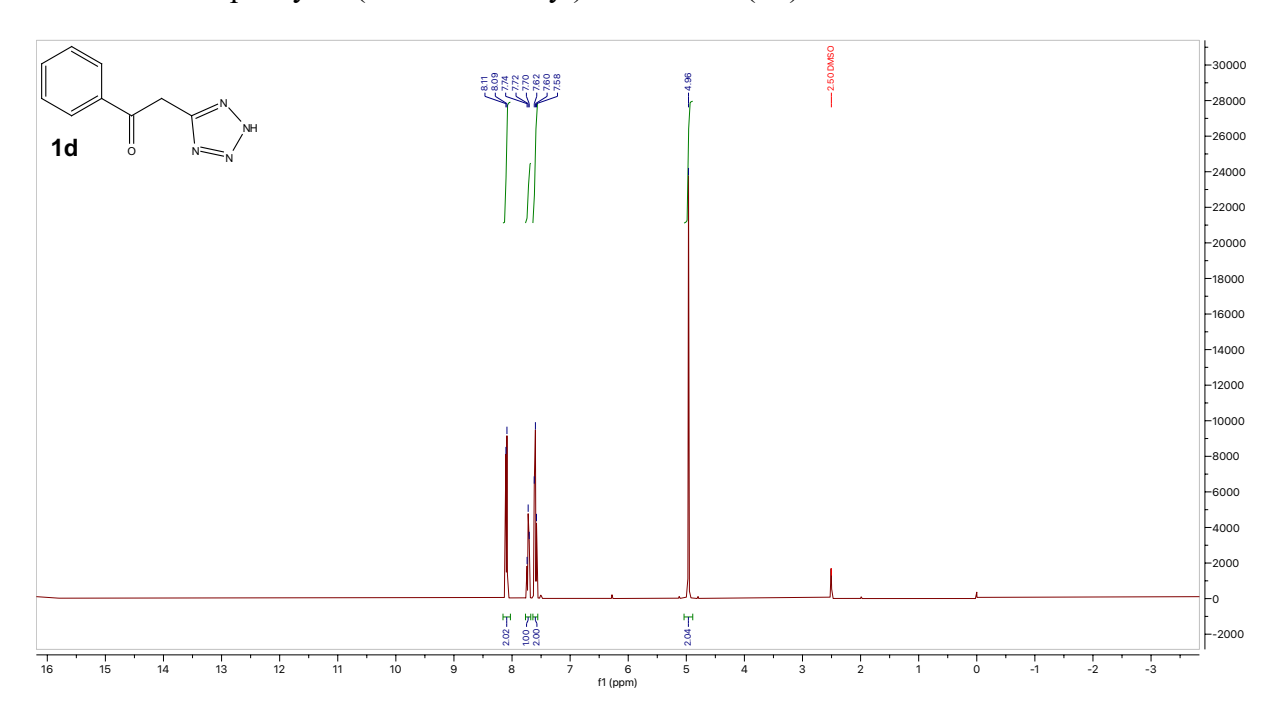
<sup>1</sup>H NMR for 3-oxo-3-phenylpropanenitrile (1c)



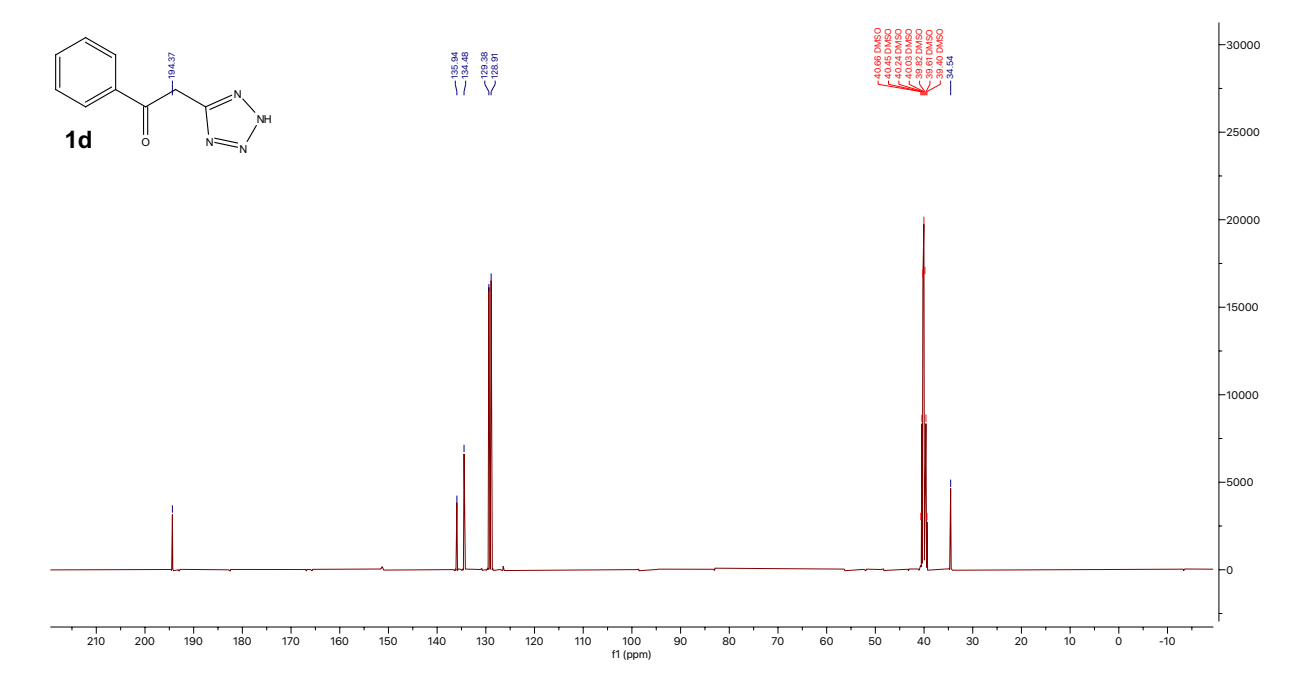
### <sup>13</sup>C NMR for 3-oxo-3-phenylpropanenitrile (1c)



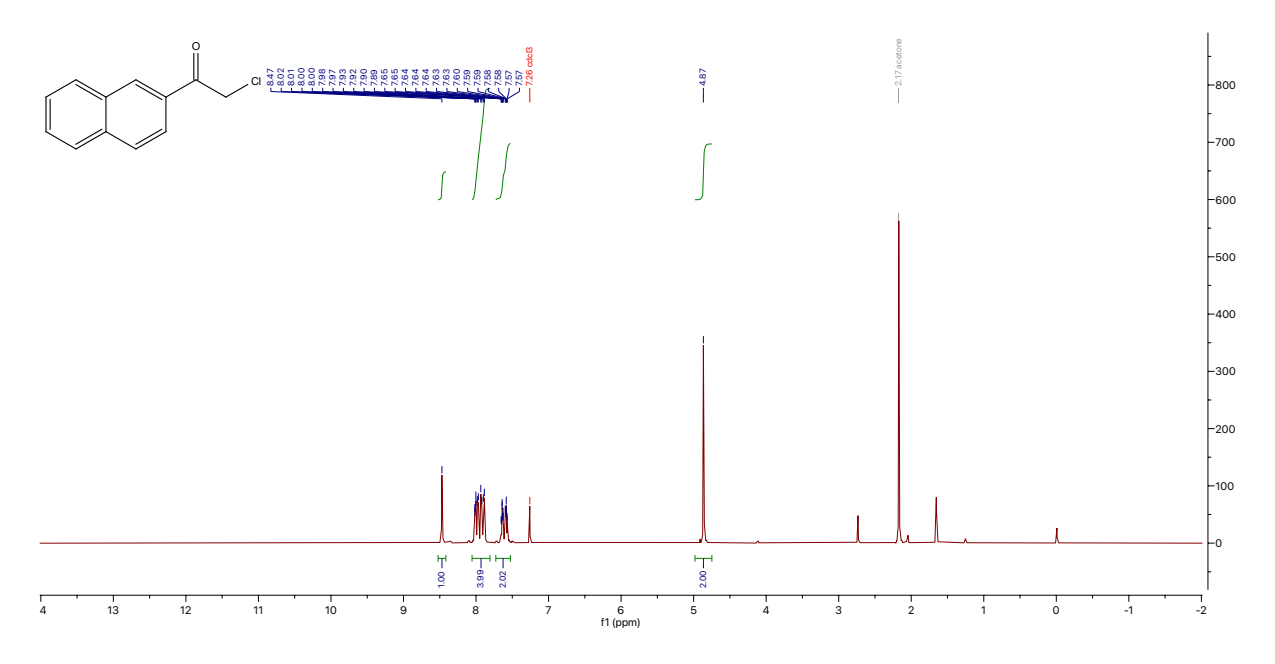
 $^{1}$ H NMR for 1-phenyl-2-(1H-tetrazol-5-yl)ethan-1-one (1 $\mathbf{d}$ )



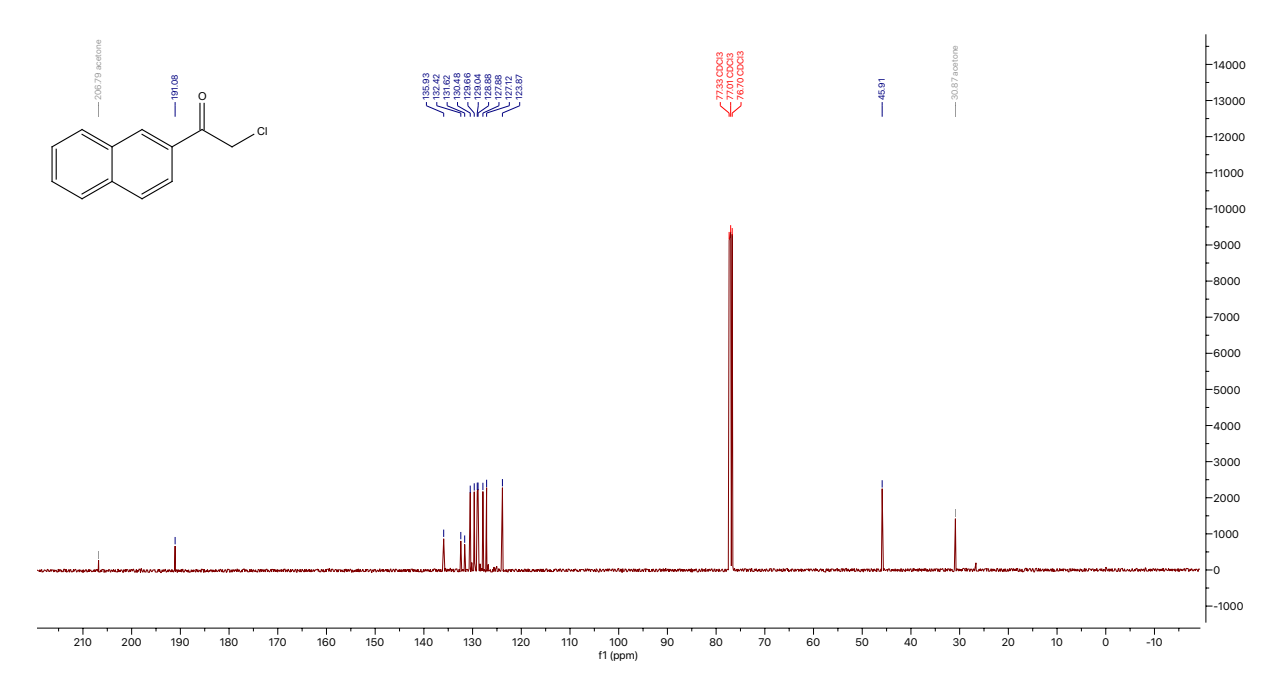
# <sup>13</sup>C NMR for 1-phenyl-2-(1*H*-tetrazol-5-yl)ethan-1-one (**1d**)



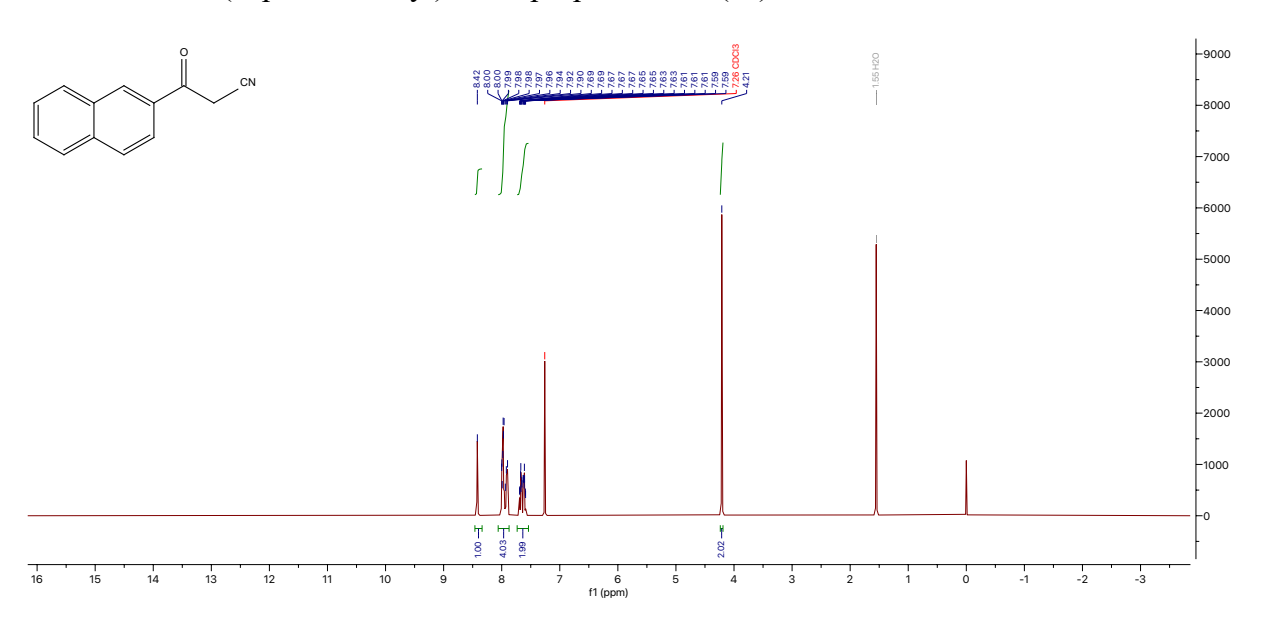
<sup>1</sup>H NMR for 2-chloro-1-(naphthalen-2-yl)ethan-1-one (**2b**)



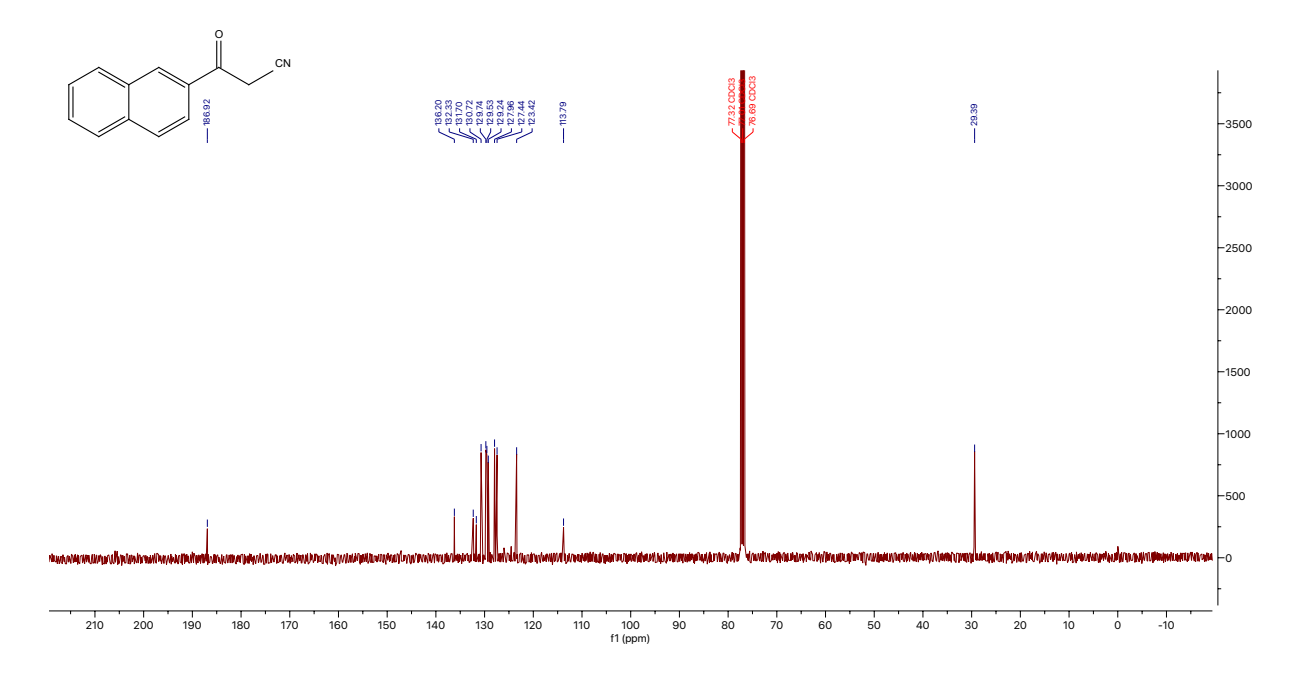
<sup>13</sup>C NMR for 2-chloro-1-(naphthalen-2-yl)ethan-1-one (**2b**)



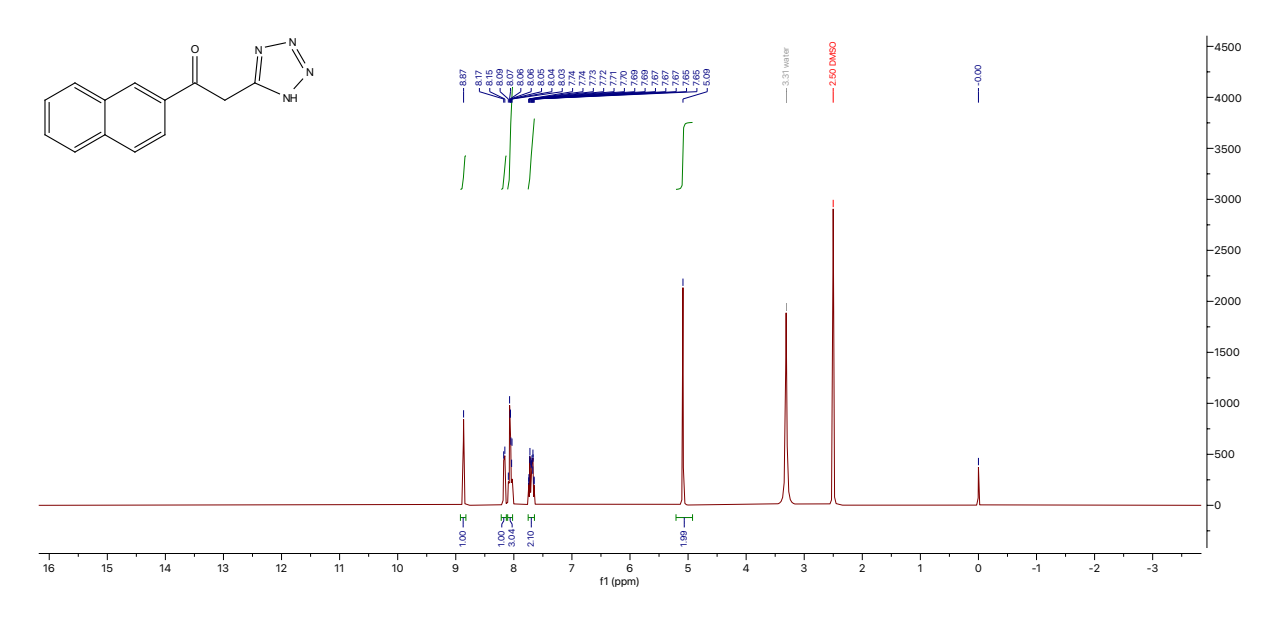
<sup>1</sup>H NMR for 3-(naphthalen-2-yl)-3-oxopropanenitrile (2c)



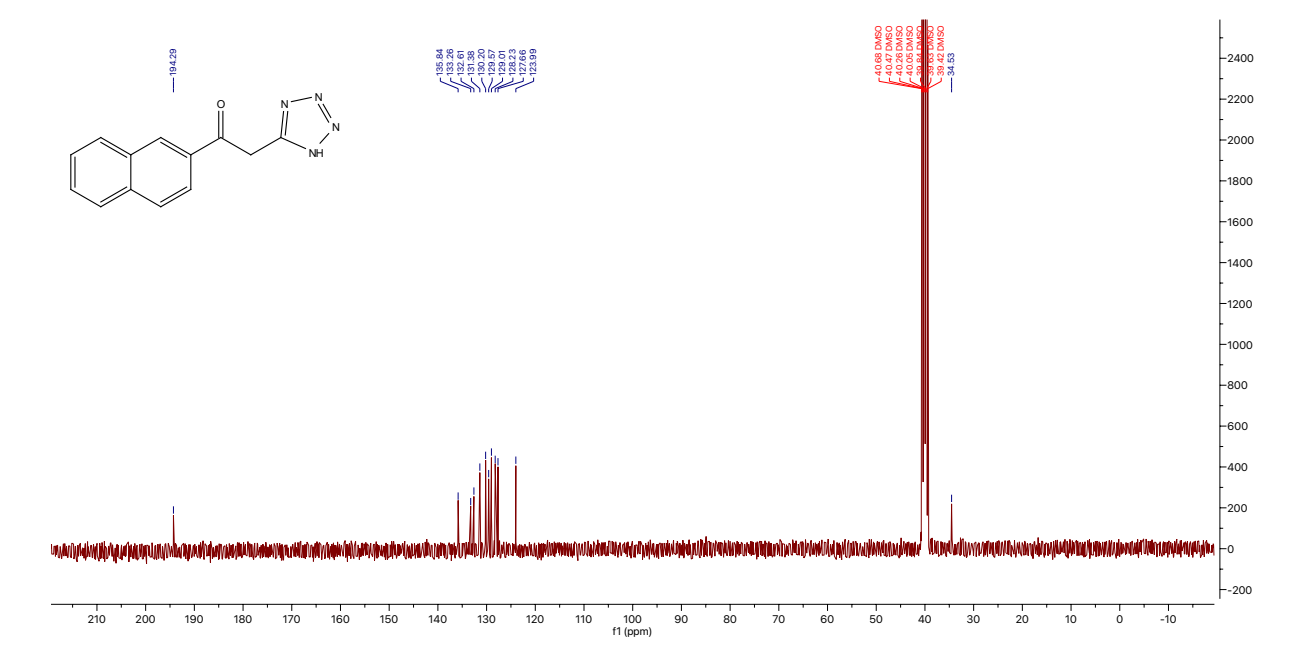
 $^{13}$ C NMR for 3-(naphthalen-2-yl)-3-oxopropanenitrile (2c)



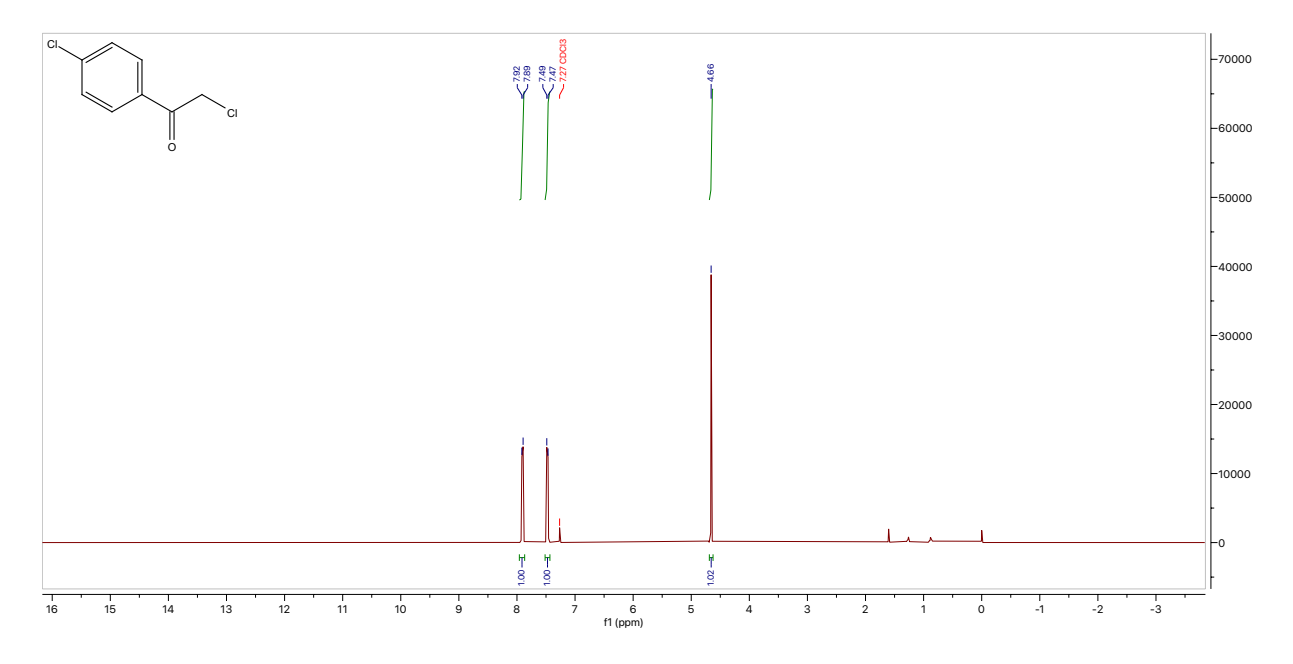
 $^1\mathrm{H}$  NMR for 1-(naphthalen-2-yl)-2-(1H-tetrazol-5-yl)ethan-1-one (2d)



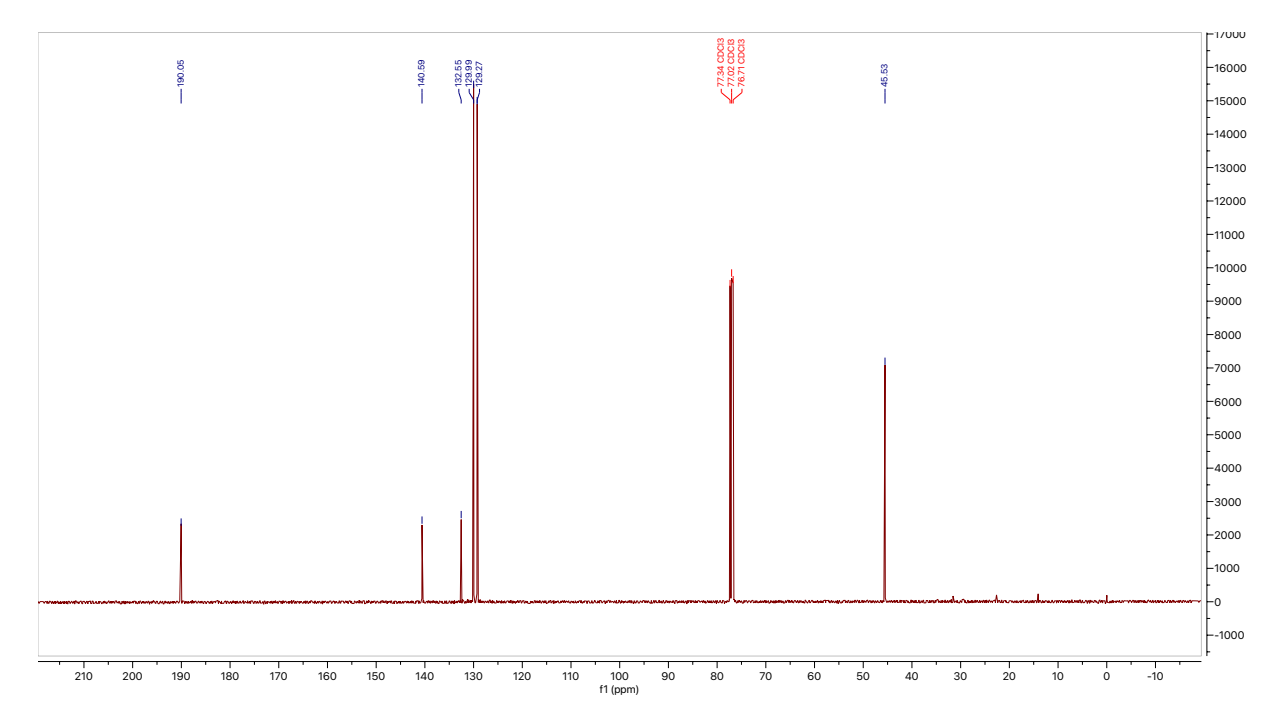
 $^{13}\mathrm{C}$  NMR for 1-(naphthalen-2-yl)-2-(1*H*-tetrazol-5-yl)ethan-1-one (\mathbf{2d})



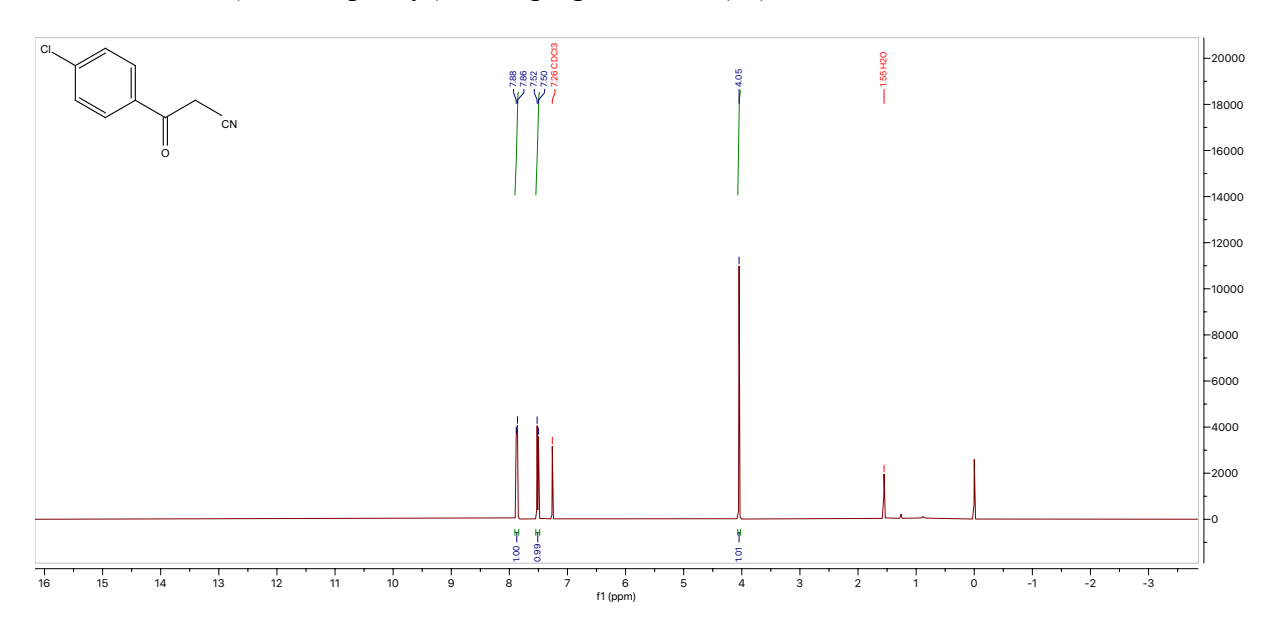
<sup>1</sup>H NMR for 2-chloro-1-(4-chlorophenyl) ethan-1-one (**3b**)



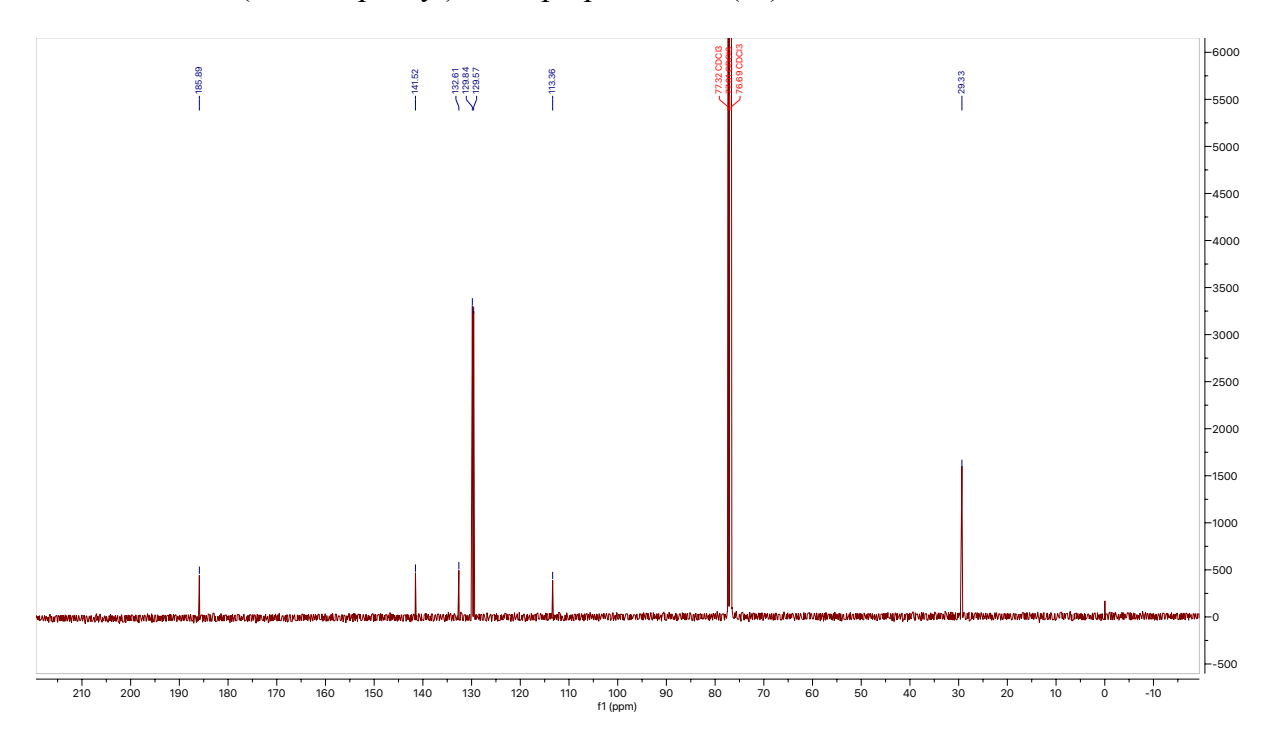
<sup>13</sup>C NMR for 2-chloro-1-(4-chlorophenyl) ethan-1-one (**b**)



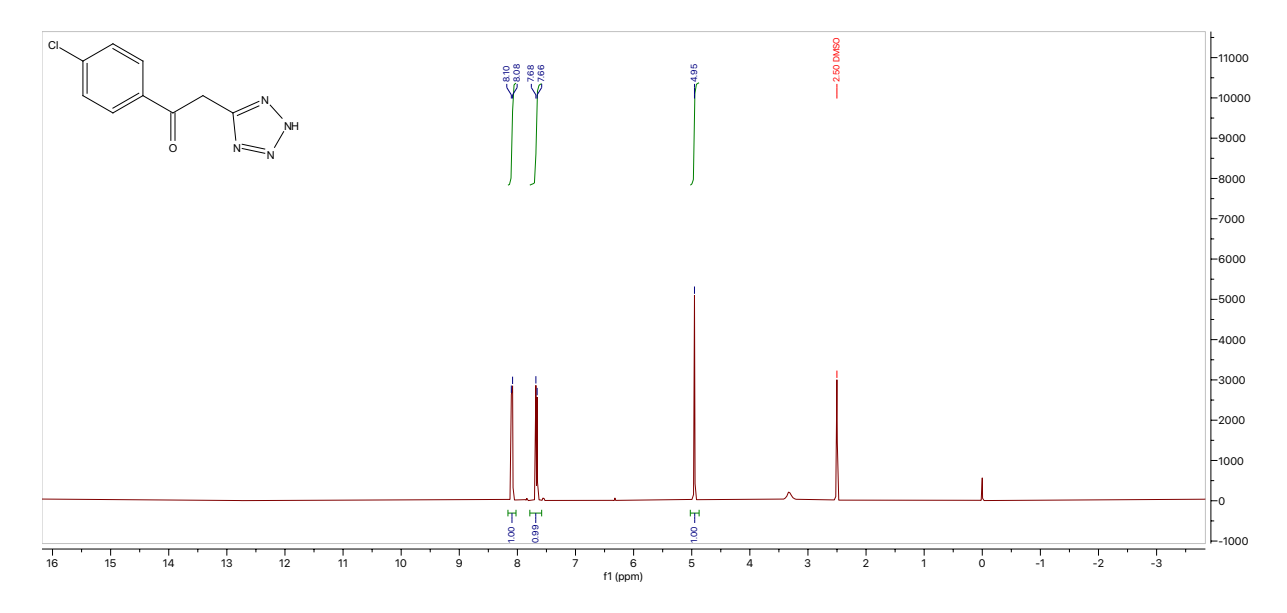
<sup>1</sup>H NMR for 3-(4-chlorophenyl)-3-oxopropanenitrile (**3c**)



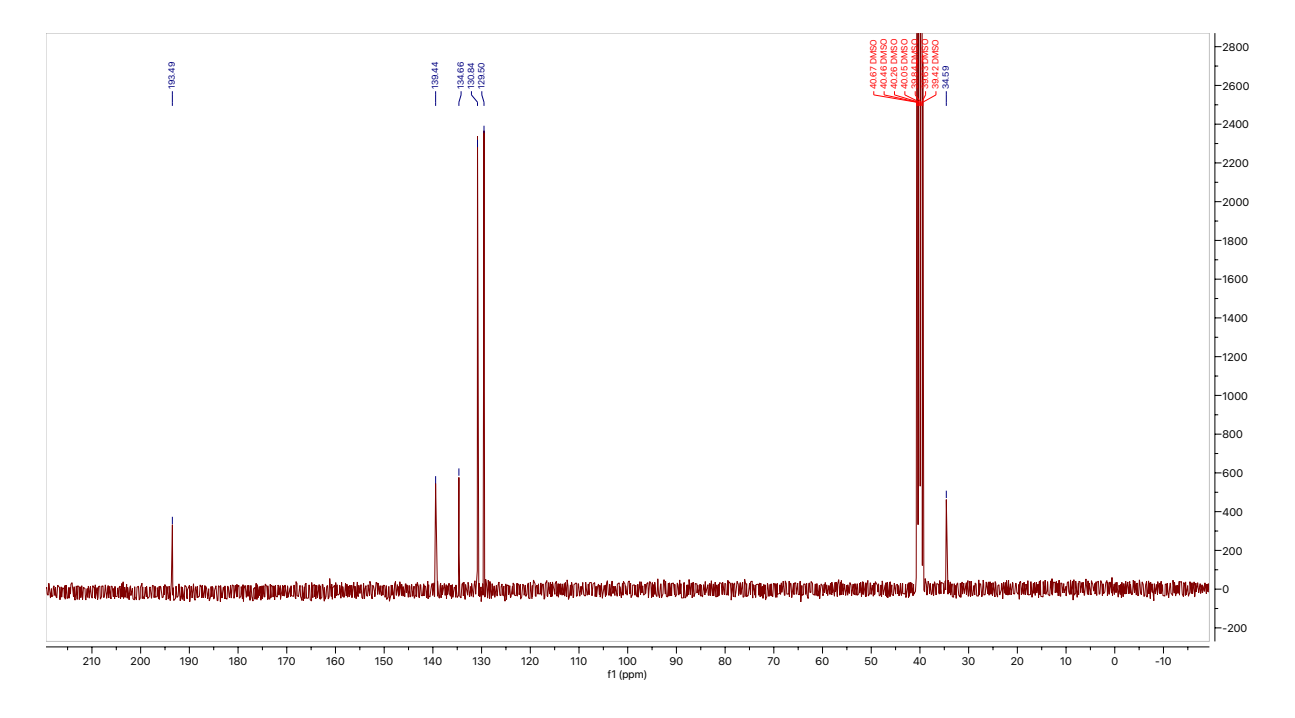
<sup>13</sup>C NMR for 3-(4-chlorophenyl)-3-oxopropanenitrile (3c)



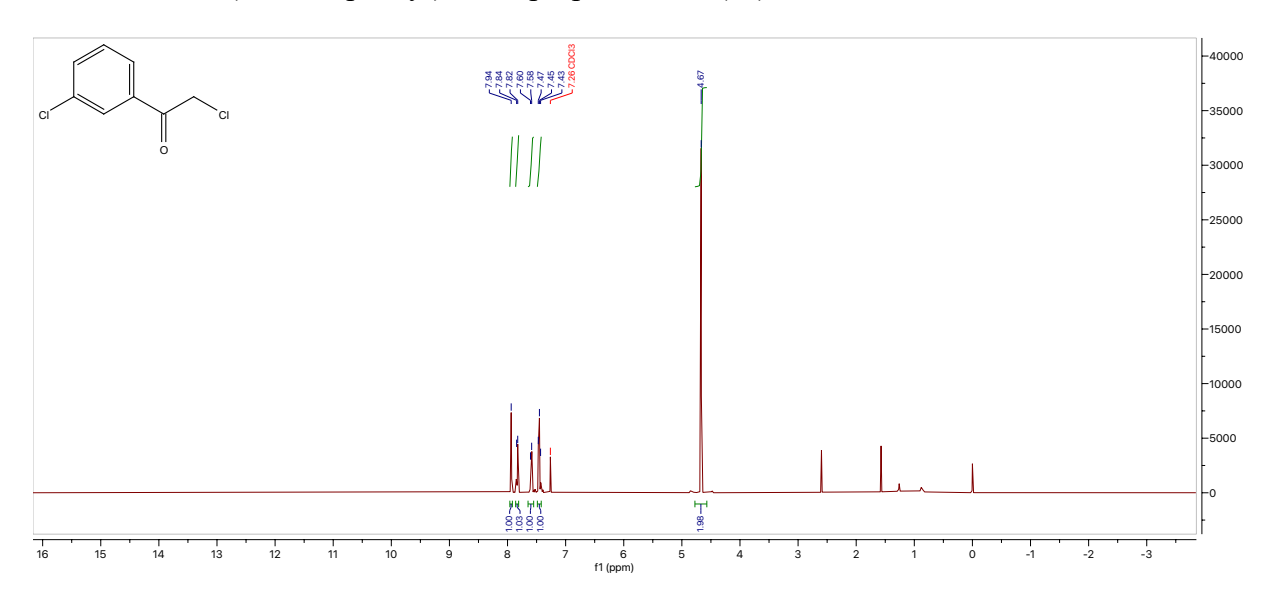
<sup>1</sup>H NMR for 1-(4-chlorophenyl)-2-(1*H*-tetrazol-5-yl)ethan-1-one (**3d**)



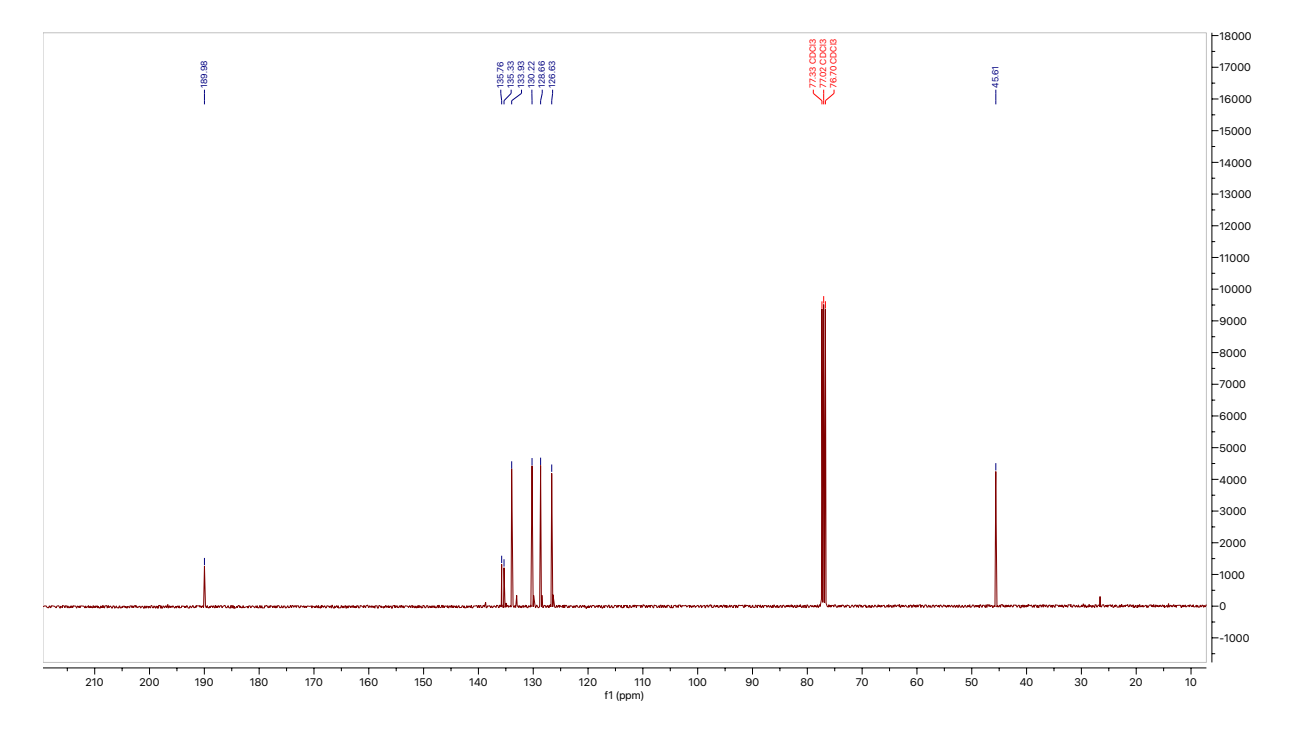
<sup>13</sup>C NMR for 1-(4-chlorophenyl)-2-(1*H*-tetrazol-5-yl)ethan-1-one (**3d**)



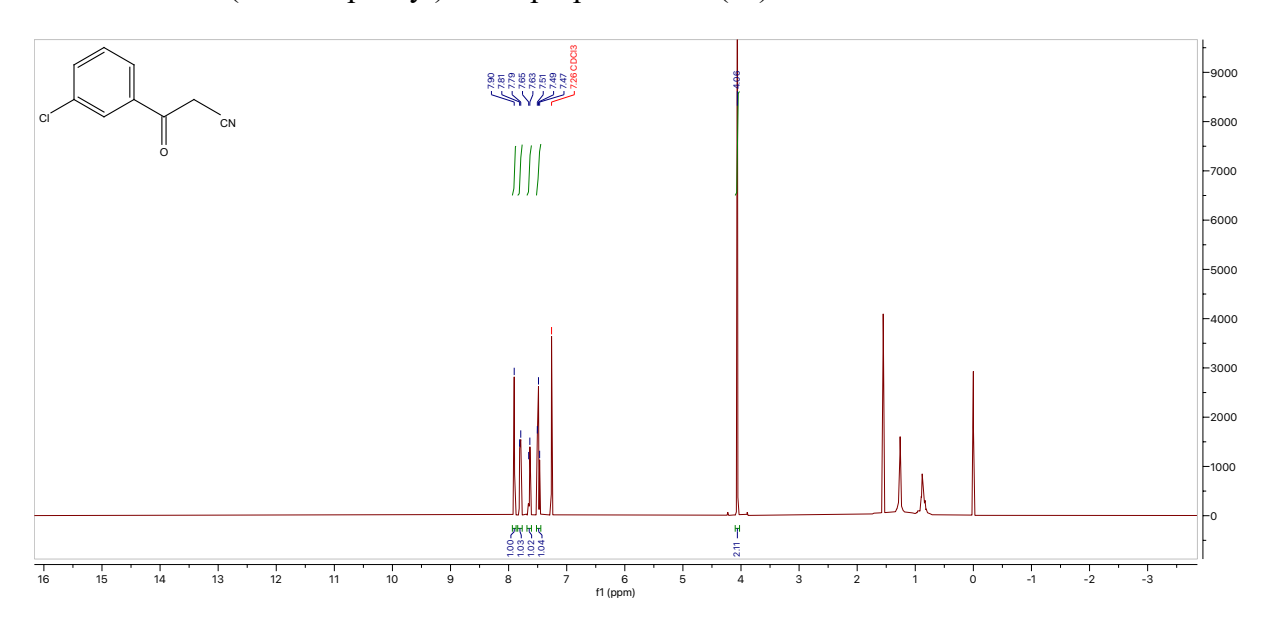
 $^{1}\text{H NMR}$  for 3-(3-chlorophenyl)-3-oxopropanenitrile (4 $\mathbf{c}$ )



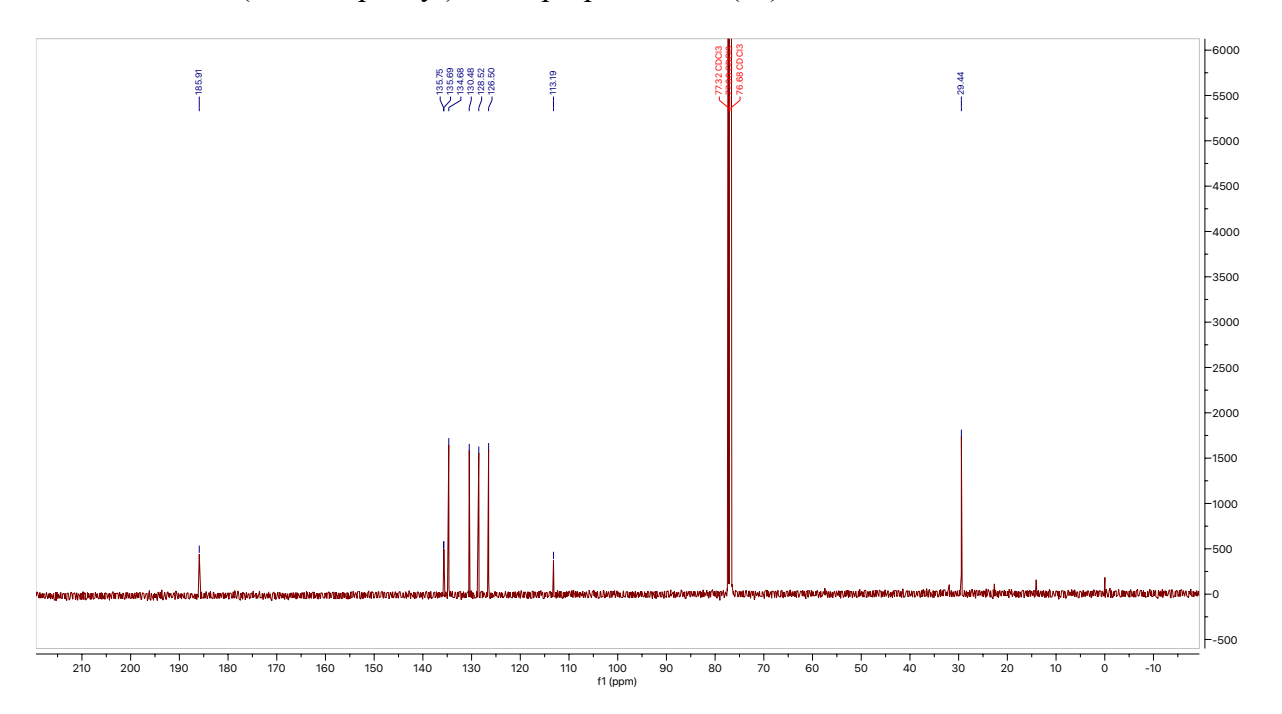
<sup>13</sup>C NMR for 3-(3-chlorophenyl)-3-oxopropanenitrile (4c)



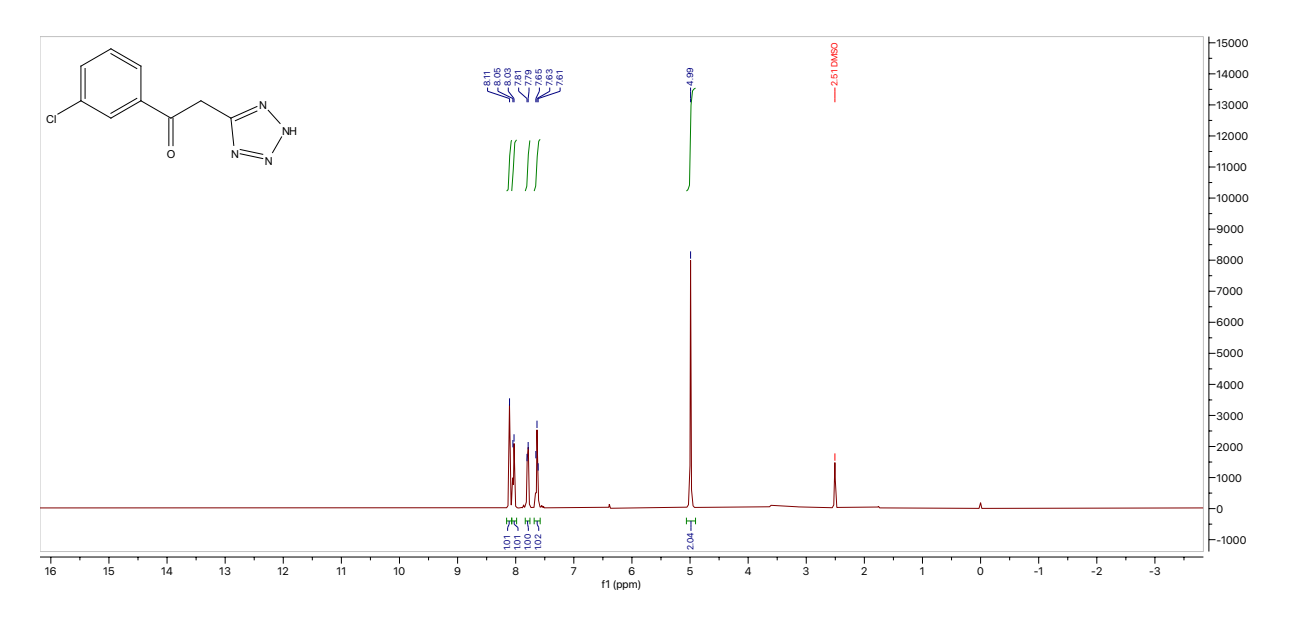
<sup>1</sup>H NMR for 3-(3-chlorophenyl)-3-oxopropanenitrile (**4c**)



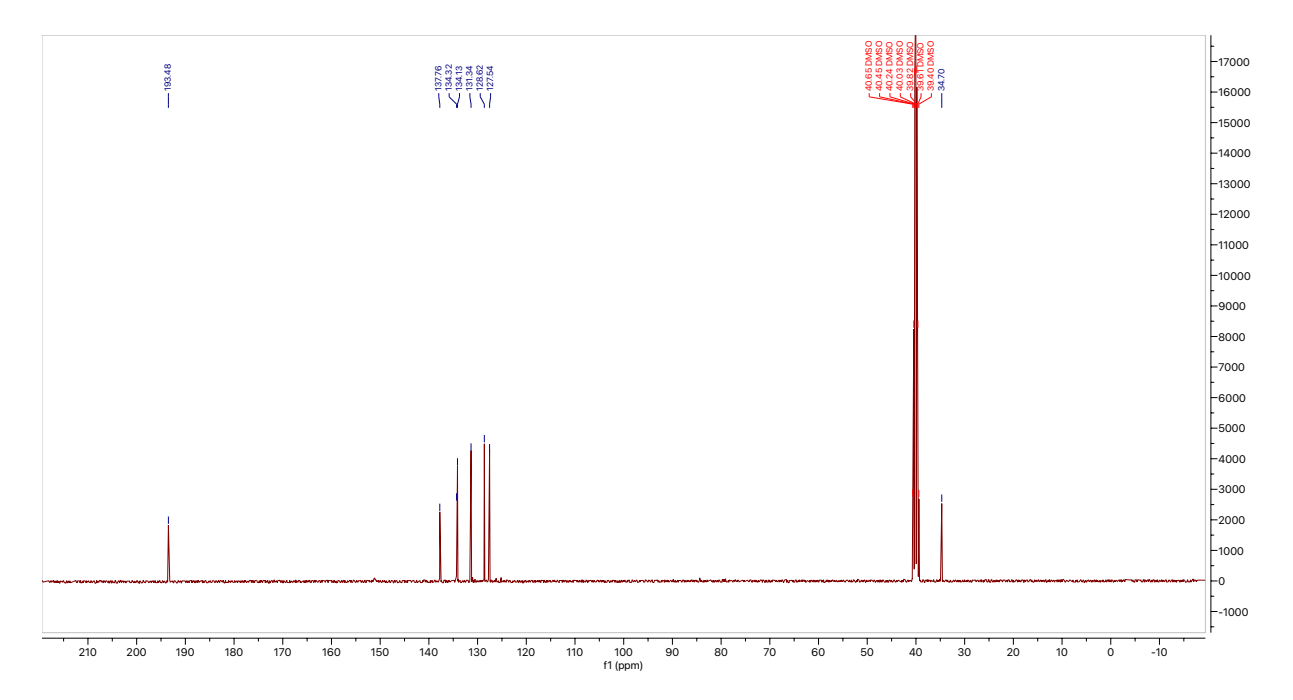
<sup>13</sup>C NMR for 3-(3-chlorophenyl)-3-oxopropanenitrile (**4c**)



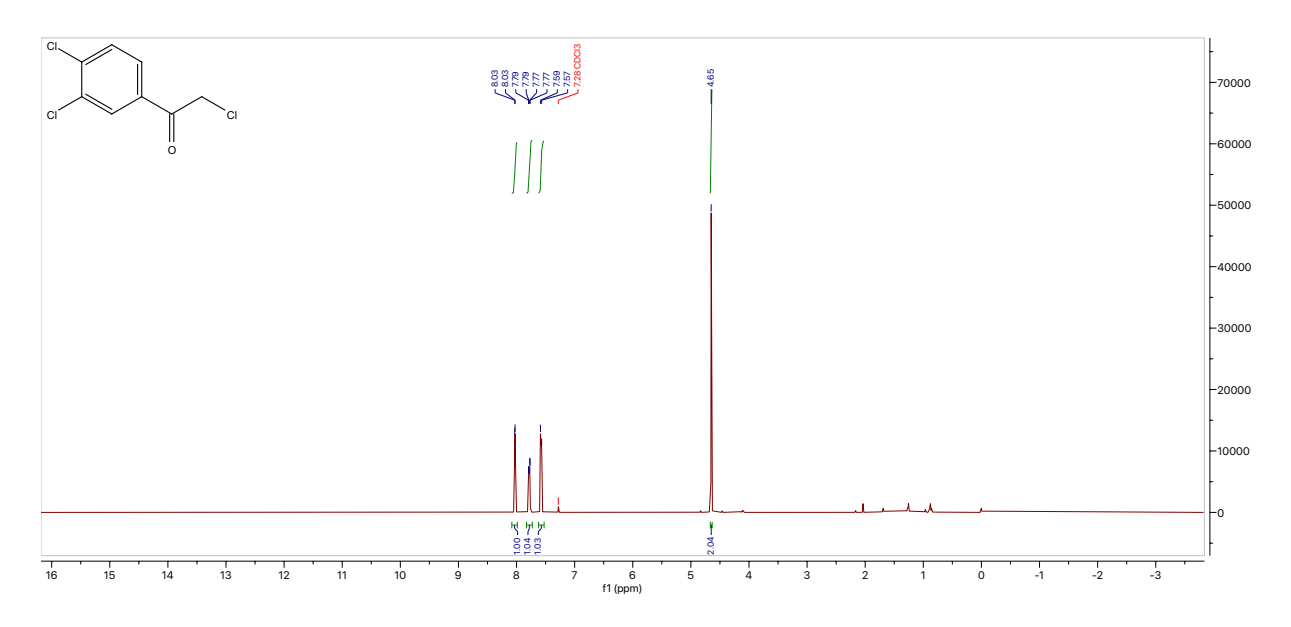
<sup>1</sup>H NMR for 1-(3-chlorophenyl)-2-(1*H*-tetrazol-5-yl)ethan-1-one (**4d**)



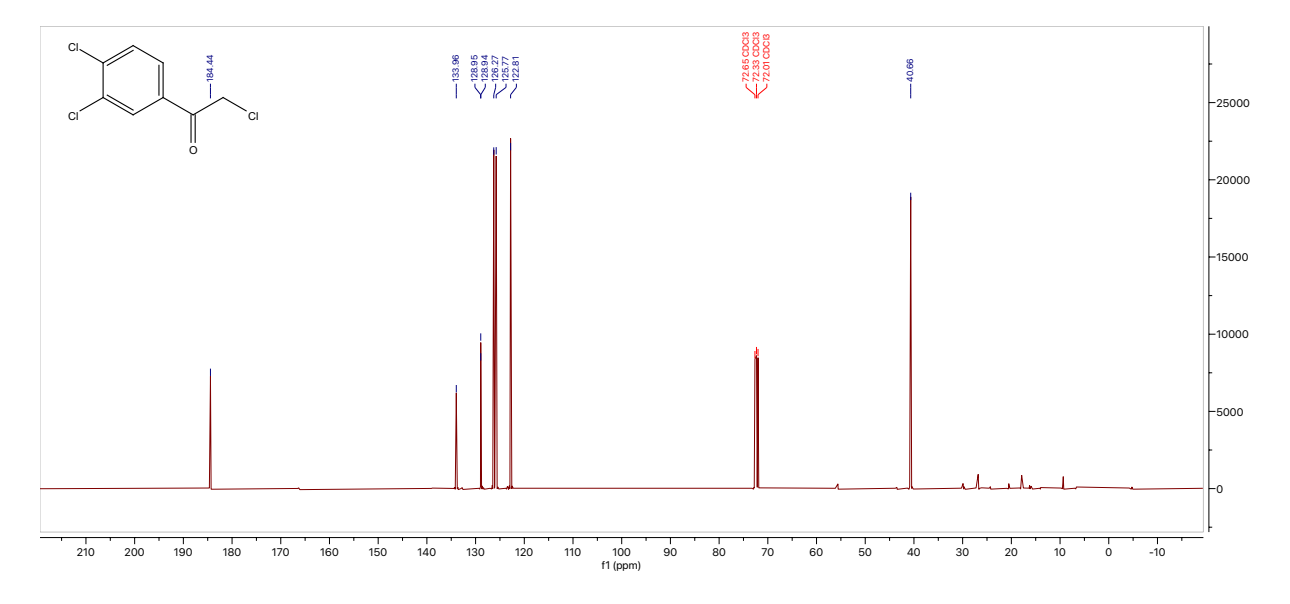
<sup>13</sup>C NMR for 1-(3-chlorophenyl)-2-(1*H*-tetrazol-5-yl)ethan-1-one (**4d**)



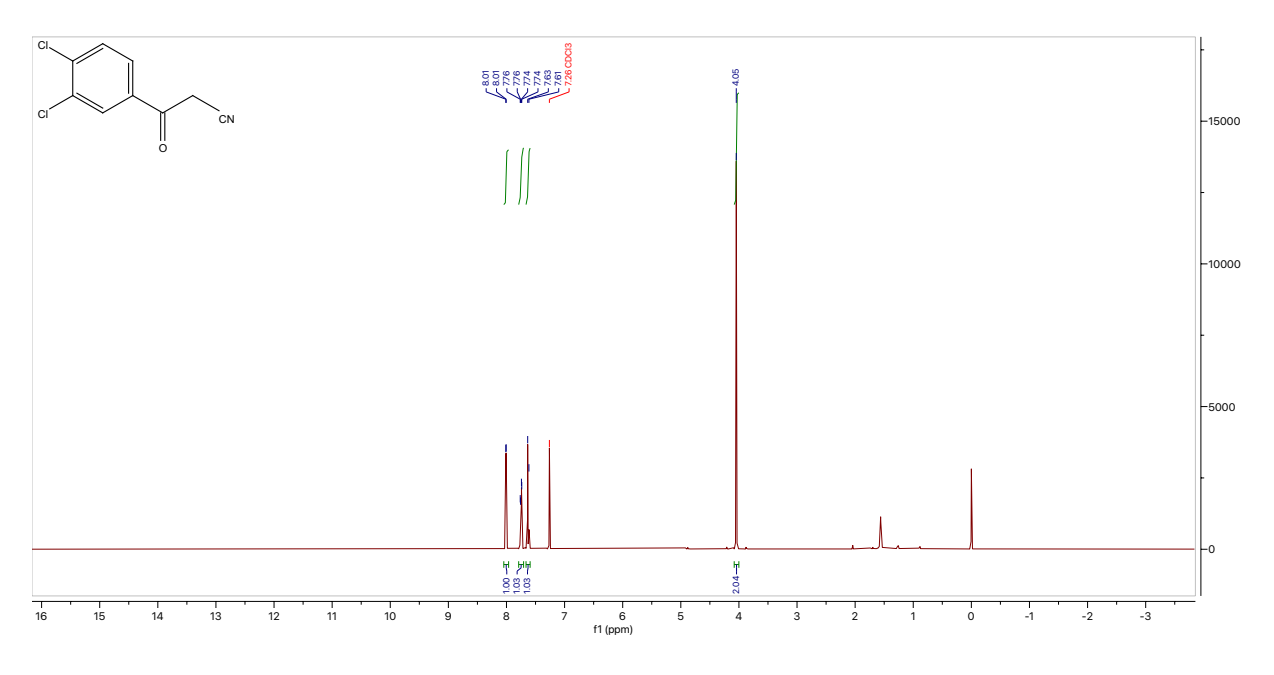
<sup>1</sup>H NMR for 2-chloro-1-(3,4-dichlorophenyl)ethan-1-one (**5b**)



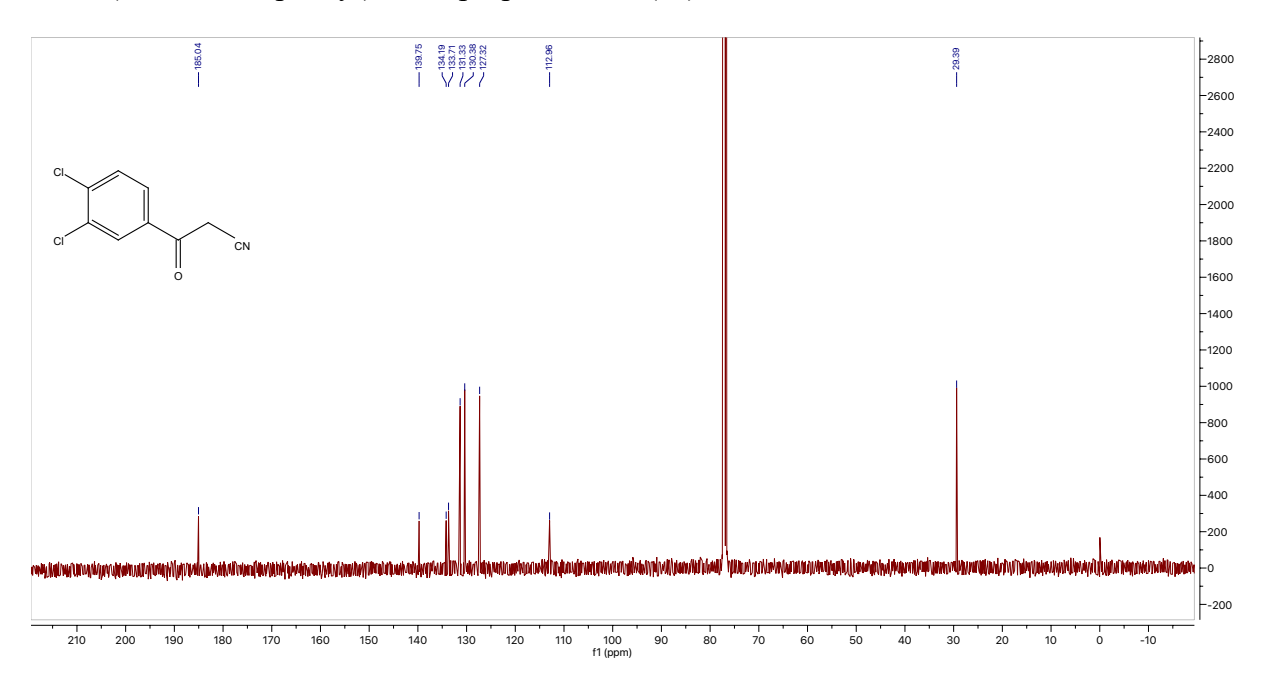
<sup>13</sup>C NMR for 2-chloro-1-(3,4-dichlorophenyl)ethan-1-one (**5b**)



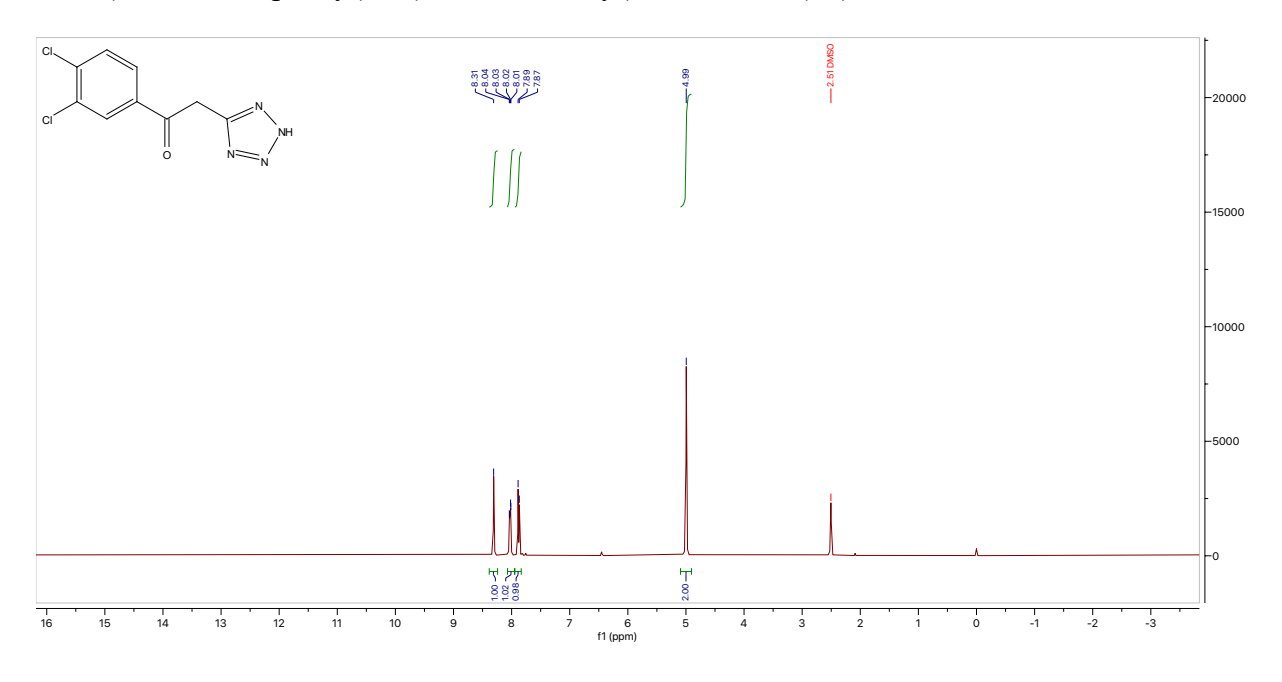
<sup>1</sup>H 3-(3,4-dichlorophenyl)-3-oxopropanenitrile (**5c**)



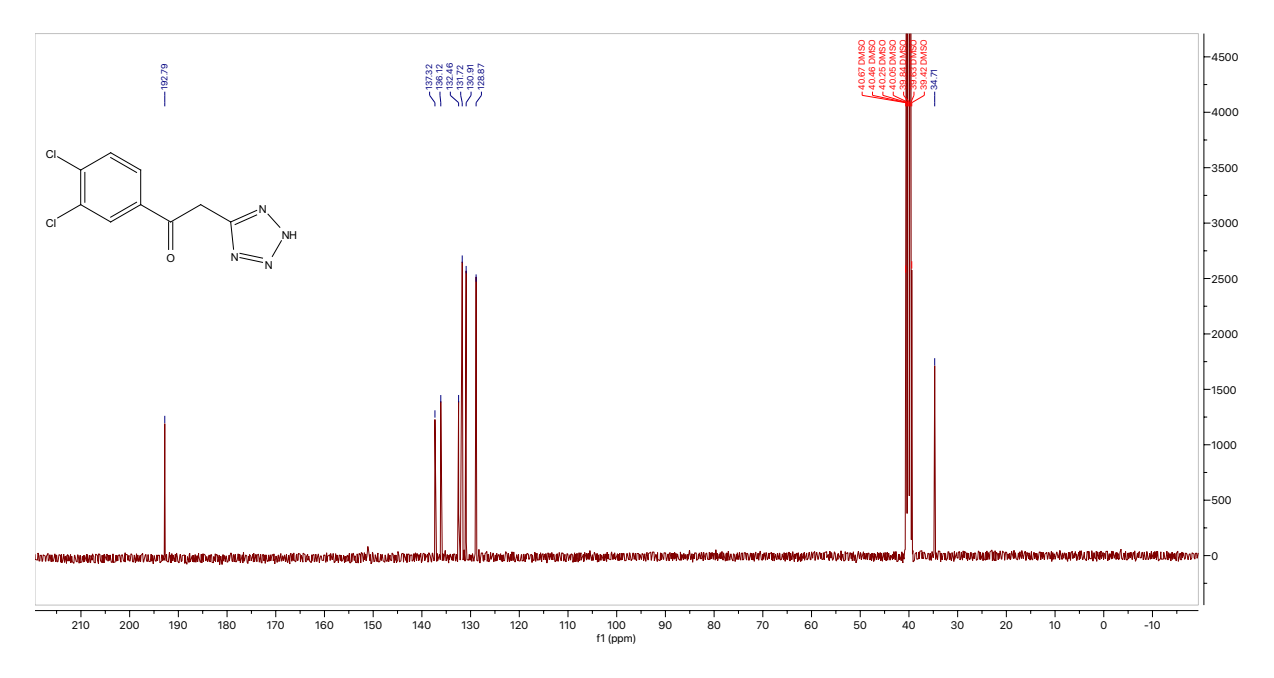
<sup>13</sup>C 3-(3,4-dichlorophenyl)-3-oxopropanenitrile (**5c**)



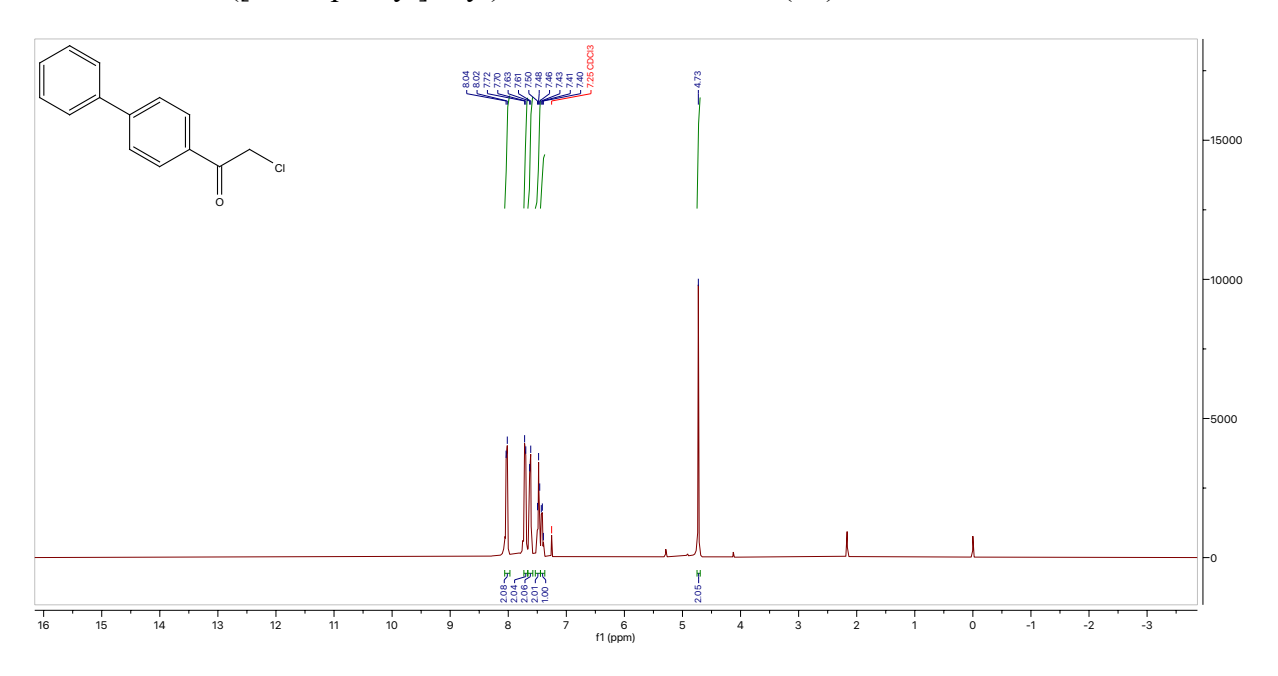
 $^{1}$ H 1-(3,4-dichlorophenyl)-2-(1H-tetrazol-5-yl)ethan-1-one (5 $\mathbf{d}$ )



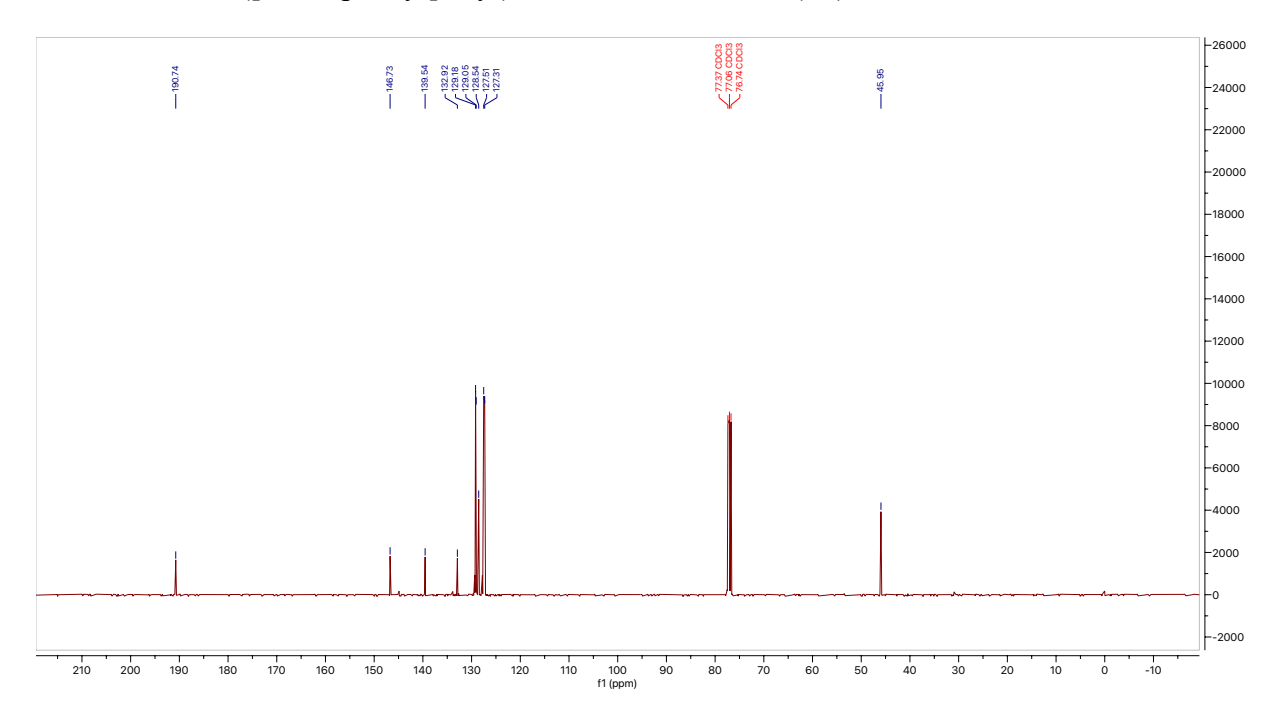
 $^{13}$ C 1-(3,4-dichlorophenyl)-2-(1H-tetrazol-5-yl)ethan-1-one (5 $\mathbf{d}$ )



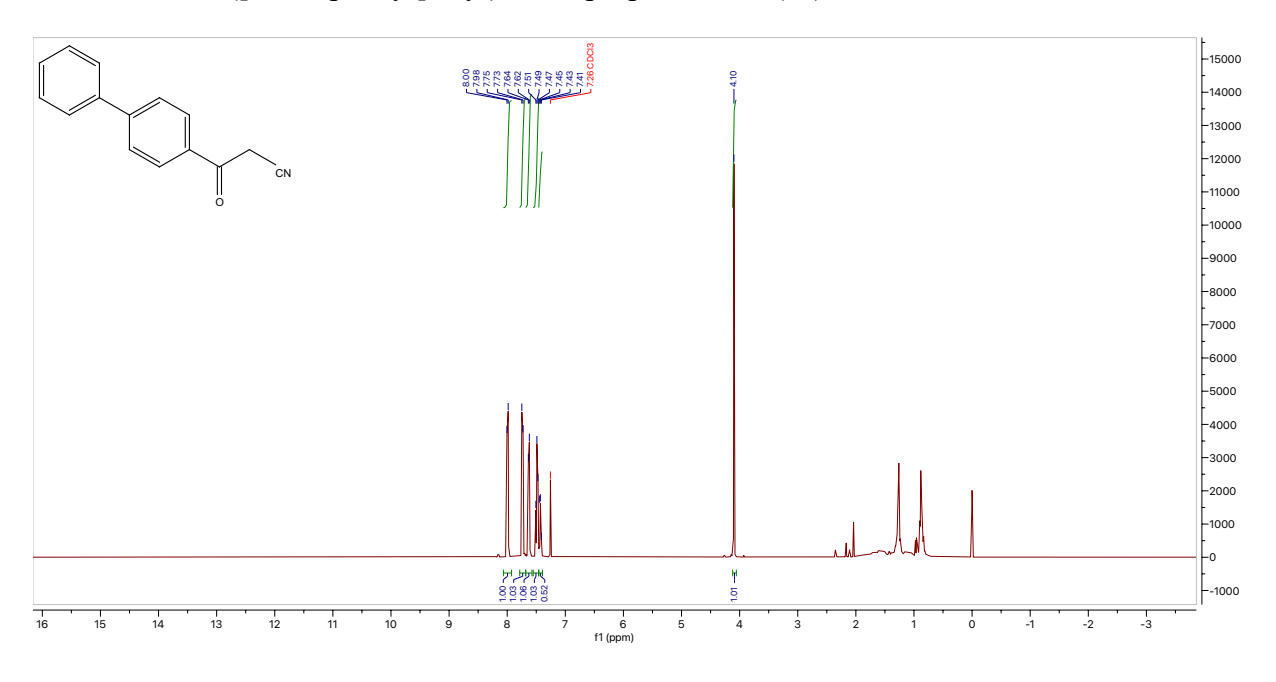
<sup>1</sup>H NMR for 1-([1,1'-biphenyl]-4-yl)-2-chloroethan-1-one (**6b**)



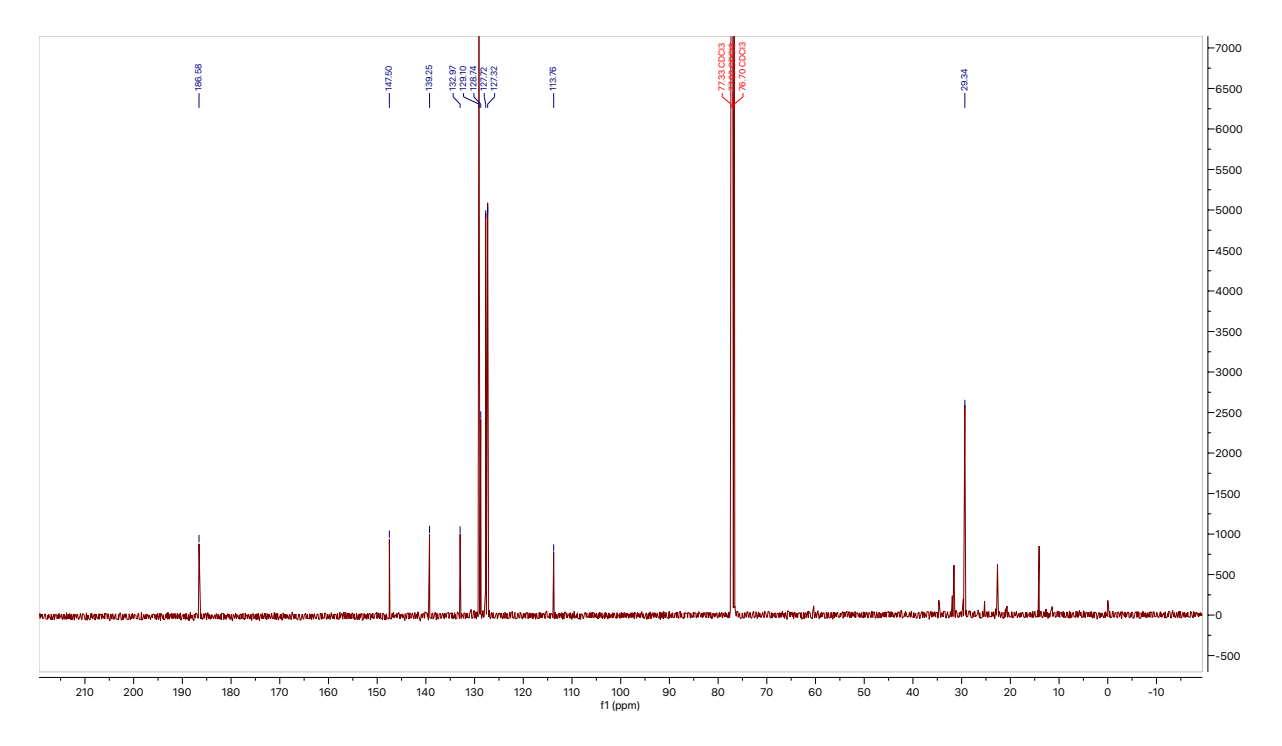
<sup>13</sup>C NMR for 1-([1,1'-biphenyl]-4-yl)-2-chloroethan-1-one (**6b**)



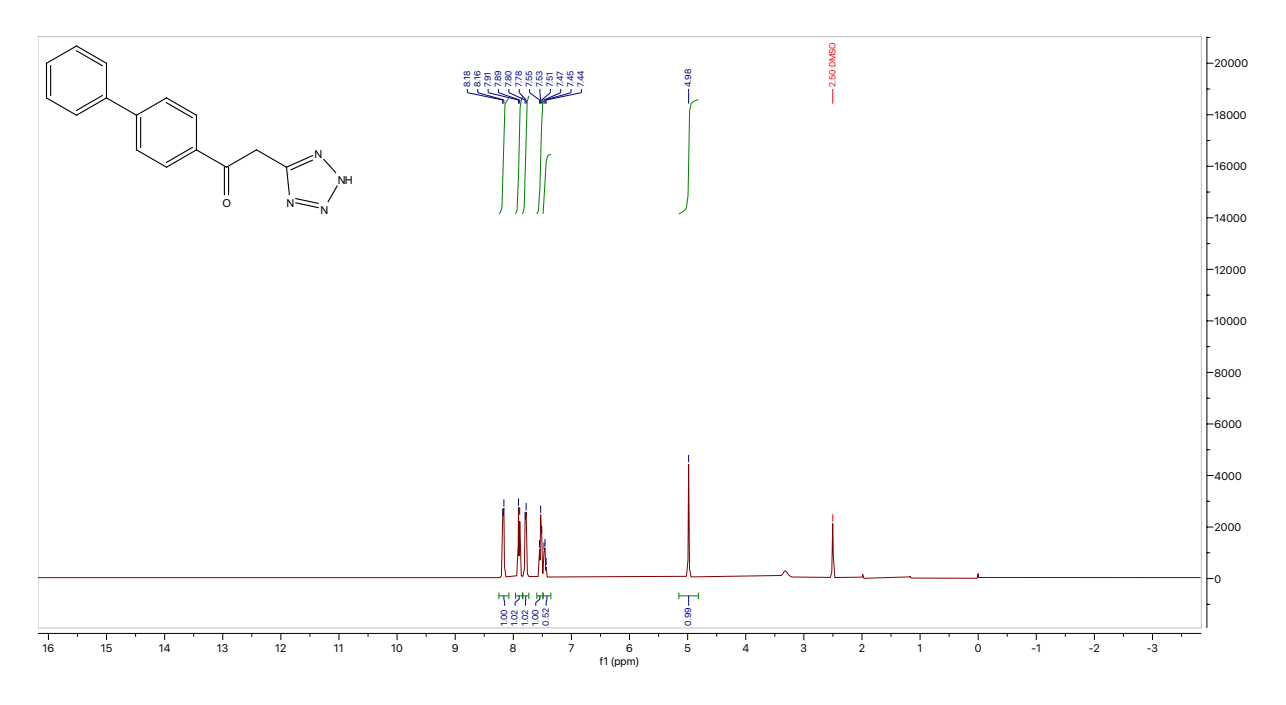
<sup>1</sup>H NMR for 3-([1,1'-biphenyl]-4-yl)-3-oxopropanenitrile (**6c**)



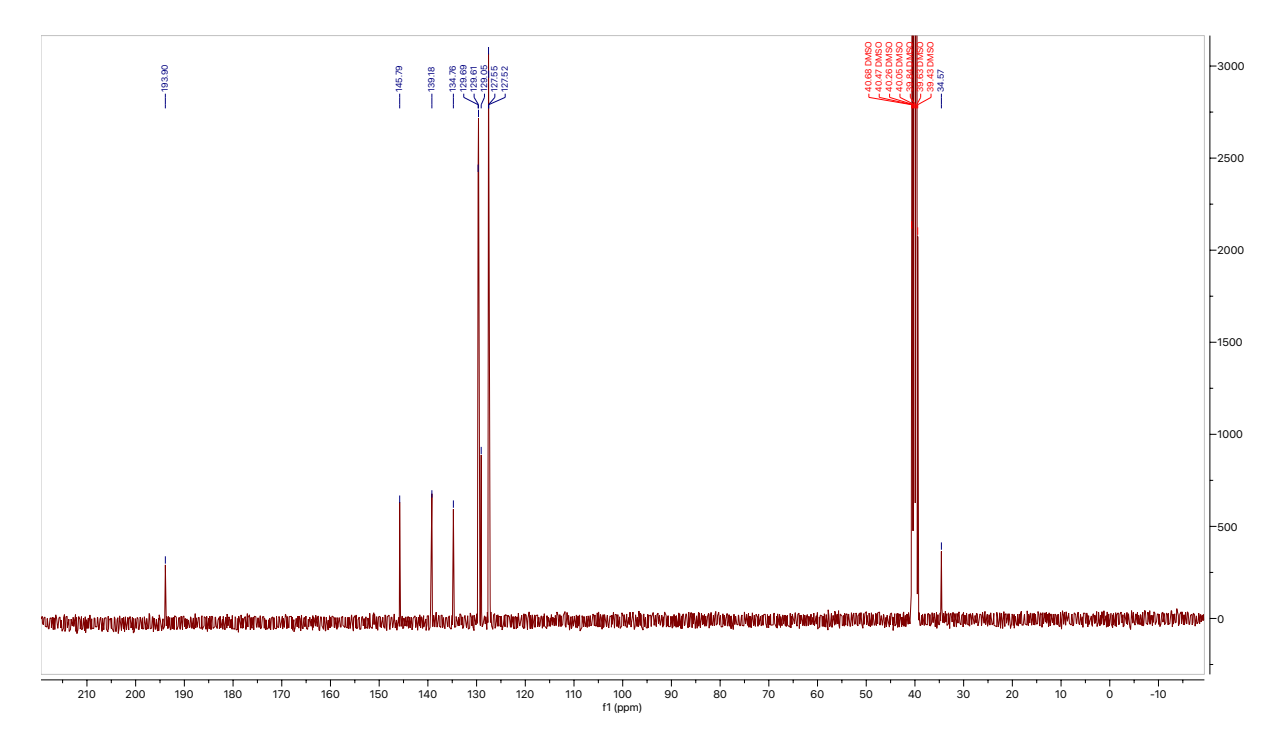
<sup>13</sup>C NMR for 3-([1,1'-biphenyl]-4-yl)-3-oxopropanenitrile (**6c**)



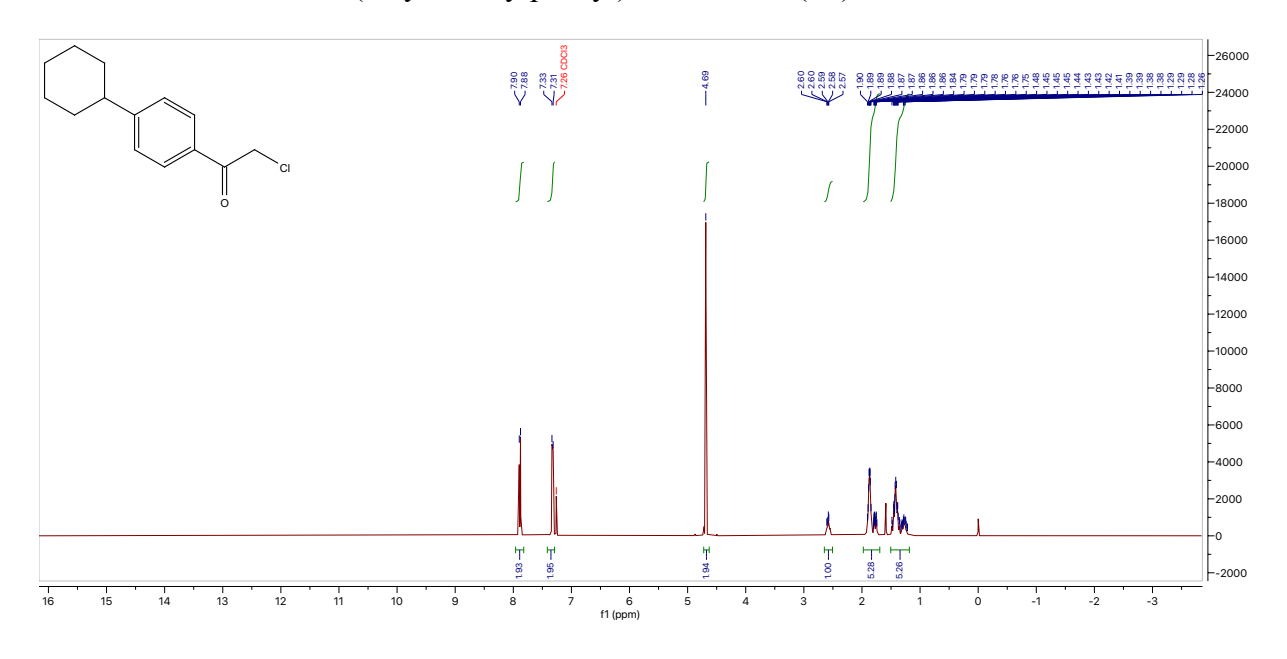
<sup>1</sup>H NMR for 1-([1,1'-biphenyl]-4-yl)-2-(1*H*-tetrazol-5-yl)ethan-1-one (**6d**)



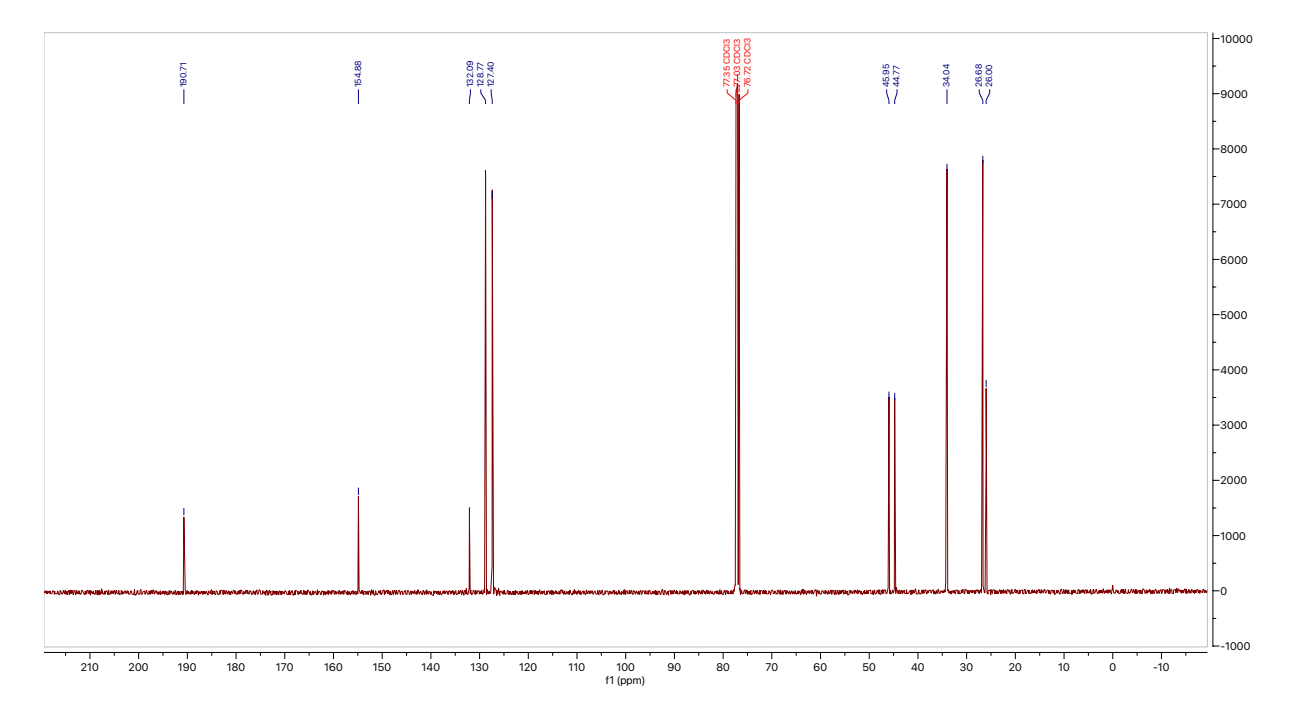
<sup>13</sup>C NMR for 1-([1,1'-biphenyl]-4-yl)-2-(1*H*-tetrazol-5-yl)ethan-1-one (**6d**)



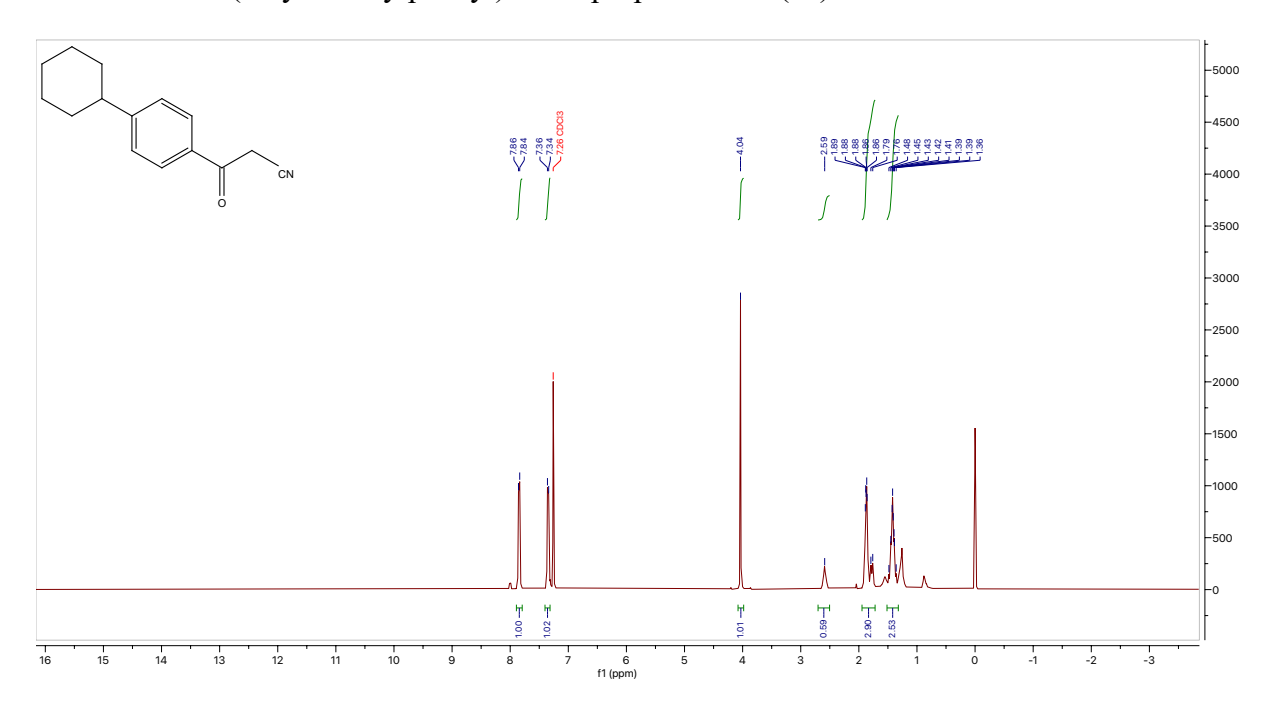
<sup>1</sup>H NMR for 2-chloro-1-(4-cyclohexylphenyl) ethan-1-one (**7b**)



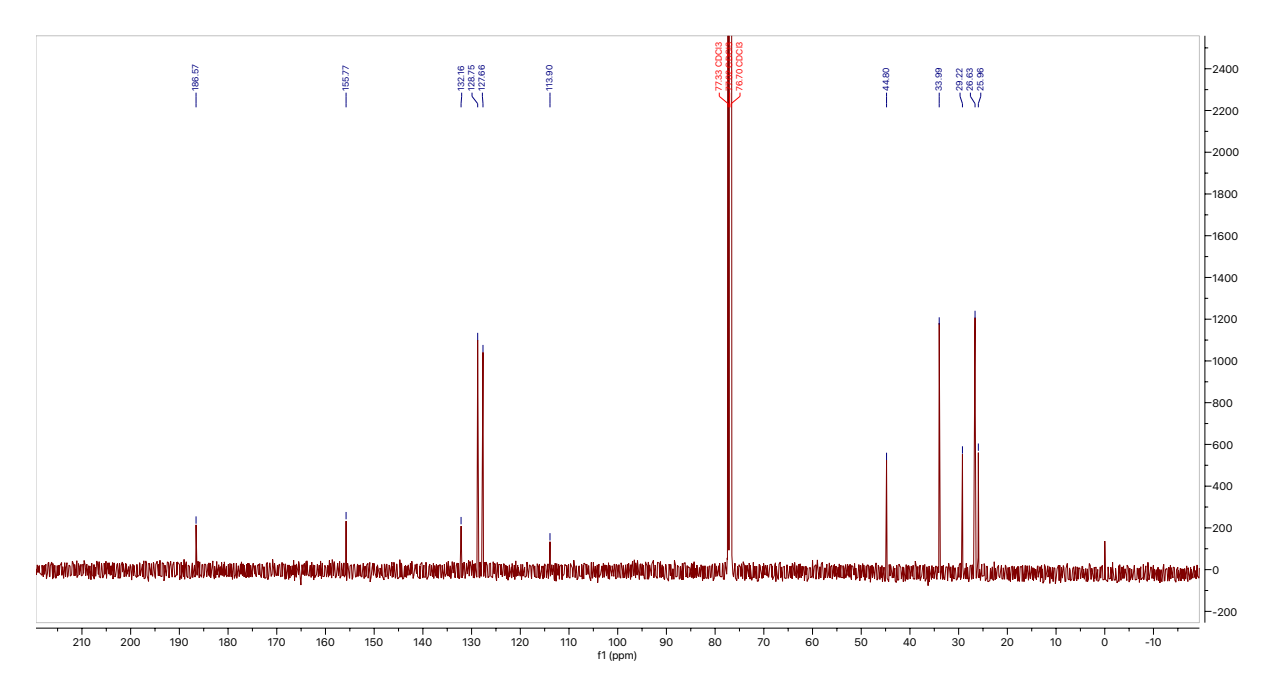
<sup>13</sup>C NMR for 2-chloro-1-(4-cyclohexylphenyl) ethan-1-one (**7b**)



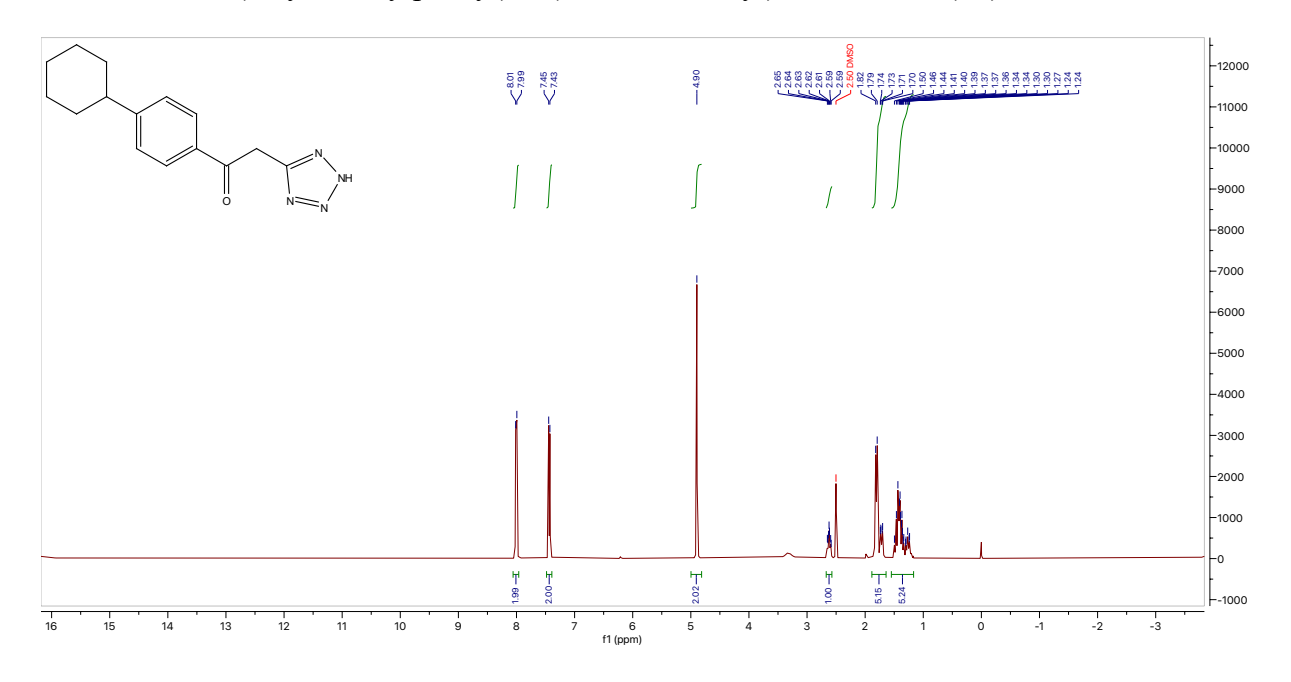
<sup>1</sup>H NMR for 3-(4-cyclohexylphenyl)-3-oxopropanenitrile (7c)



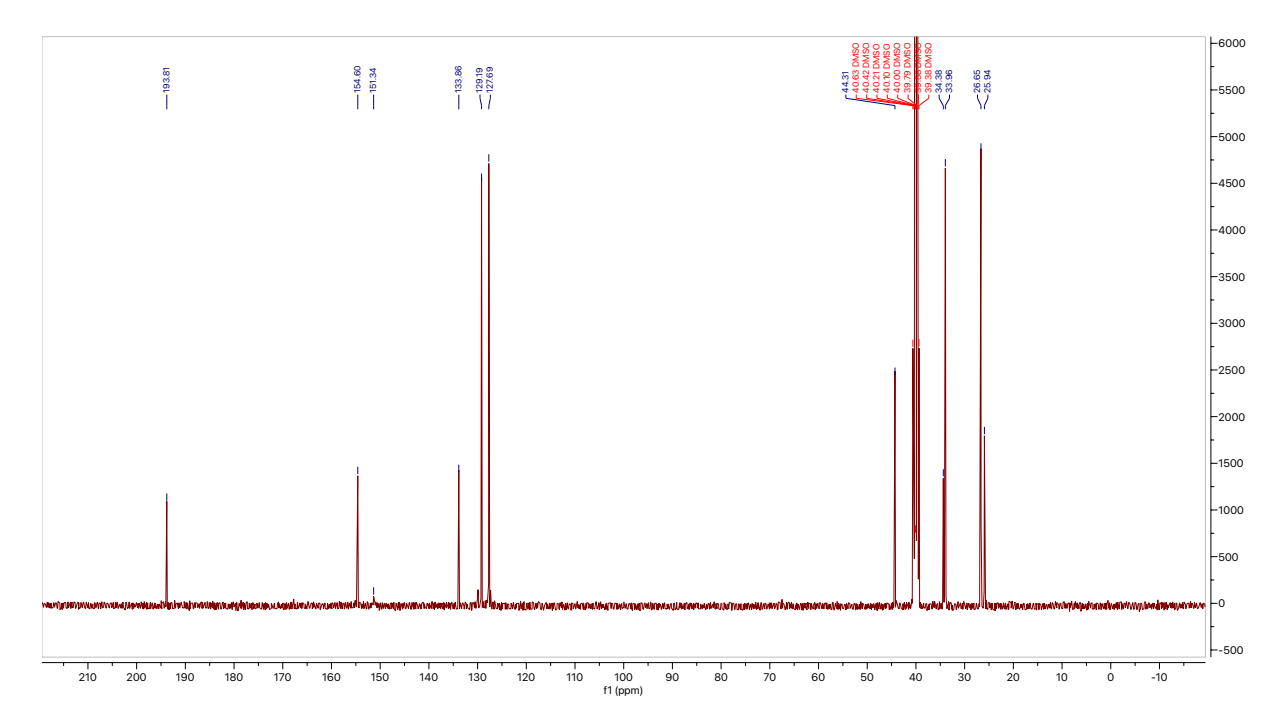
<sup>13</sup>C NMR for 3-(4-cyclohexylphenyl)-3-oxopropanenitrile (7c)



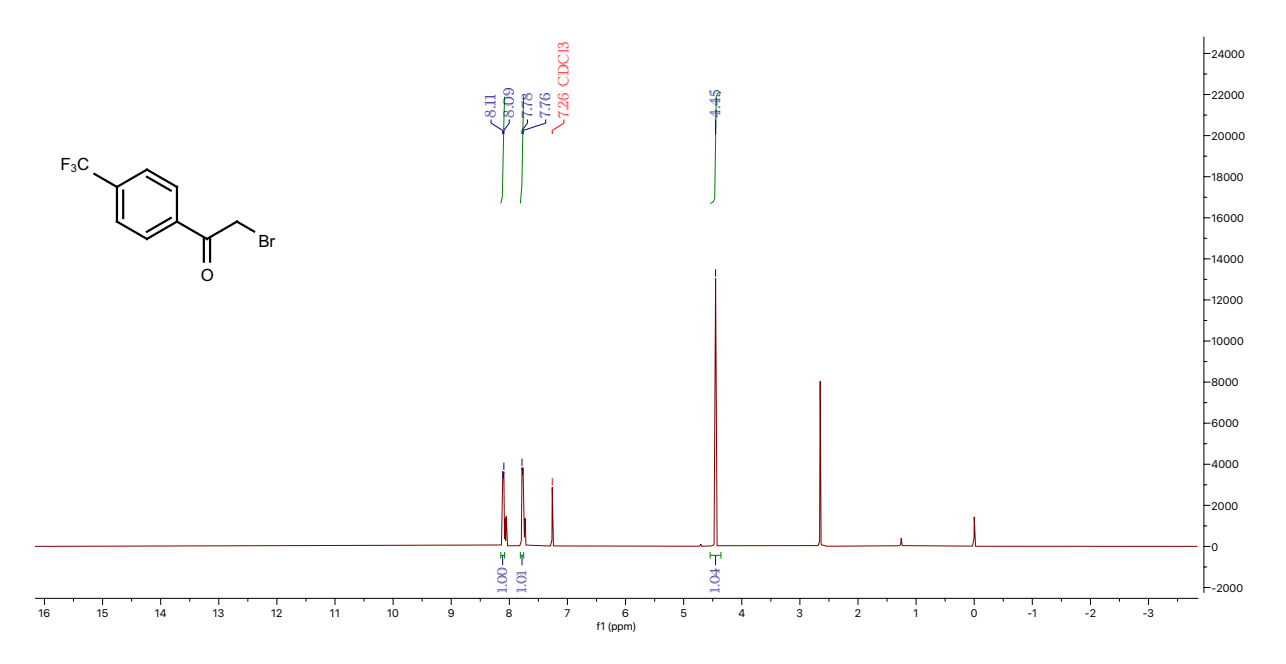
 $^1\mathrm{H}$  NMR for 1-(4-cyclohexylphenyl)-2-(1H-tetrazol-5-yl) ethan-1-one (7**d**)



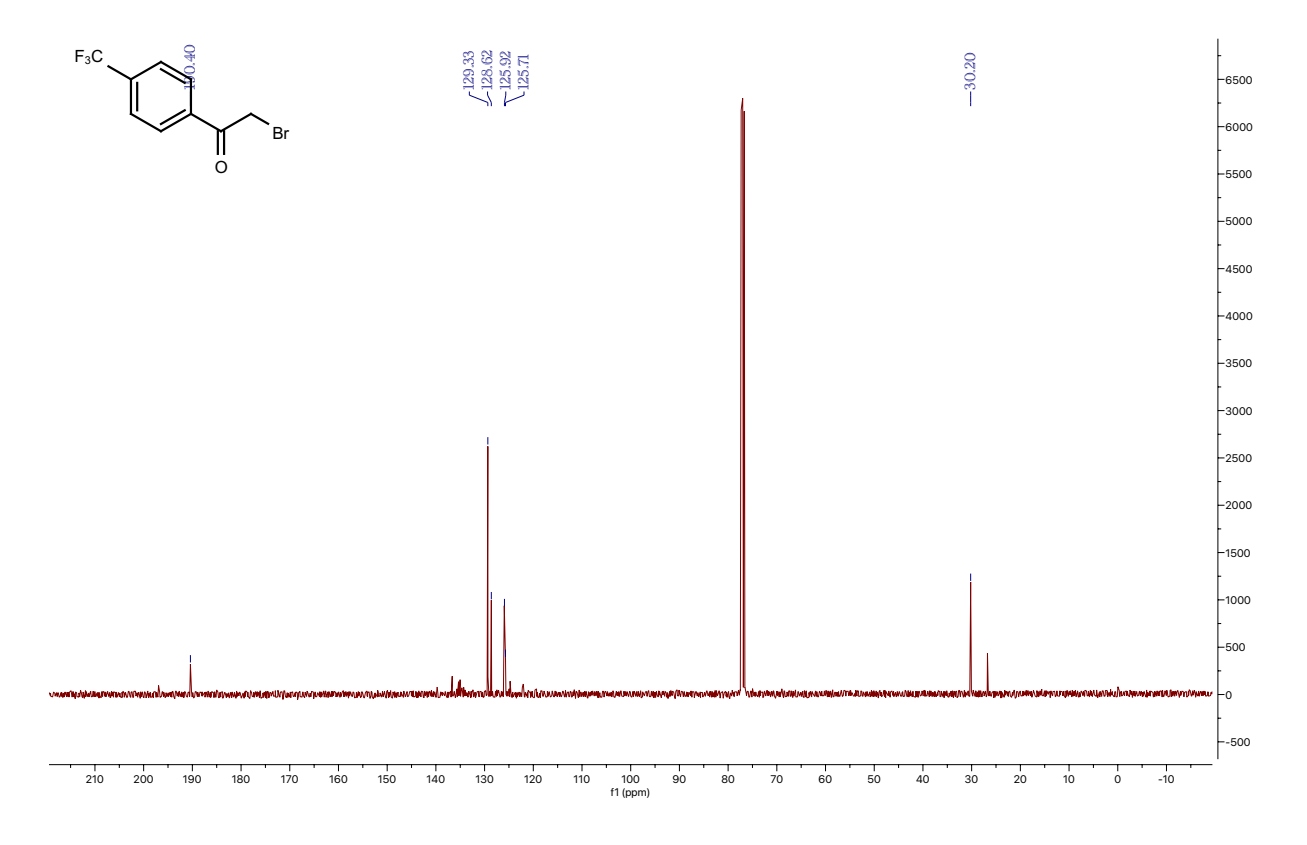
 $^{13}$ C NMR for 1-(4-cyclohexylphenyl)-2-(1H-tetrazol-5-yl) ethan-1-one (7**d**)



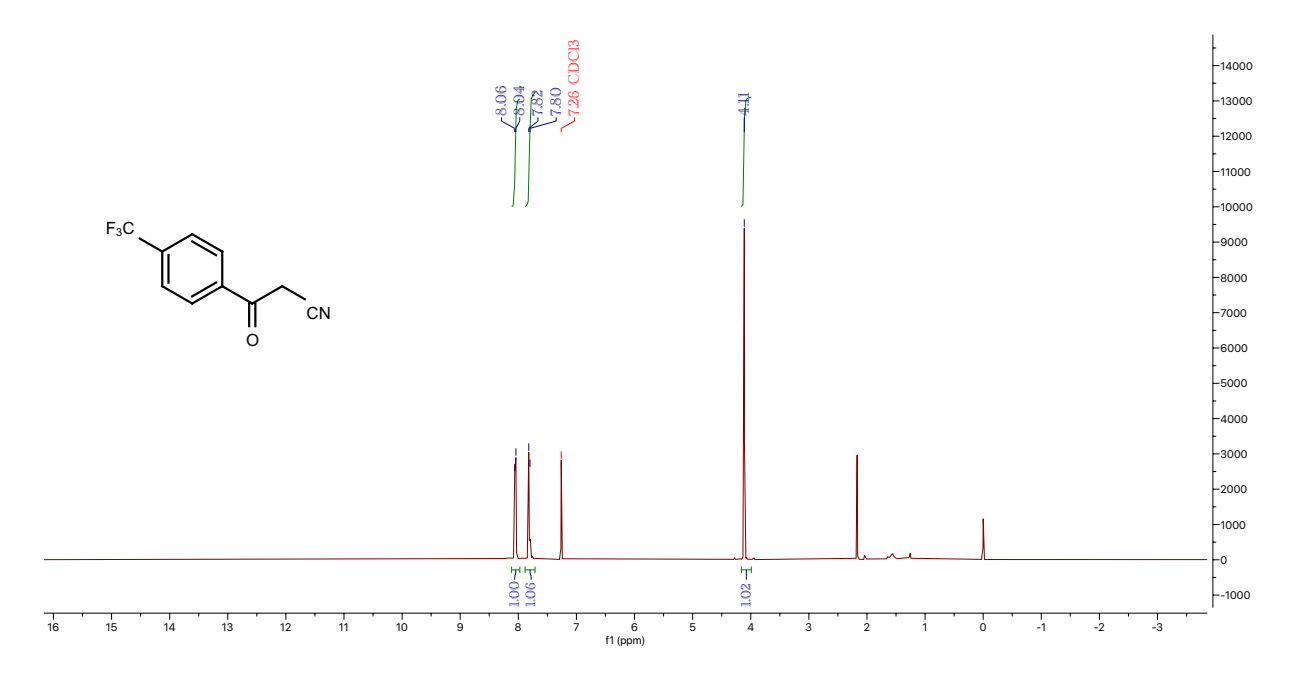
<sup>1</sup>H NMR for 2-bromo-1-(4-(trifluoromethyl)phenyl)ethan-1-one (**8b**)



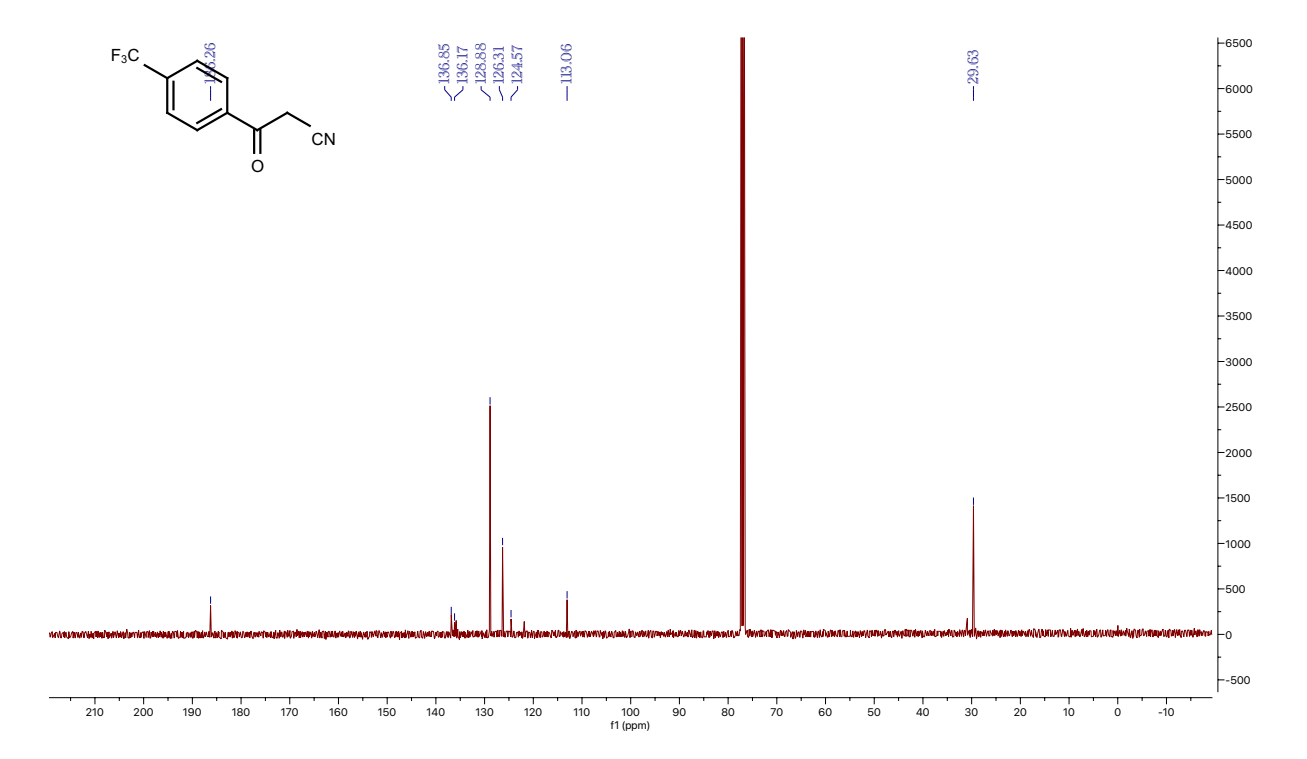
<sup>13</sup>C NMR for 2-bromo-1-(4-(trifluoromethyl)phenyl)ethan-1-one (8b)



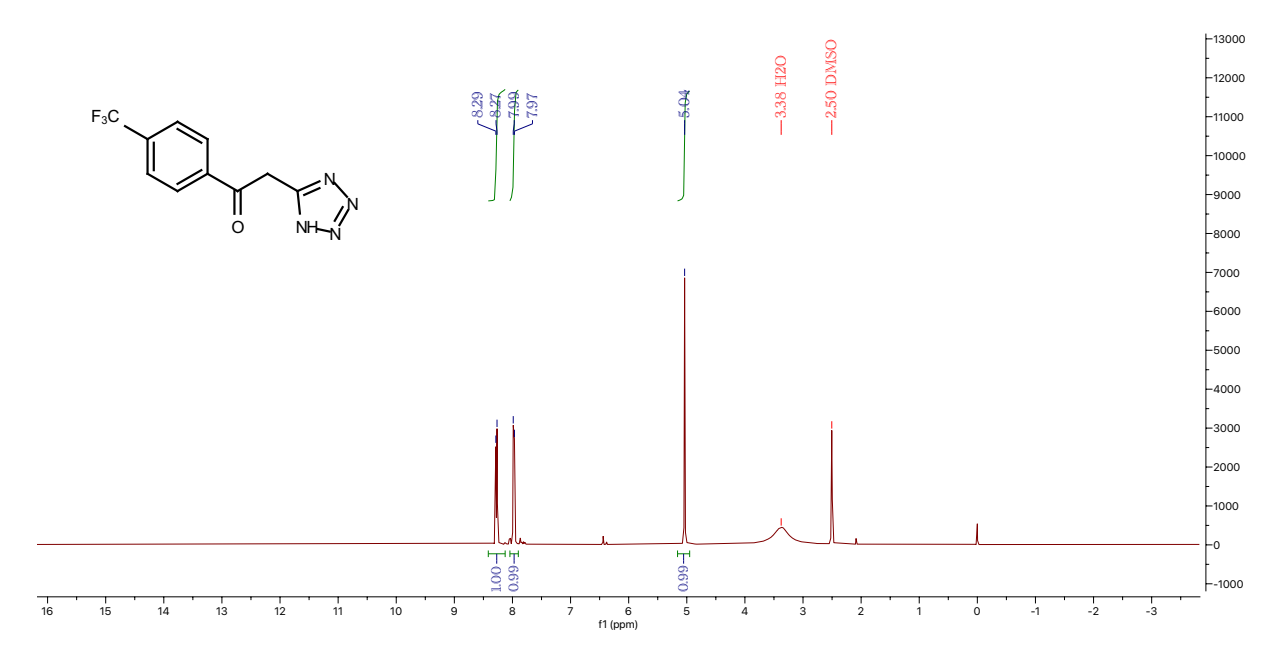
# <sup>1</sup>H NMR for 3-oxo-3-(4-(trifluoromethyl)phenyl)propanenitrile (8c)



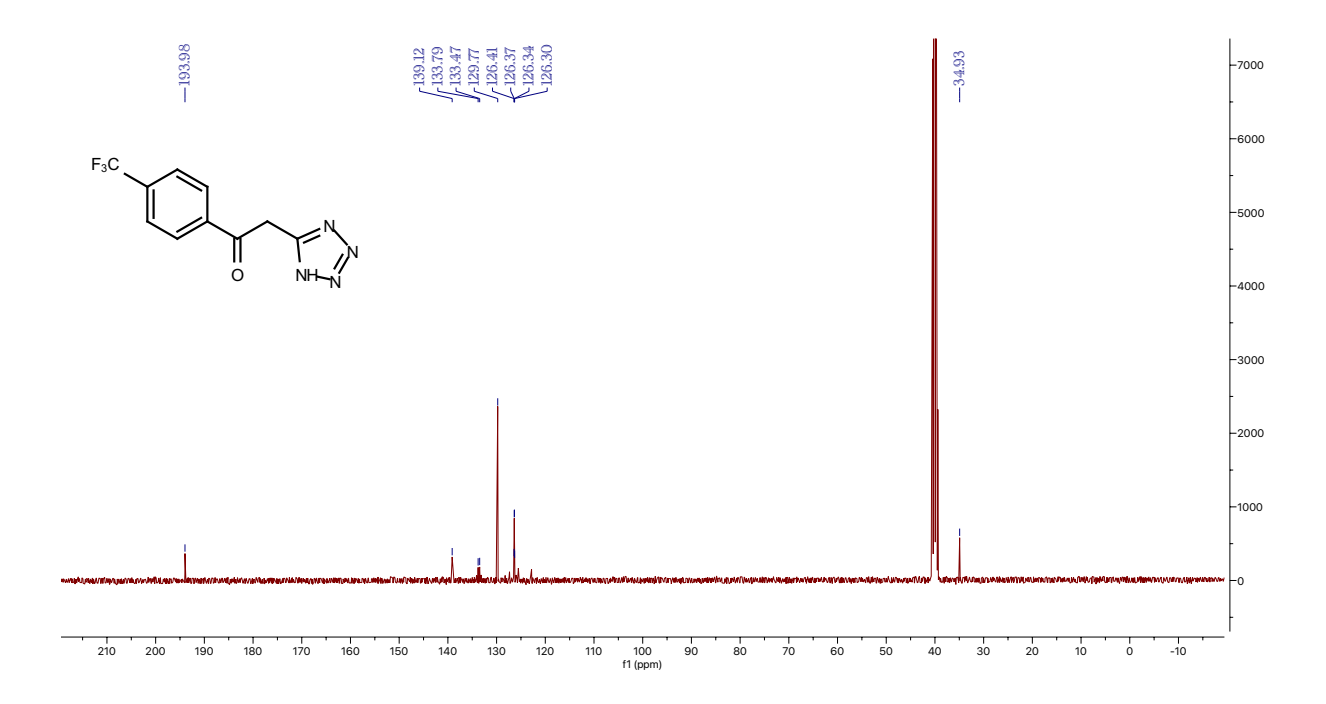
#### <sup>13</sup>C NMR for 3-oxo-3-(4-(trifluoromethyl)phenyl)propanenitrile (8c)



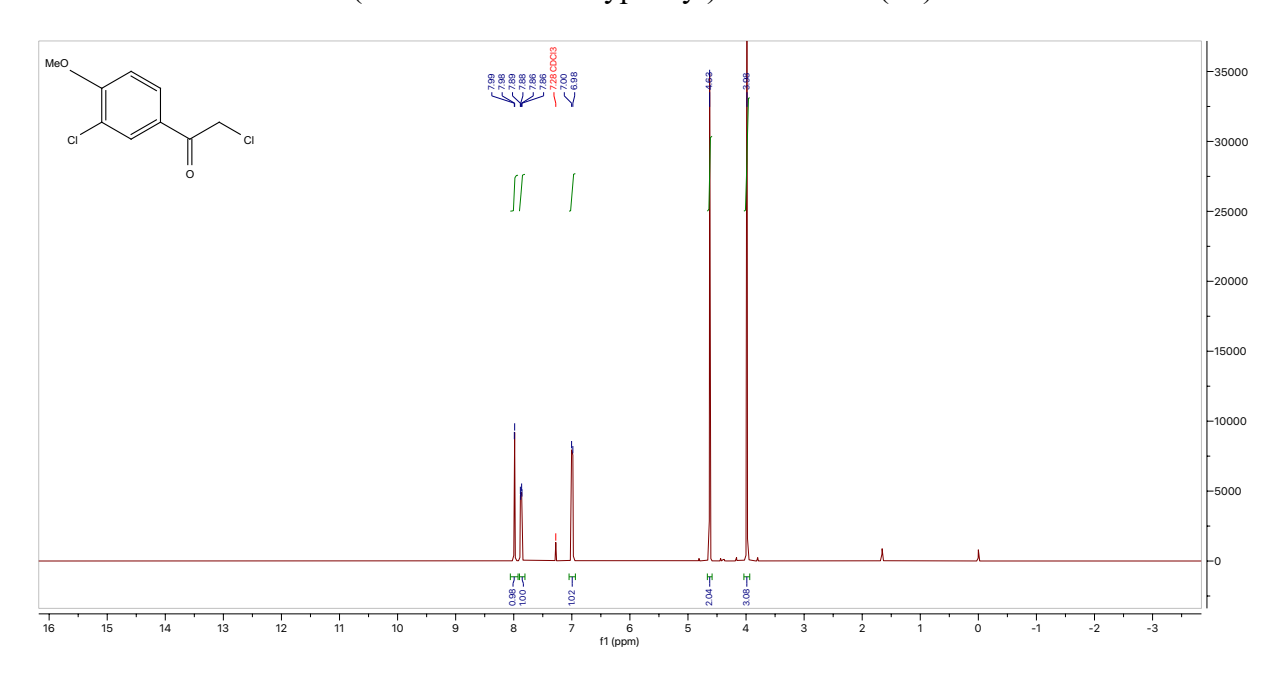
<sup>1</sup>H NMR for 2-(1H-tetrazol-5-yl)-1-(4-(trifluoromethyl)phenyl)ethan-1-one (8d)



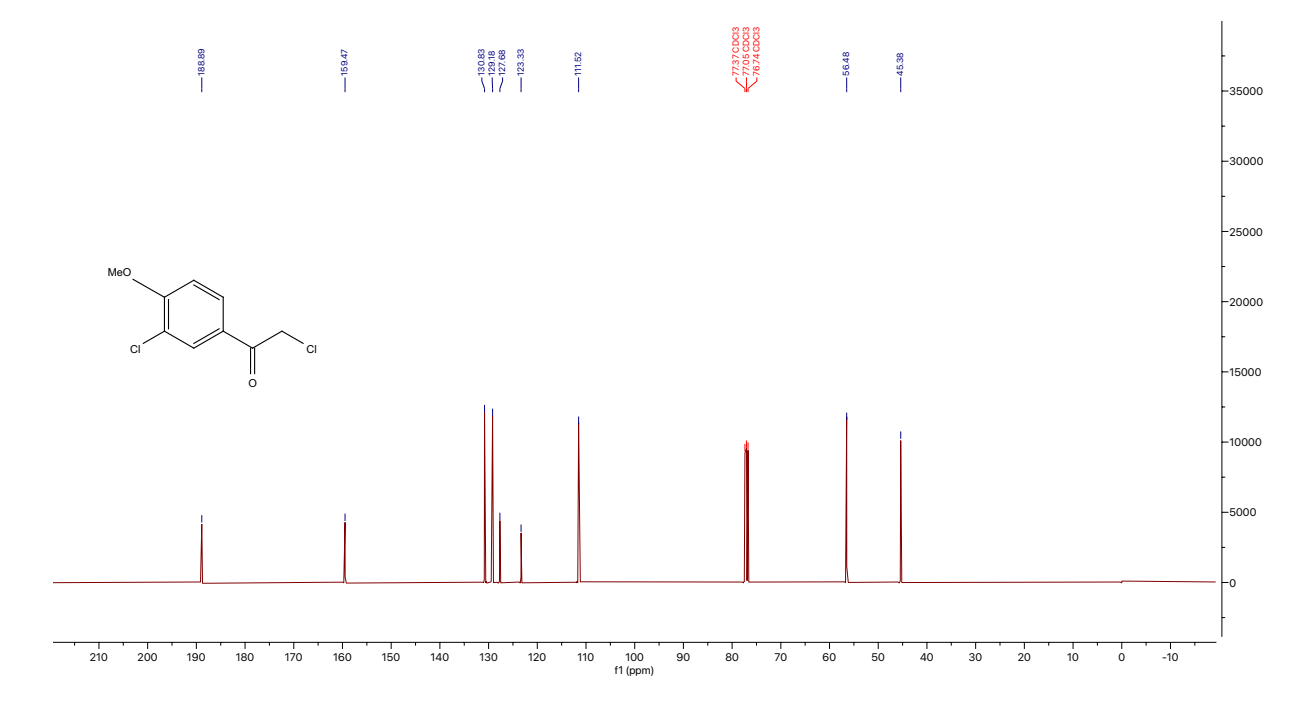
<sup>13</sup>C NMR for 2-(1H-tetrazol-5-yl)-1-(4-(trifluoromethyl)phenyl)ethan-1-one (8d)



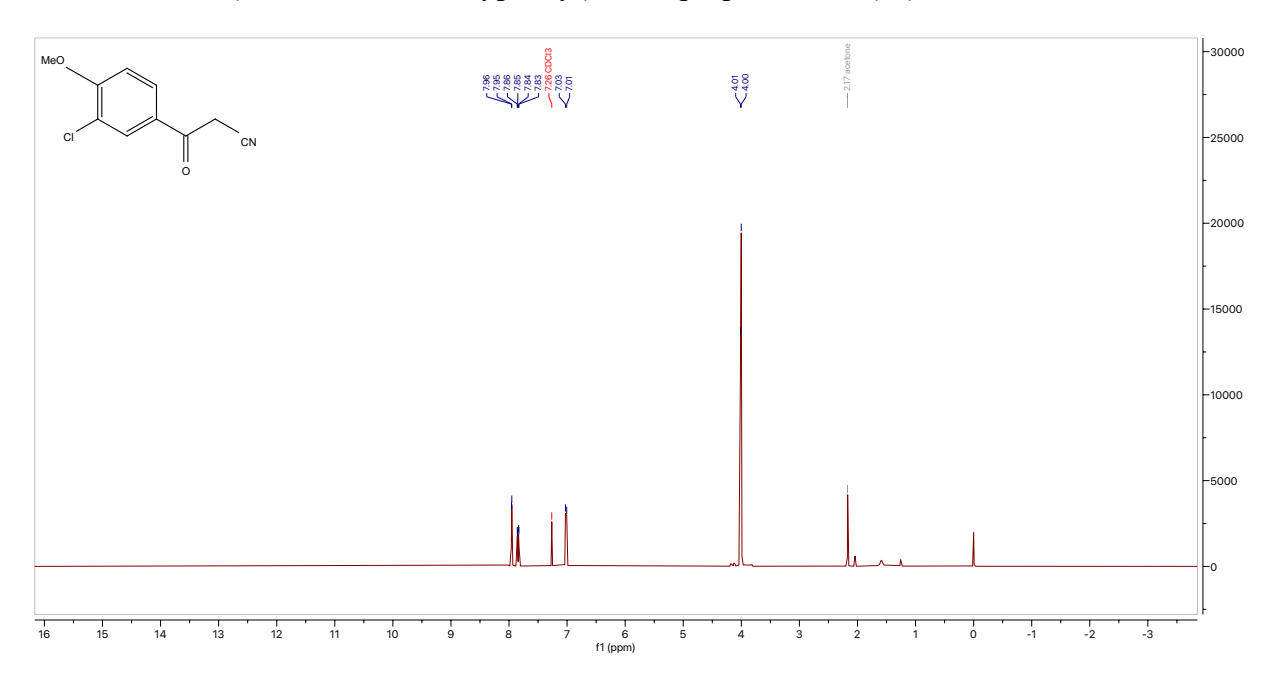
<sup>1</sup>H NMR for 2-chloro-1-(3-chloro-4-methoxyphenyl)ethan-1-one (**9b**)



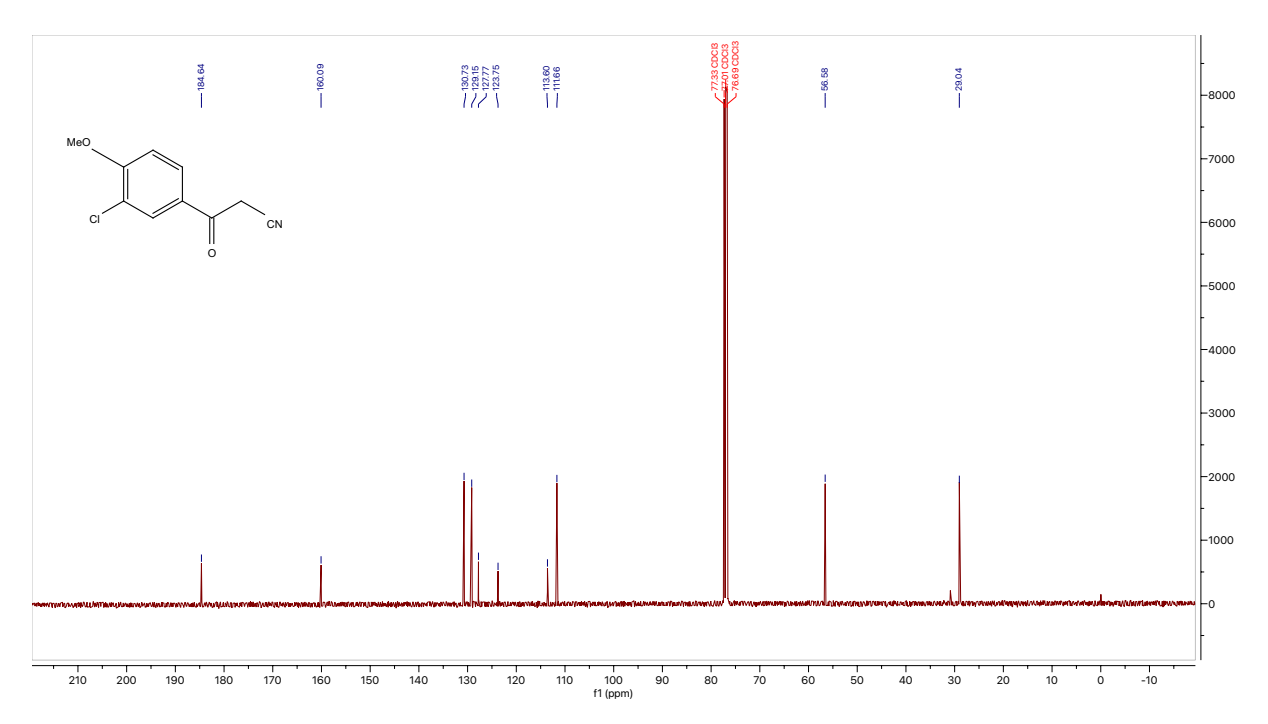
<sup>13</sup>C NMR for 2-chloro-1-(3-chloro-4-methoxyphenyl)ethan-1-one (9b)



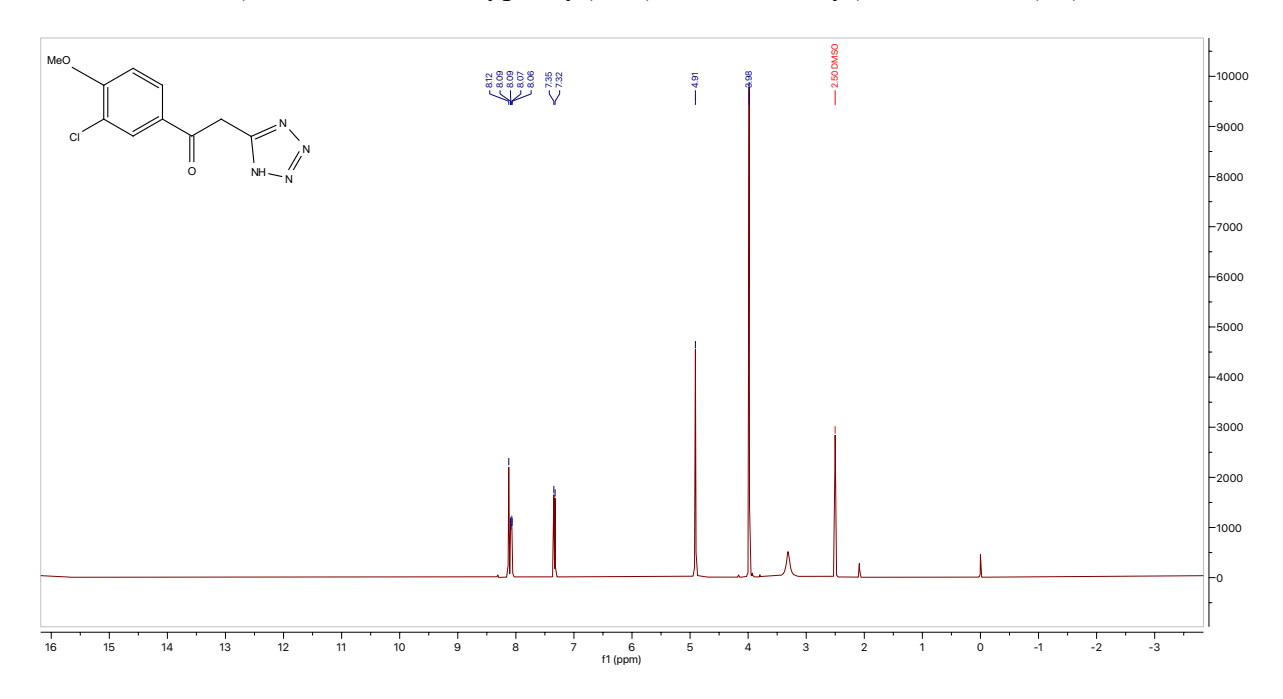
<sup>1</sup>H NMR for 3-(3-chloro-4-methoxyphenyl)-3-oxopropanenitrile (**9c**)



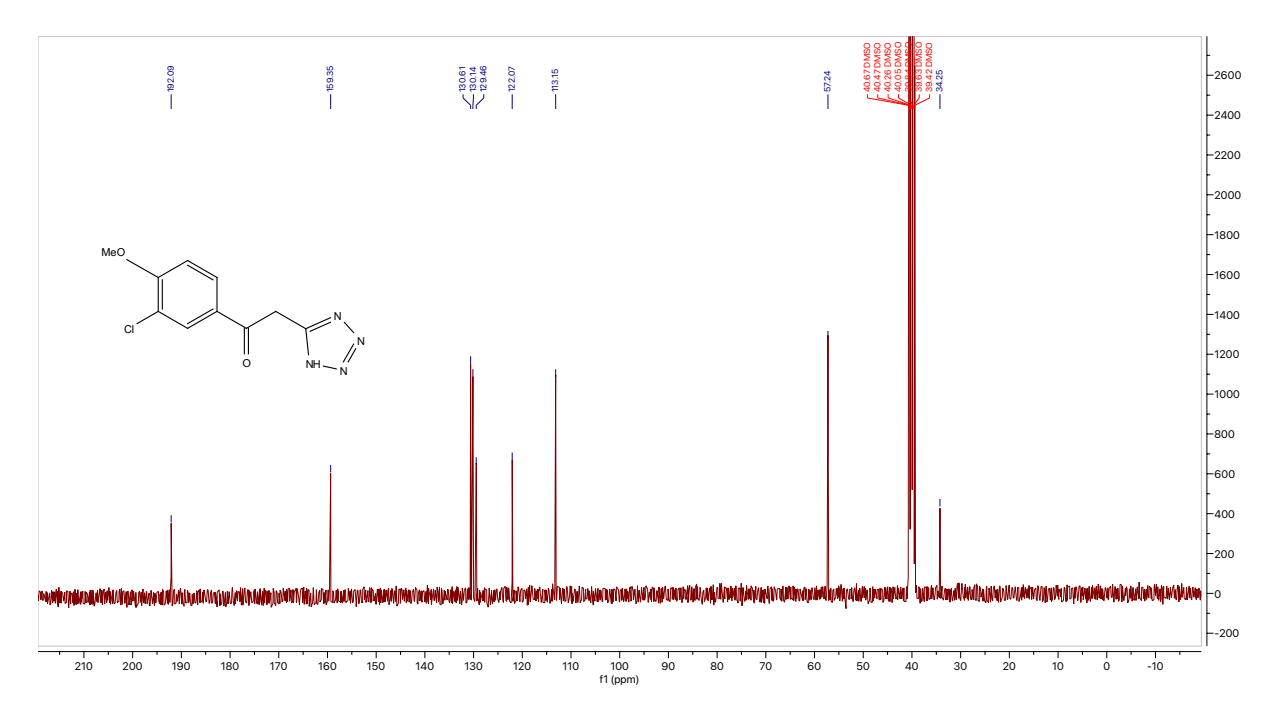
<sup>13</sup>C NMR for 3-(3-chloro-4-methoxyphenyl)-3-oxopropanenitrile (9c)



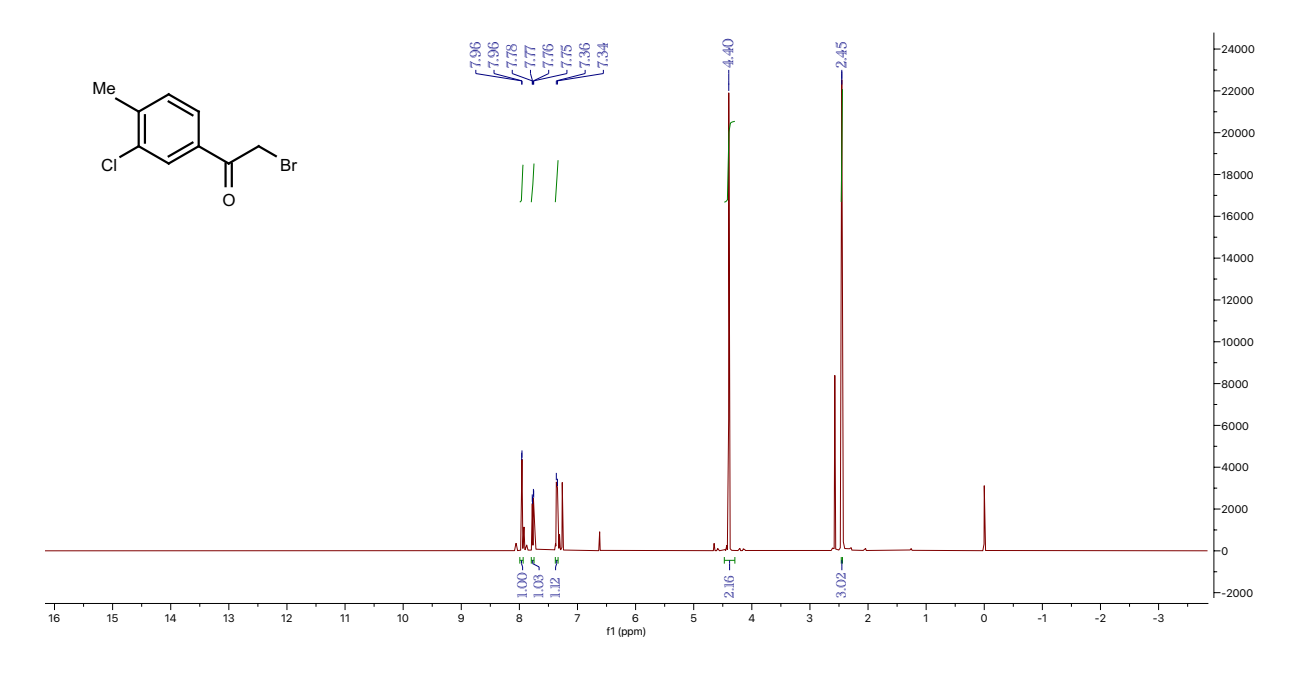
<sup>1</sup>H NMR for 1-(3-chloro-4-methoxyphenyl)-2-(1*H*-tetrazol-5-yl)ethan-1-one (**9d**)



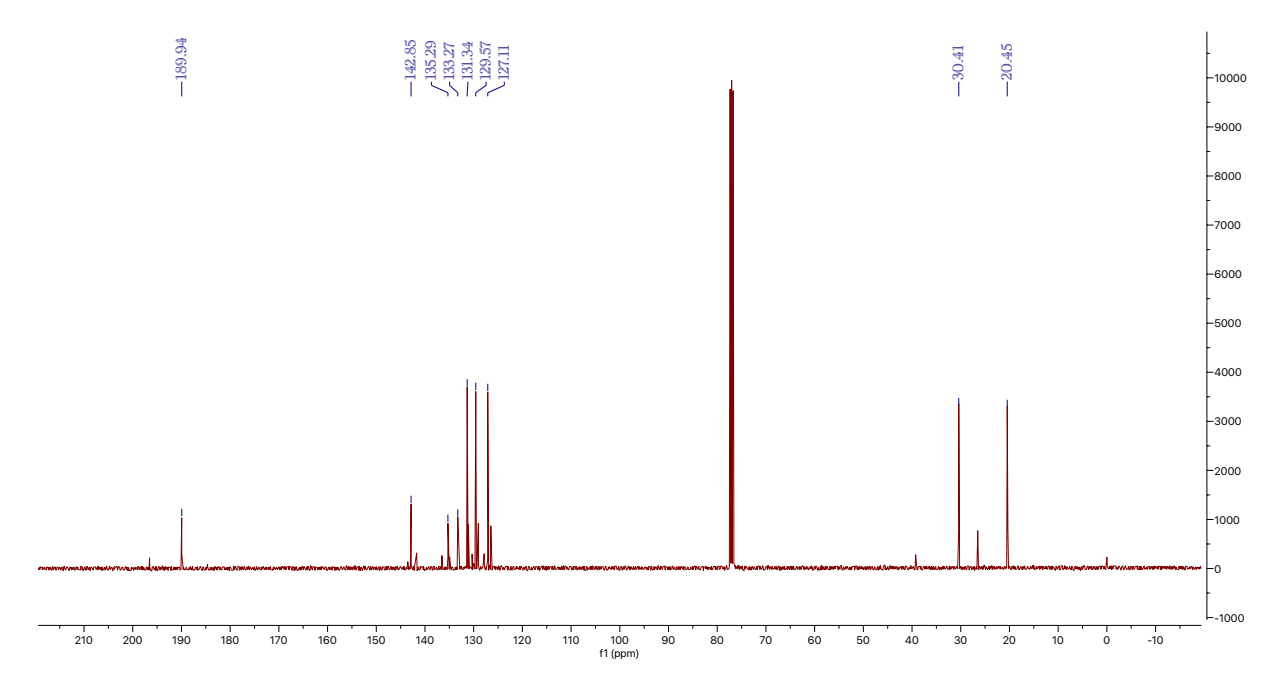
<sup>13</sup>C NMR for 1-(3-chloro-4-methoxyphenyl)-2-(1*H*-tetrazol-5-yl)ethan-1-one (**9d**)



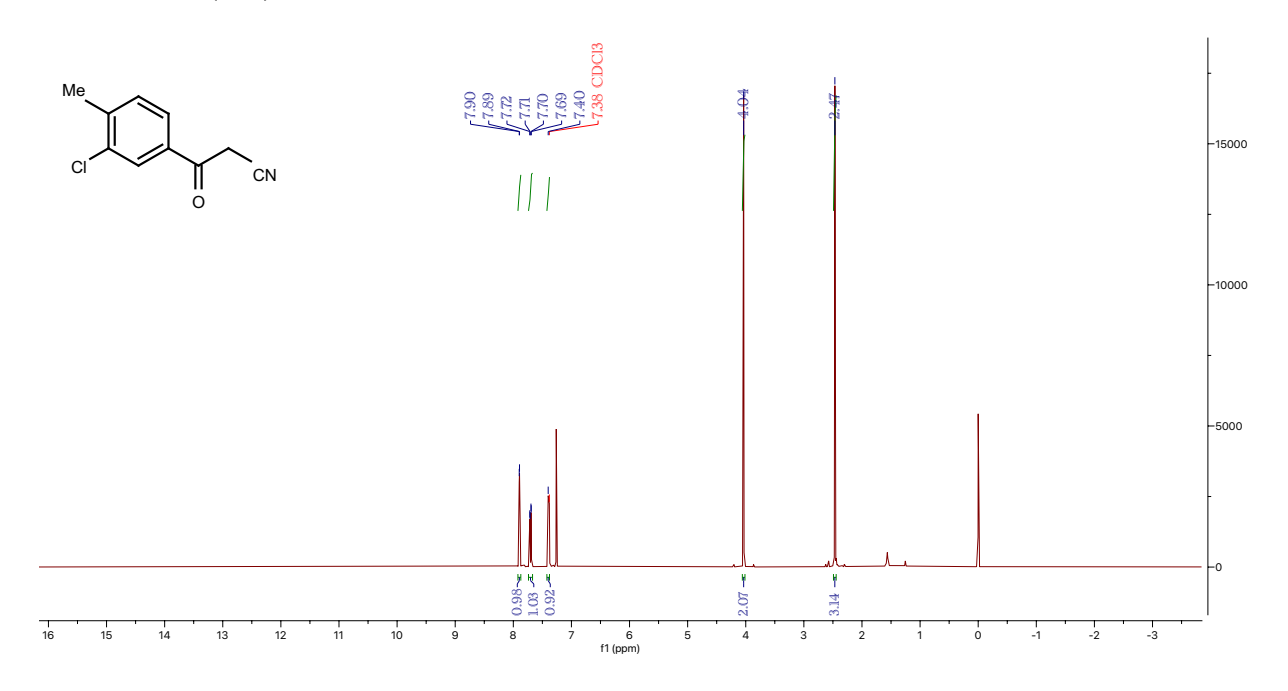
# <sup>1</sup>H NMR for (**10b**)



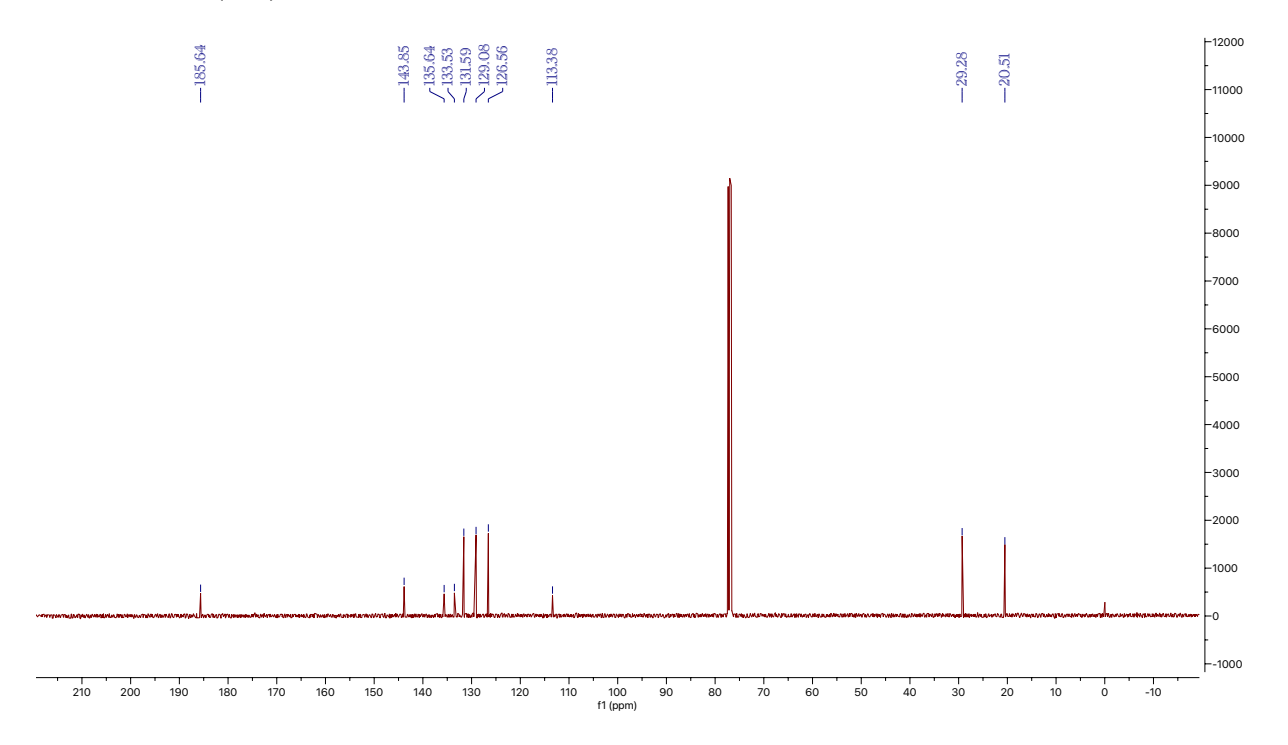
# <sup>13</sup>C NMR for (**10b**)



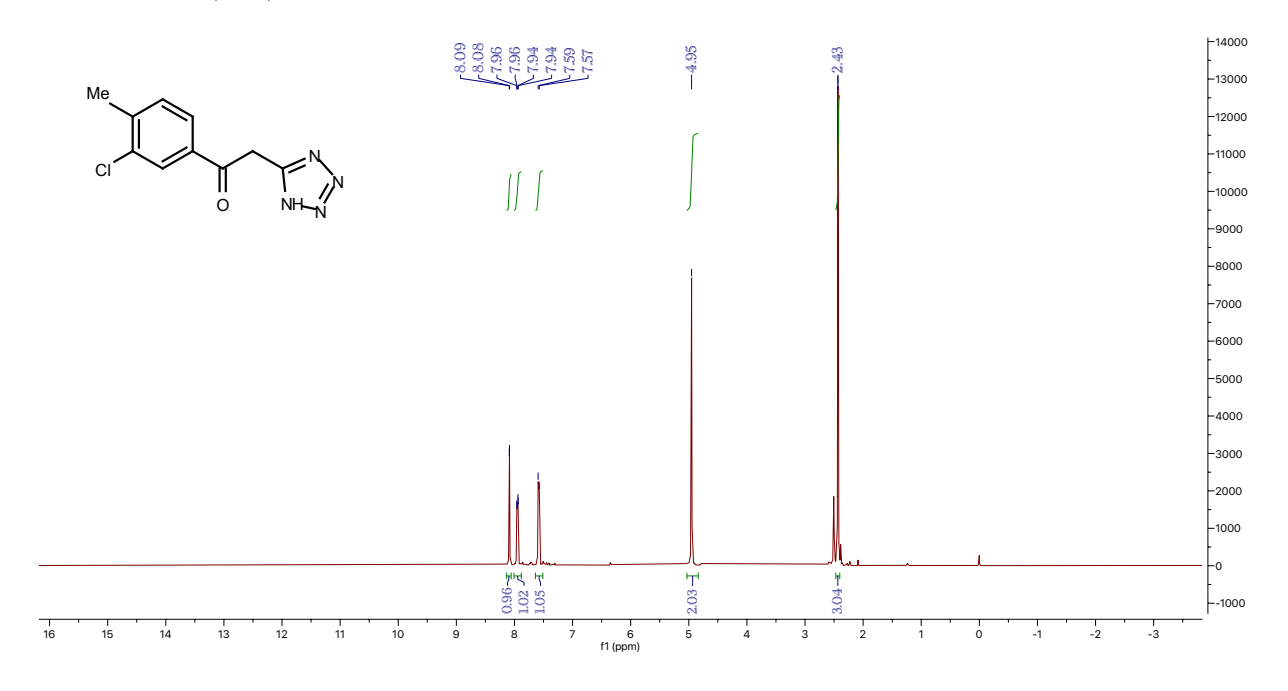
# <sup>1</sup>H NMR for (**10c**)



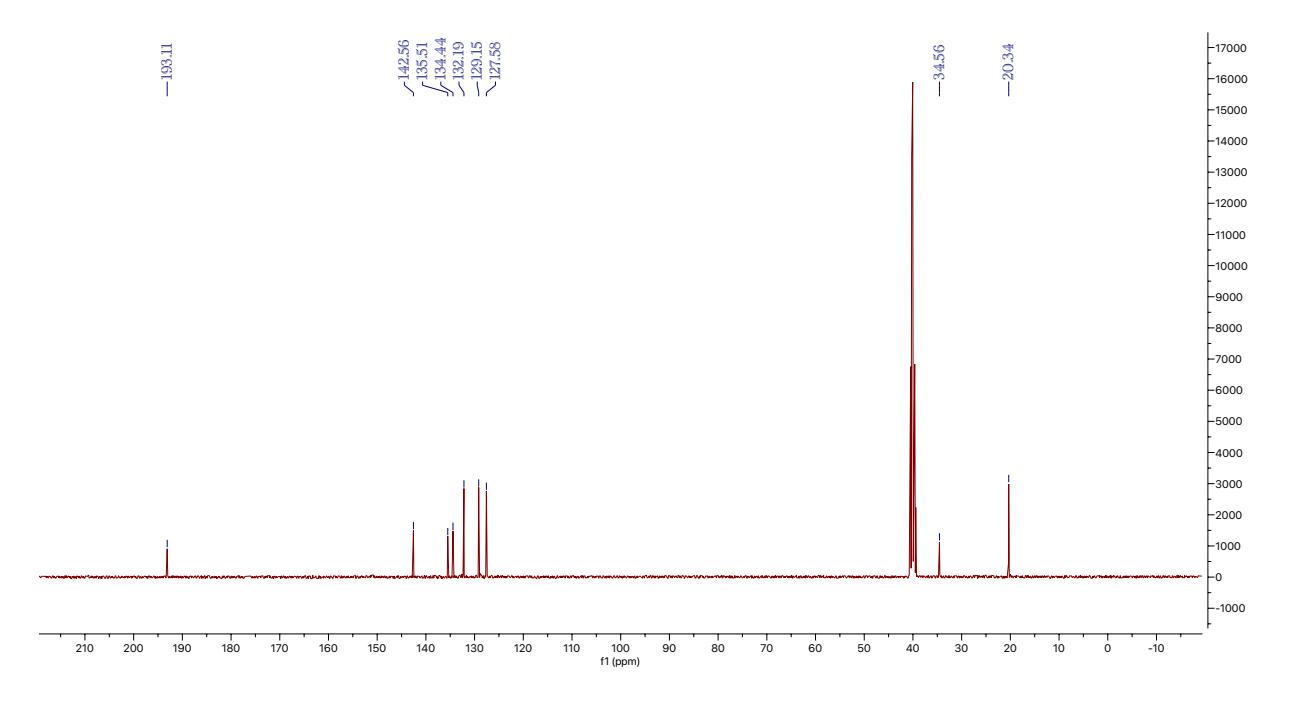
# <sup>13</sup>C NMR for (**10c**)



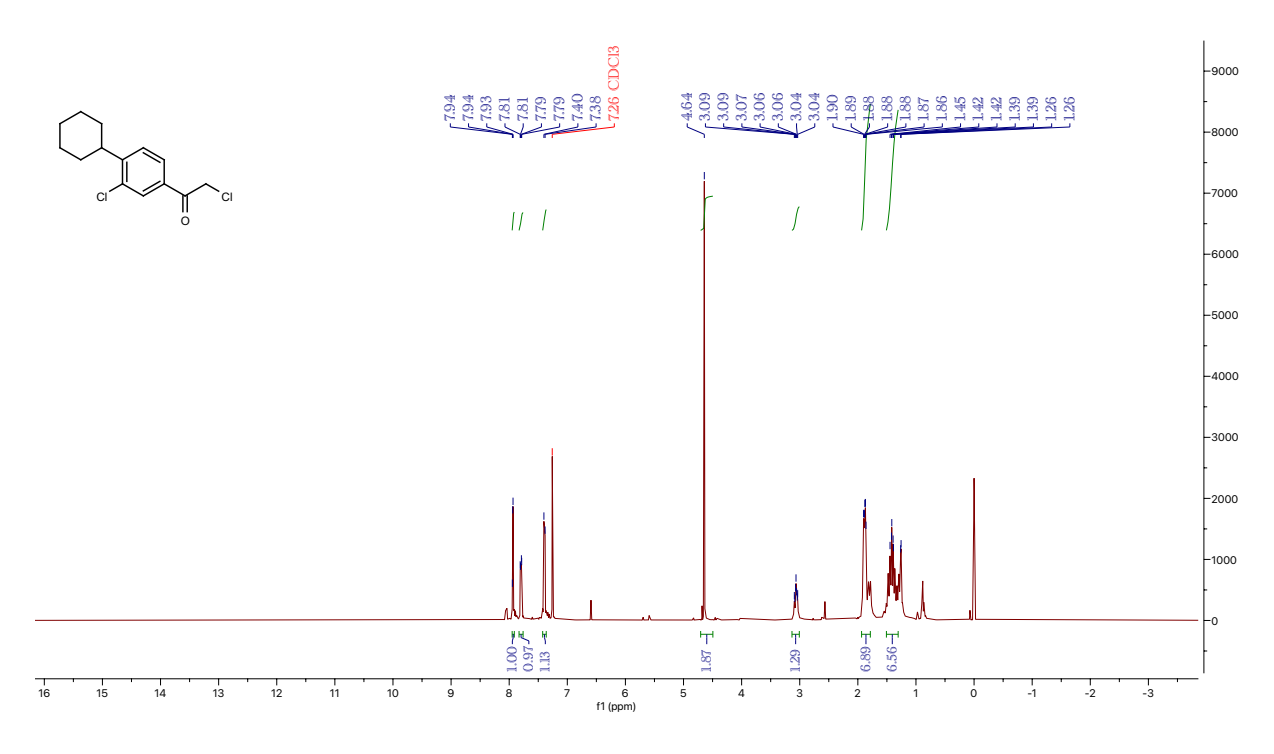
## <sup>1</sup>H NMR for (**10d**)



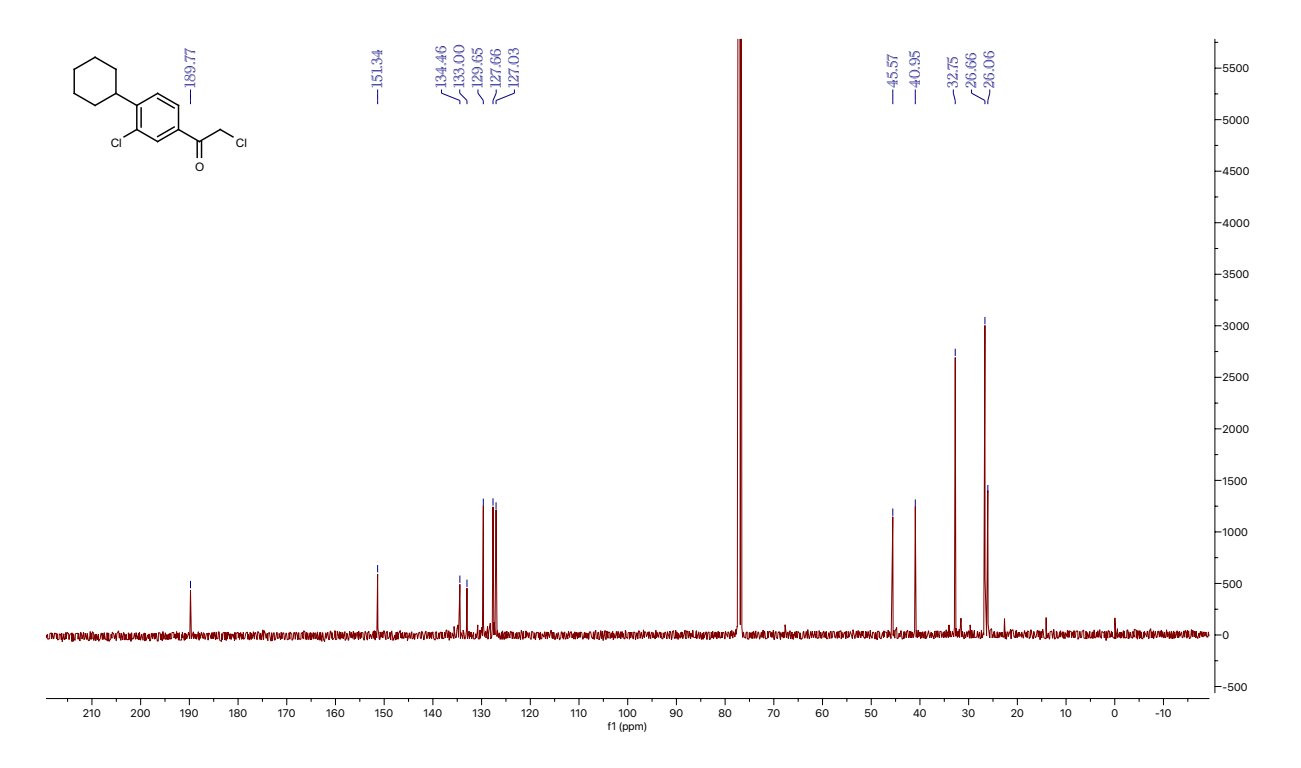
## <sup>13</sup>C NMR for (**10d**)



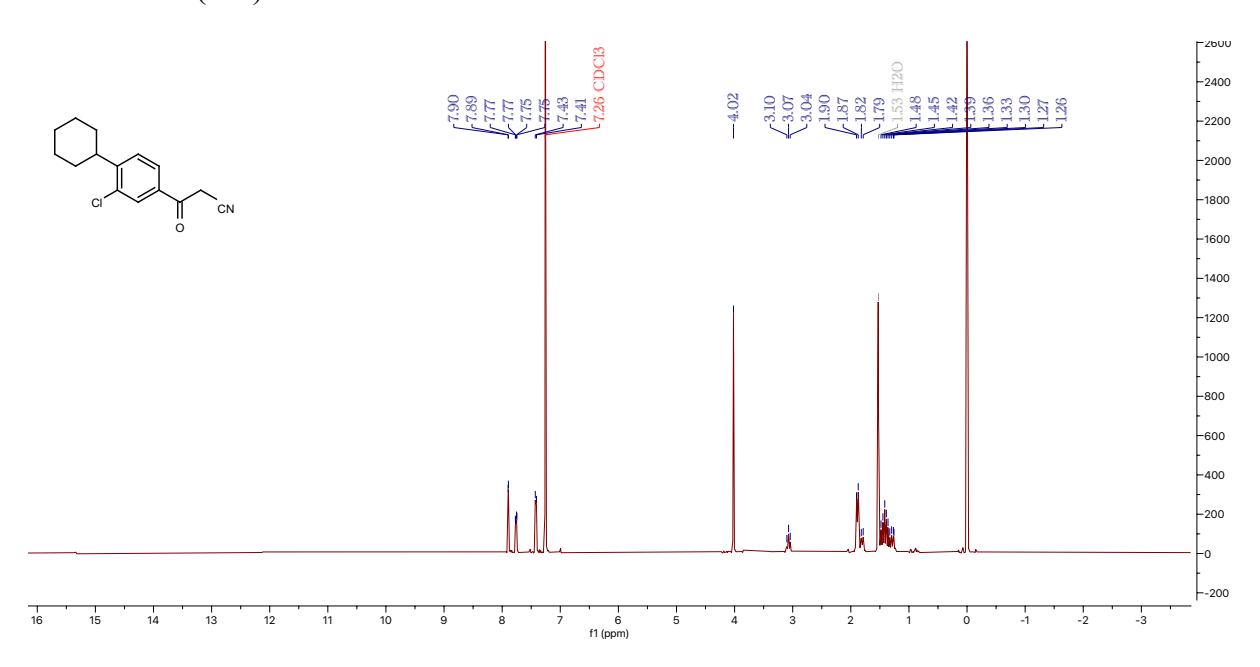
### <sup>1</sup>H NMR for **11b**



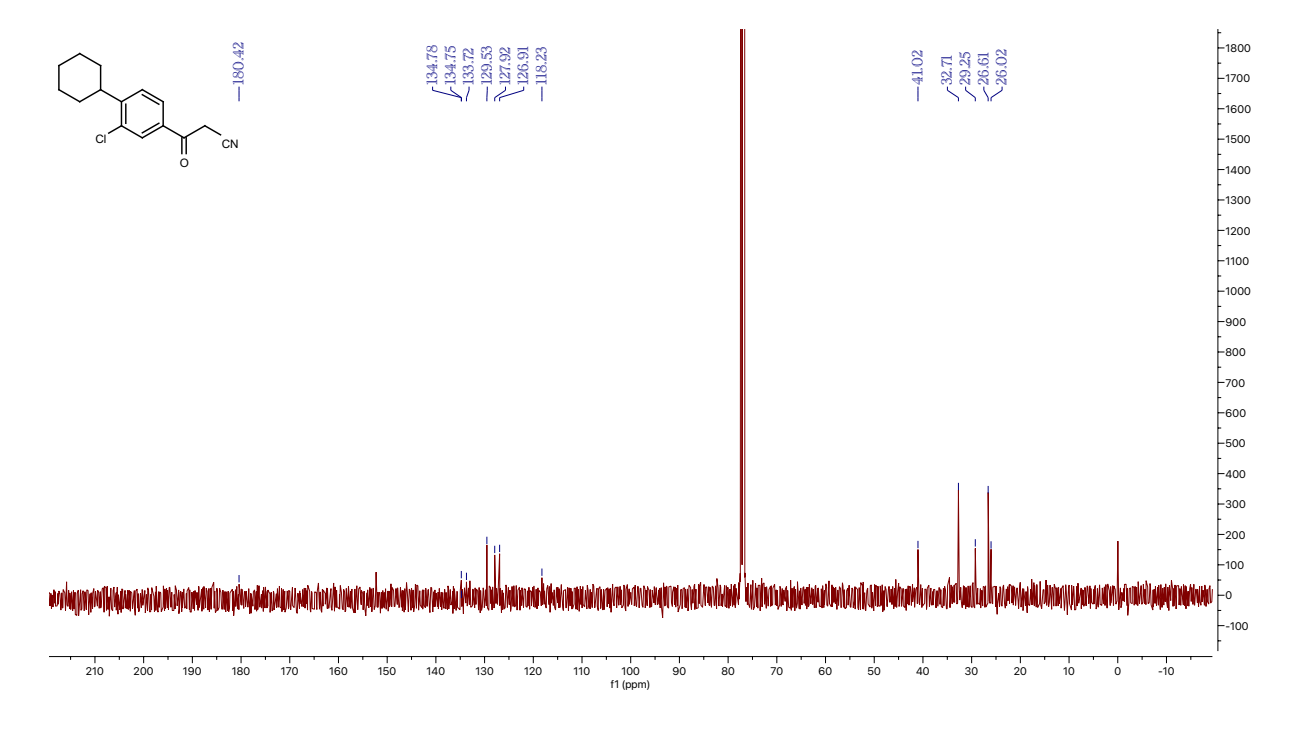
### <sup>13</sup>C NMR for **11b**



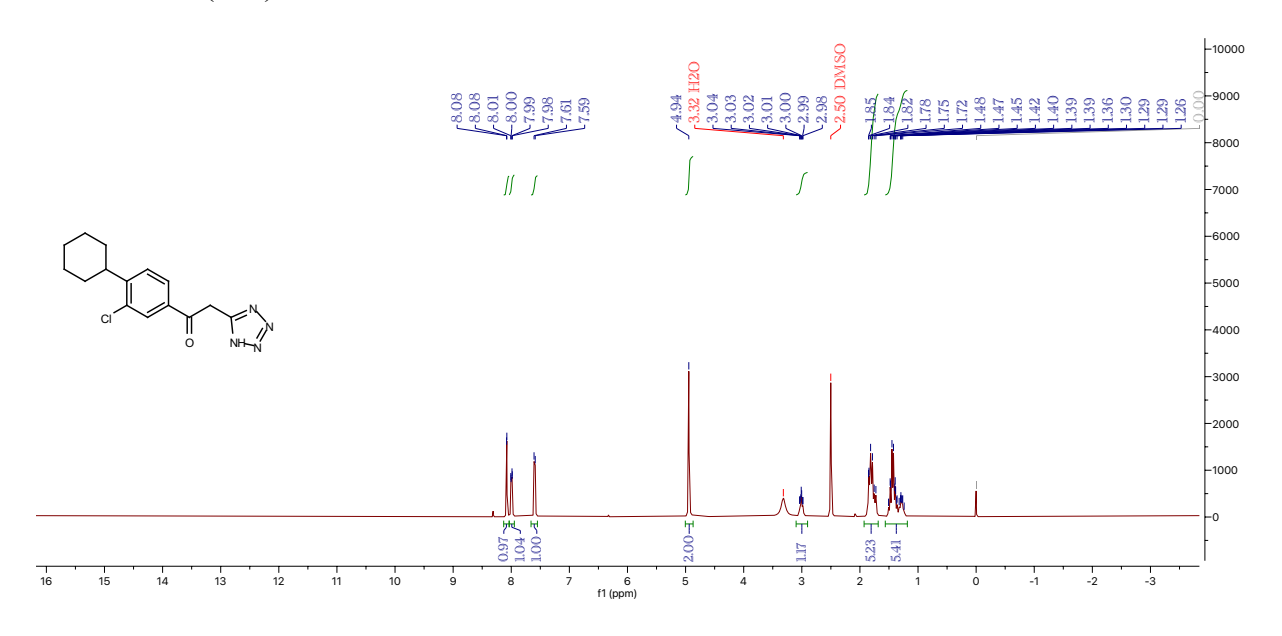
### <sup>1</sup>H NMR for (**11c**)



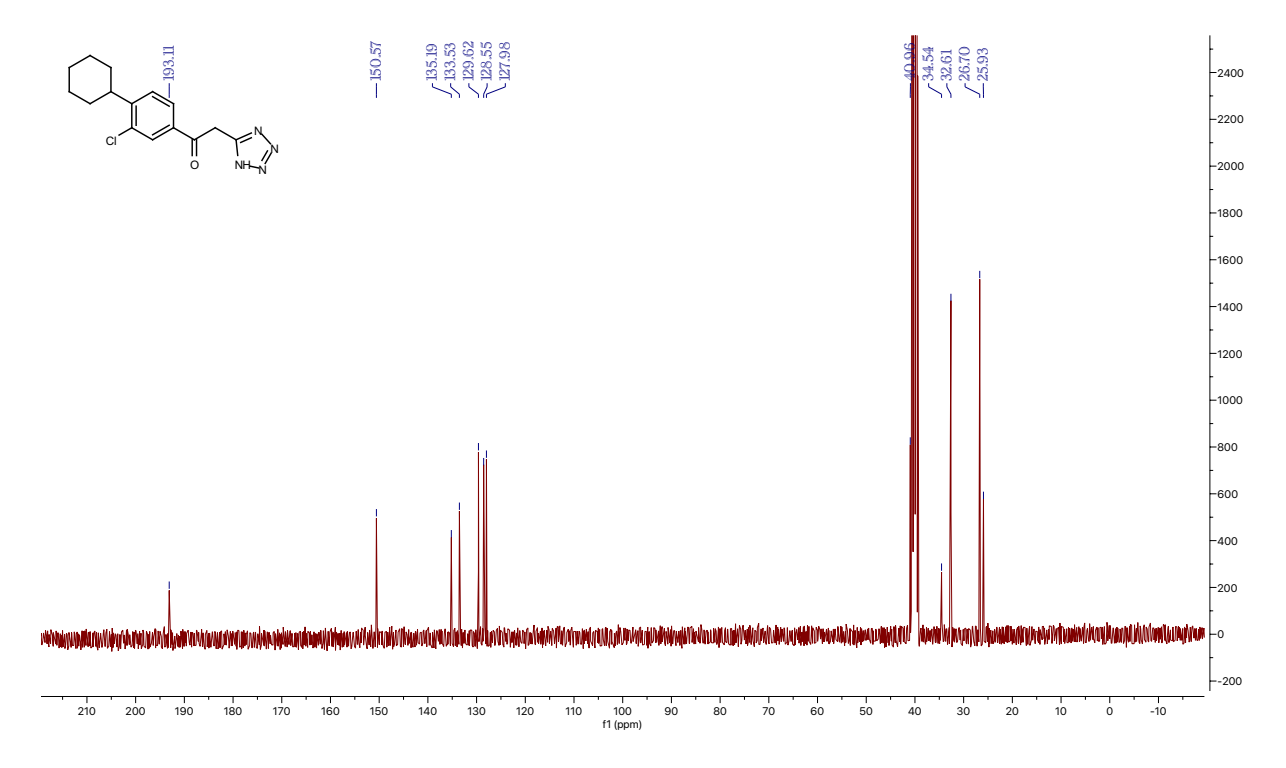
### <sup>13</sup>C NMR for (**11c**)



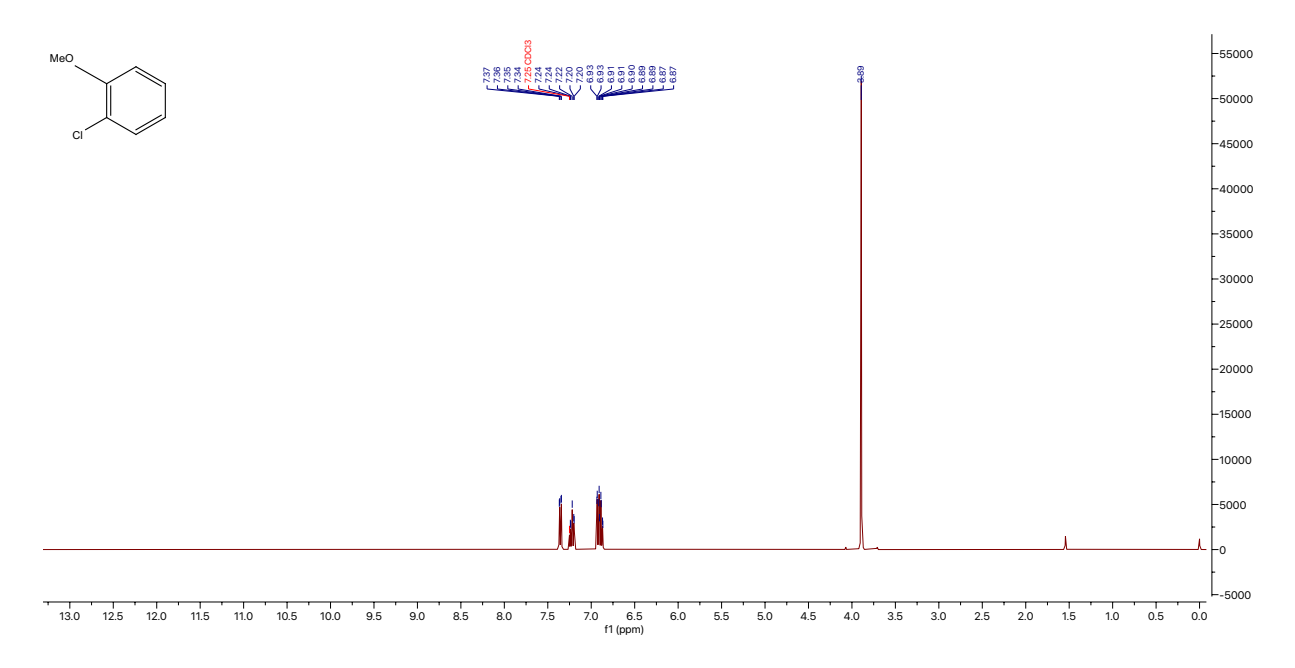
### <sup>1</sup>H NMR for (**11d**)



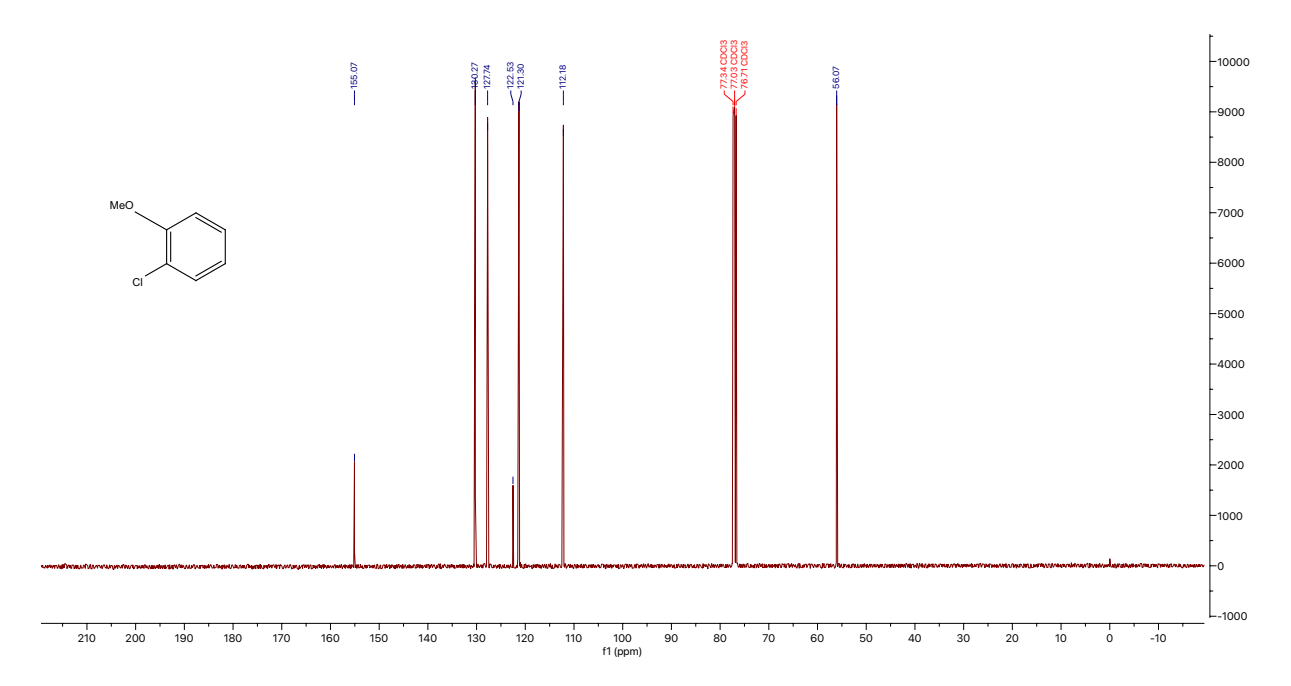
## <sup>13</sup>C NMR for (**11d**)



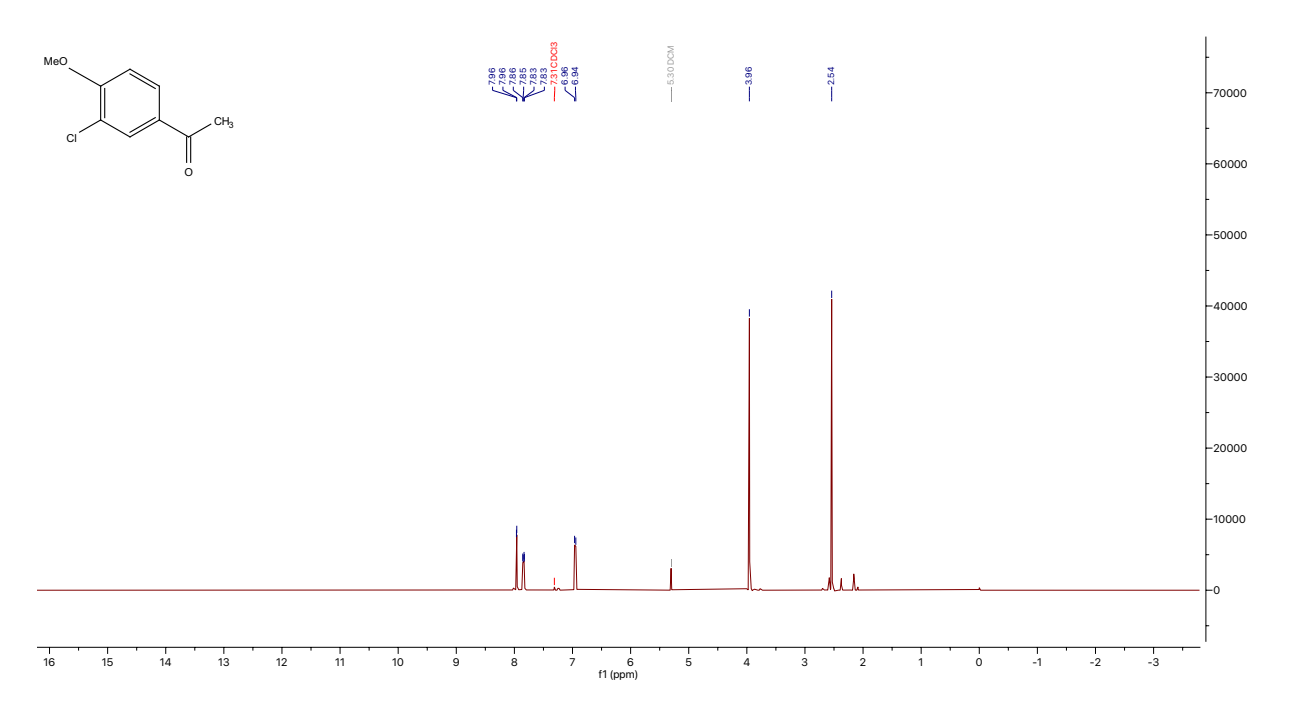
<sup>1</sup>H NMR for 1-chloro-2-methoxybenzene (**12ab**)



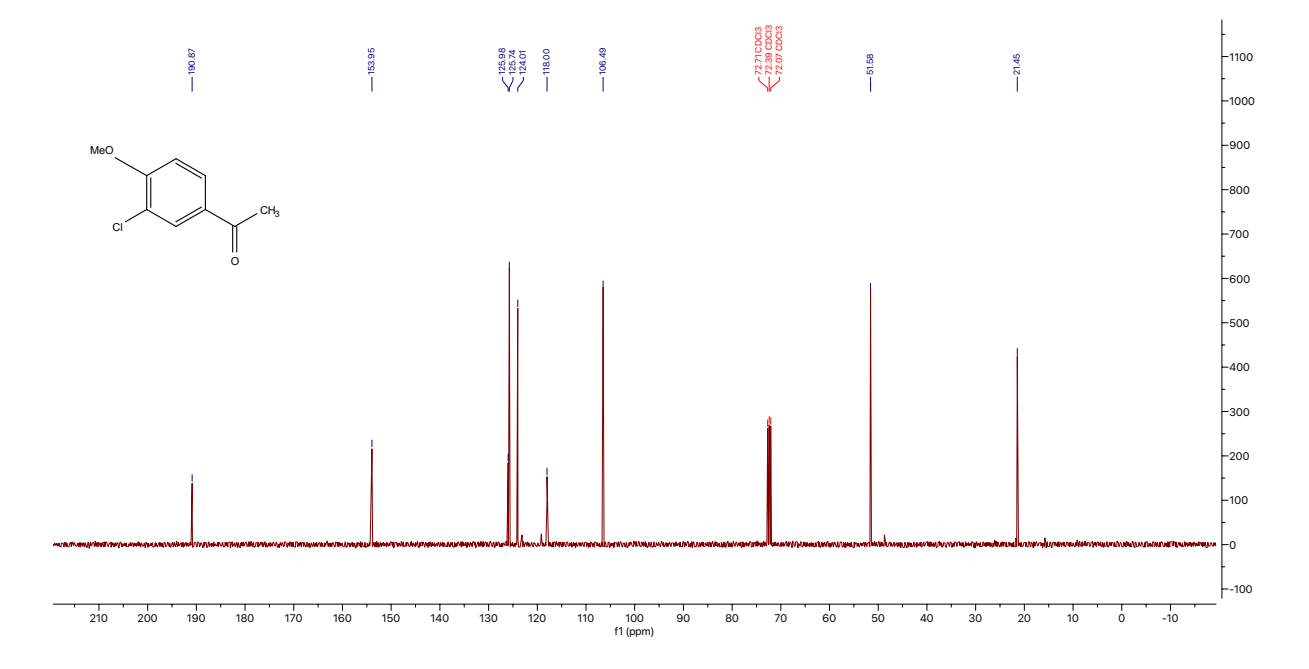
<sup>13</sup>C NMR for 1-chloro-2-methoxybenzene (**12ab**)



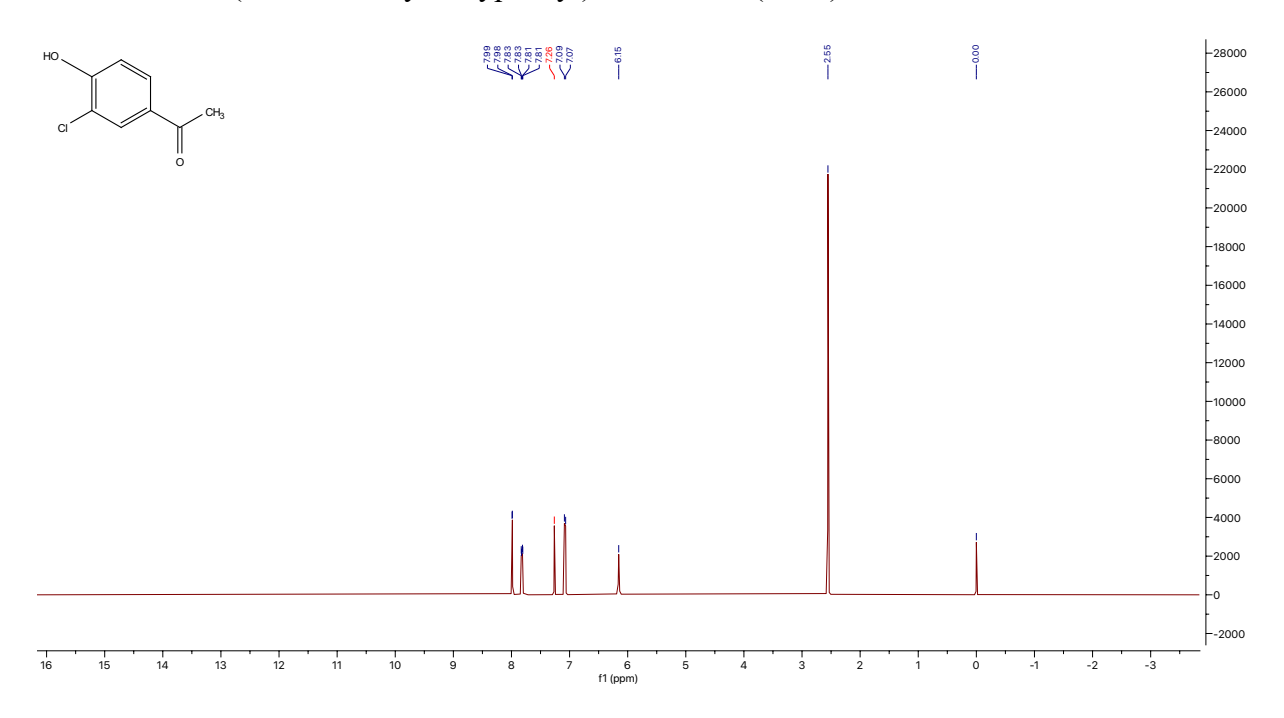
## <sup>1</sup>H NMR for 1-(3-chloro-4-methoxyphenyl)ethan-1-one (**12ac**)



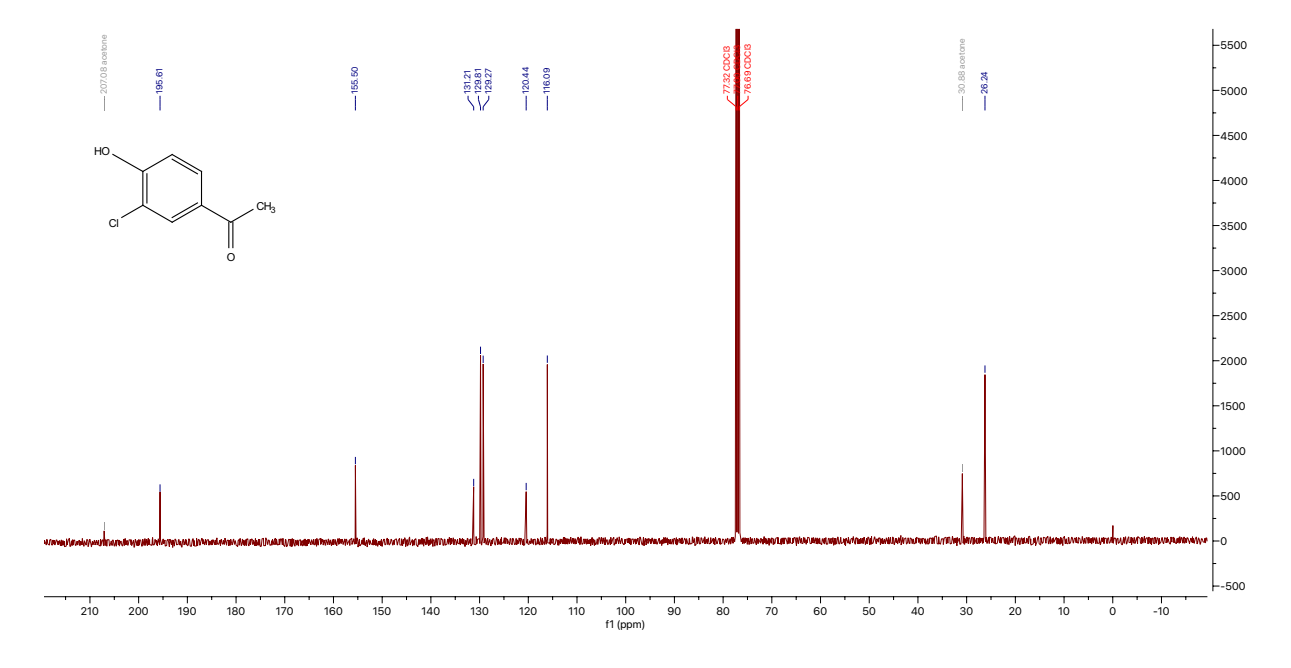
### <sup>13</sup>C NMR for 1-(3-chloro-4-methoxyphenyl)ethan-1-one (12ac)



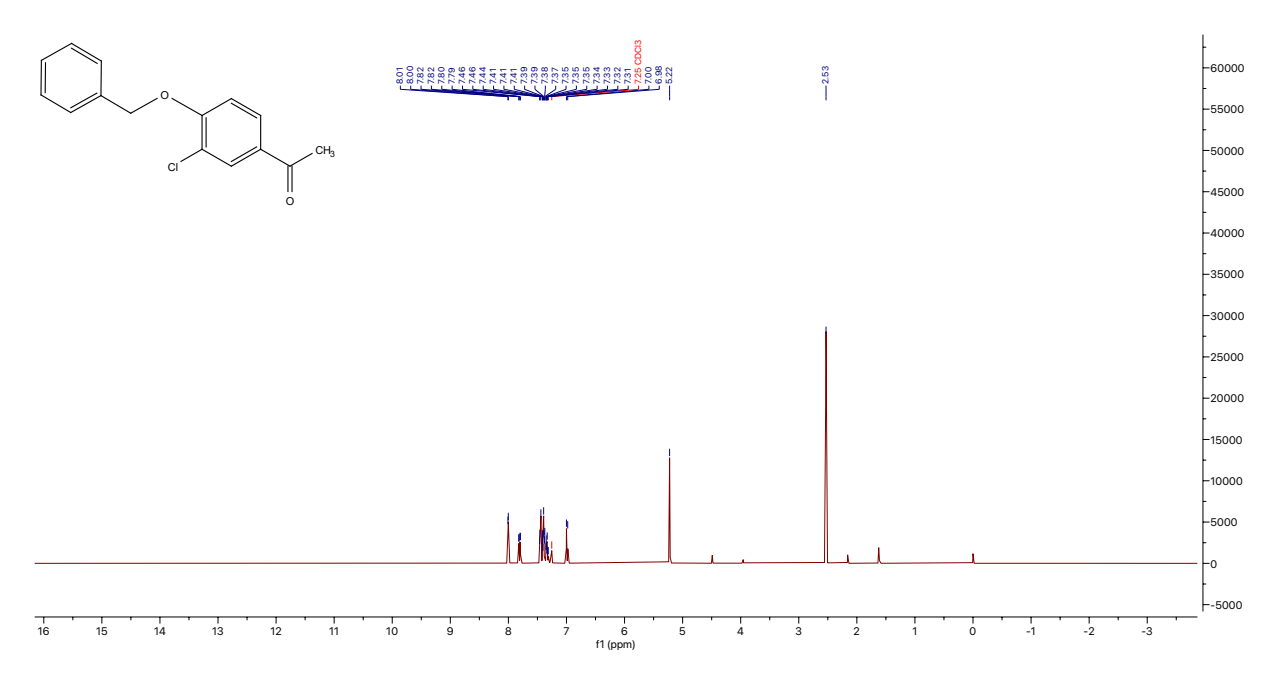
## <sup>1</sup>H NMR for 1-(3-chloro-4-hydroxyphenyl)ethan-1-one (**12ad**)



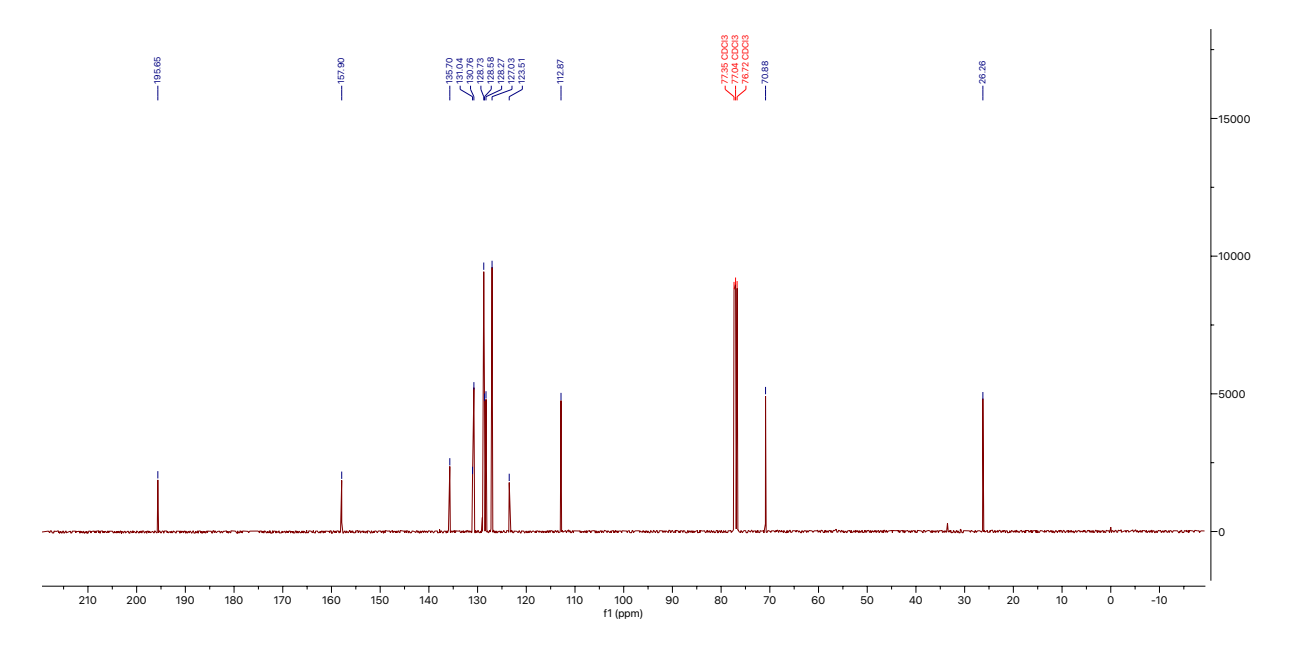
### <sup>13</sup>C NMR for 1-(3-chloro-4-hydroxyphenyl)ethan-1-one (**12ad**)



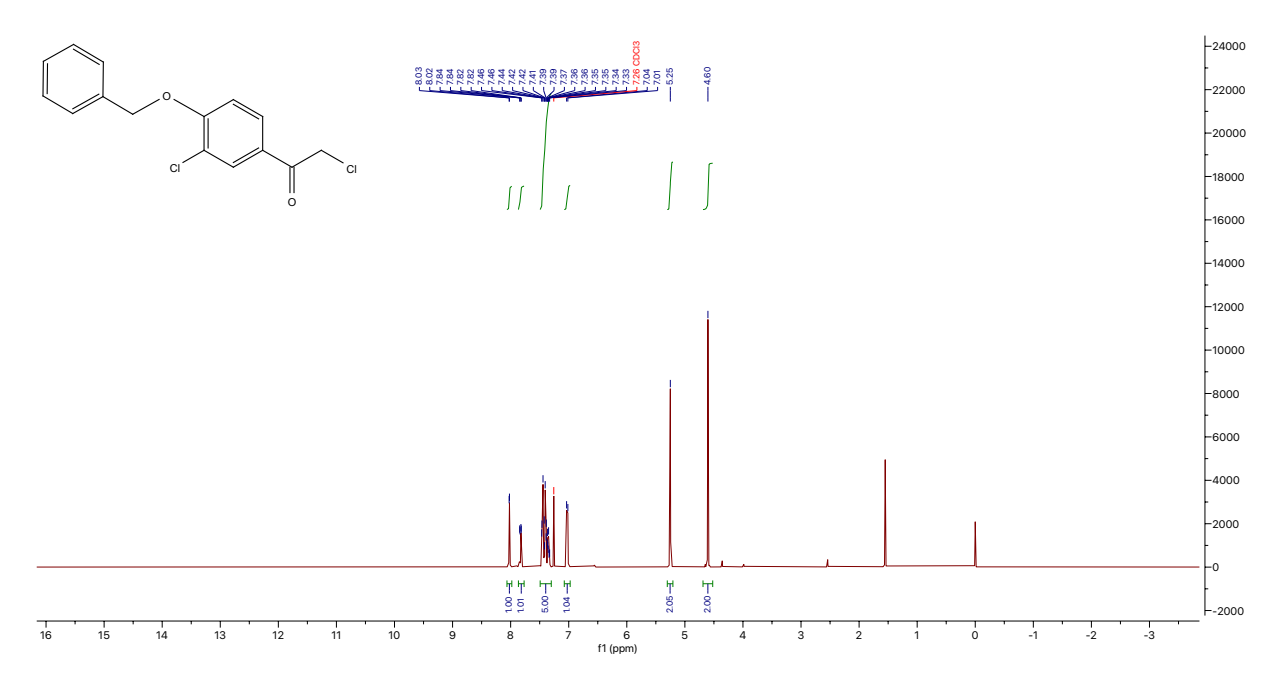
## <sup>1</sup>H NMR for 1-(4-(benzyloxy)-3-chlorophenyl)ethan-1-one (**12ae**)



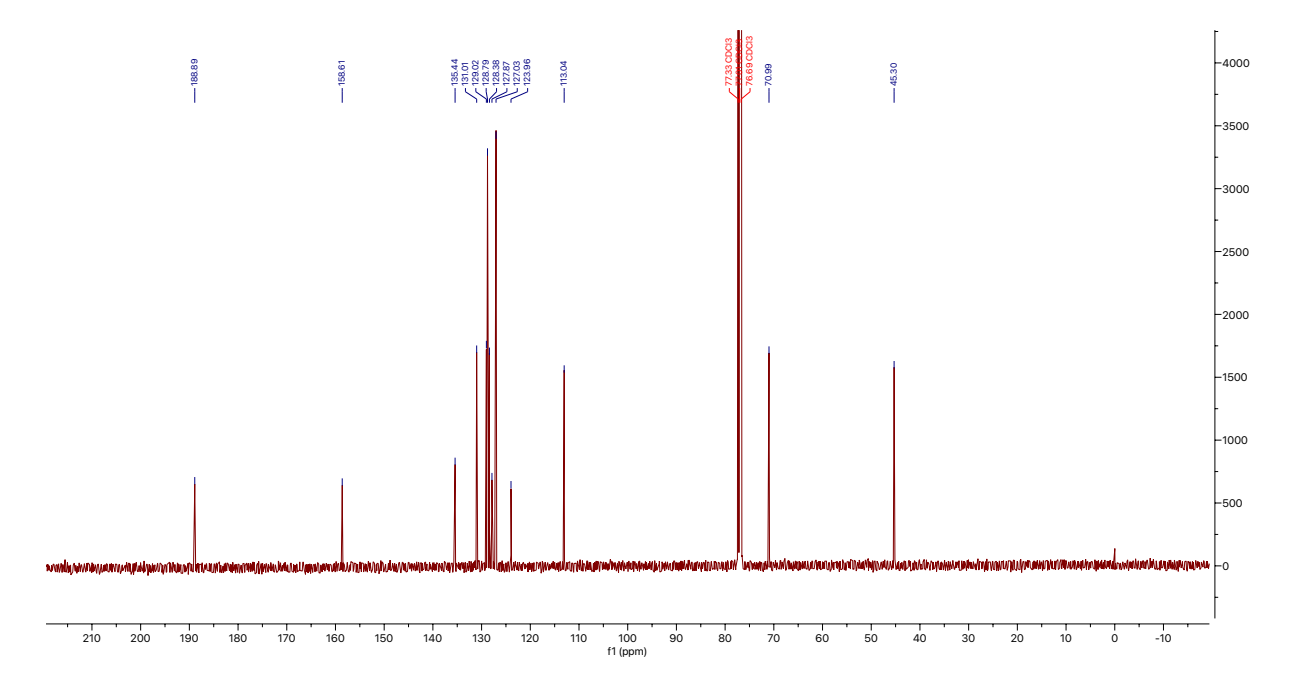
### <sup>13</sup>C NMR for 1-(4-(benzyloxy)-3-chlorophenyl)ethan-1-one (**12ae**)



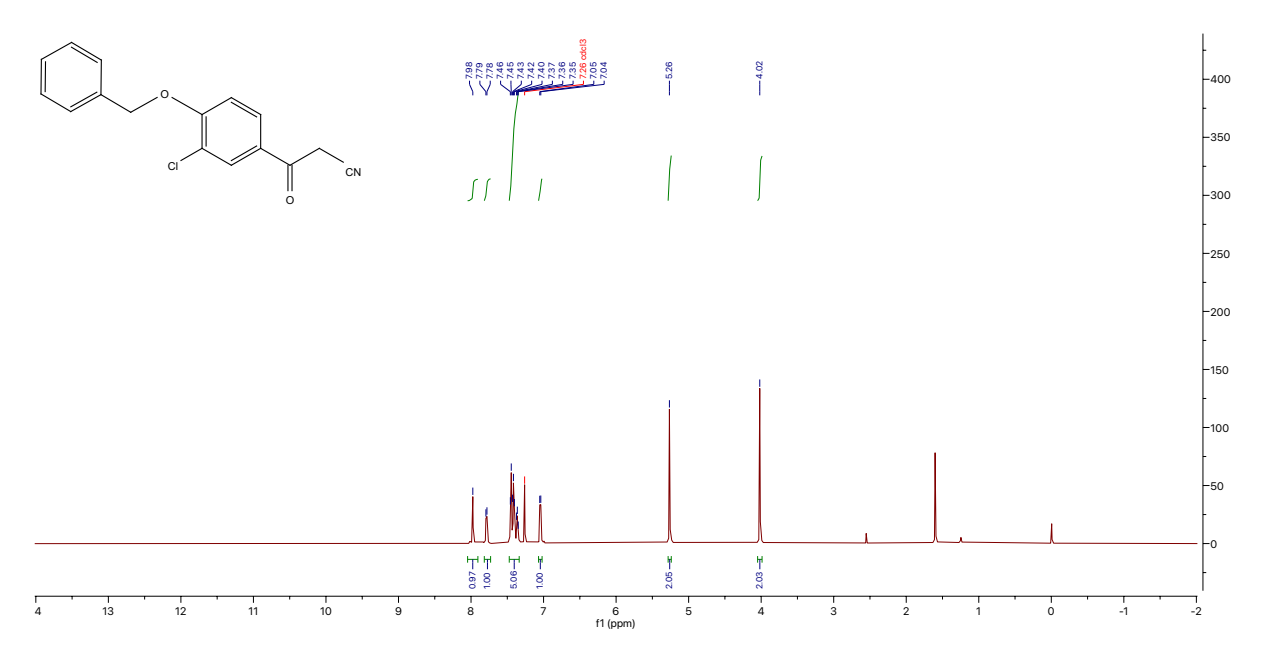
 $^1\mathrm{H}$  NMR for 1-(4-(benzyloxy)-3-chlorophenyl)-2-chloroethan-1-one (12b)



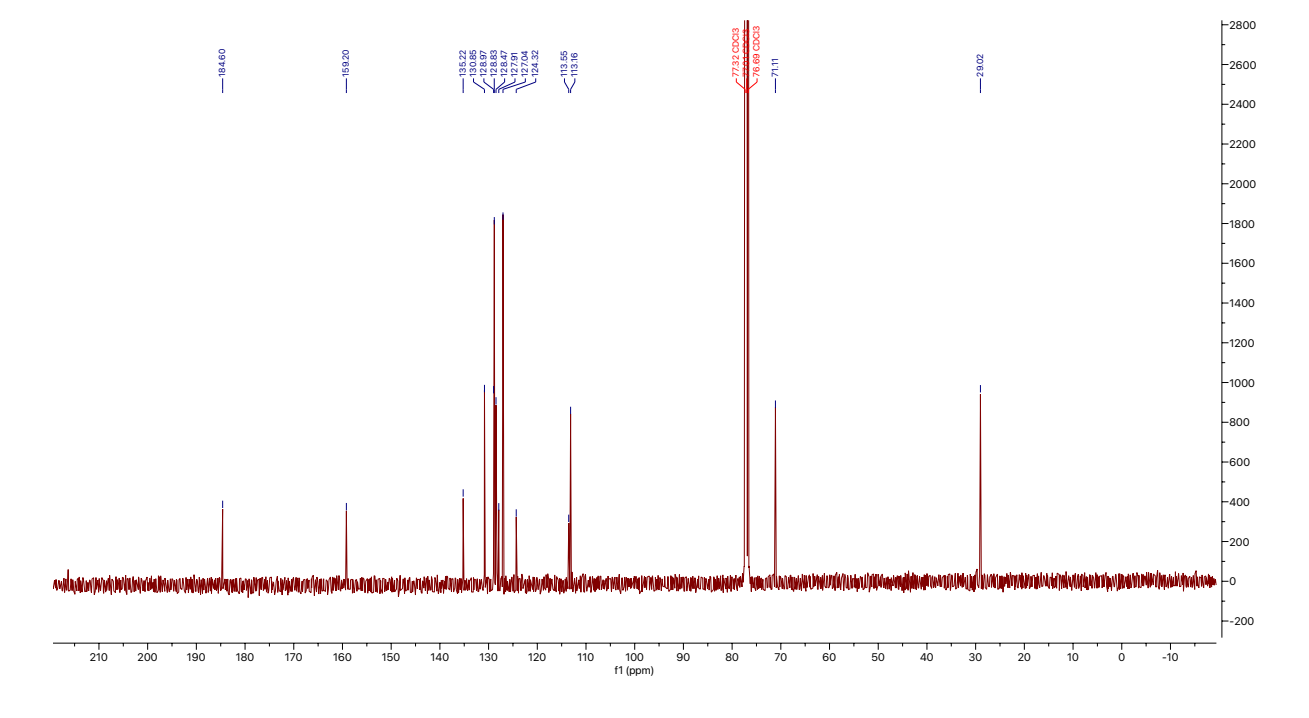
<sup>13</sup>C NMR for 1-(4-(benzyloxy)-3-chlorophenyl)-2-chloroethan-1-one (12b)



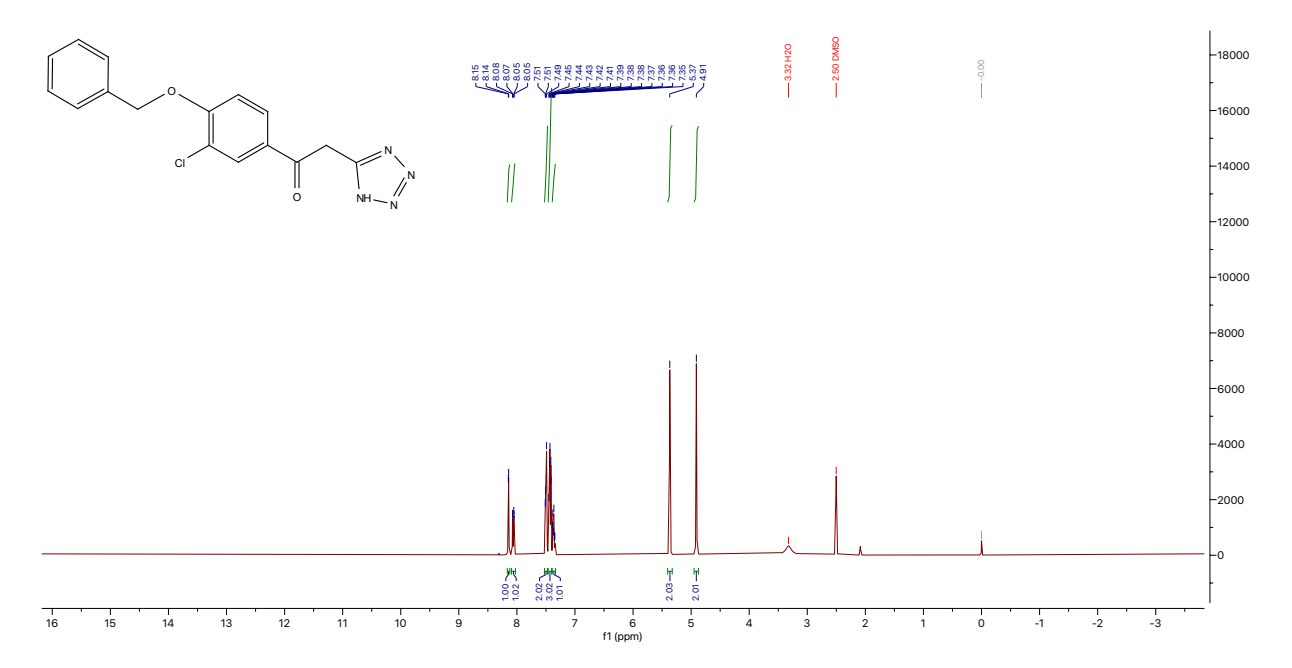
<sup>1</sup>H NMR for 3-(4-(benzyloxy)-3-chlorophenyl)-3-oxopropanenitrile (**12c**)



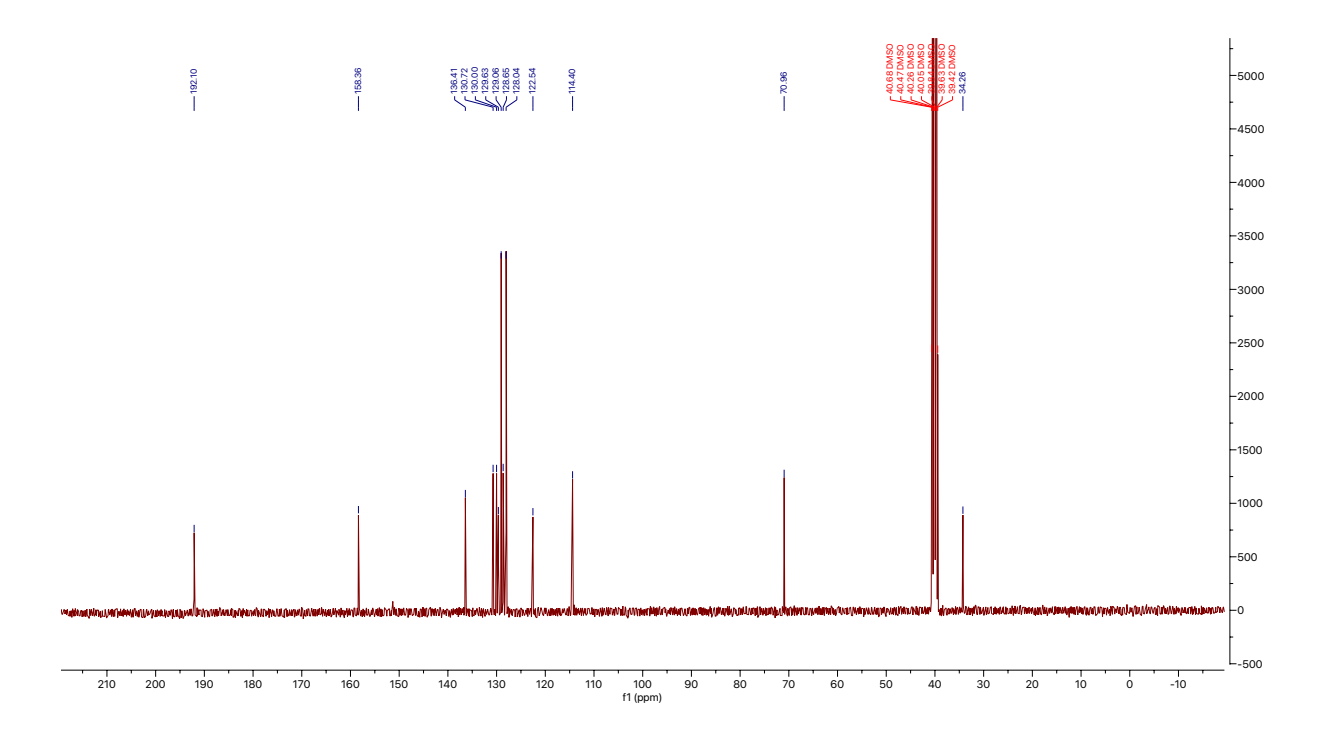
<sup>13</sup>C NMR for 3-(4-(benzyloxy)-3-chlorophenyl)-3-oxopropanenitrile (12c)



<sup>1</sup>H NMR 1-(4-(benzyloxy)-3-chlorophenyl)-2-(1*H*-tetrazol-5-yl)ethan-1-one for (**12d**)

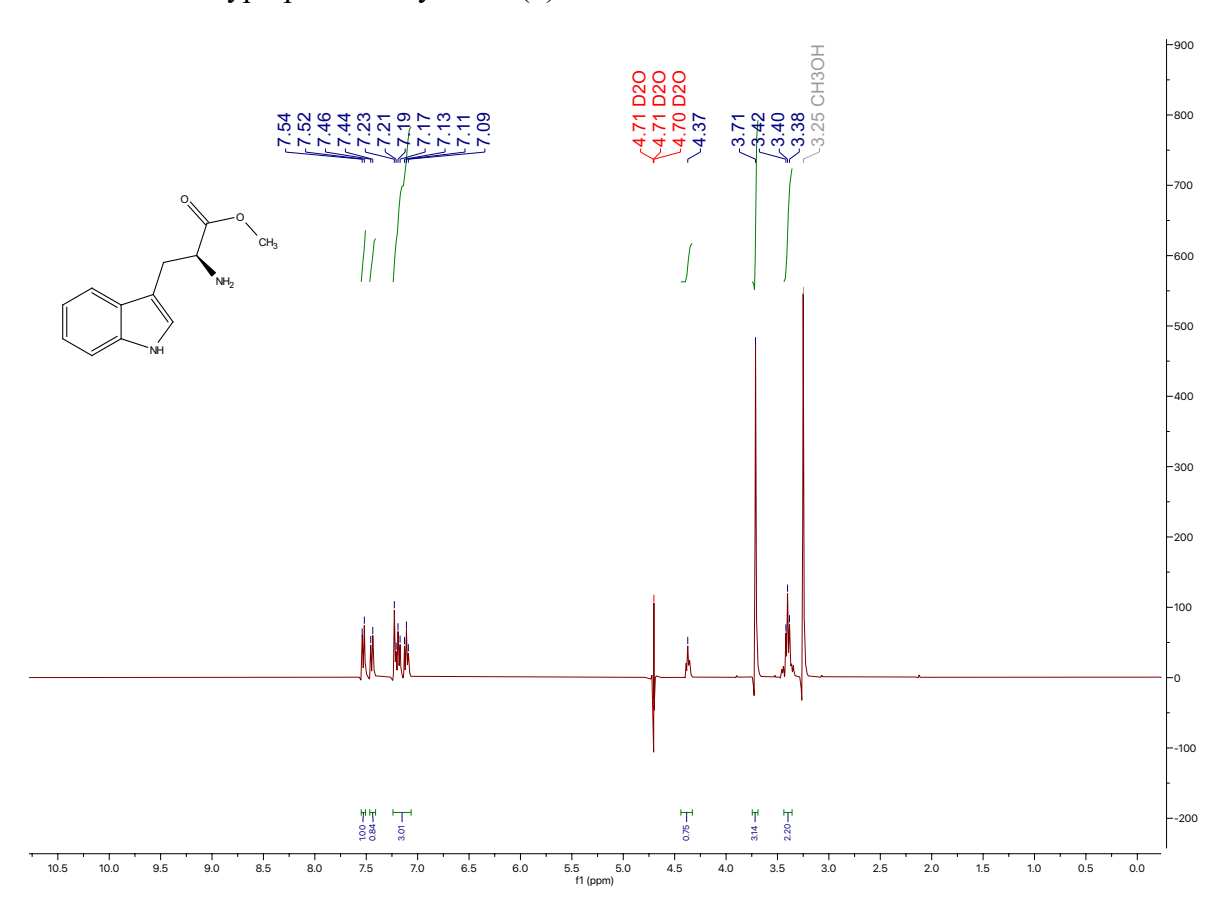


 $^{13}$ C NMR for 1-(4-(benzyloxy)-3-chlorophenyl)-2-(1H-tetrazol-5-yl)ethan-1-one (12d)

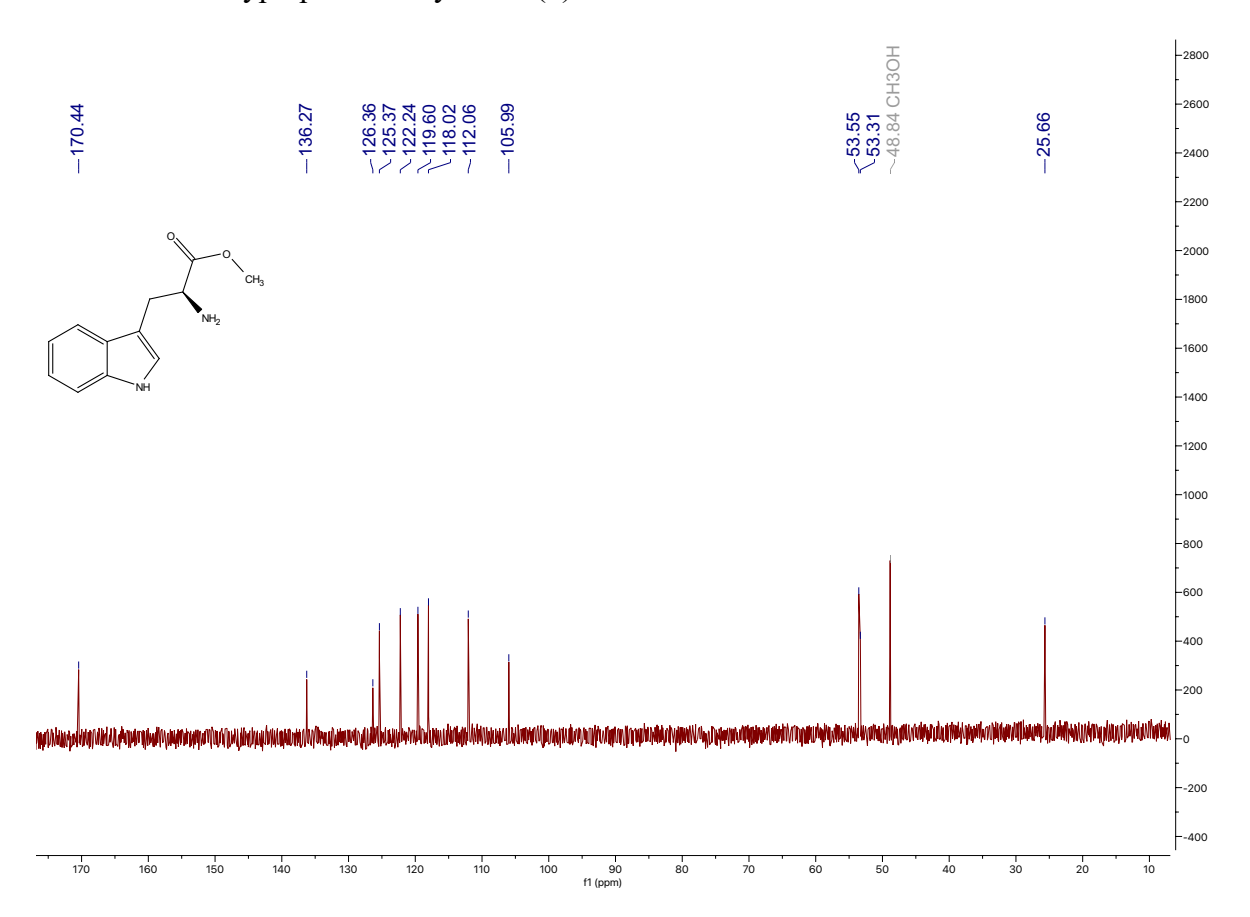


# C. <sup>1</sup>H and <sup>13</sup>C NMR for 5-Nitrokynurenine synthesis

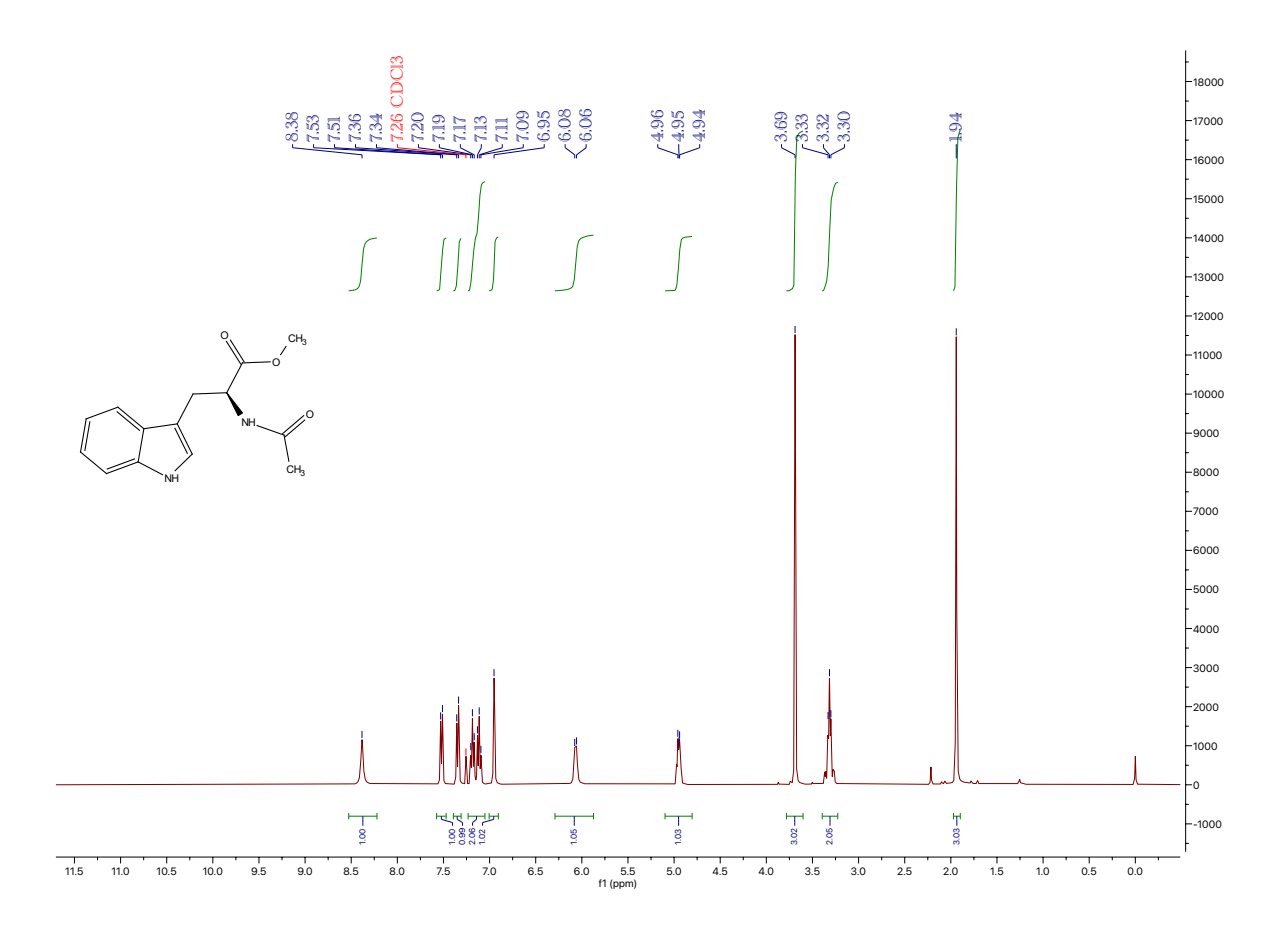
<sup>1</sup>H NMR for Tryptophan methyl ester (2)



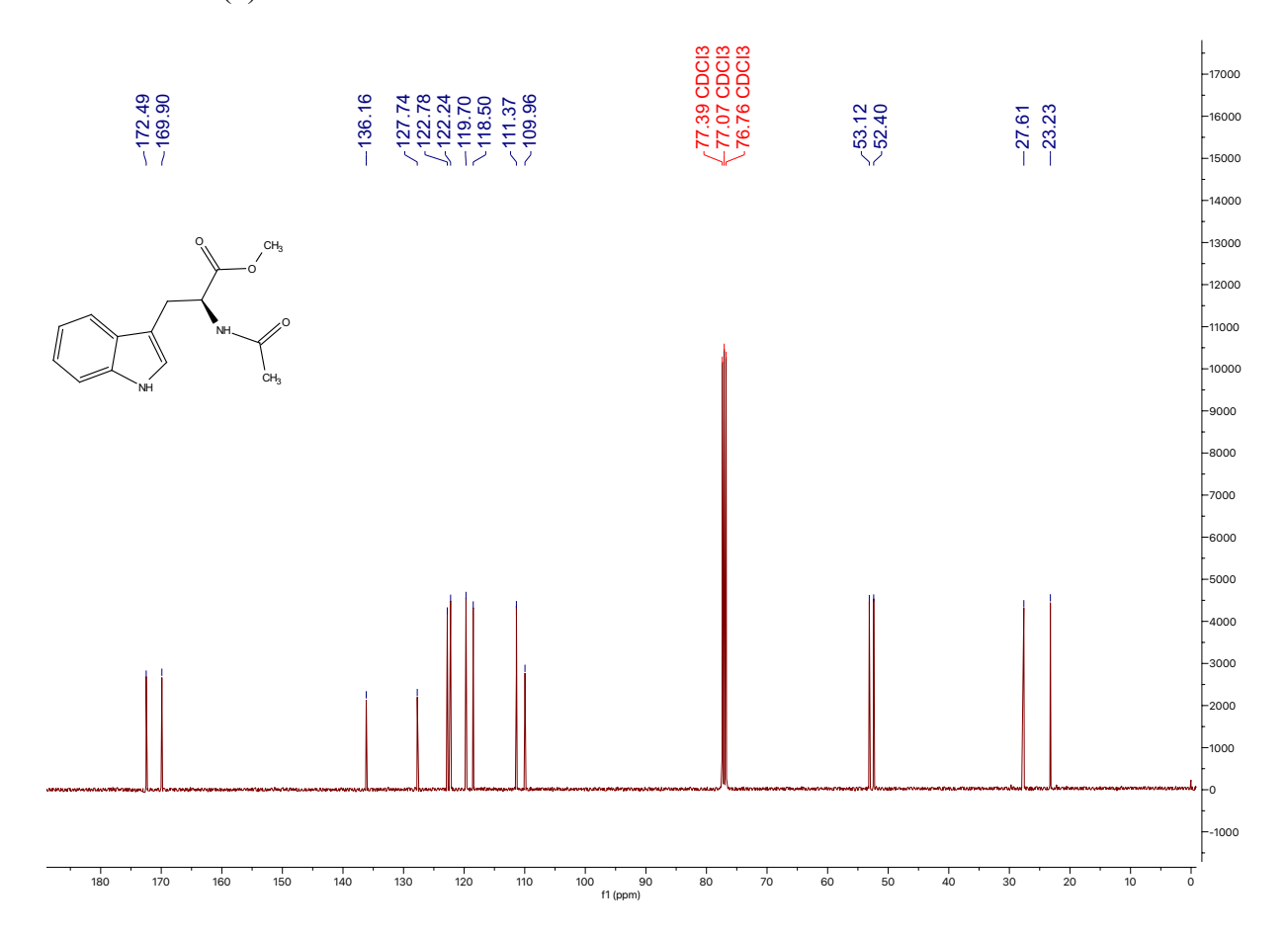
# <sup>13</sup>C NMR for Tryptophan methyl ester (2)



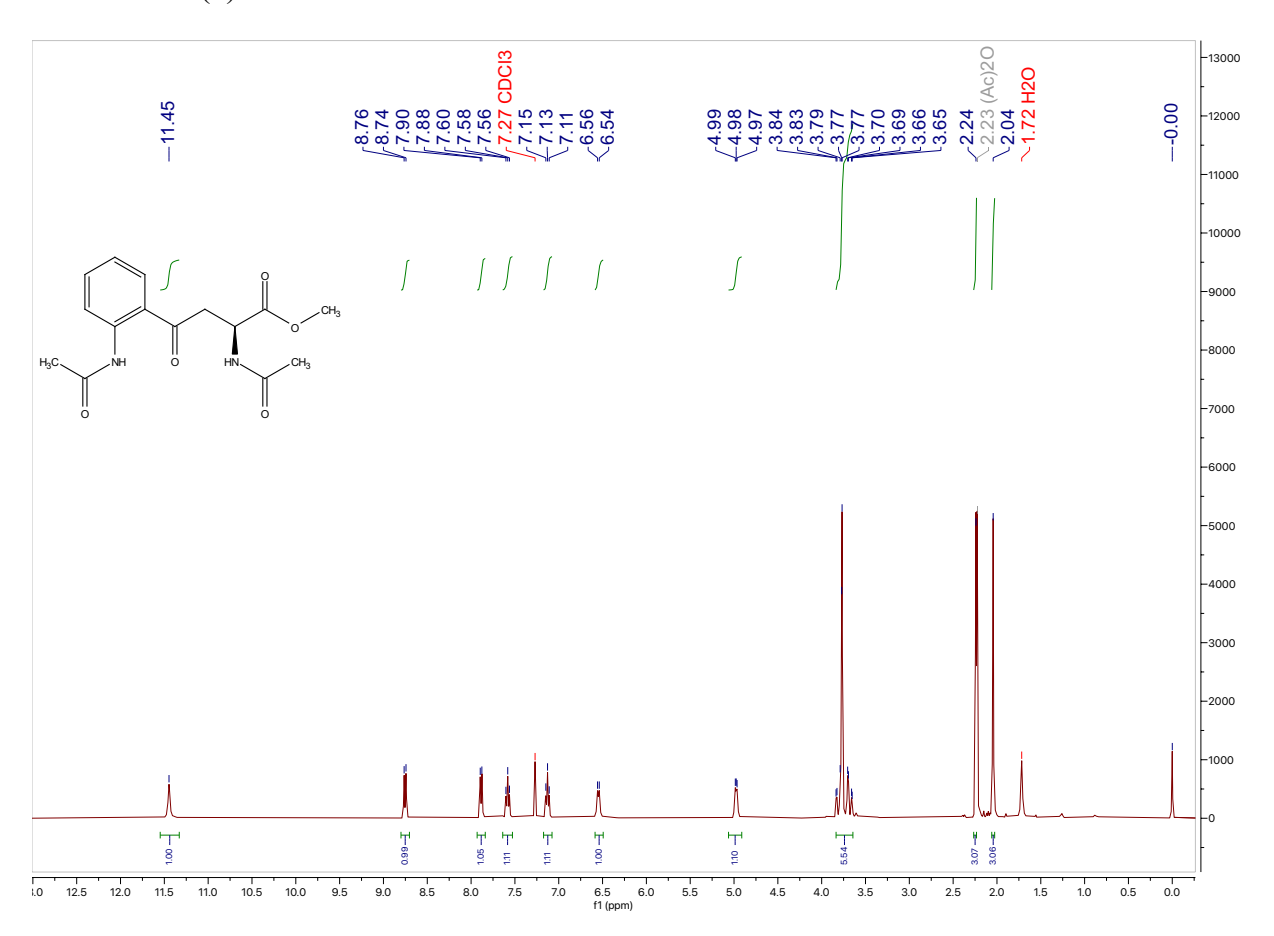
# <sup>1</sup>H NMR for (**3**)



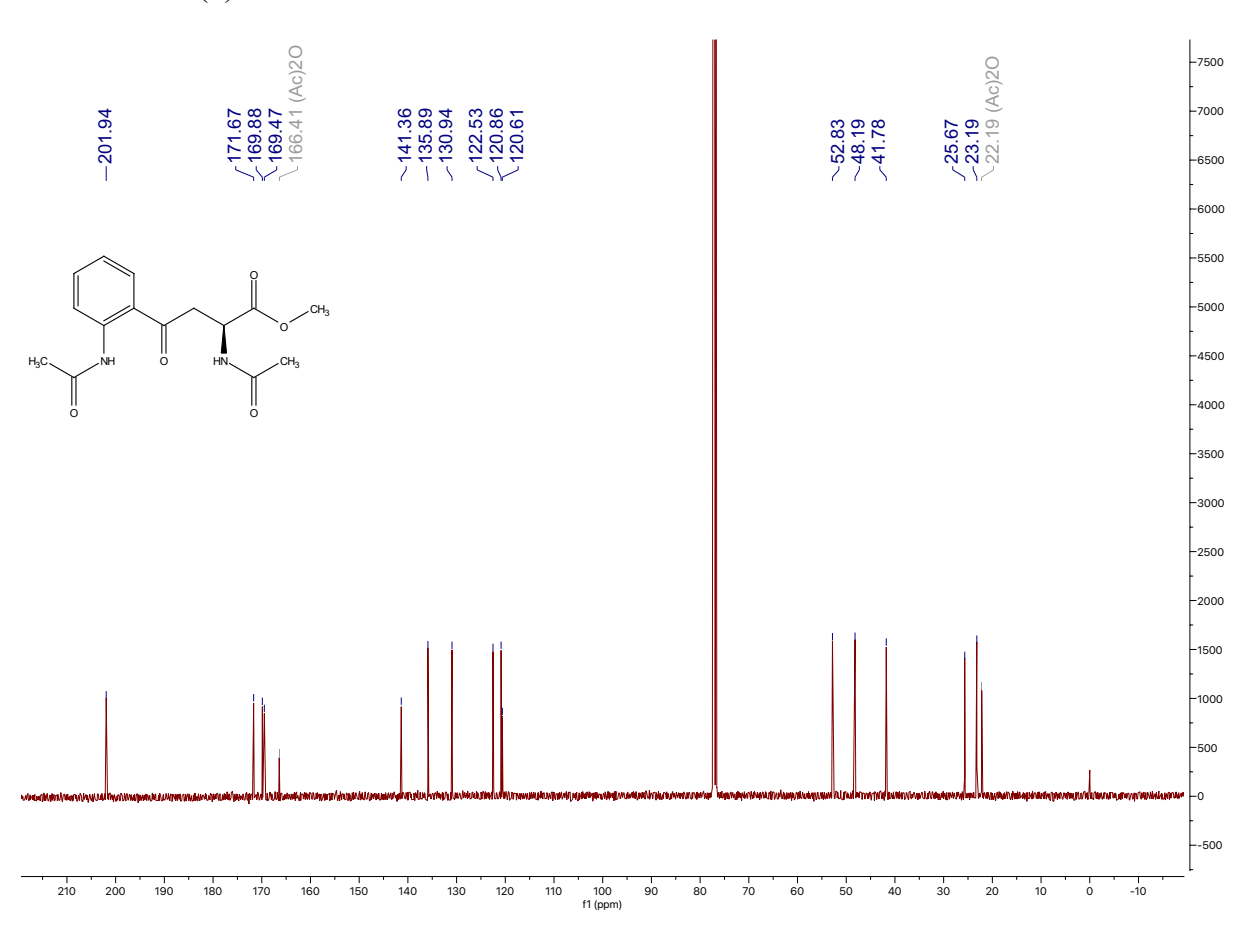
# <sup>13</sup>C NMR for (**3**)



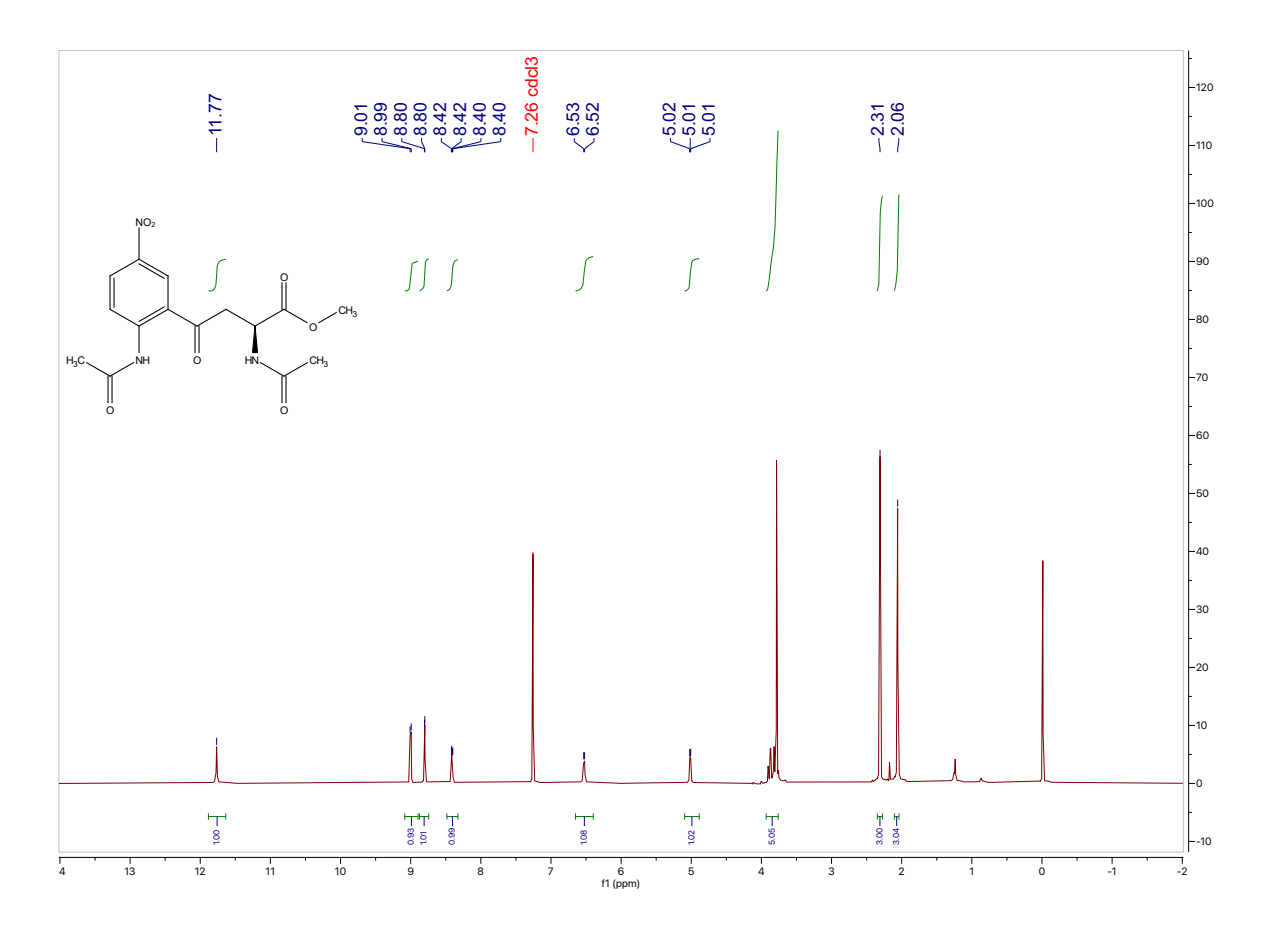
# <sup>1</sup>H NMR for (**4**)



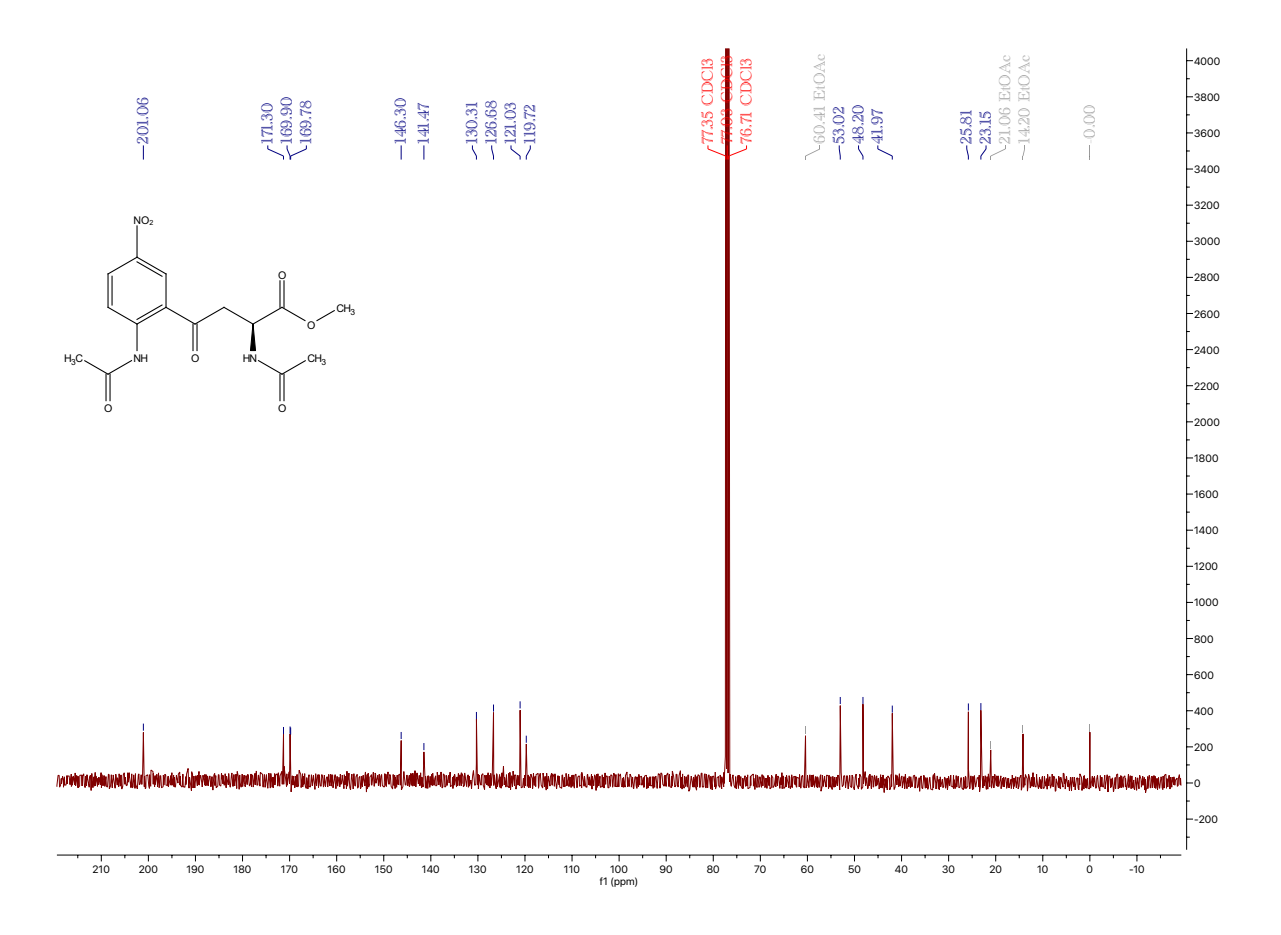
# <sup>13</sup>C NMR for (**4**)



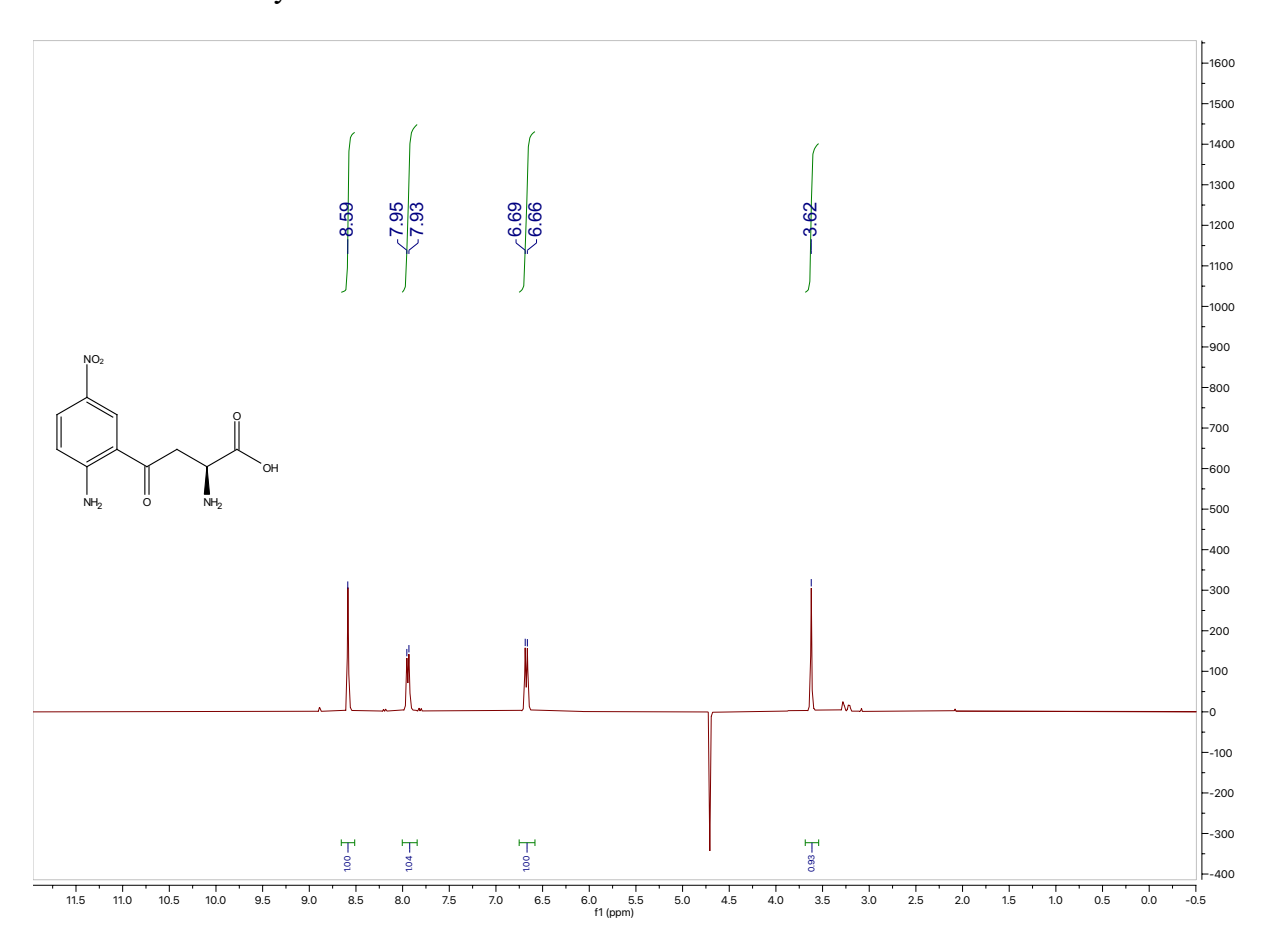
# <sup>1</sup>H NMR for (**5**)



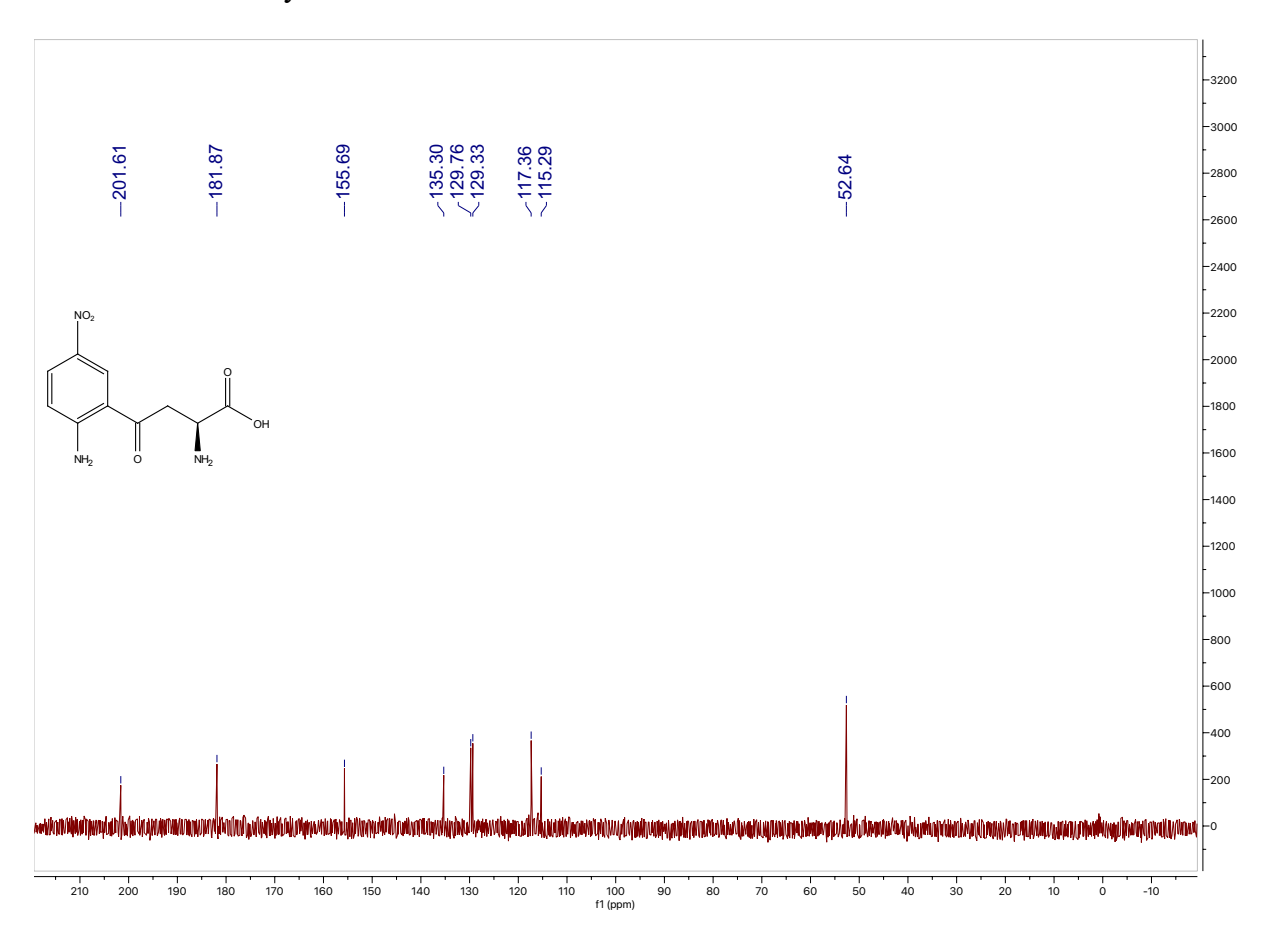
# <sup>13</sup>C NMR for (5)



<sup>1</sup>H NMR for 5-NKyn

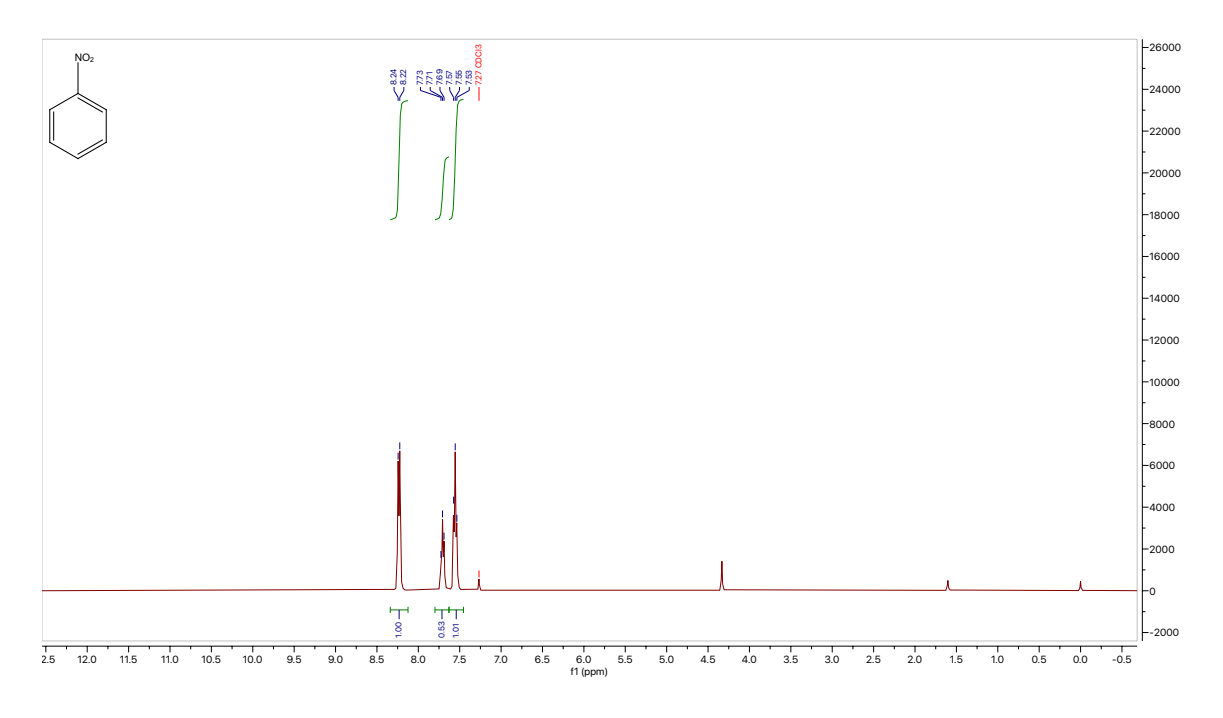


 $^{13}$ C NMR for 5-NKyn

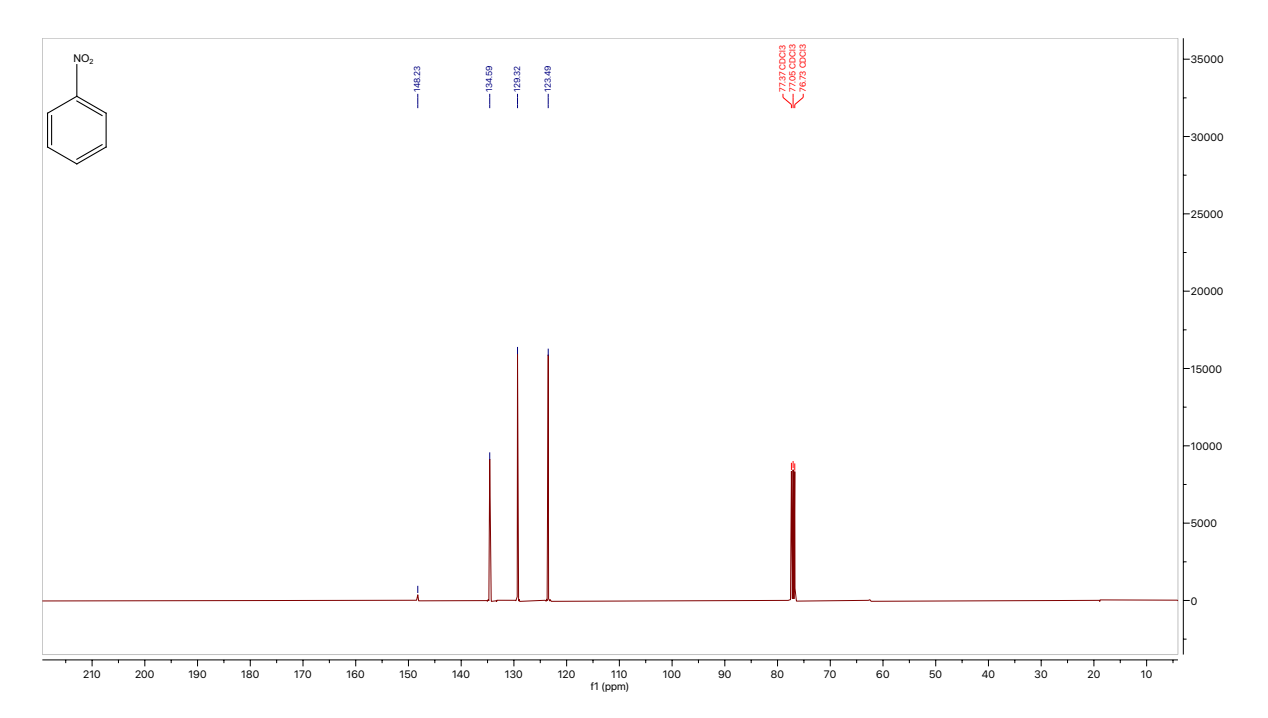


### D. <sup>1</sup>H and <sup>13</sup>C NMR for nitration

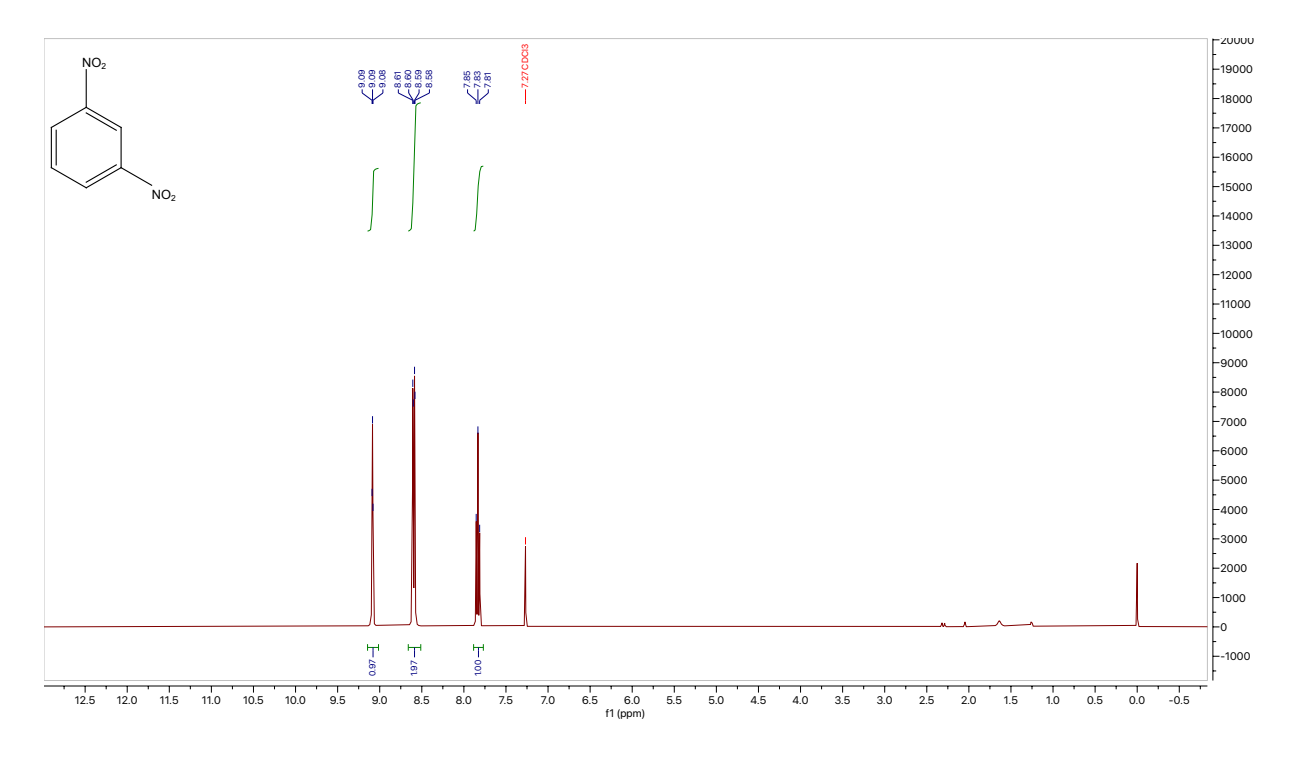
#### <sup>1</sup>H NMR for **1**



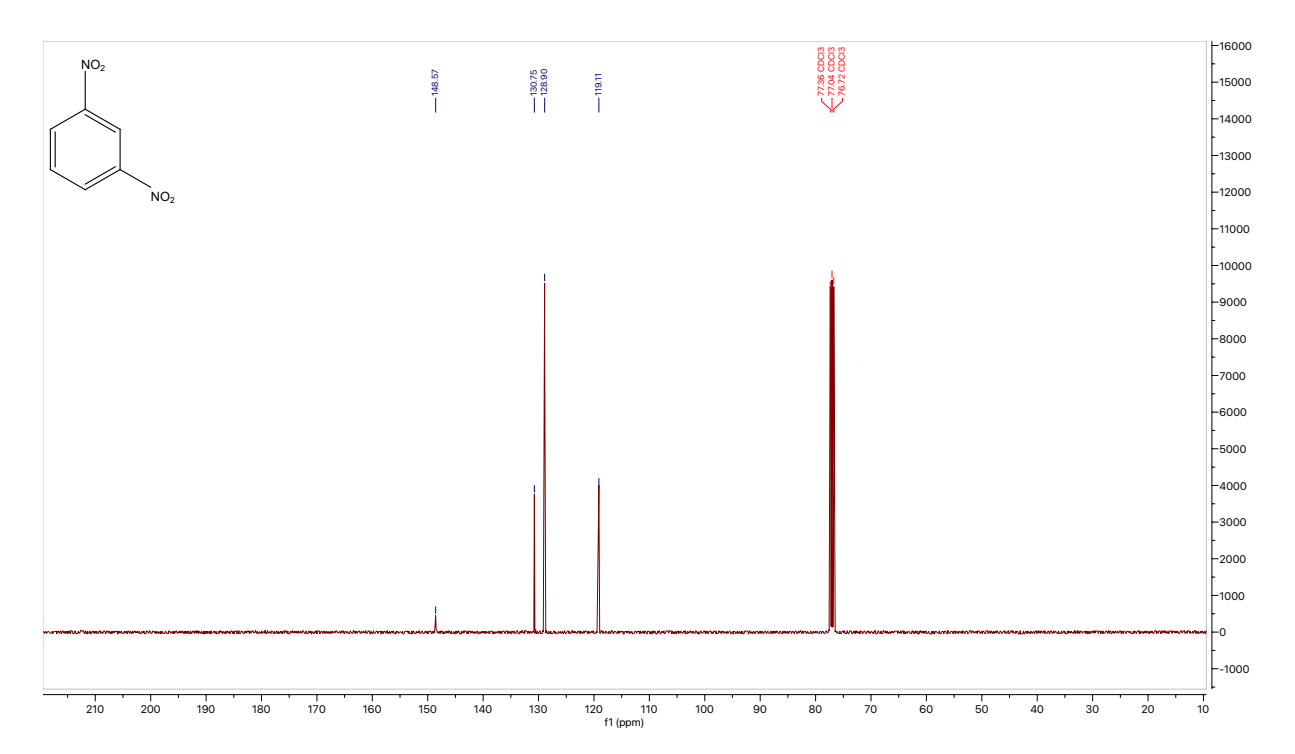
# <sup>13</sup>C NMR for **1**



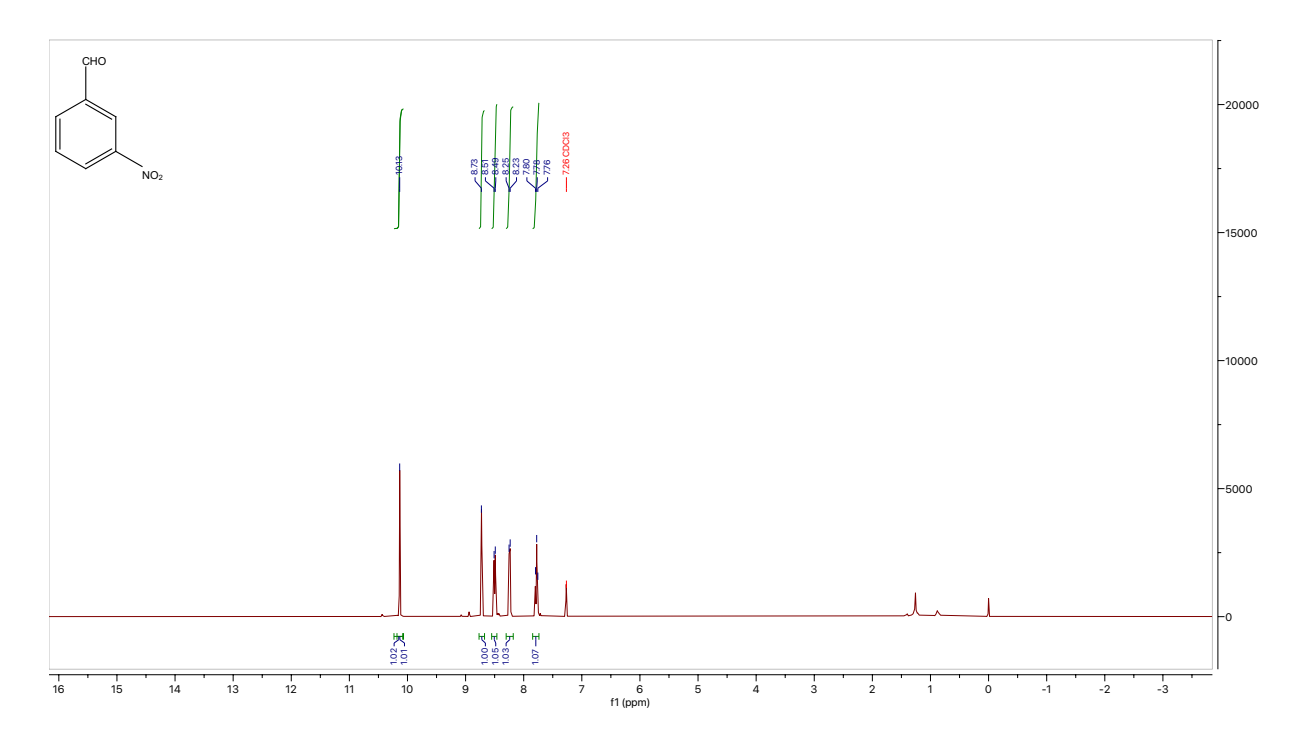
<sup>1</sup>H NMR for **2** 



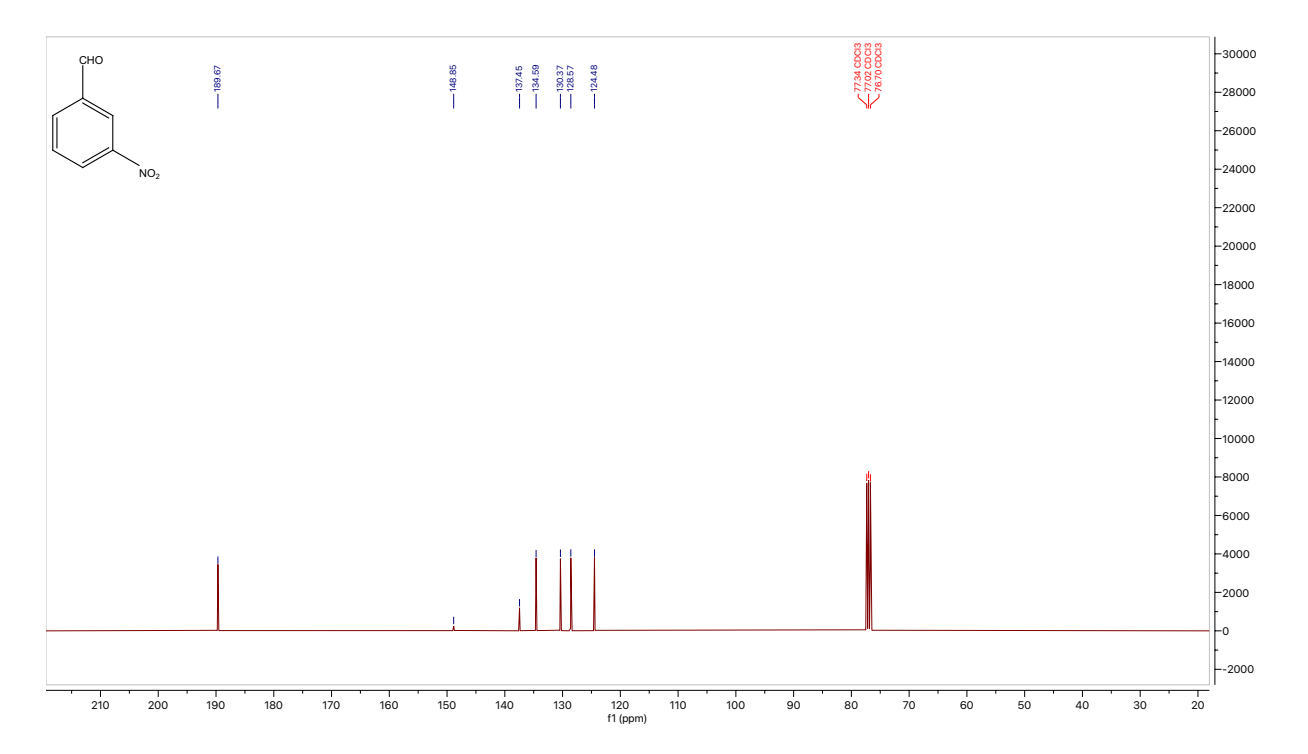
#### <sup>13</sup>C NMR for 2



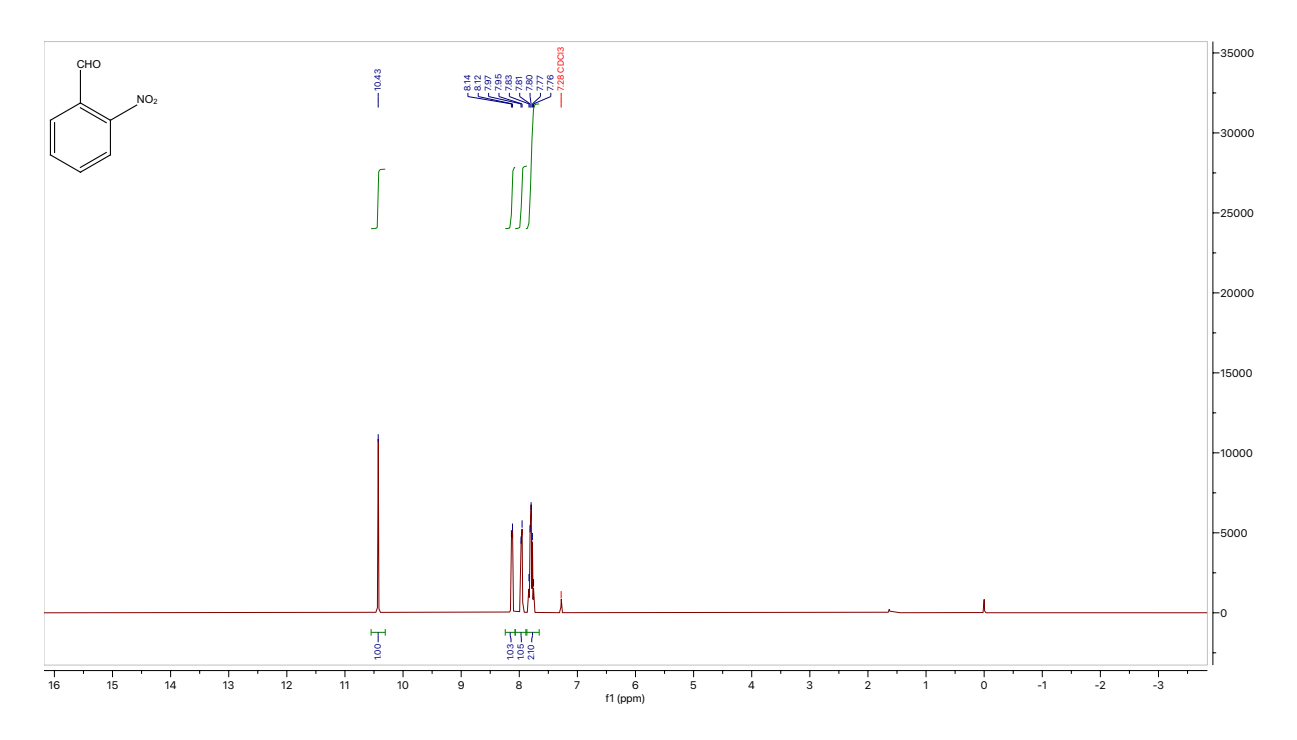
<sup>1</sup>H NMR for **3a** 



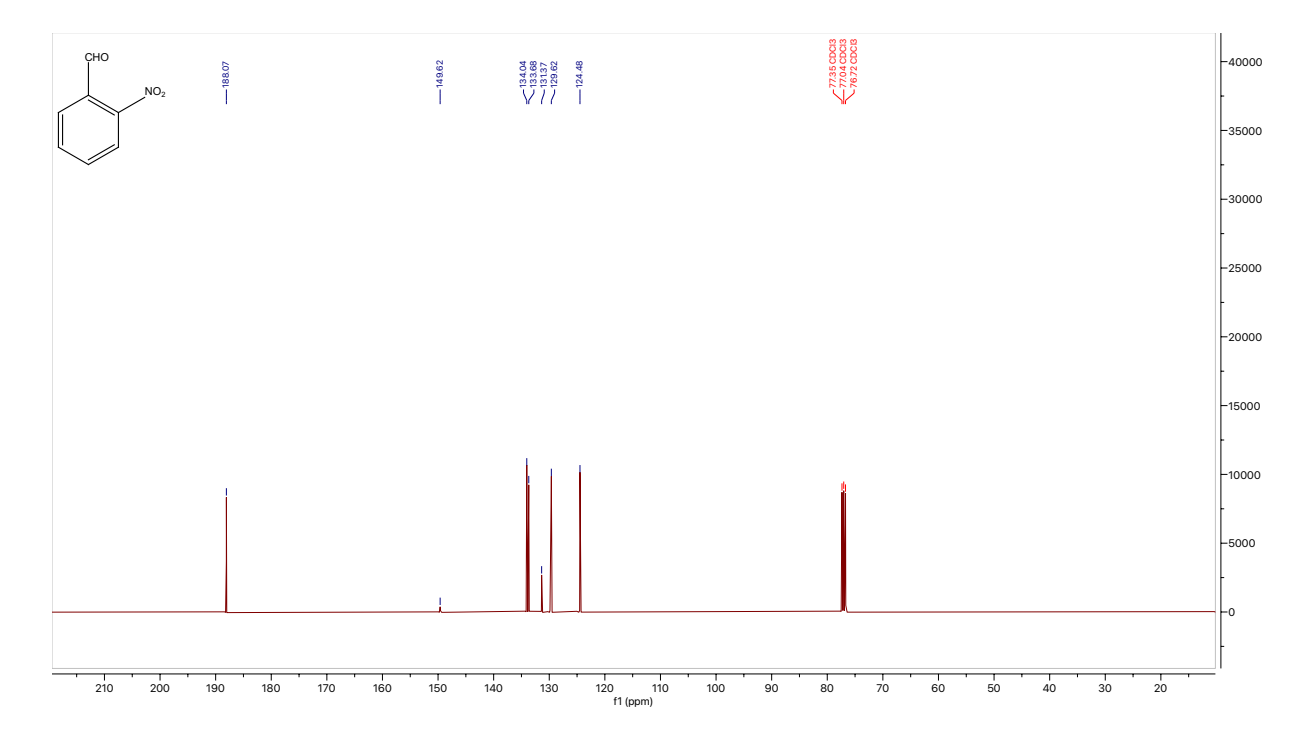
### <sup>13</sup>C NMR for **3a**



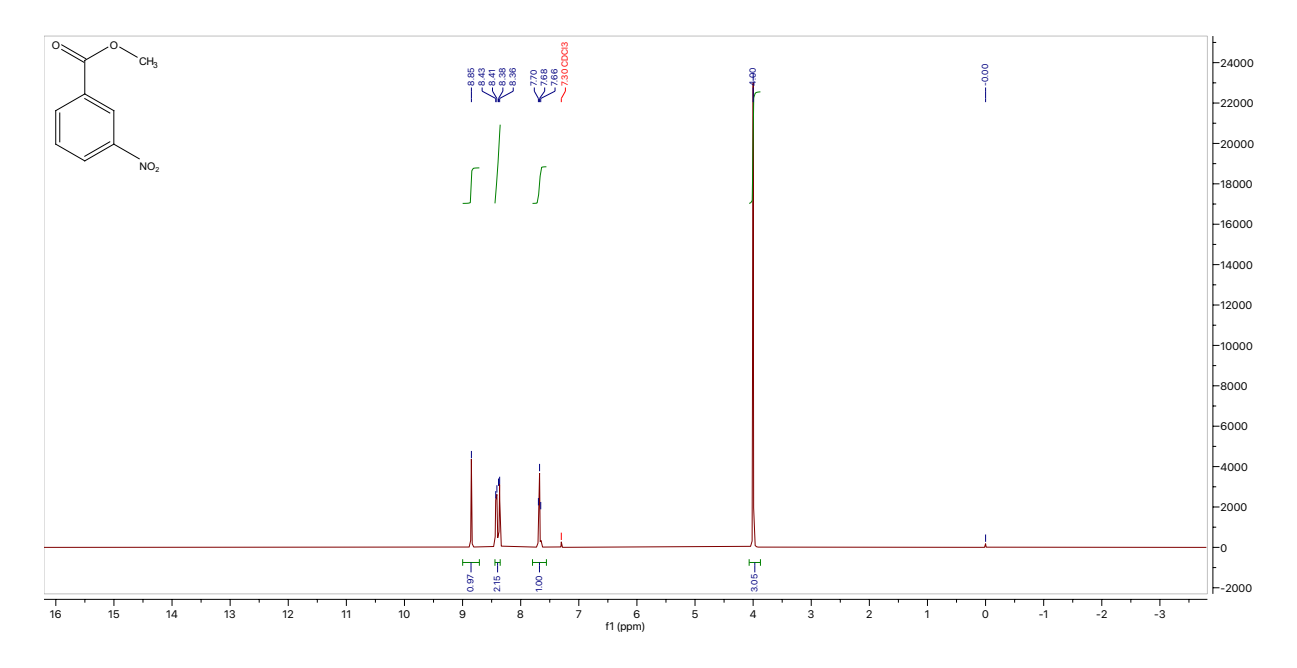
#### <sup>1</sup>H NMR for **3b**



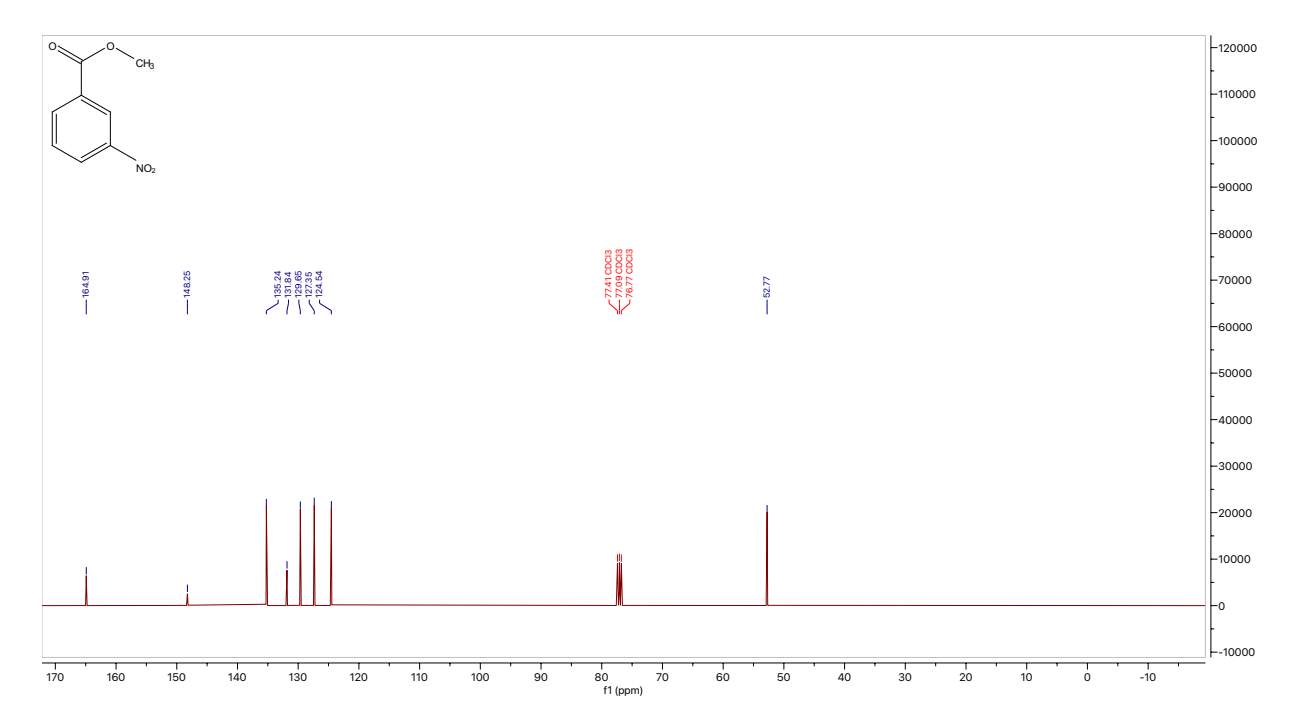
#### <sup>13</sup>C NMR for **3b**



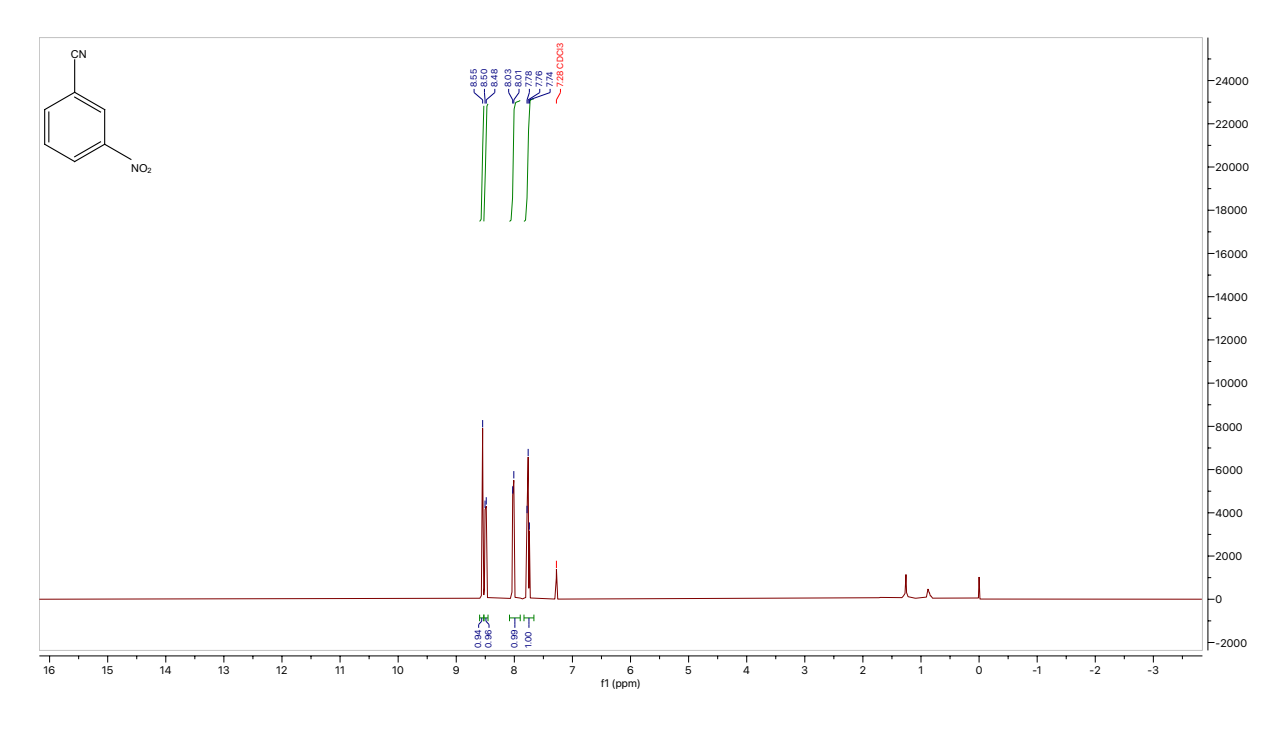
<sup>1</sup>H NMR for **4** 



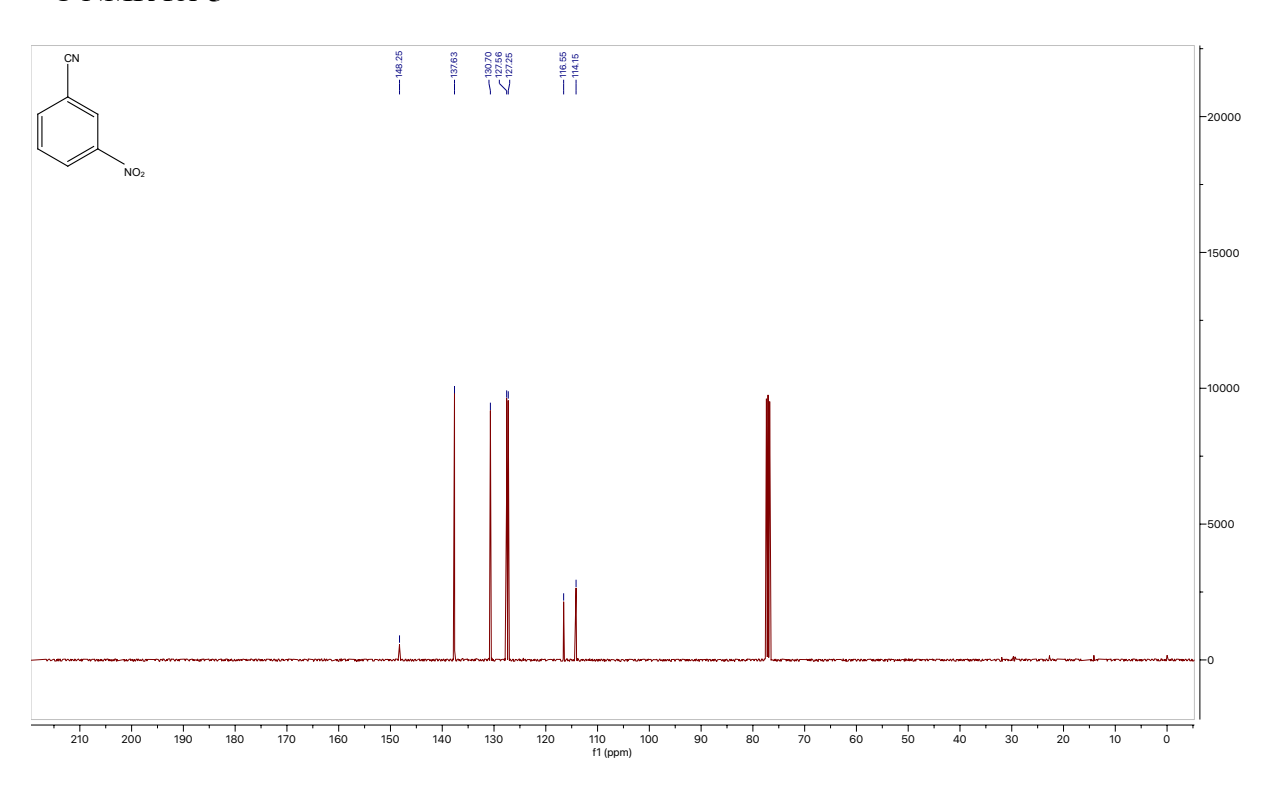
### <sup>13</sup>C NMR for 4



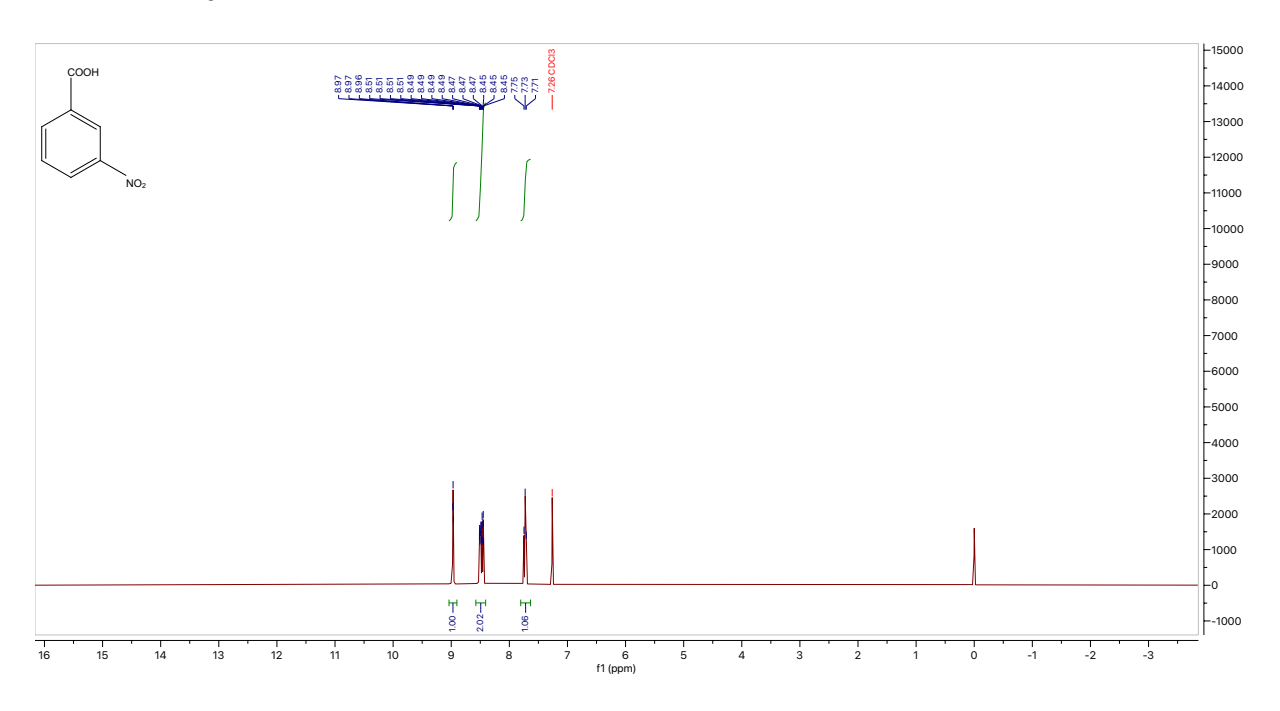
<sup>1</sup>H NMR for **5** 



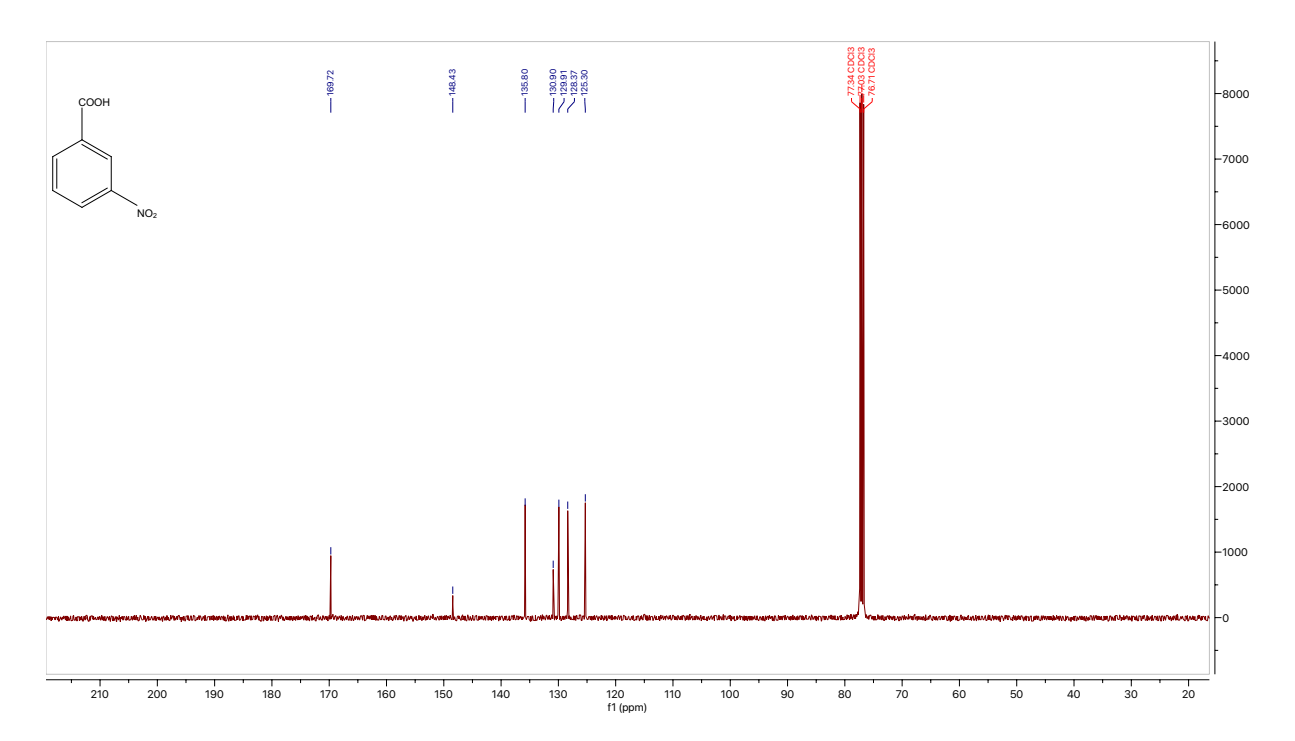
## $^{13}$ C NMR for **5**



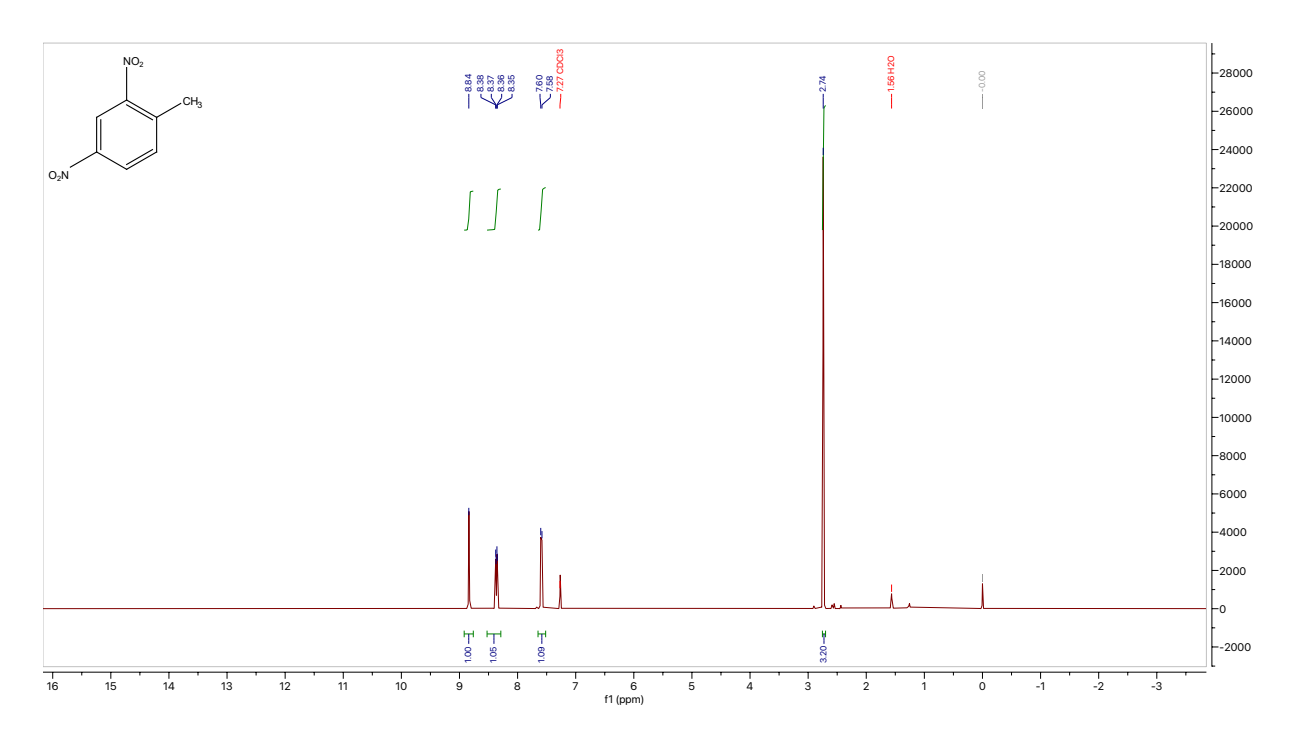
#### <sup>1</sup>H NMR for **6**



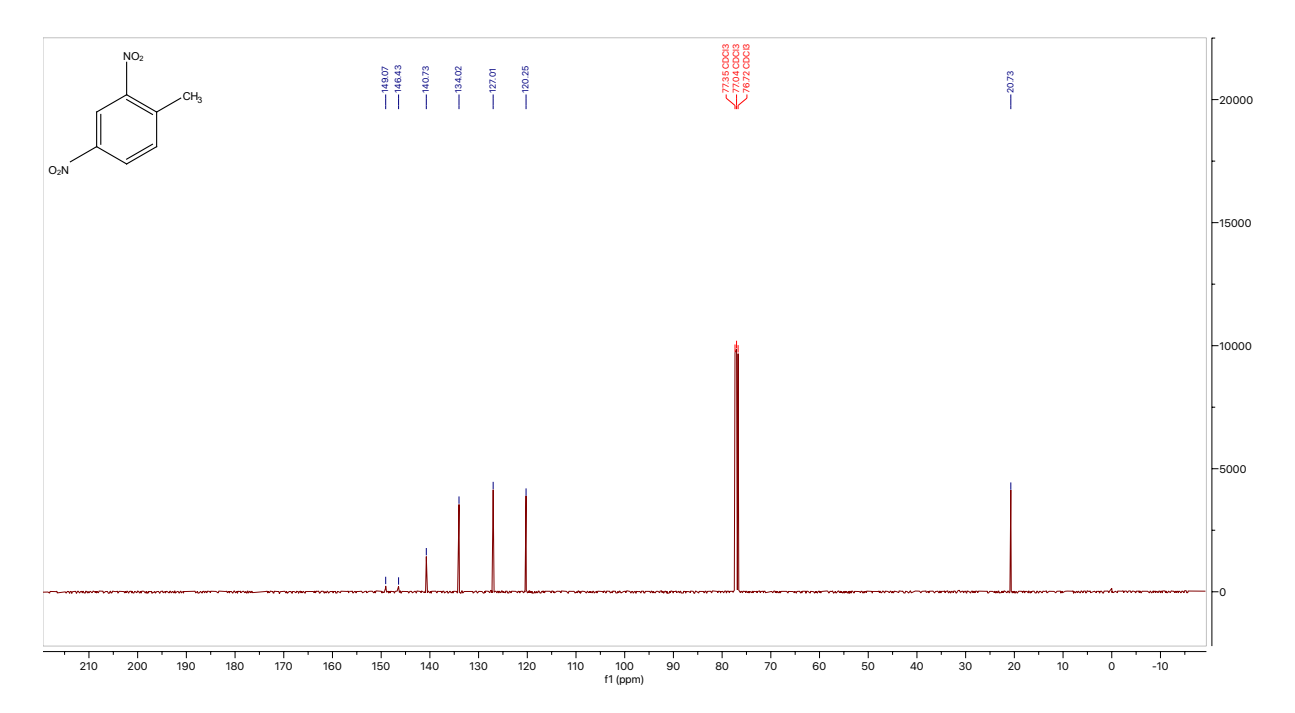
#### <sup>13</sup>C NMR for **6**



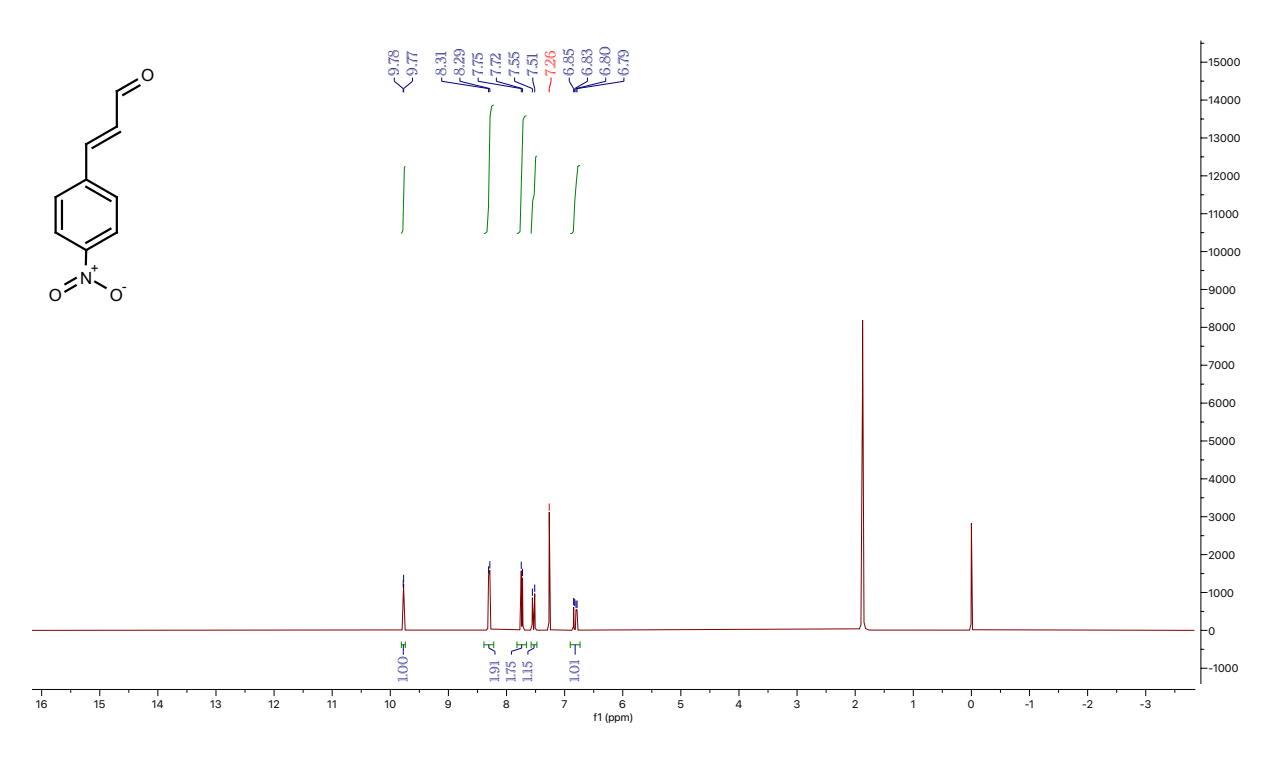
#### <sup>1</sup>H NMR for **7a and 26a**



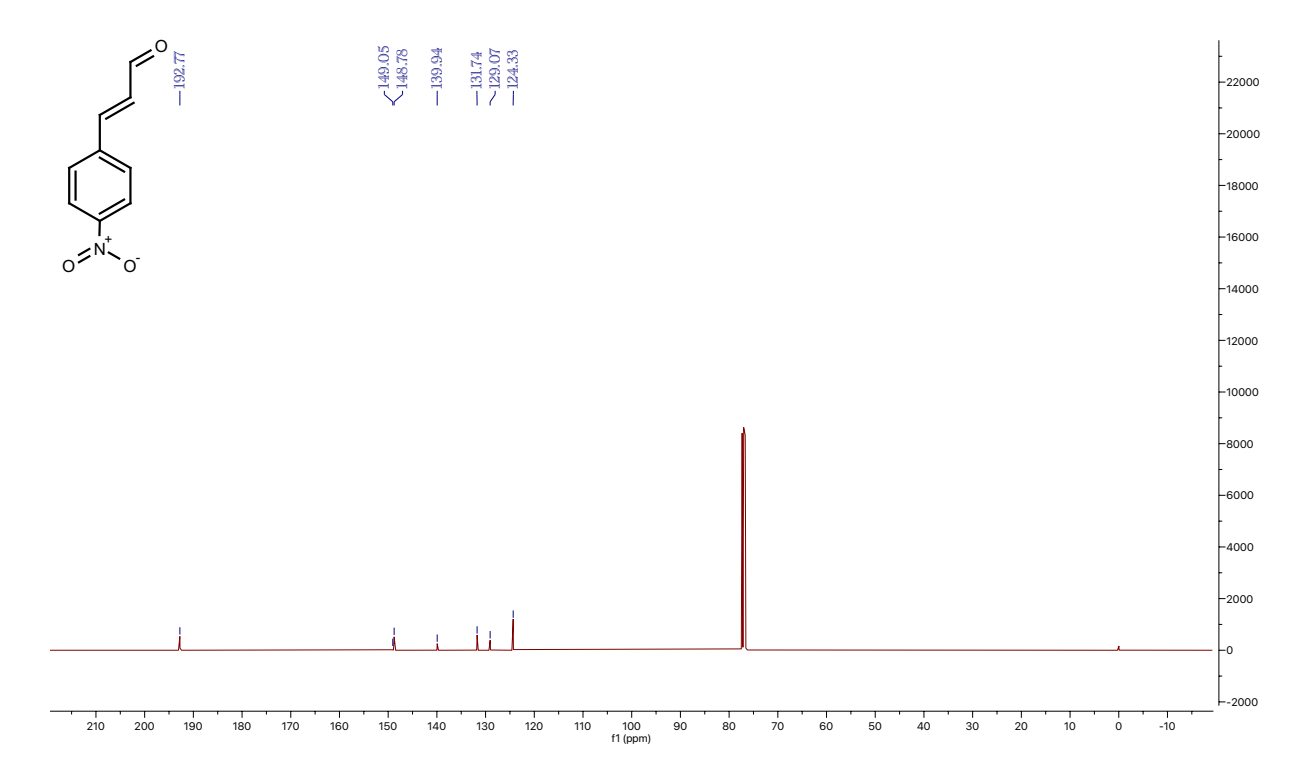
### <sup>13</sup>C NMR for 7a and 26a



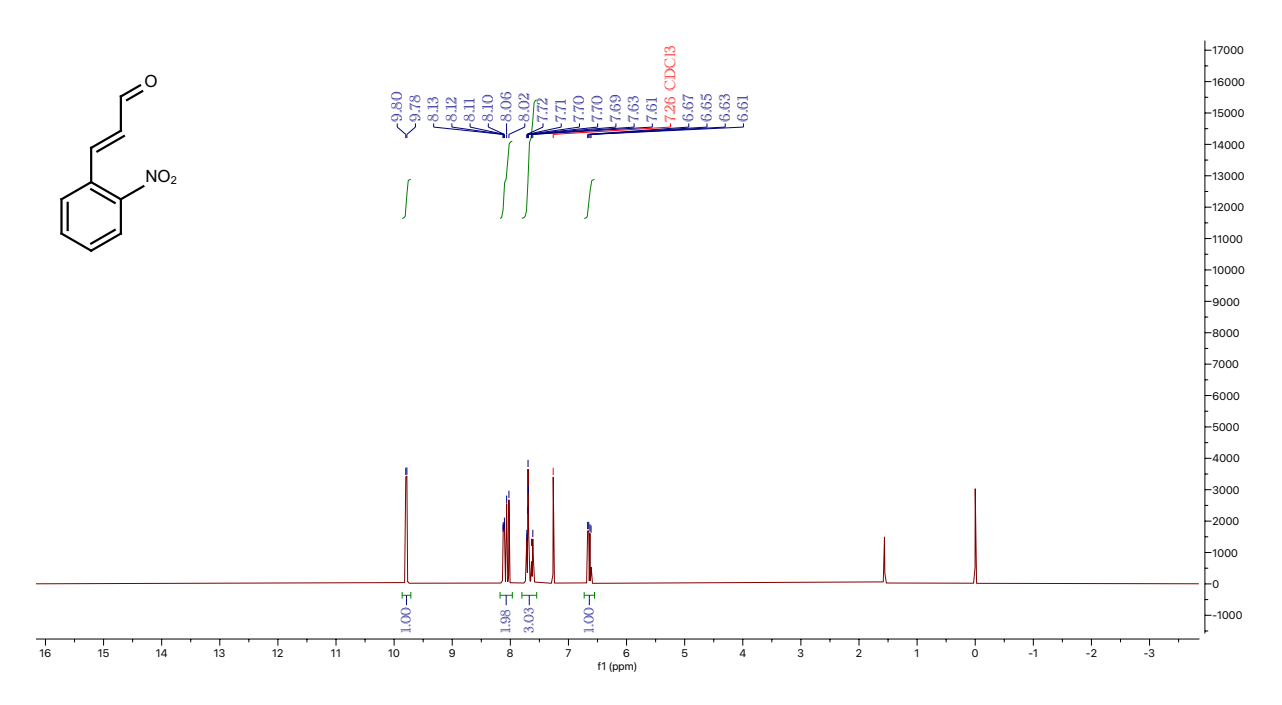
<sup>1</sup>H NMR for **8a** 



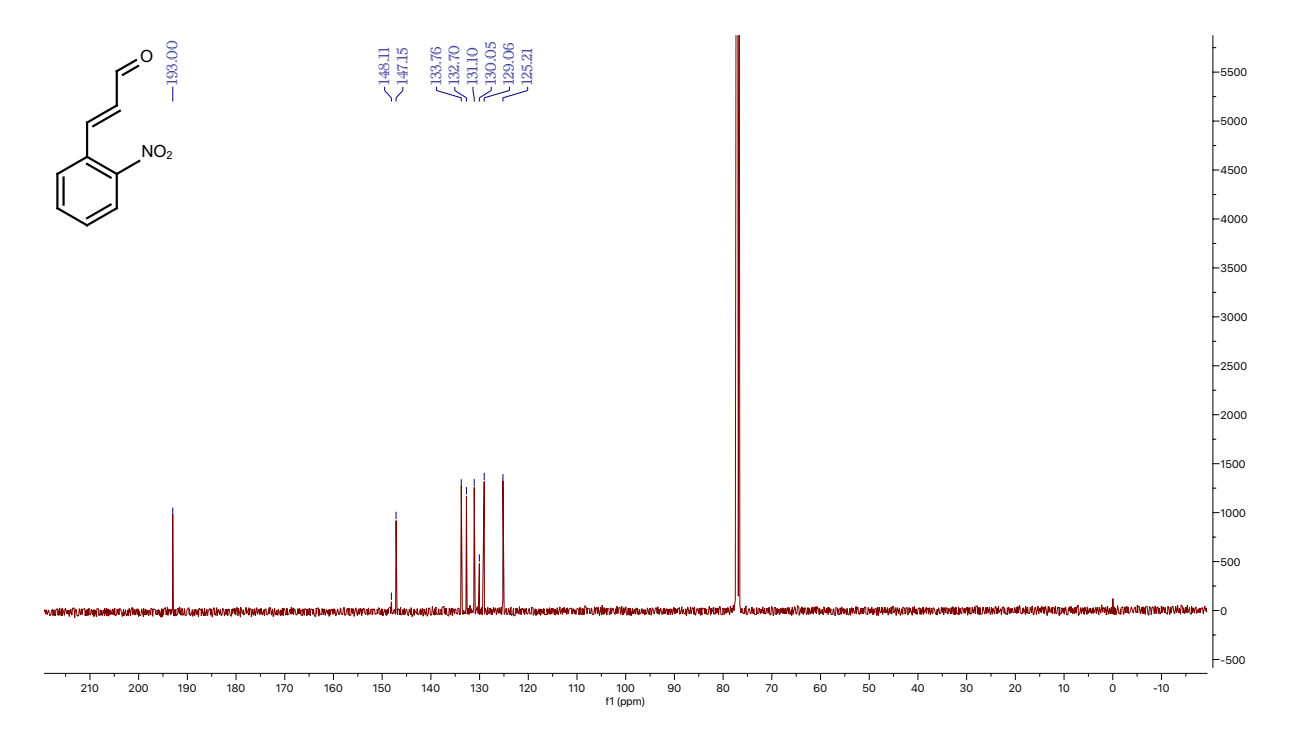
## <sup>13</sup>C NMR for **8a**



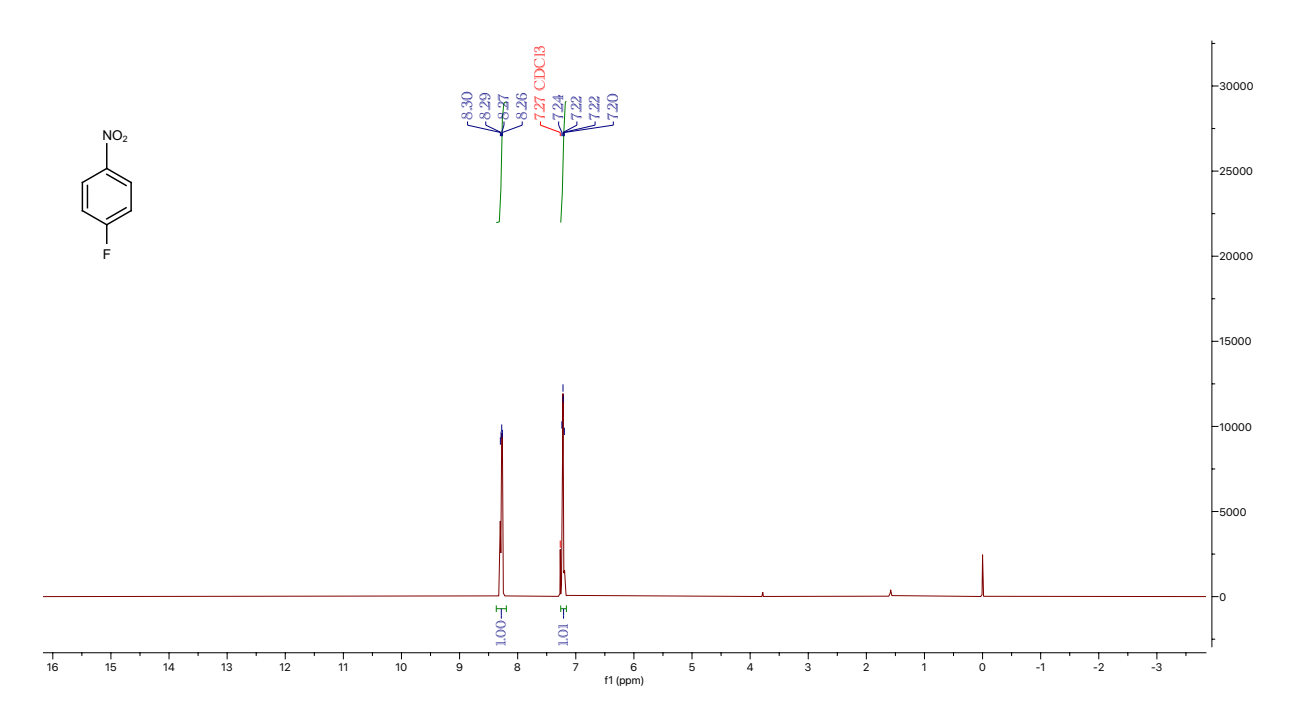
#### <sup>1</sup>H NMR for **8b**



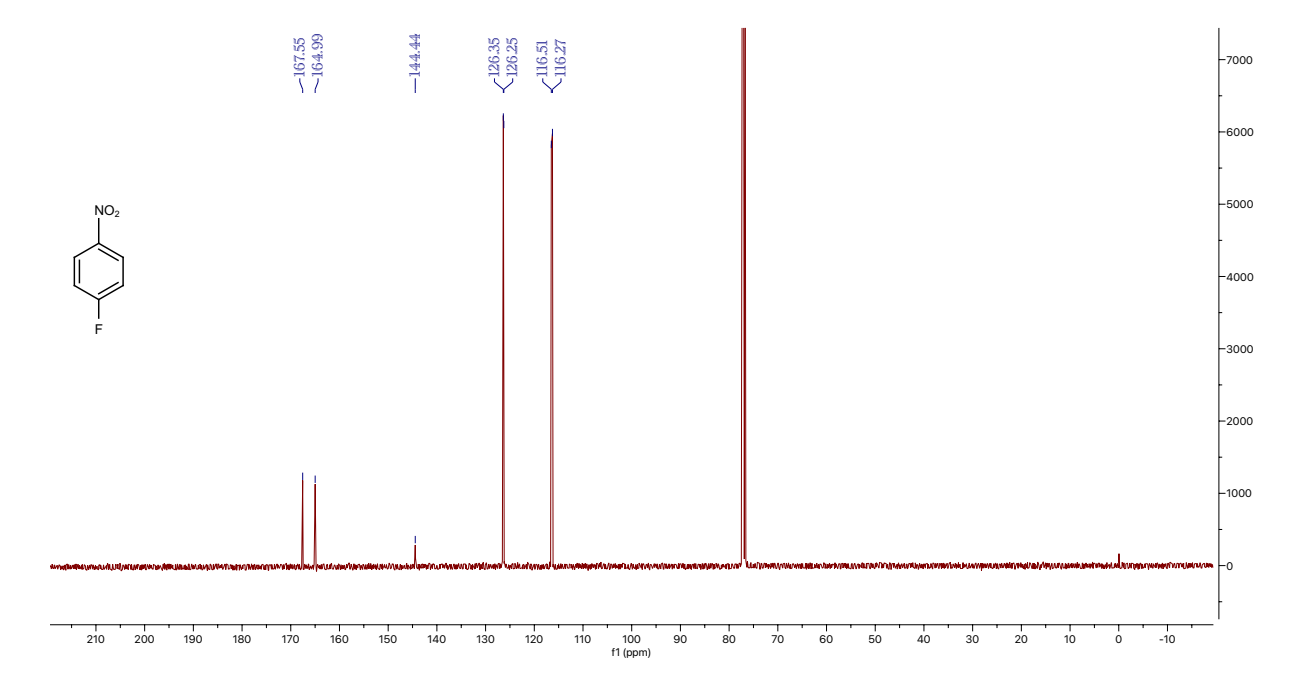
#### <sup>13</sup>C NMR for **8b**



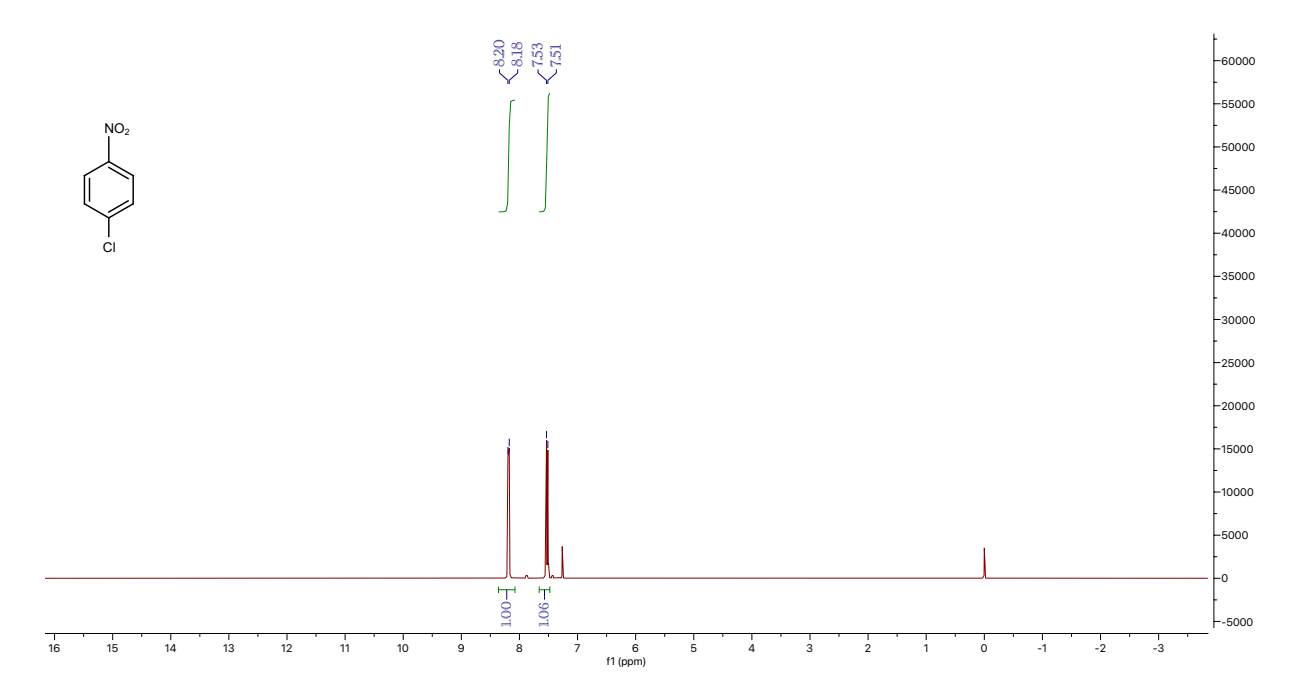
<sup>1</sup>H NMR for **9** 

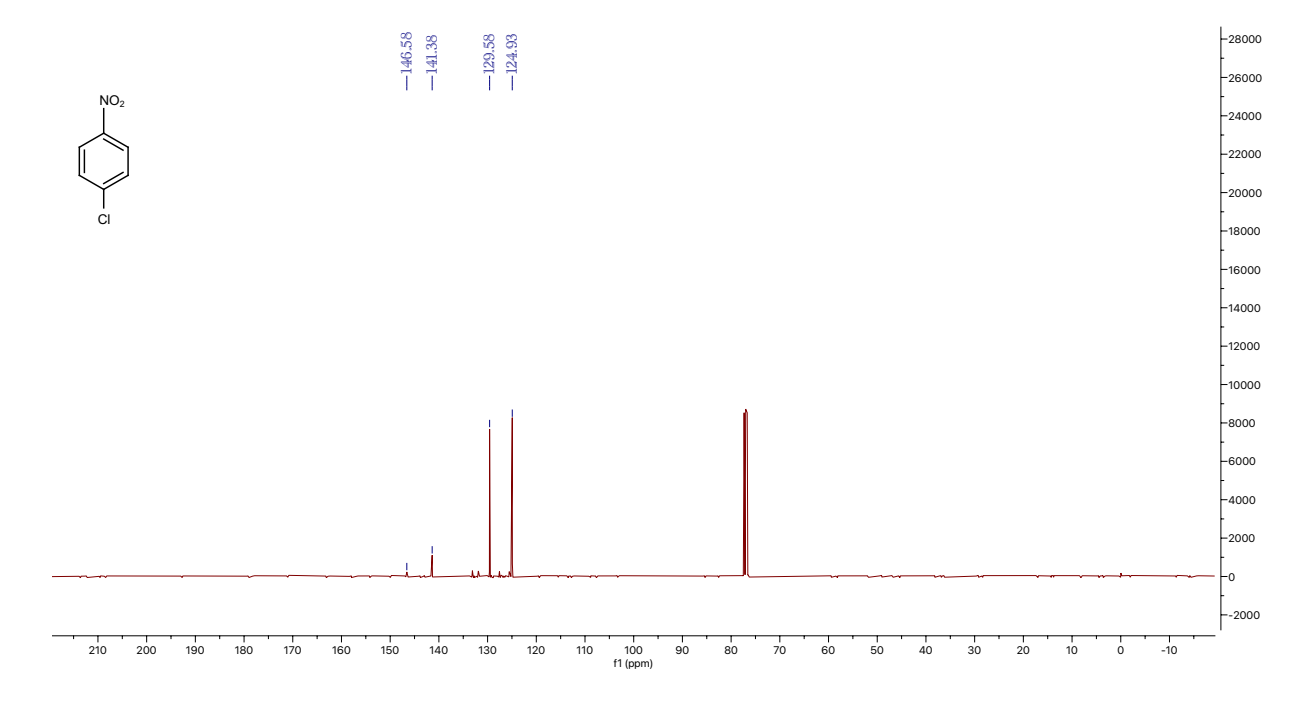


## <sup>13</sup>C NMR for 9

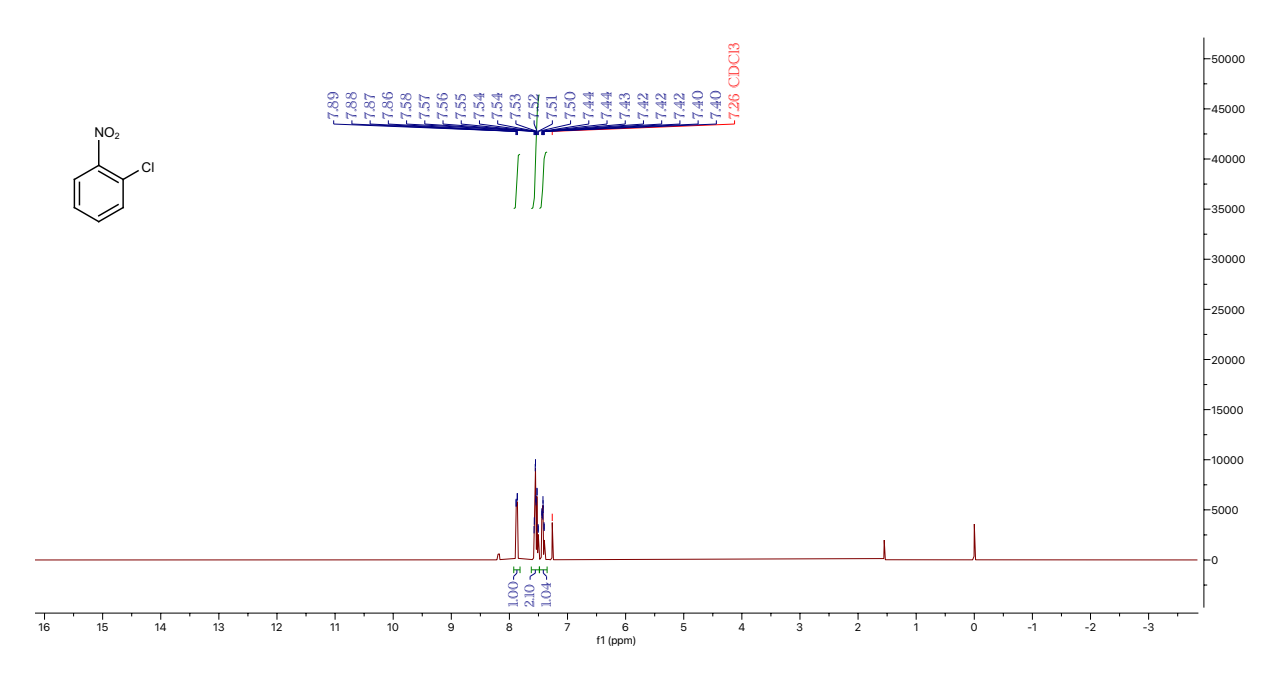


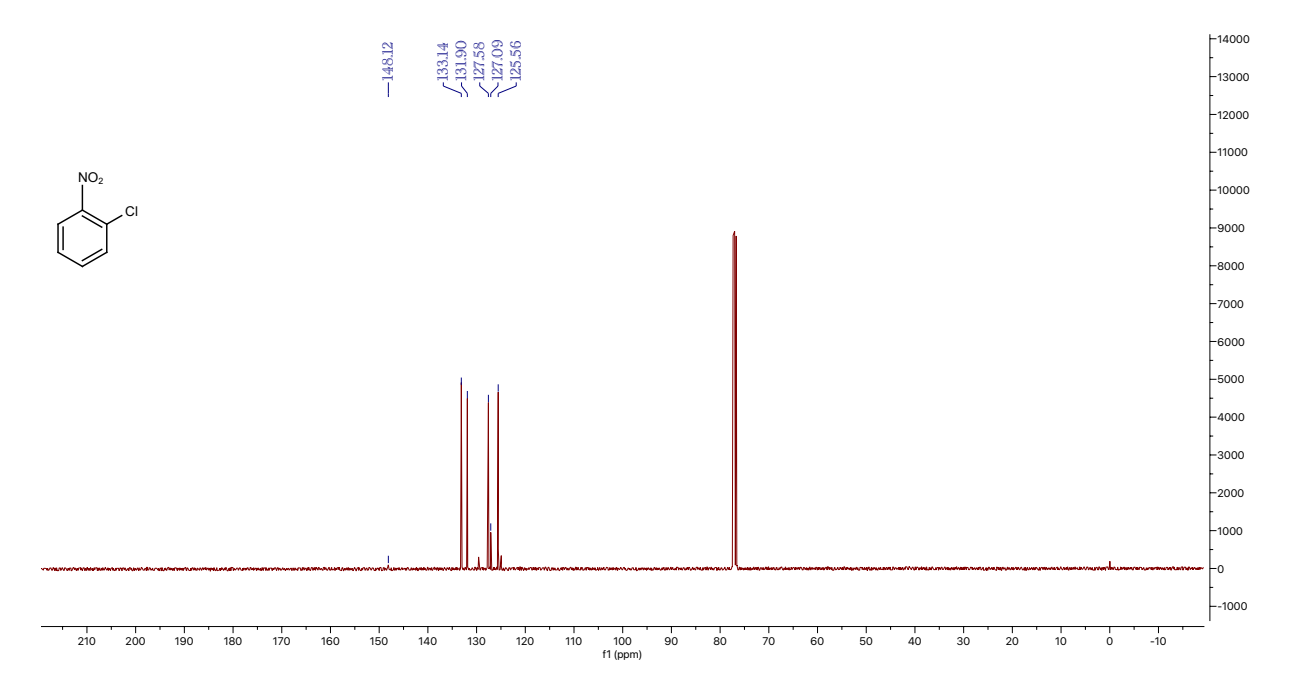
### <sup>1</sup>H NMR for **10a**



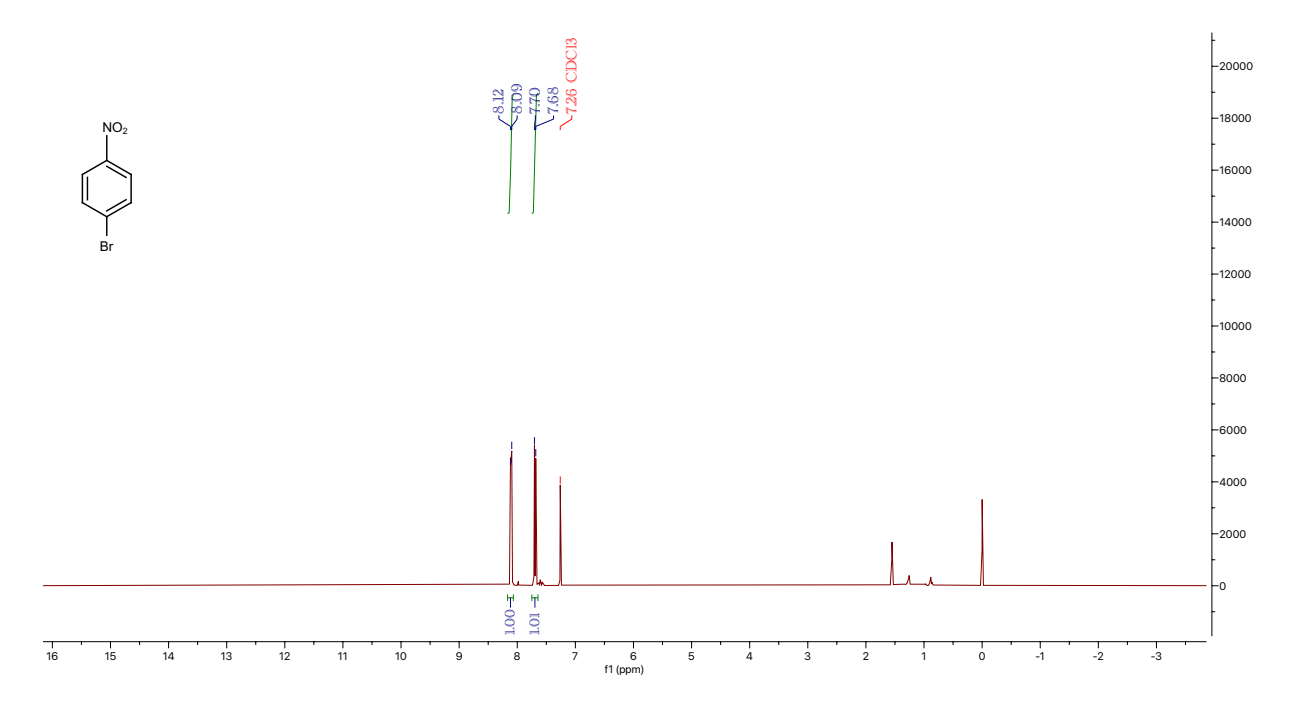


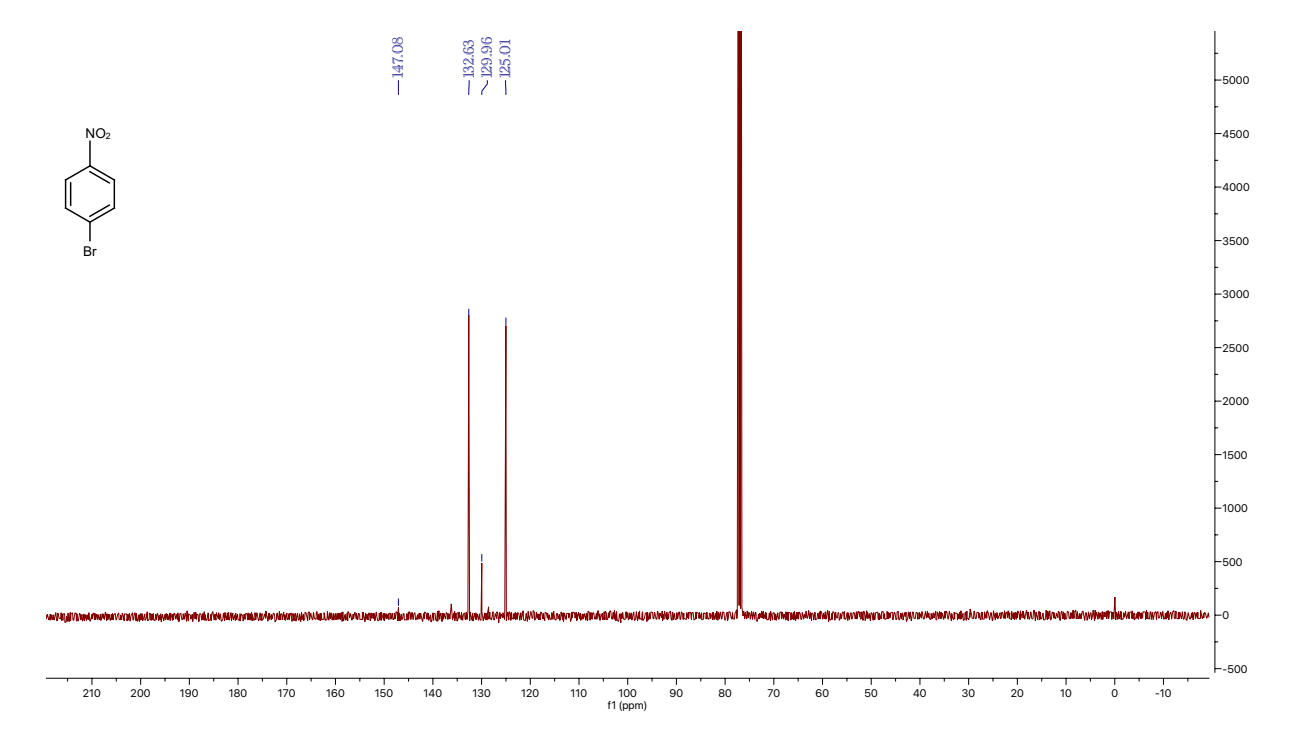
### <sup>1</sup>H NMR for **10b**



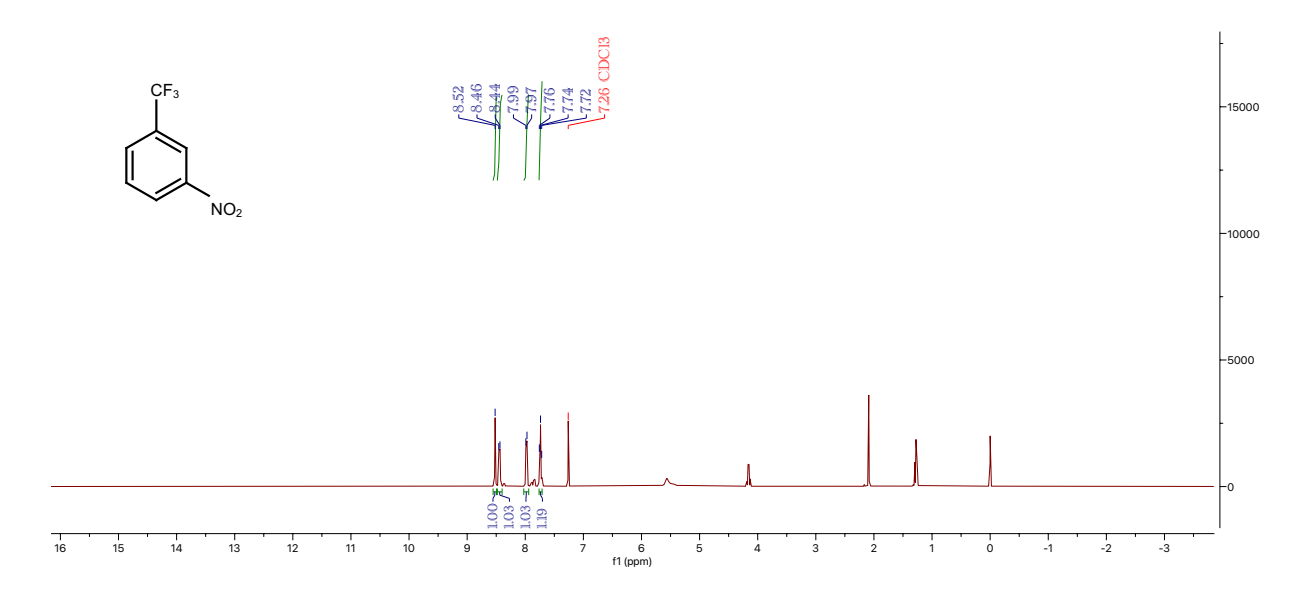


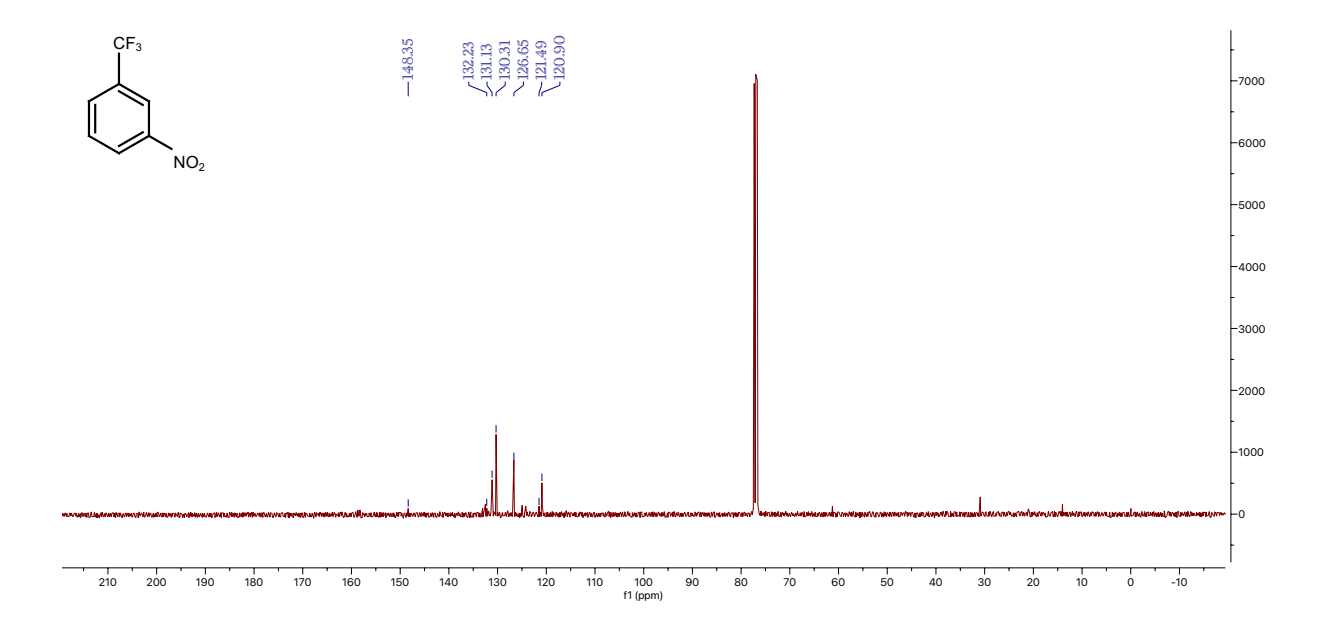
<sup>1</sup>H NMR for **11** 



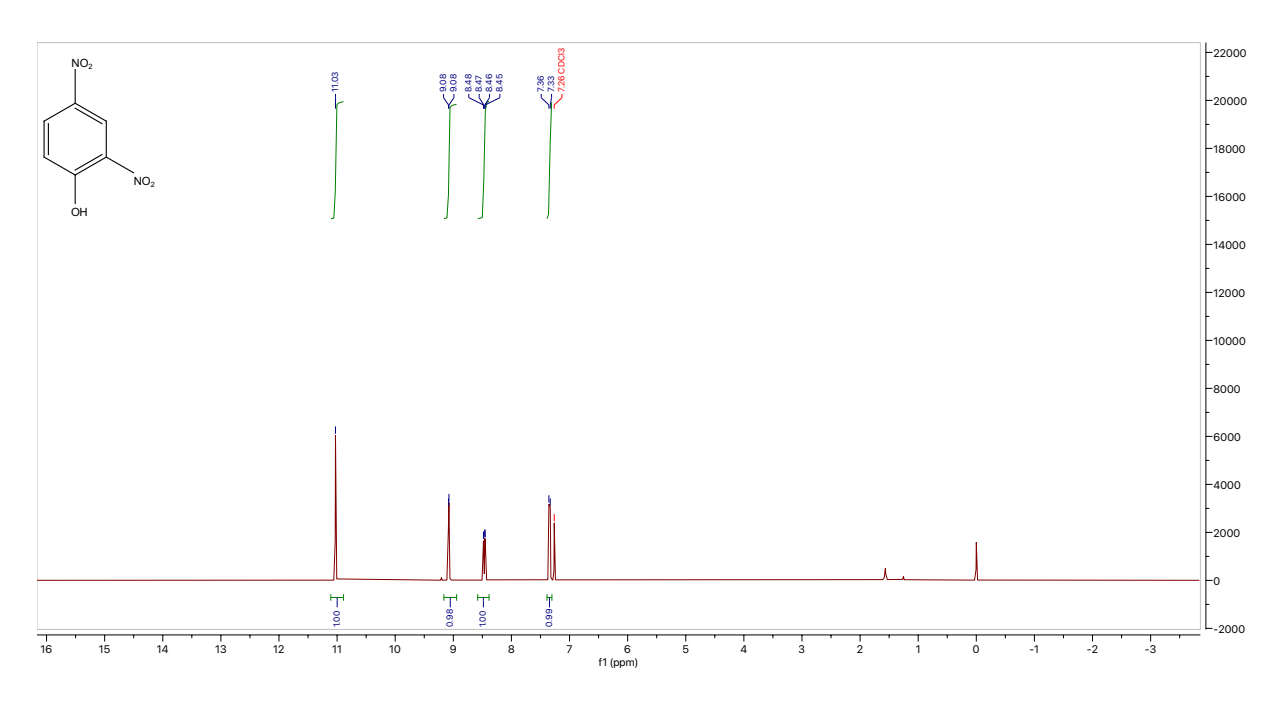


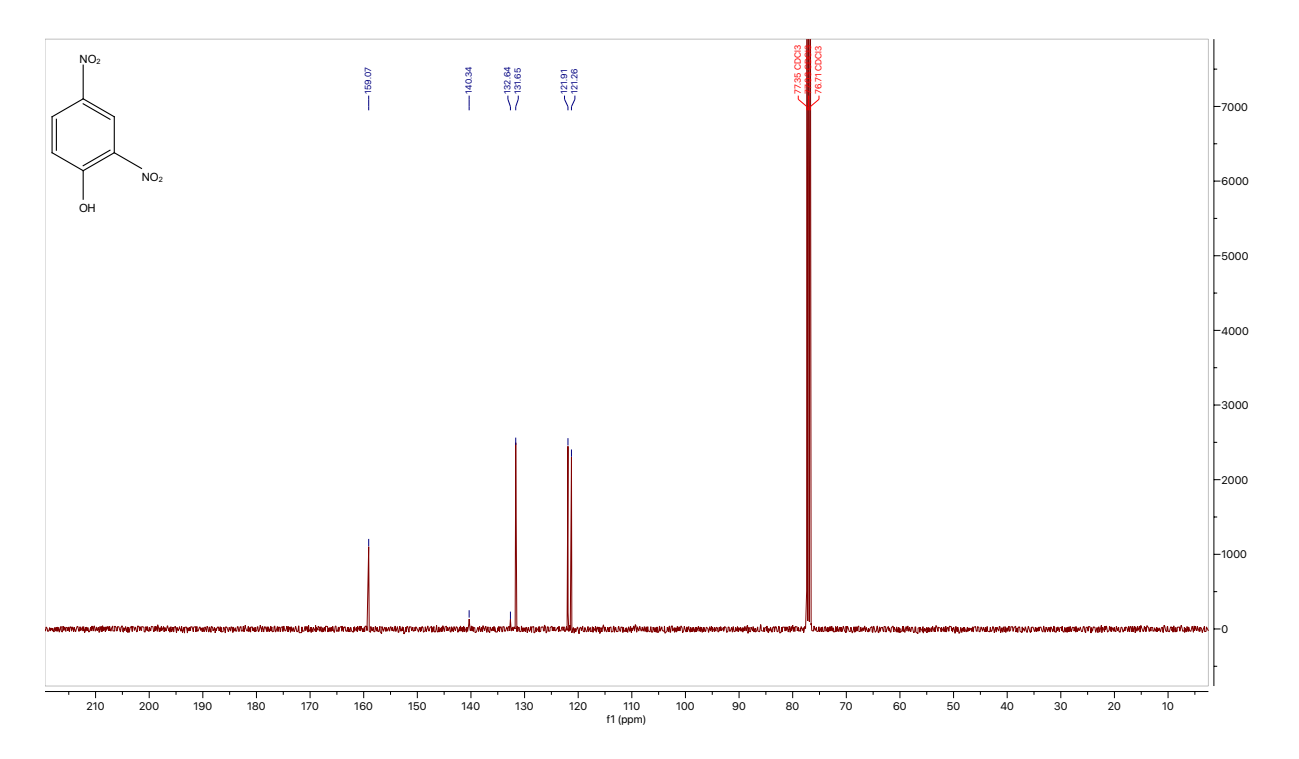
<sup>1</sup>H NMR for **12** 



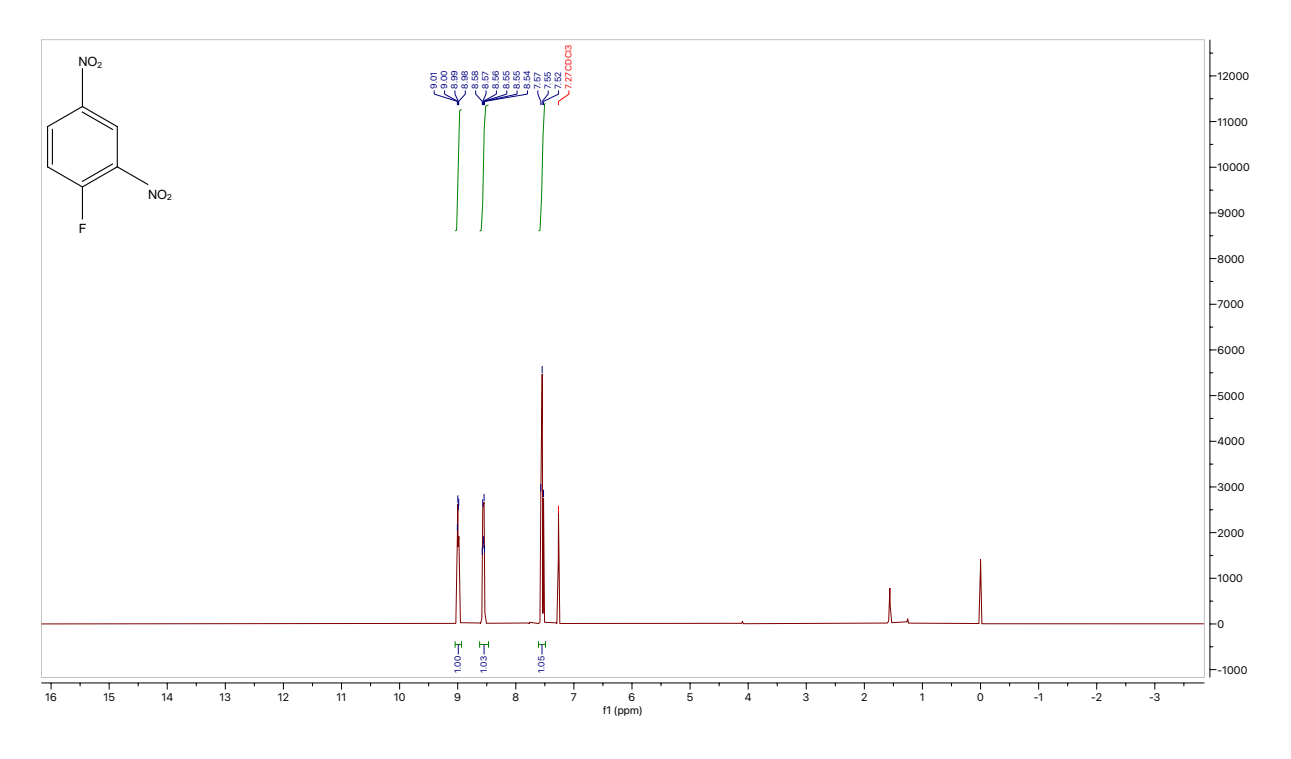


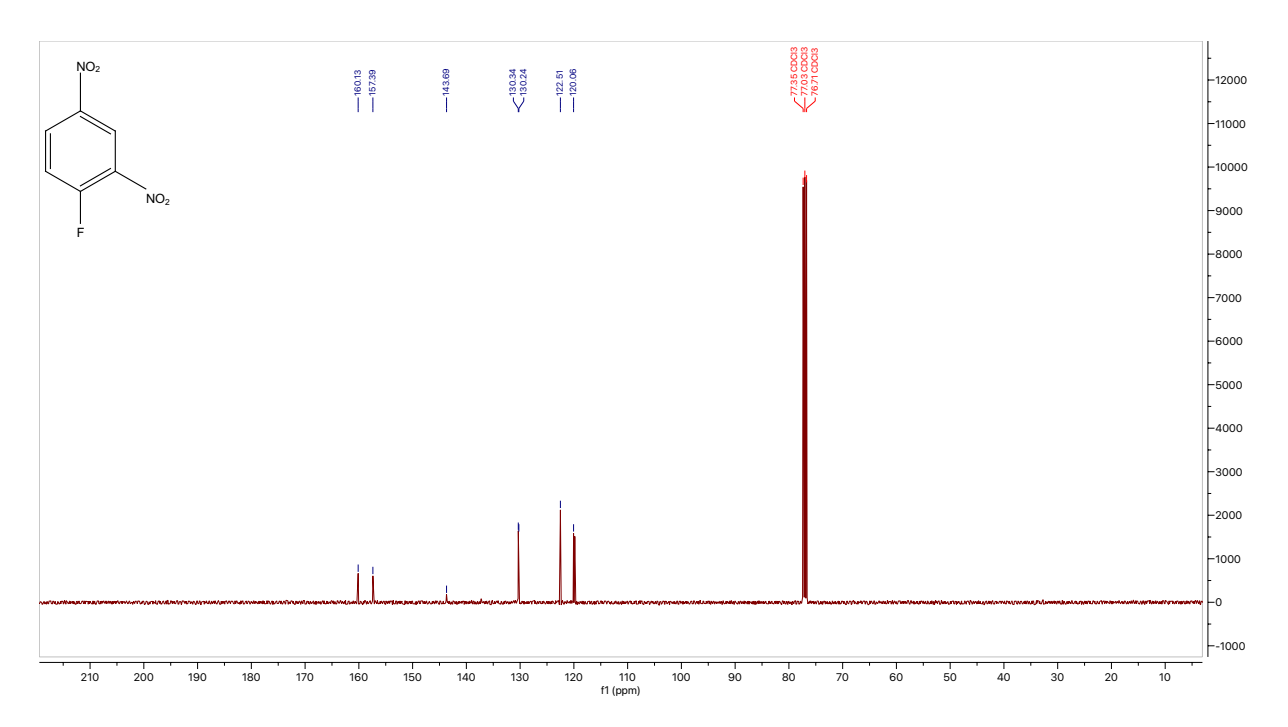
<sup>1</sup>H NMR for **13** 



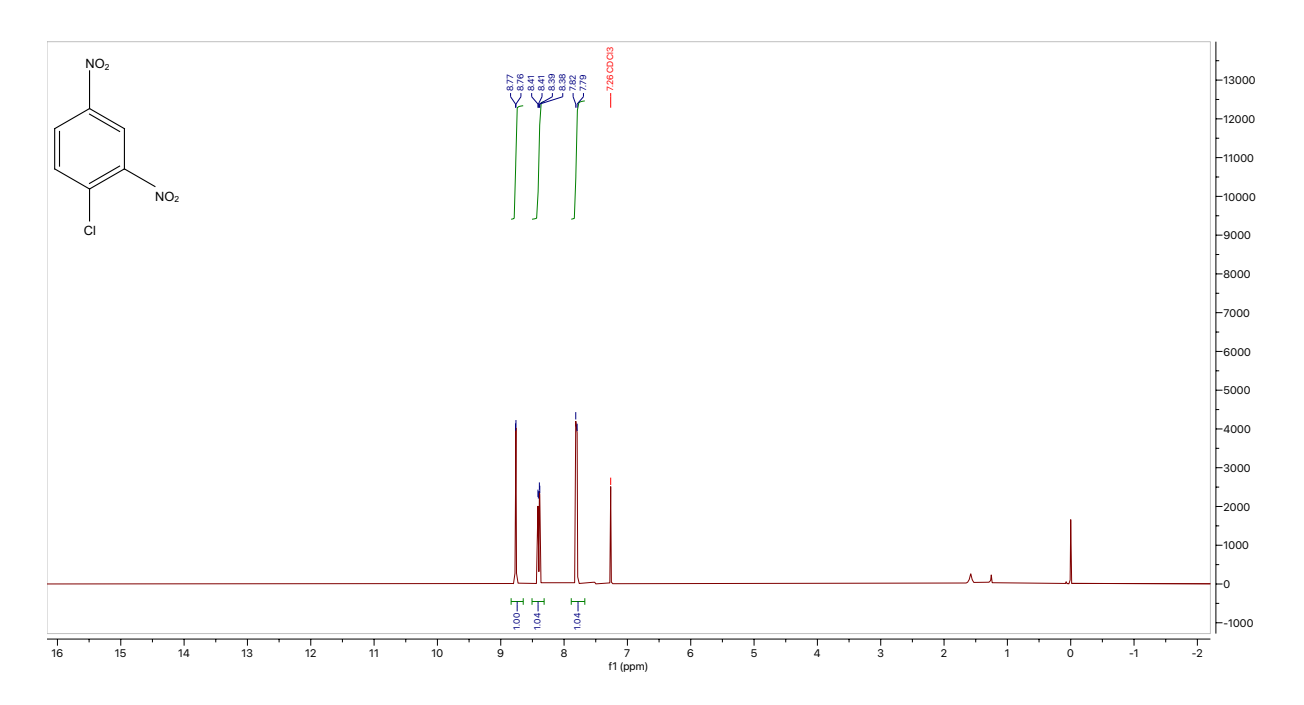


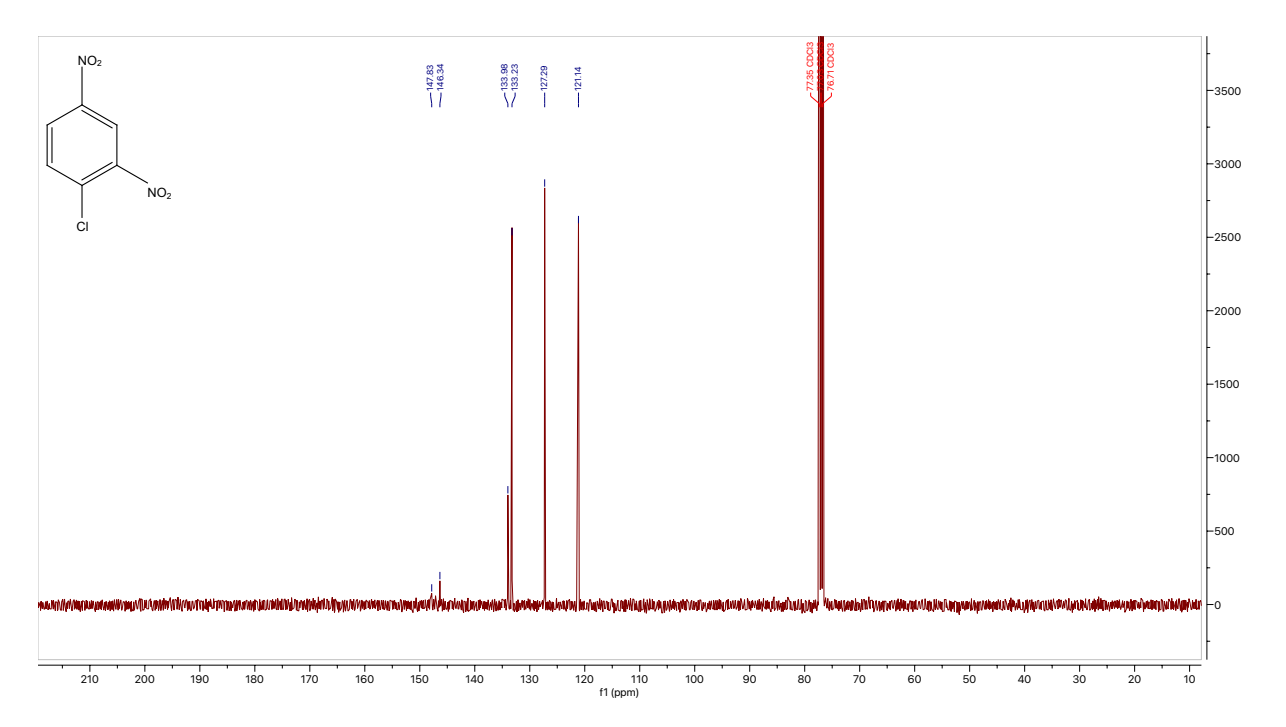
<sup>1</sup>H NMR for **14** 

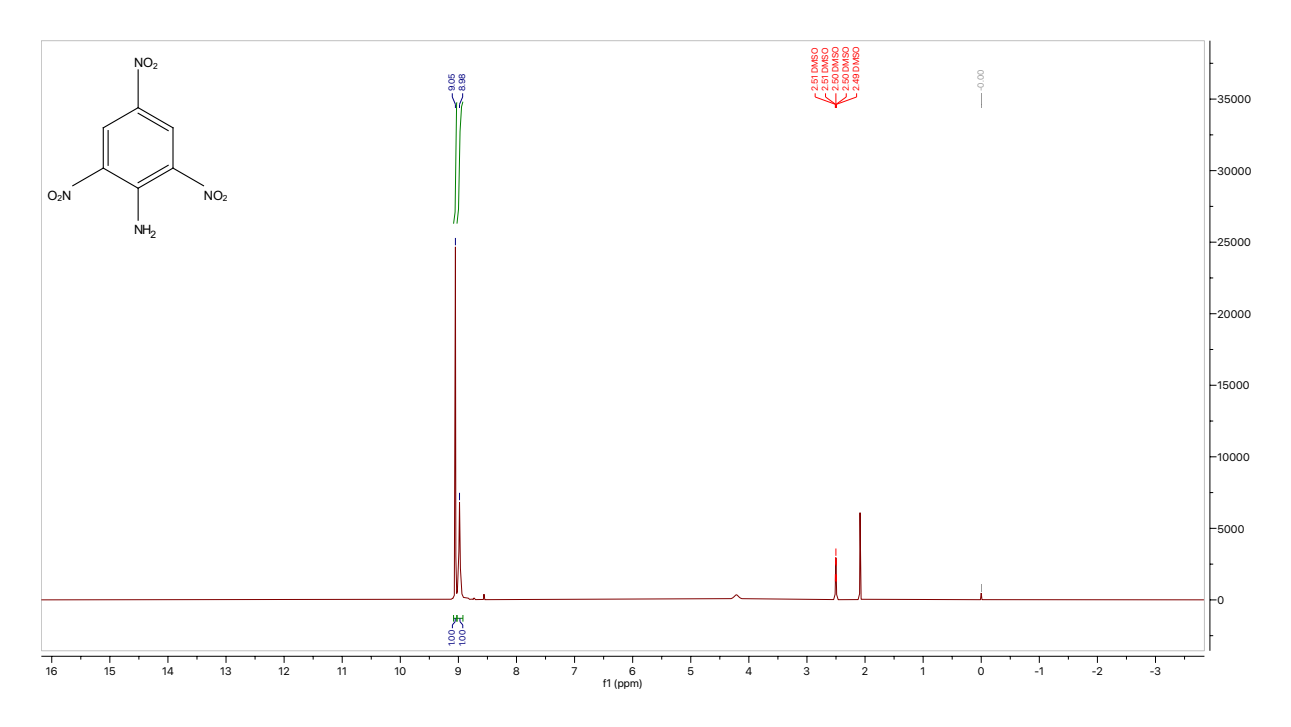


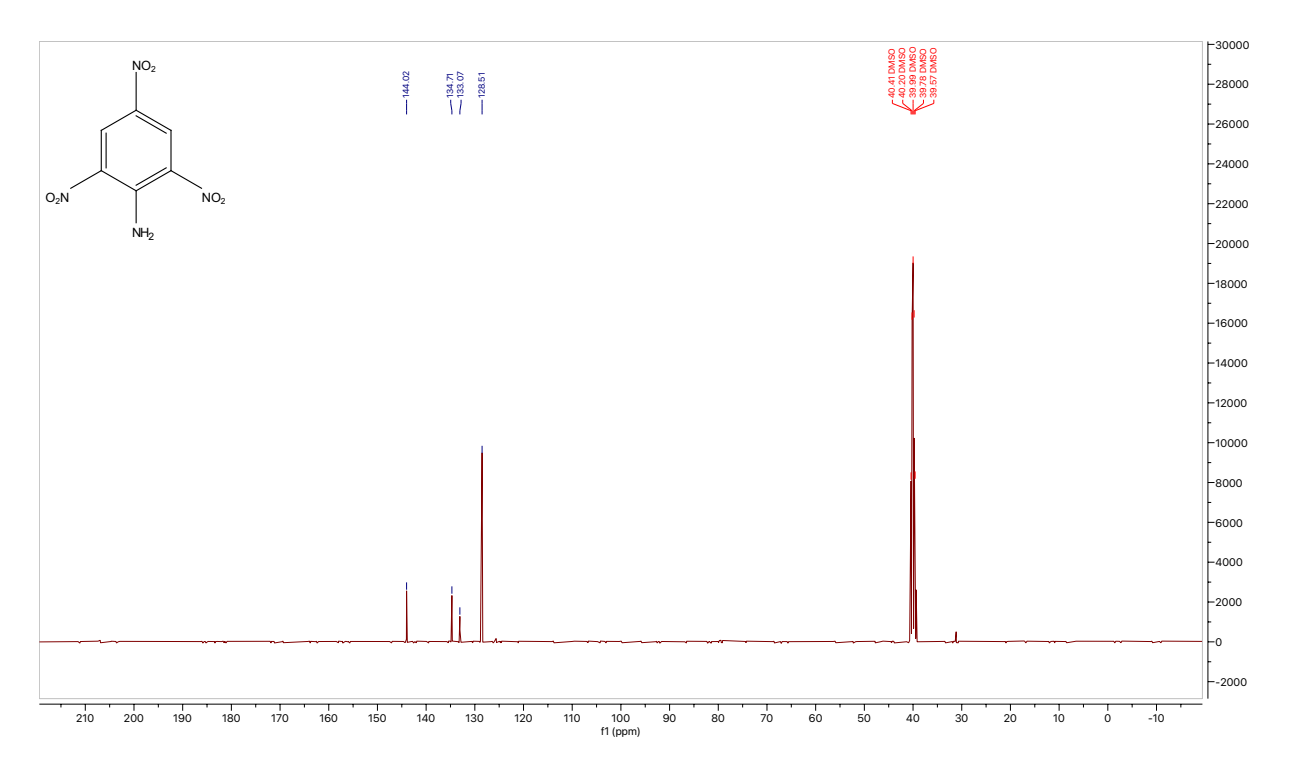


<sup>1</sup>H NMR for **15** 

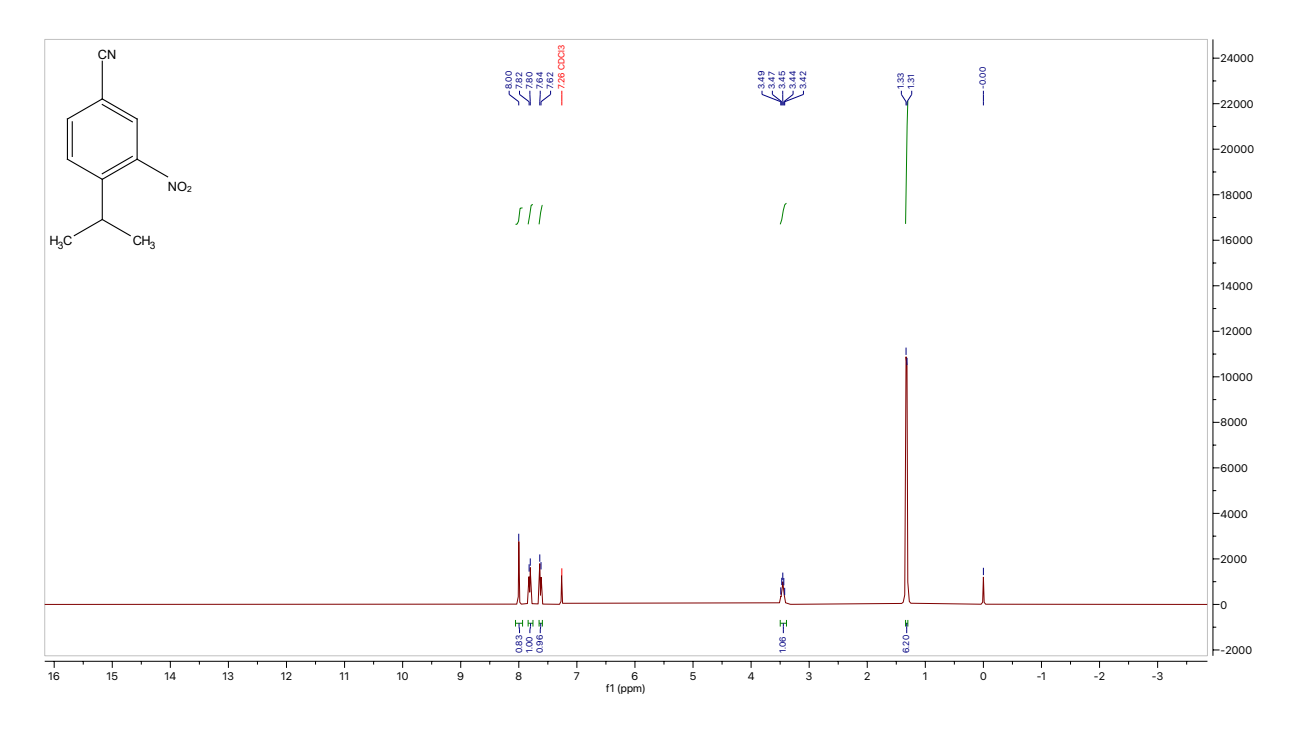


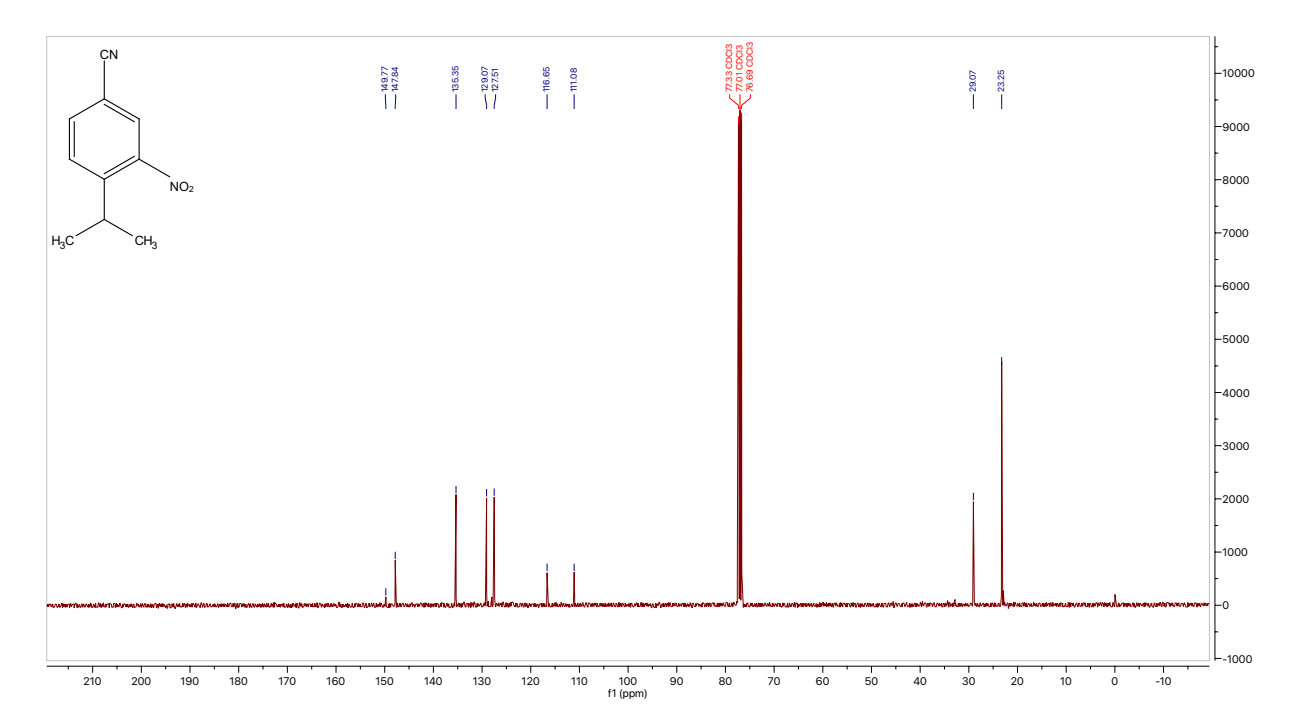




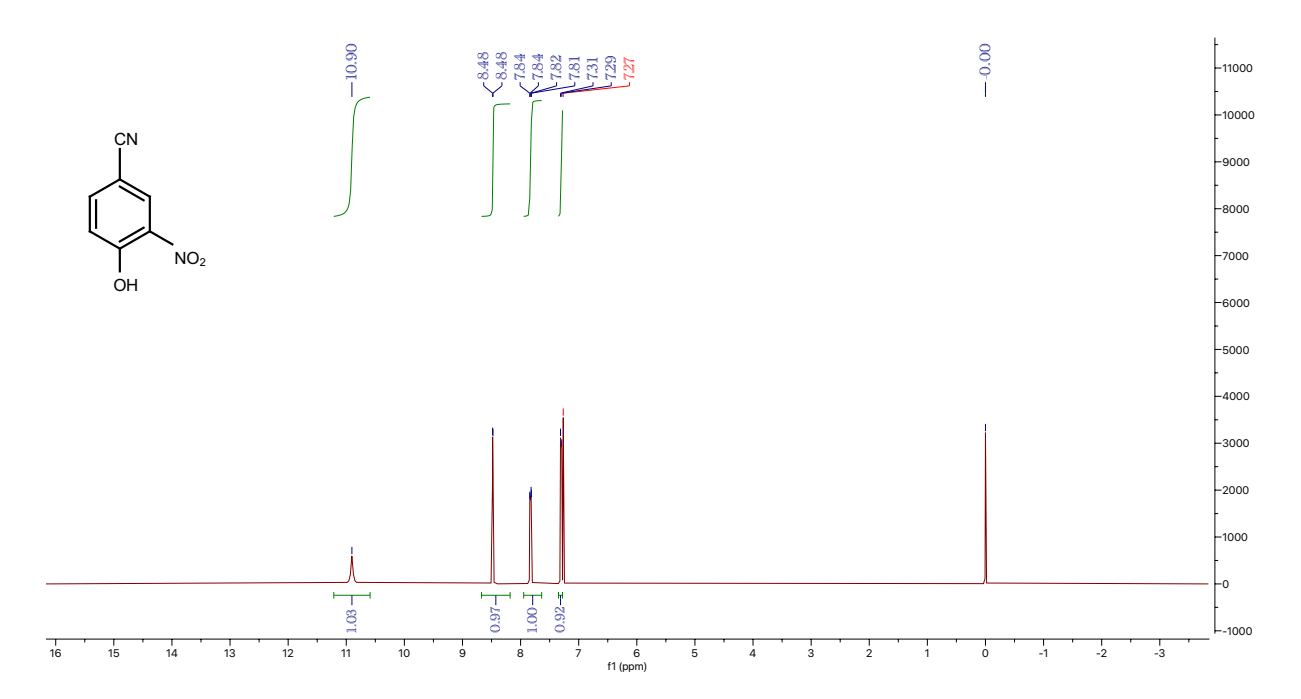


<sup>1</sup>H NMR for **17** 

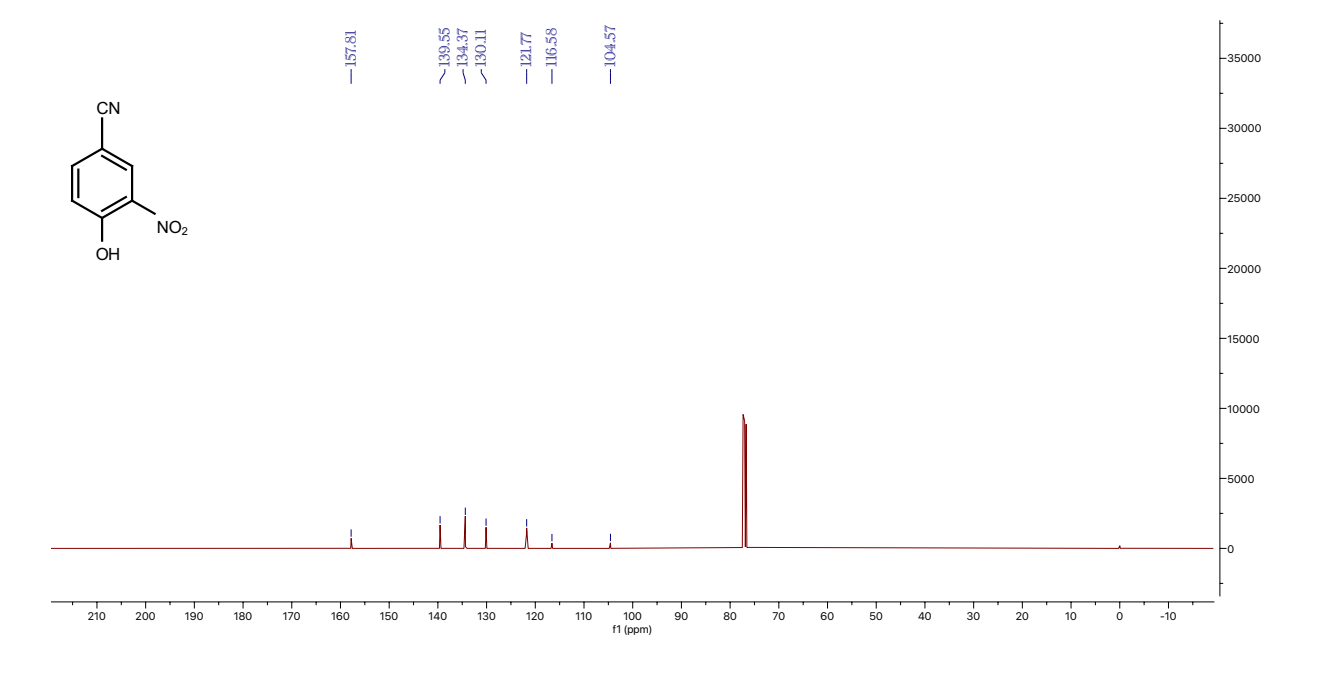


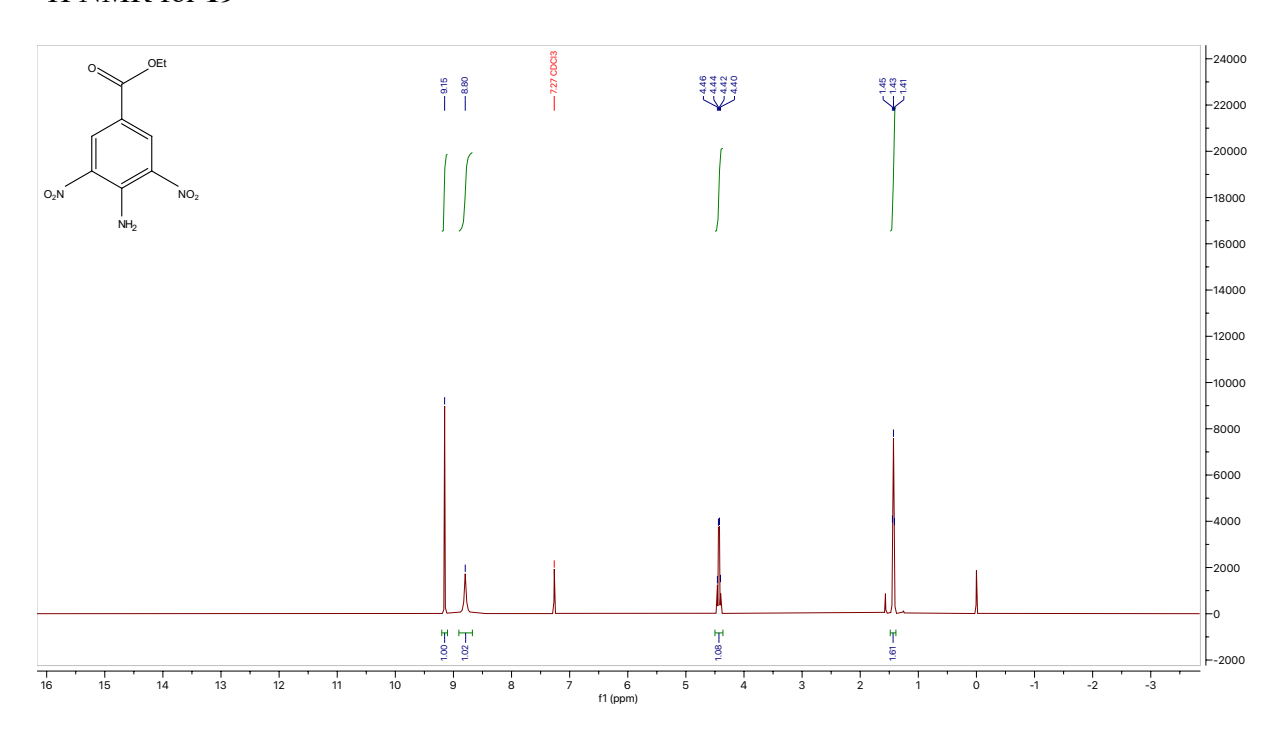


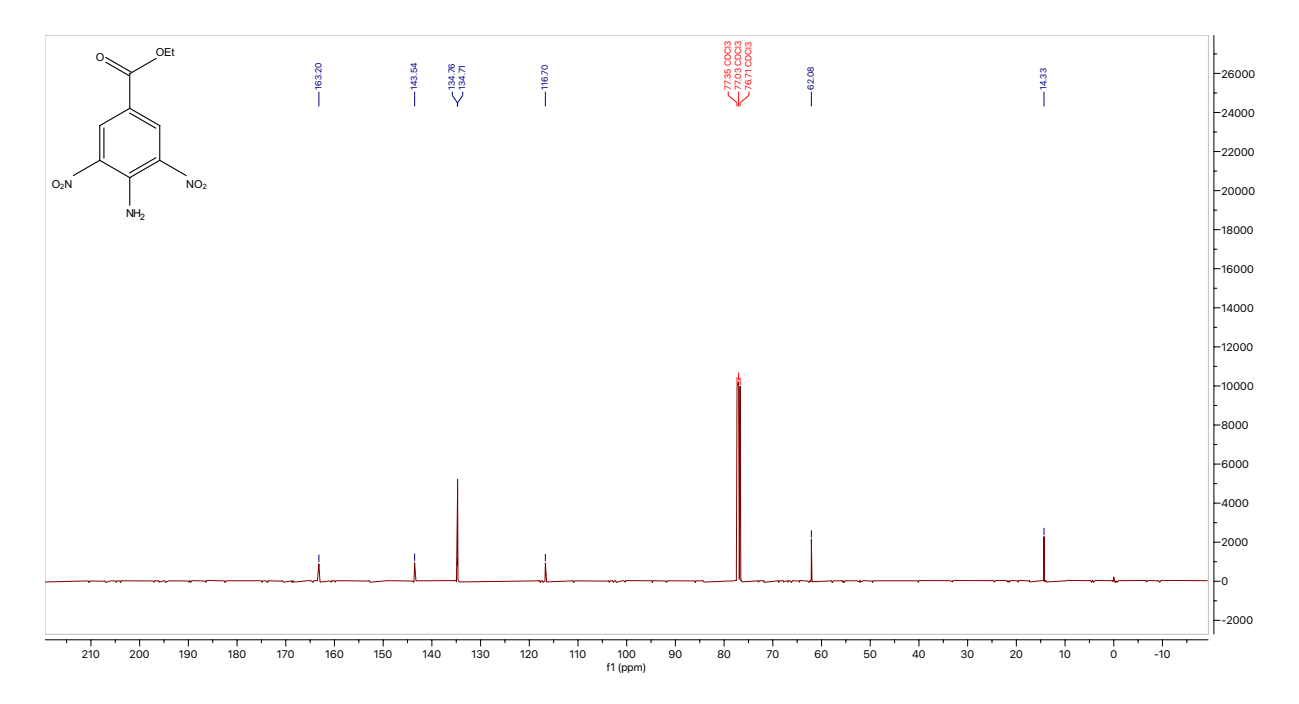
<sup>1</sup>H NMR for **18** 



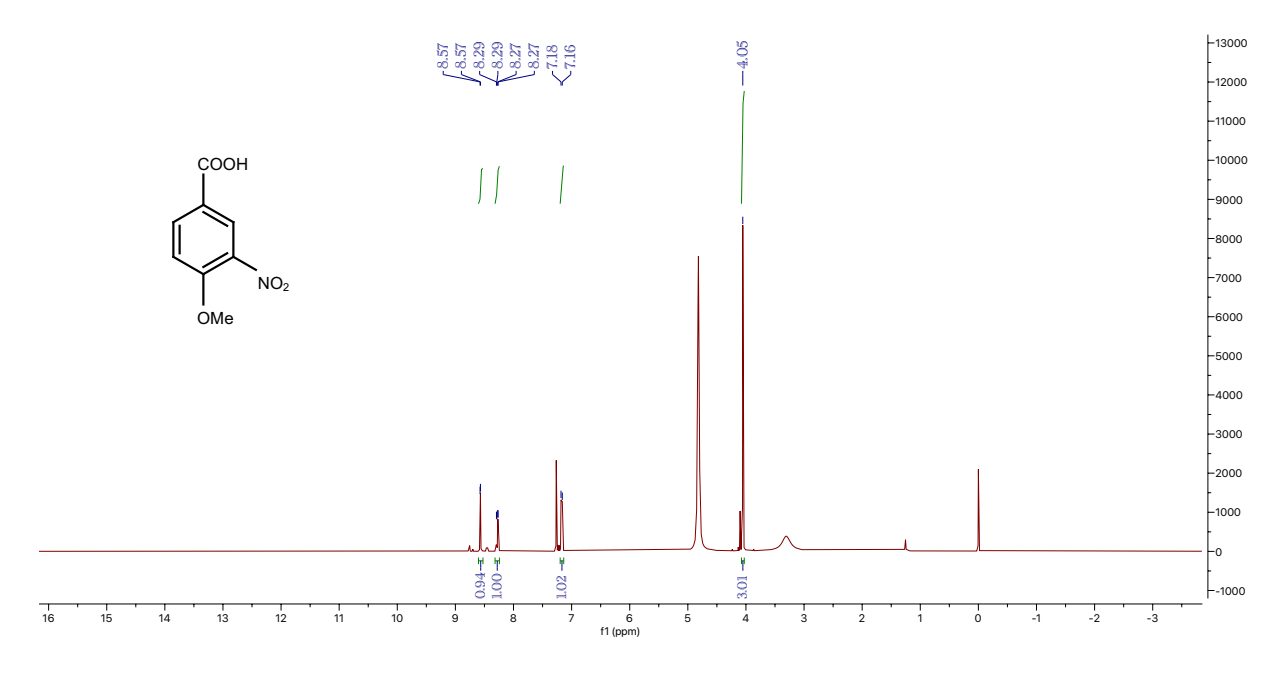
<sup>13</sup>C NMR for **18** 

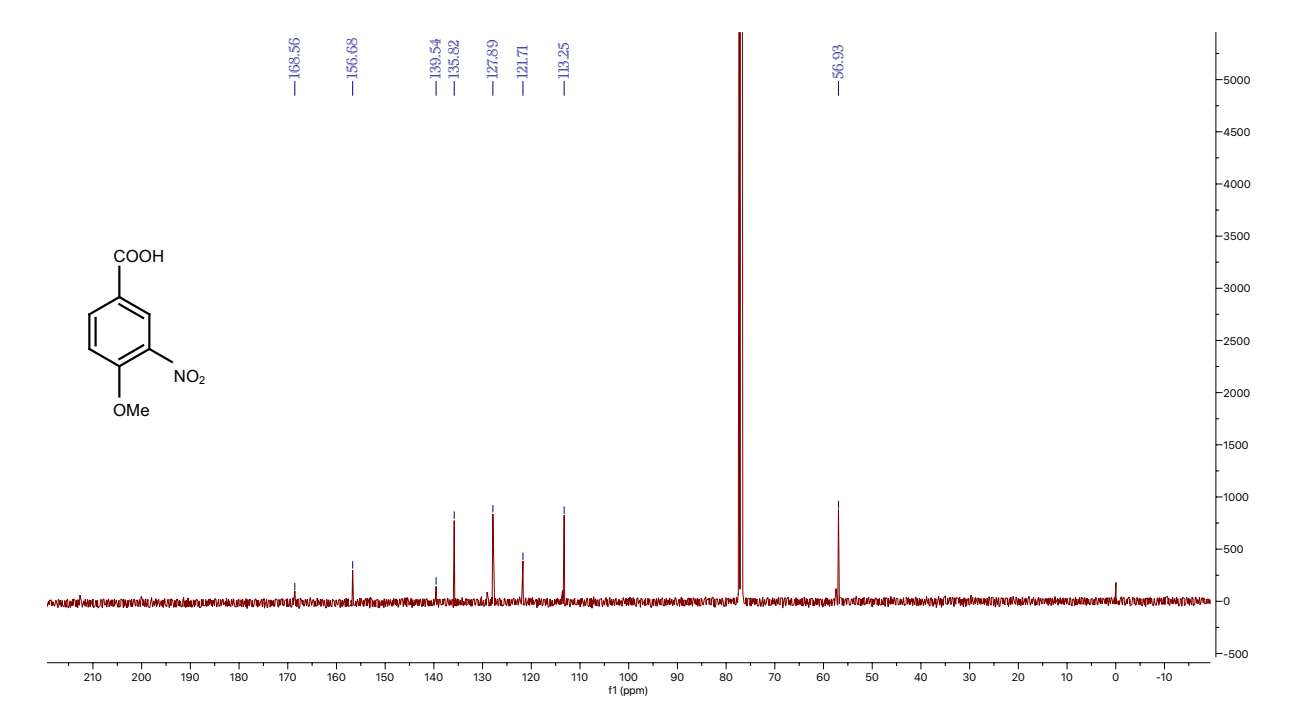


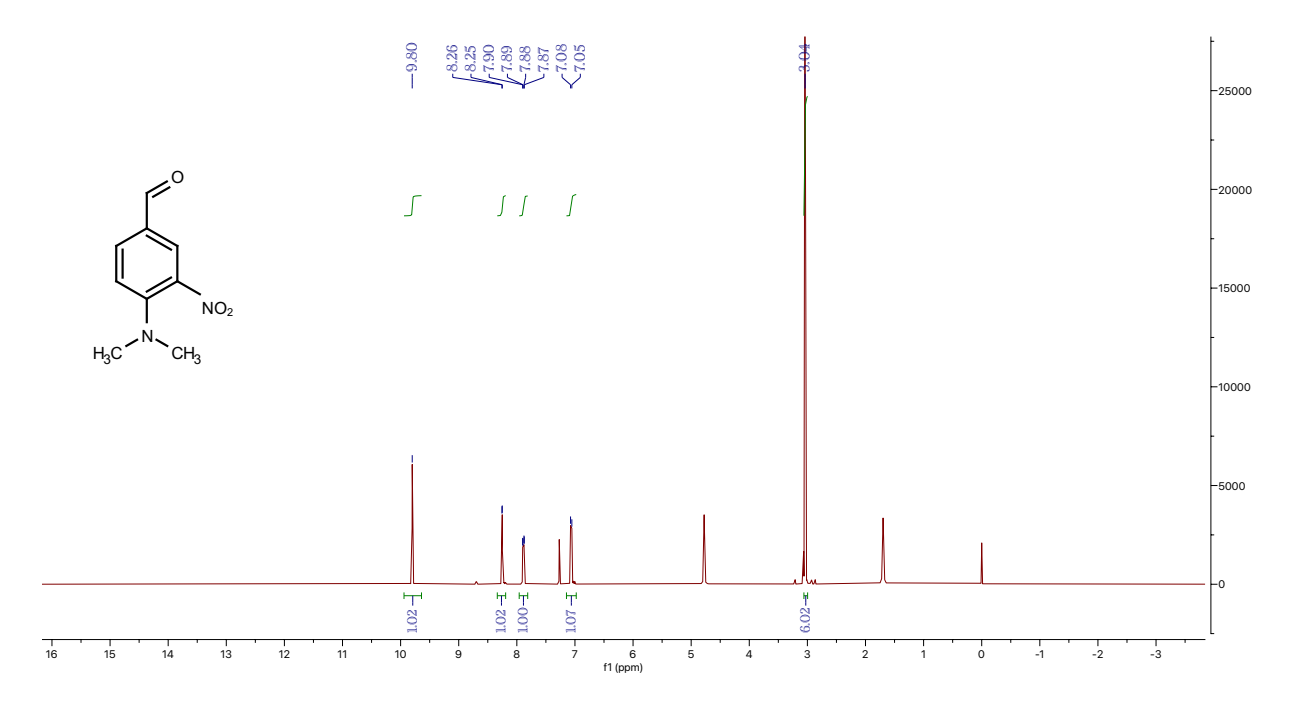




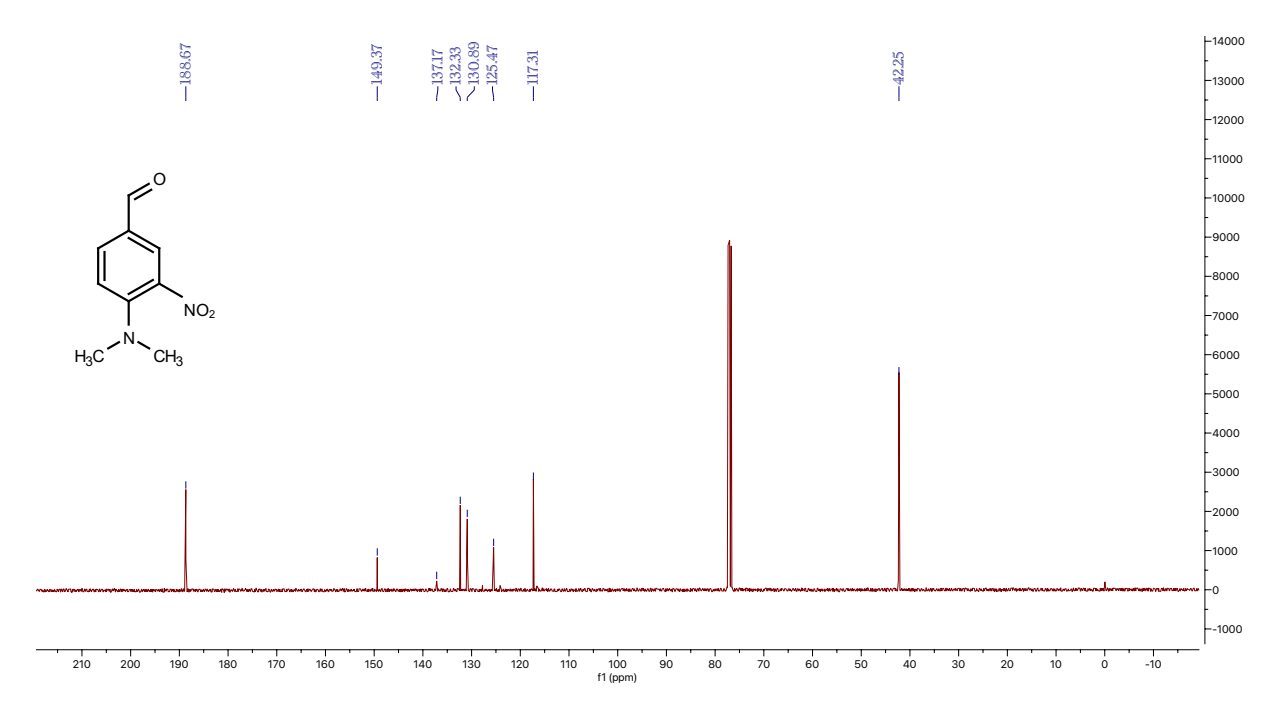
<sup>1</sup>H NMR for **20** 



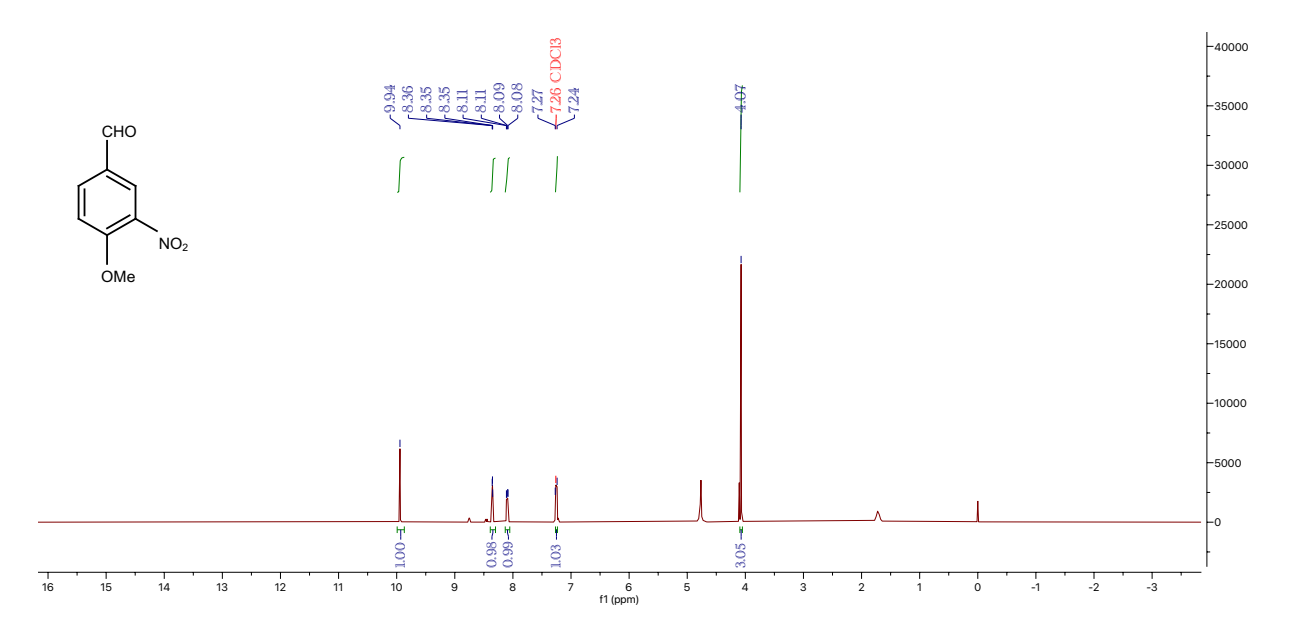




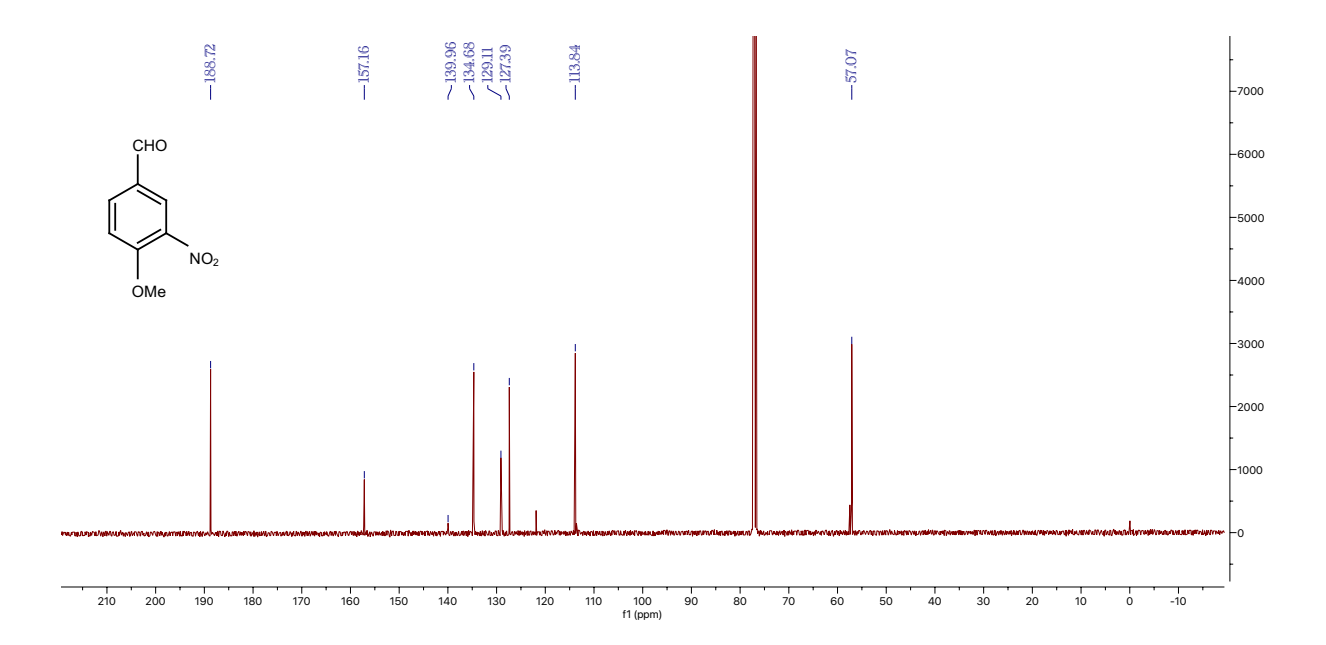
<sup>13</sup>C NMR for **21** 



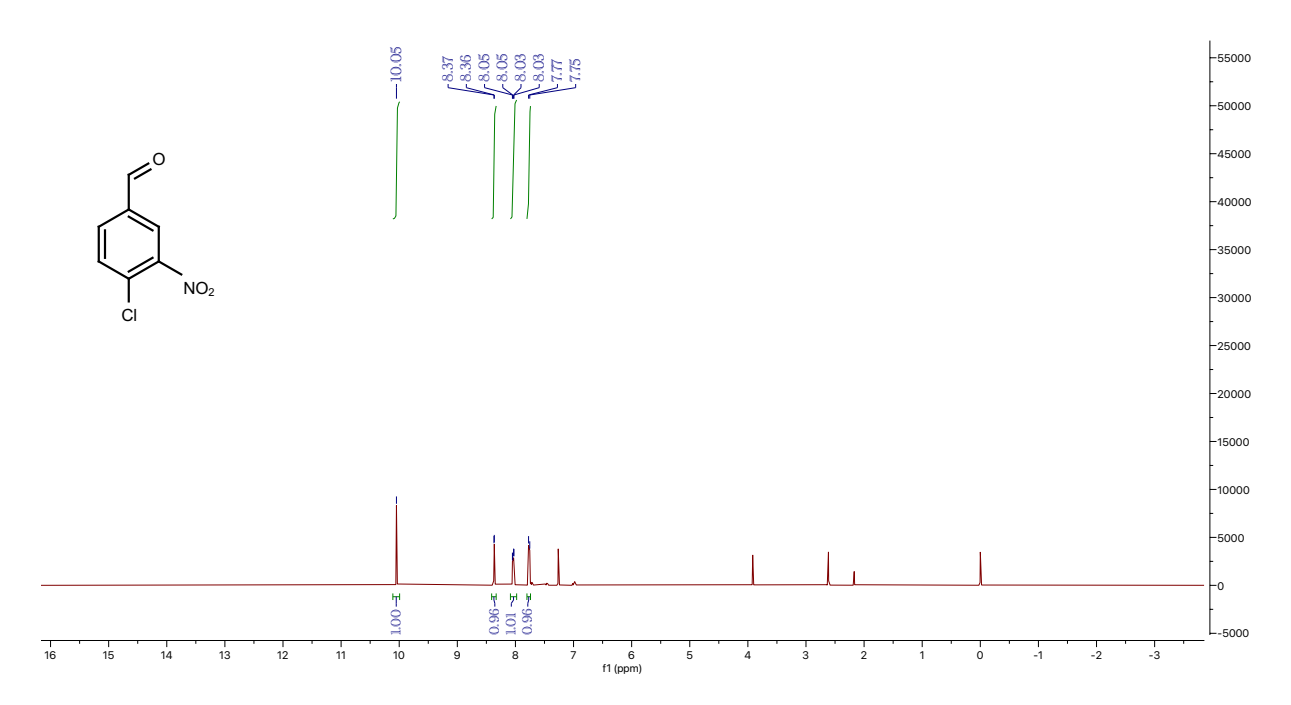
<sup>1</sup>H NMR for **22** 

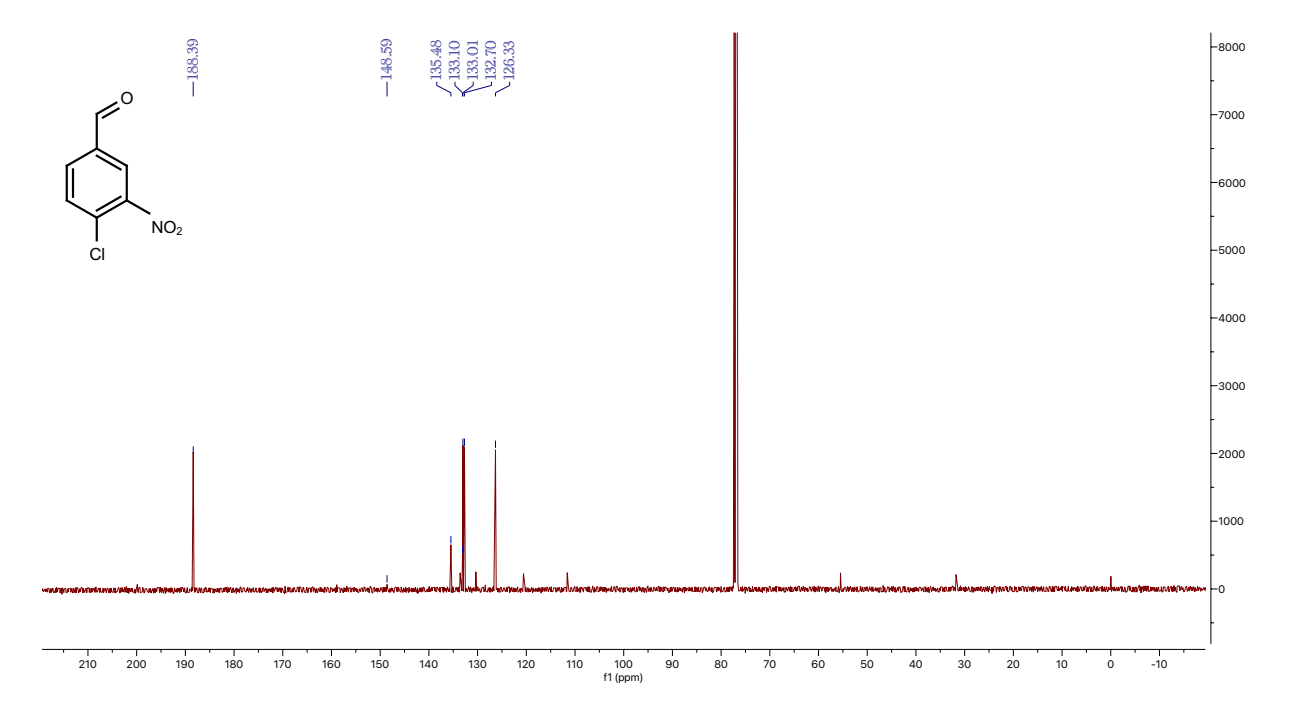


<sup>13</sup>C NMR for **22** 

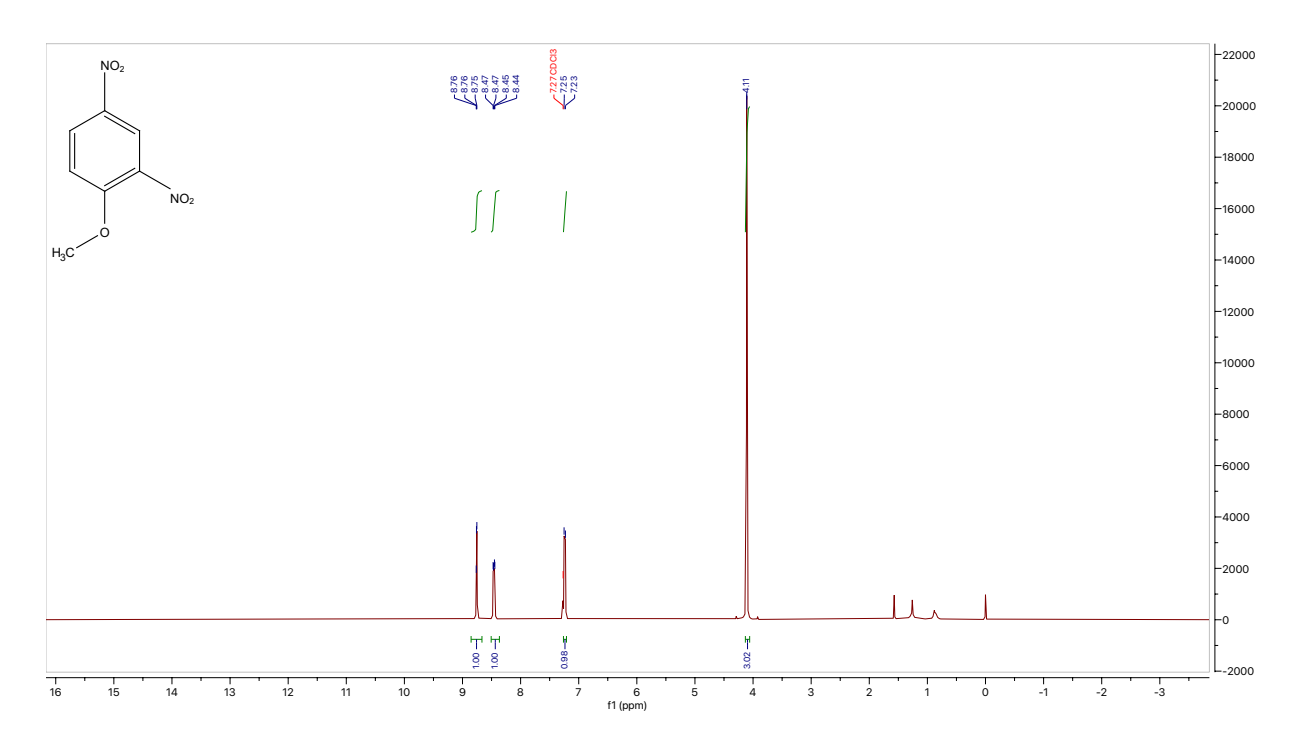


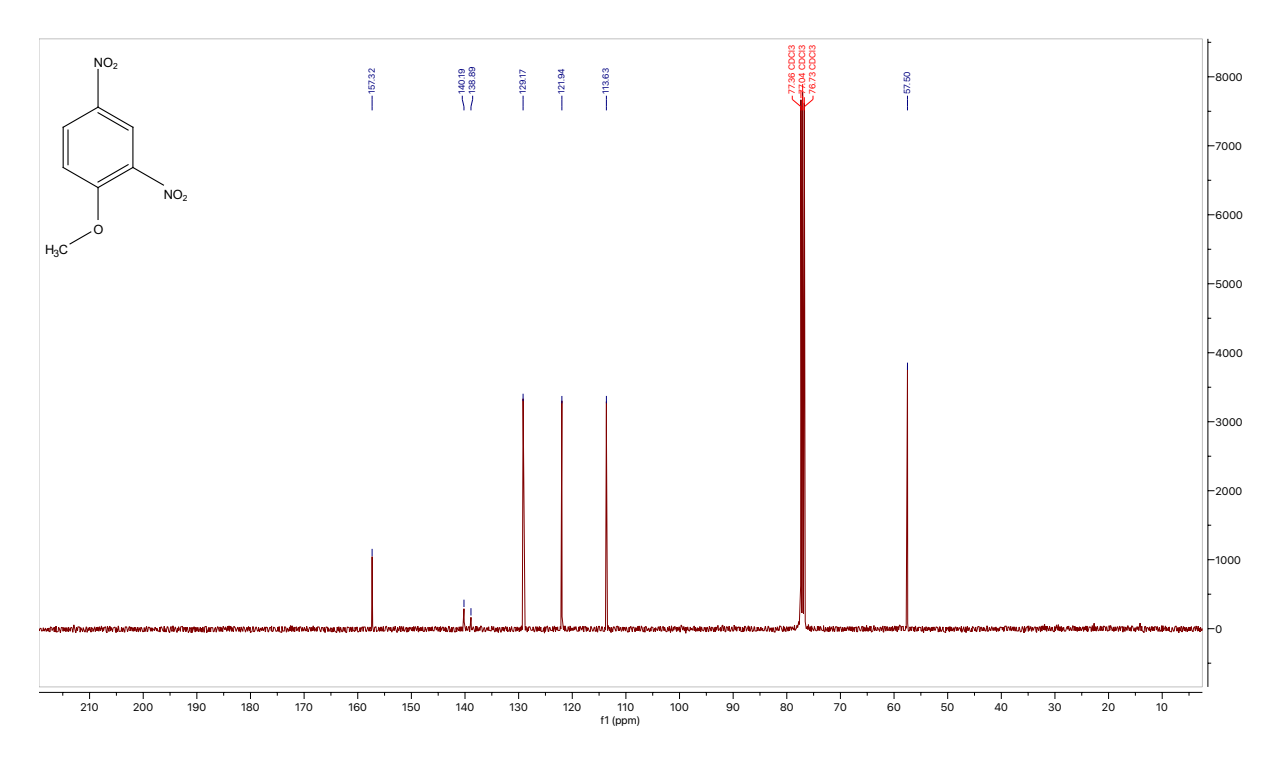
<sup>1</sup>H NMR for **23** 



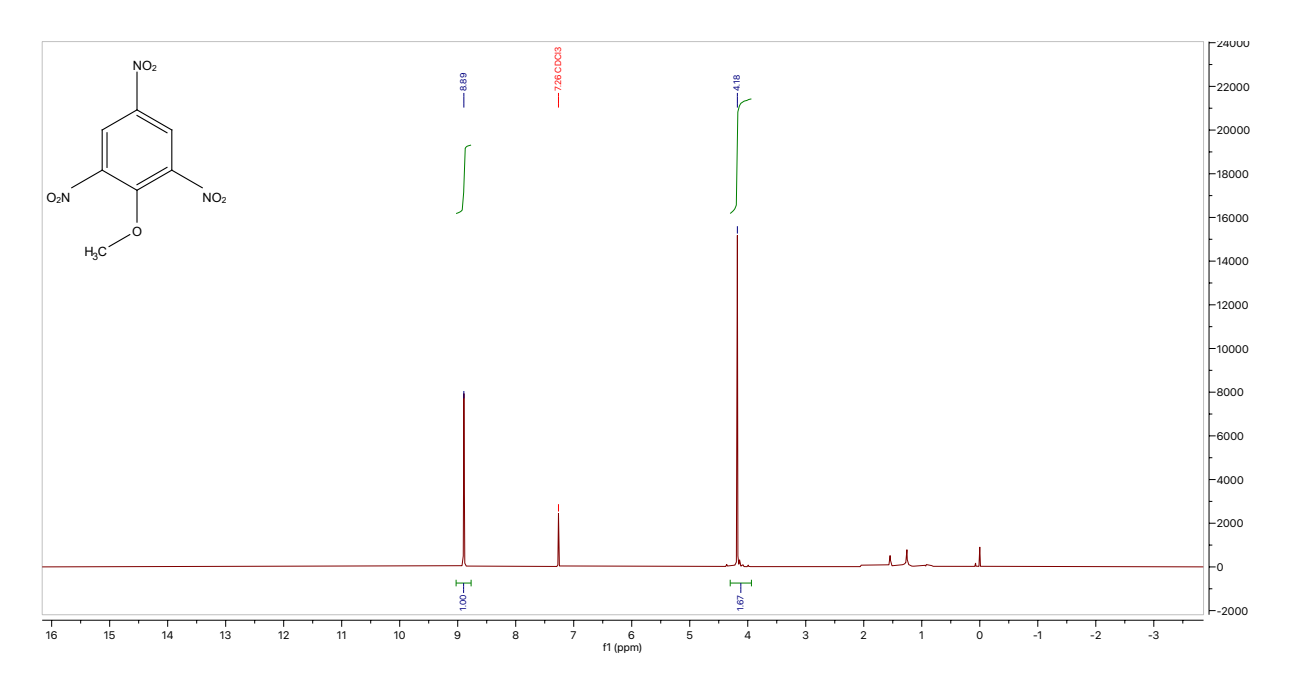


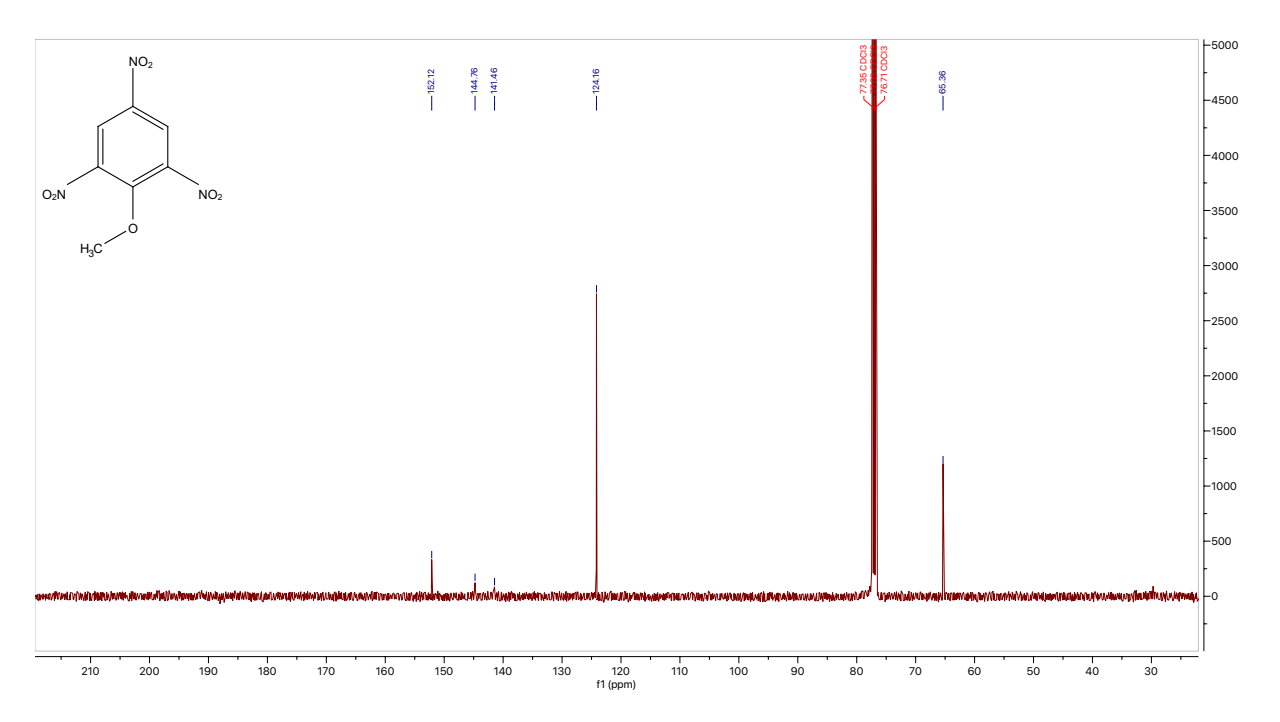
### <sup>1</sup>H NMR for **24a**



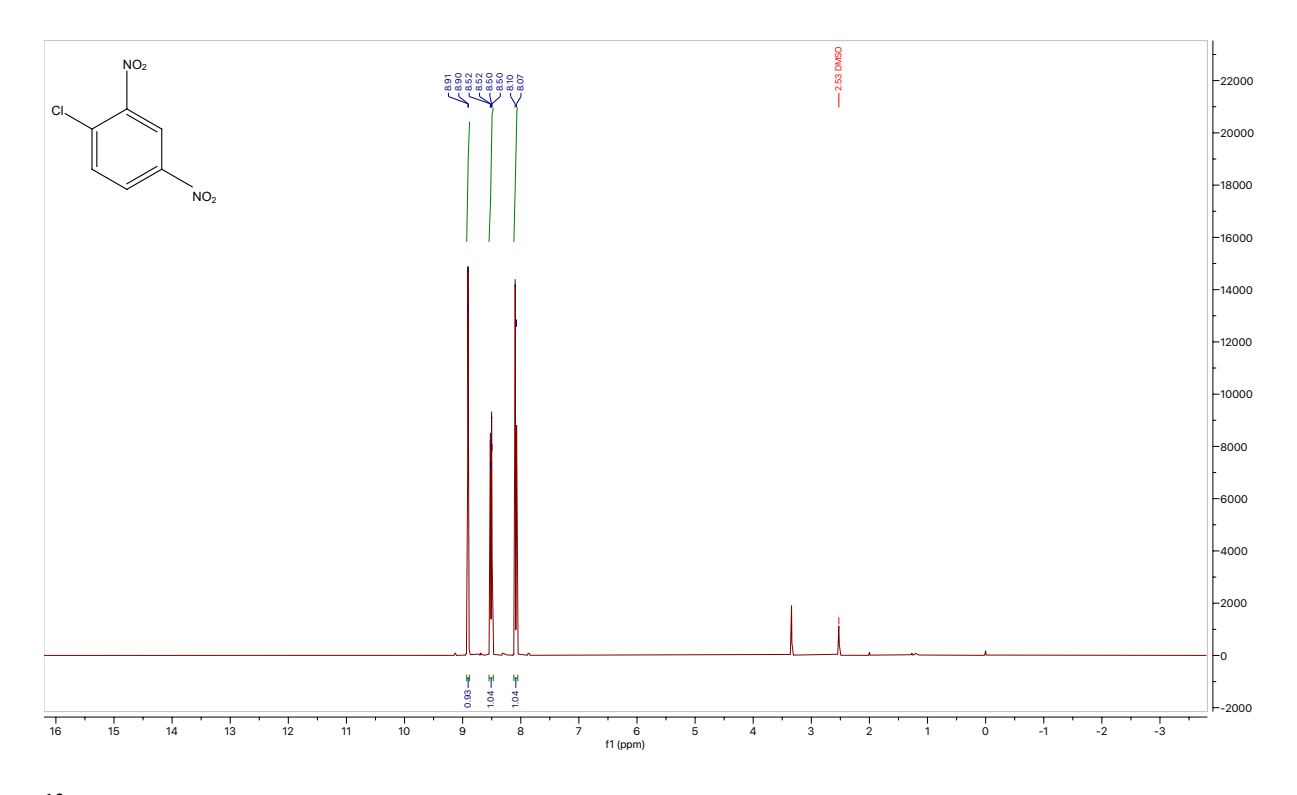


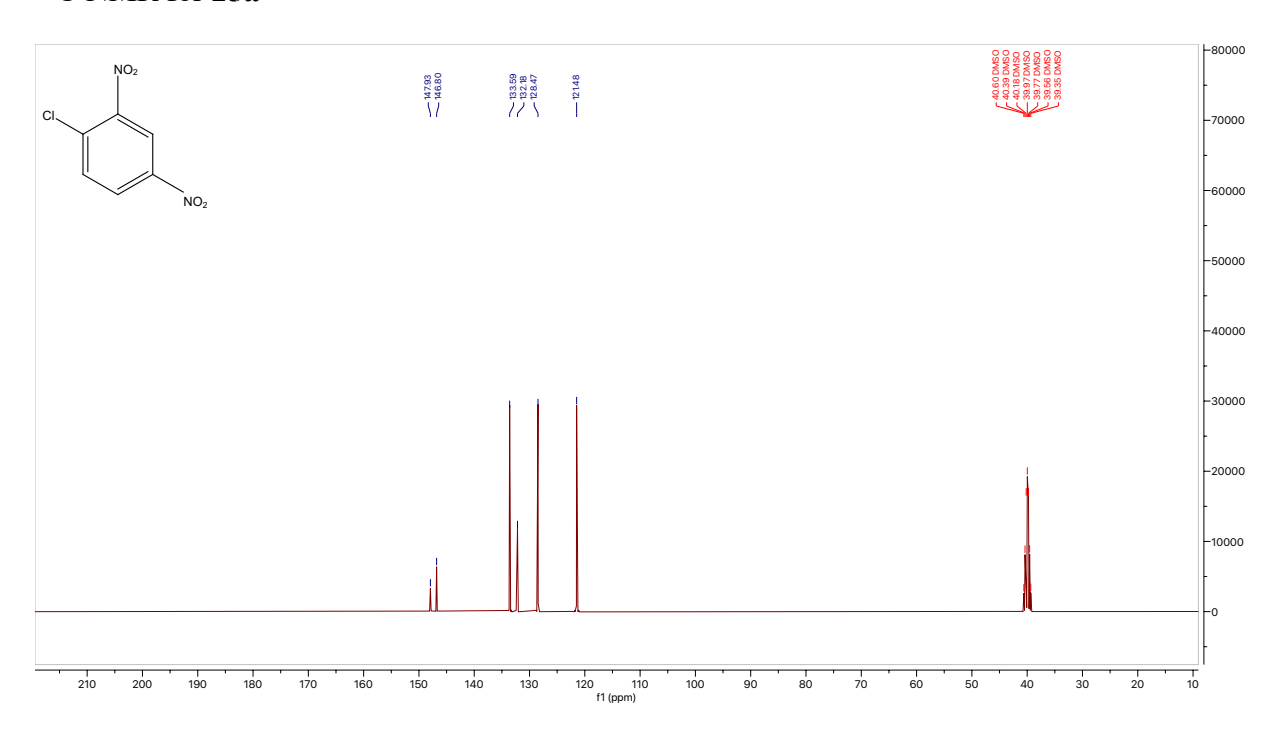
### <sup>1</sup>H NMR for **24b**



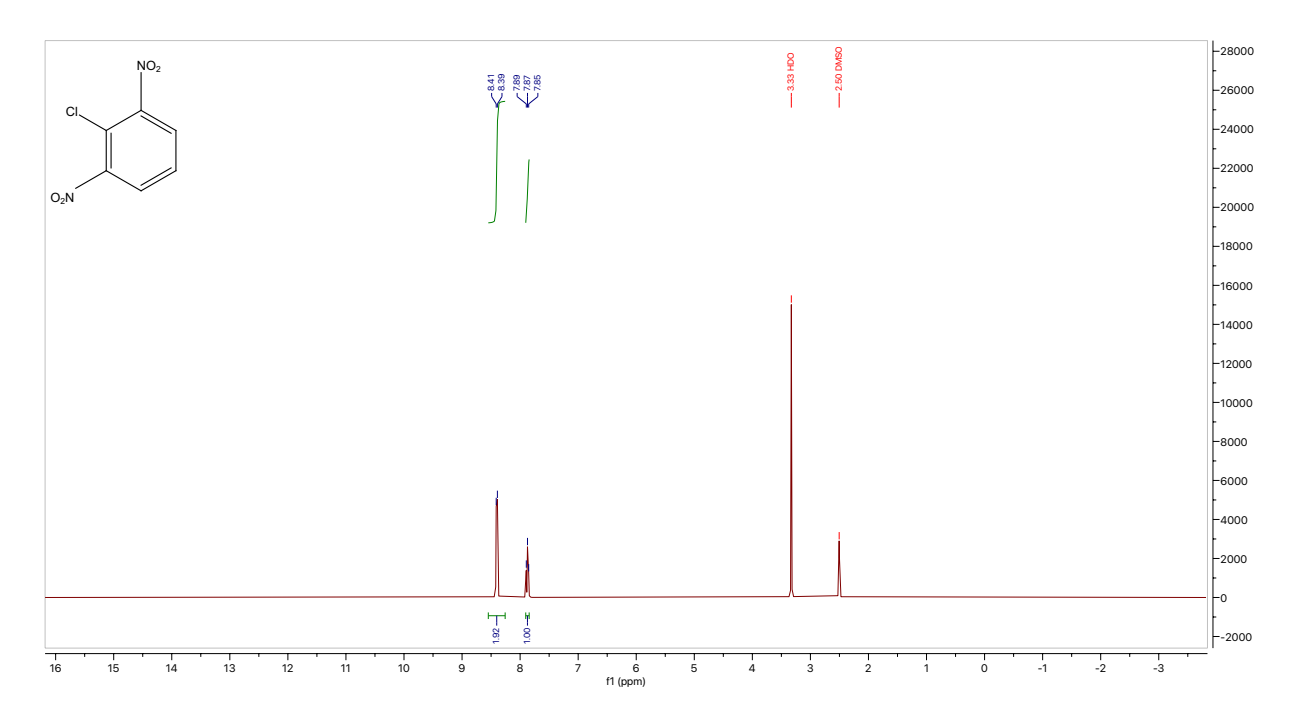


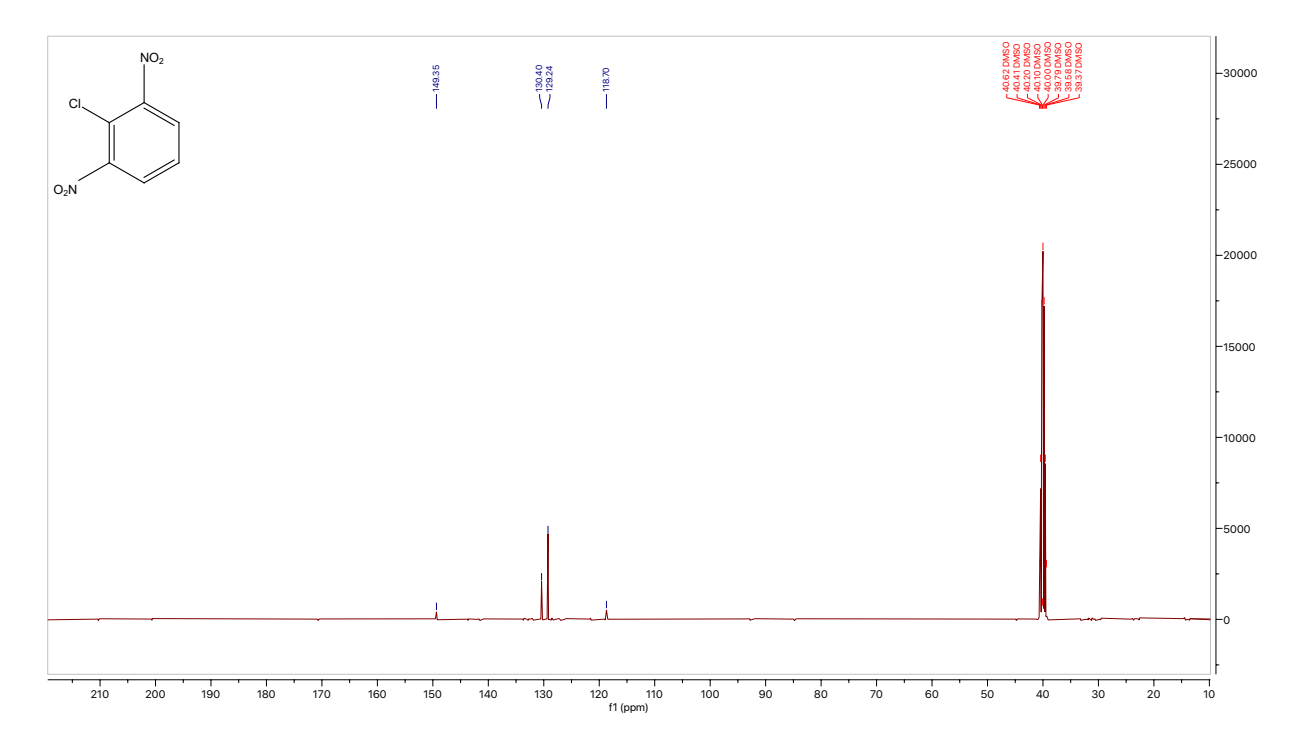
### <sup>1</sup>H NMR for **25a**



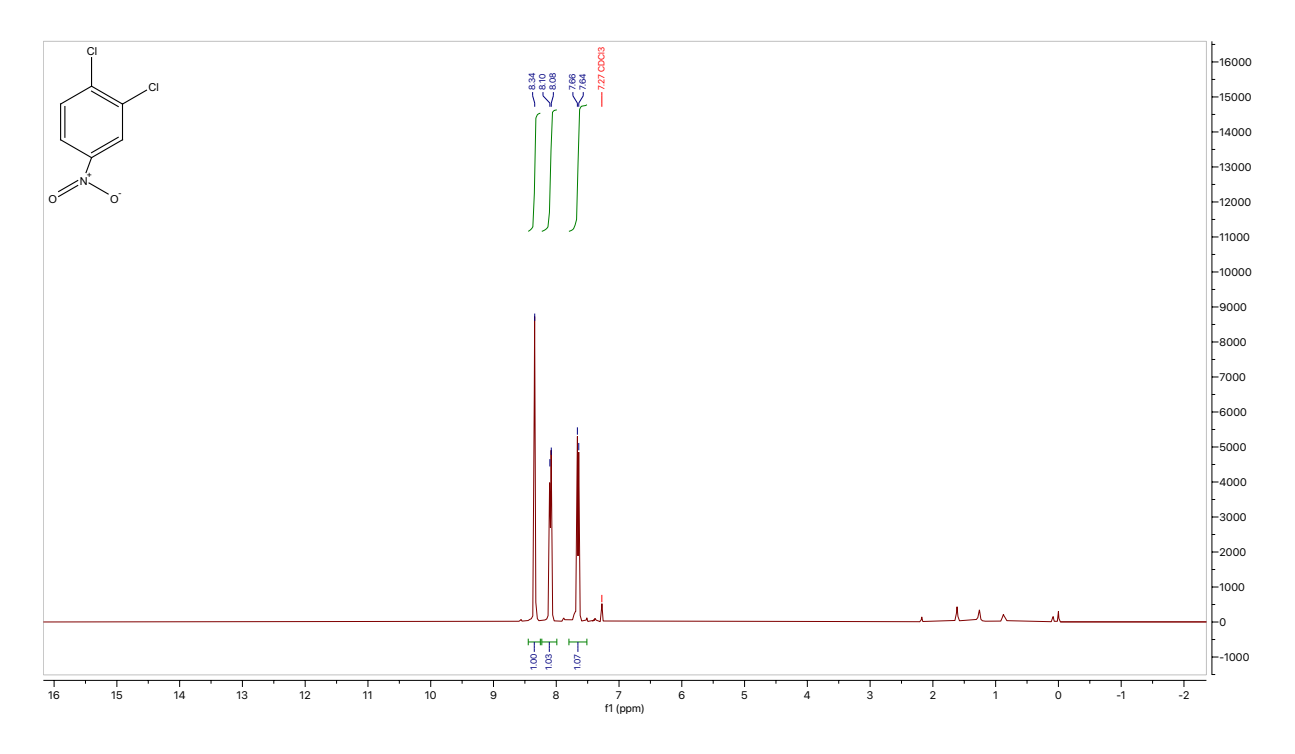


### <sup>1</sup>H NMR for **25b**

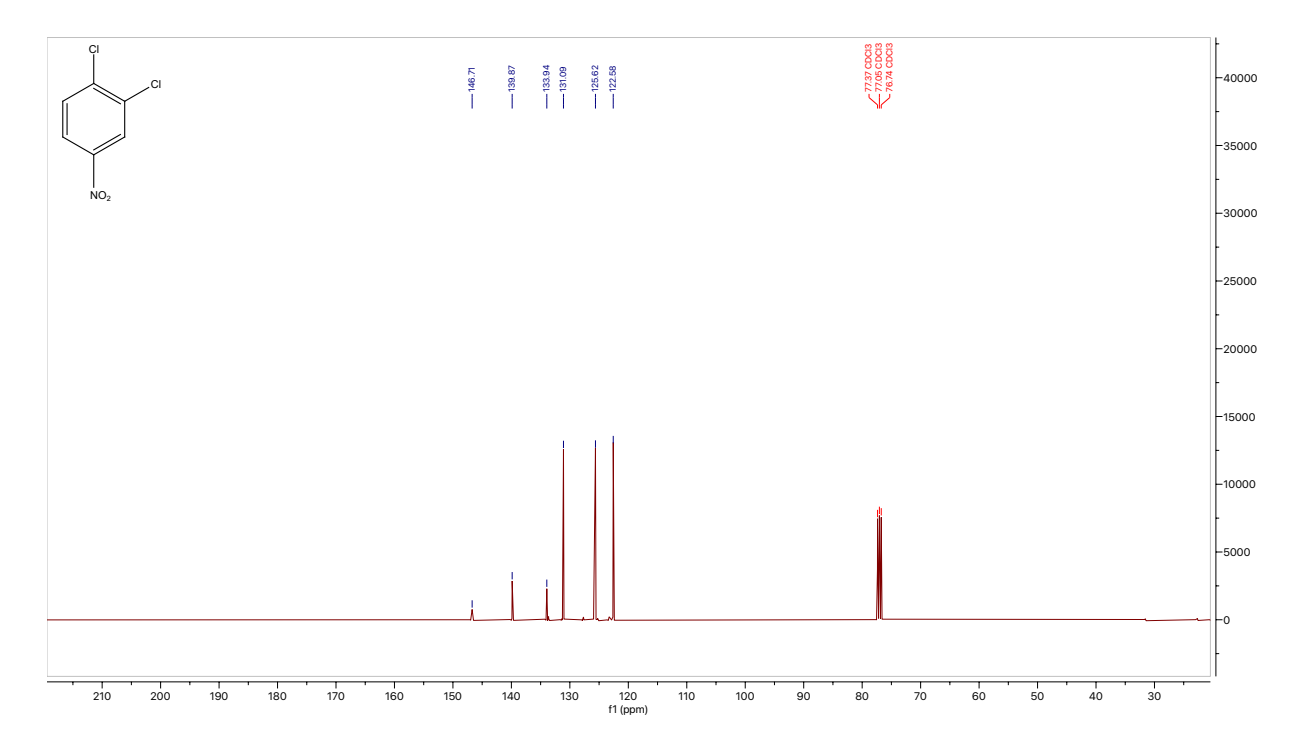




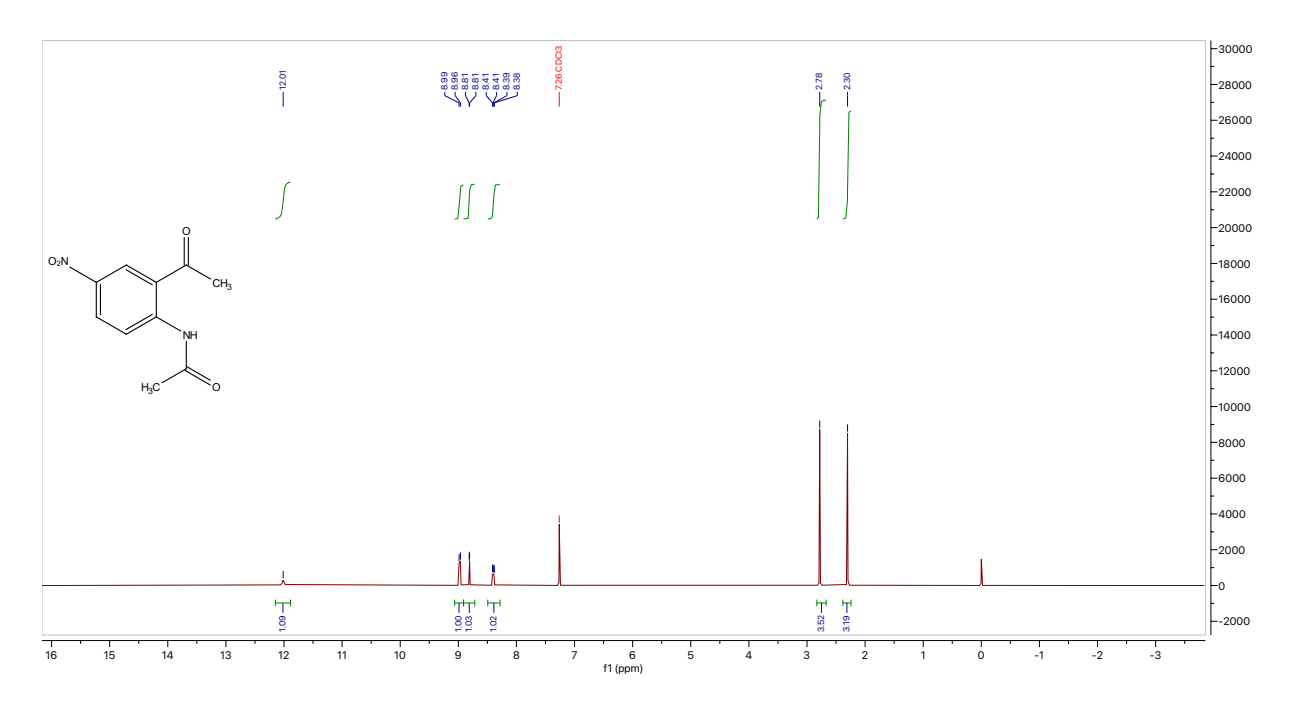
<sup>1</sup>H NMR for **27** 

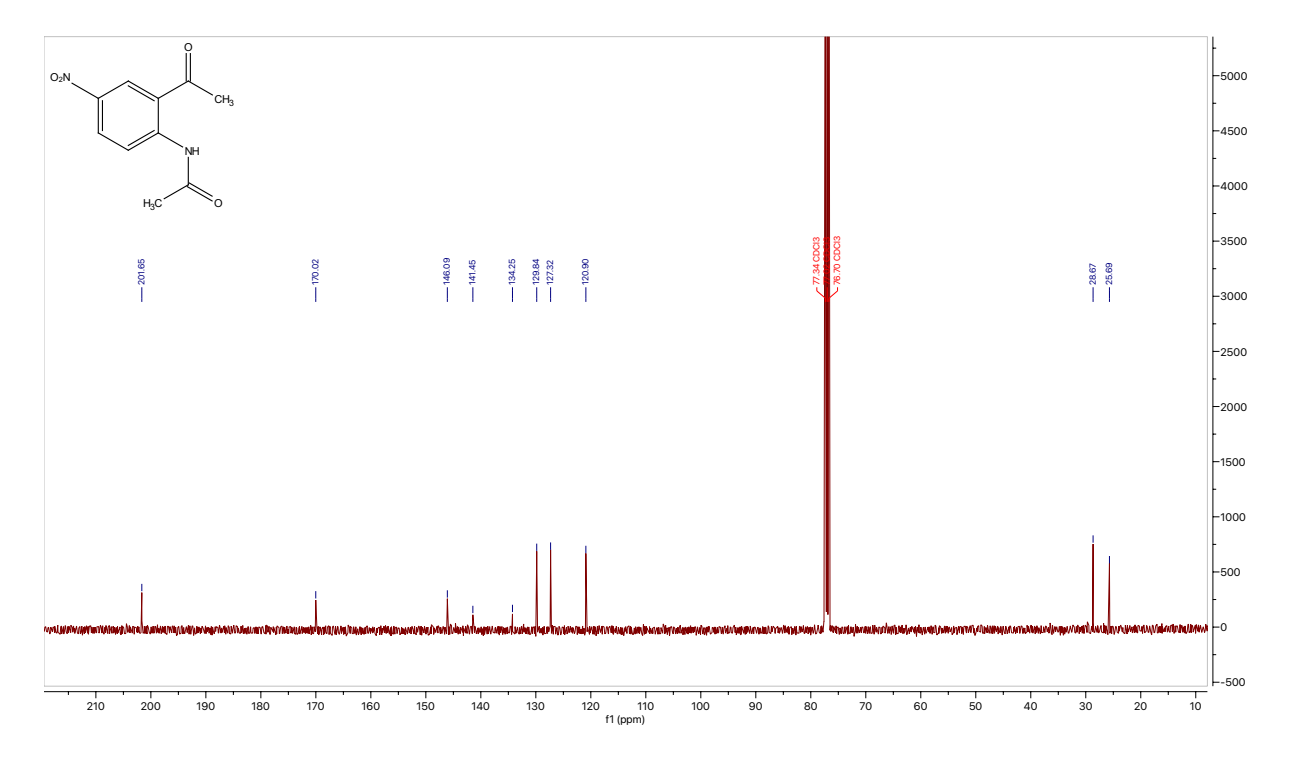


<sup>13</sup>C NMR for **27** 

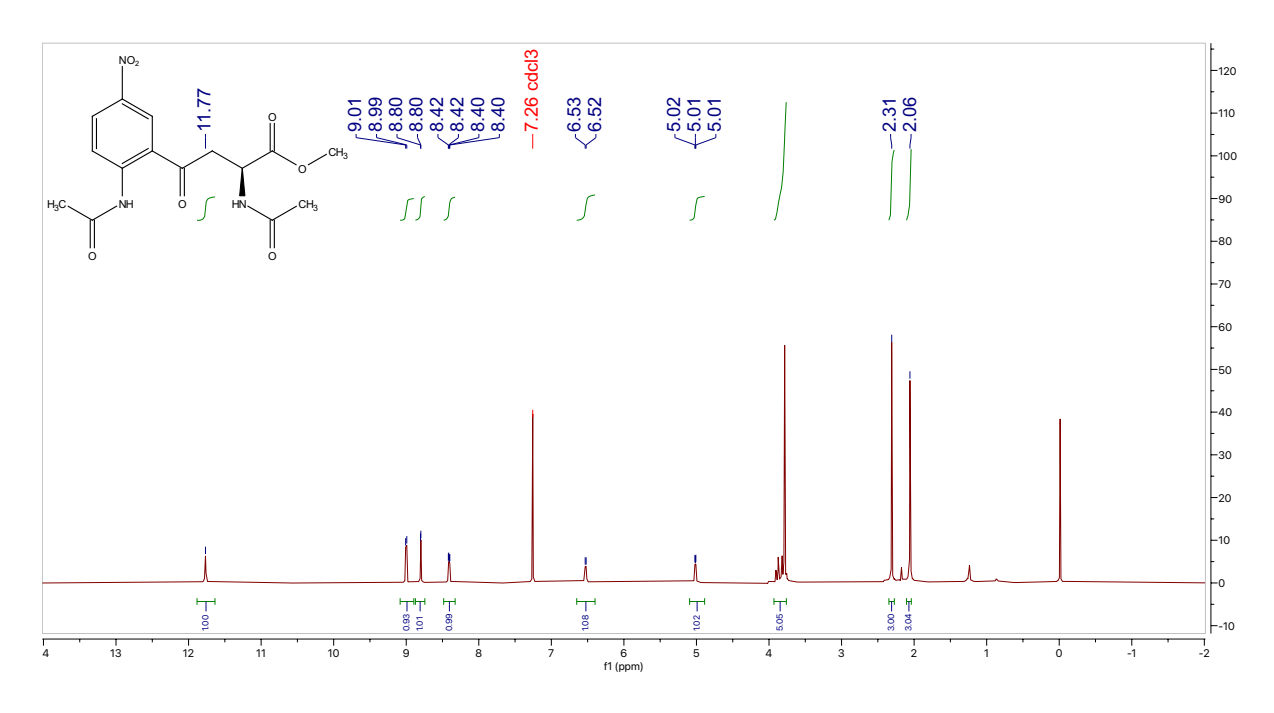


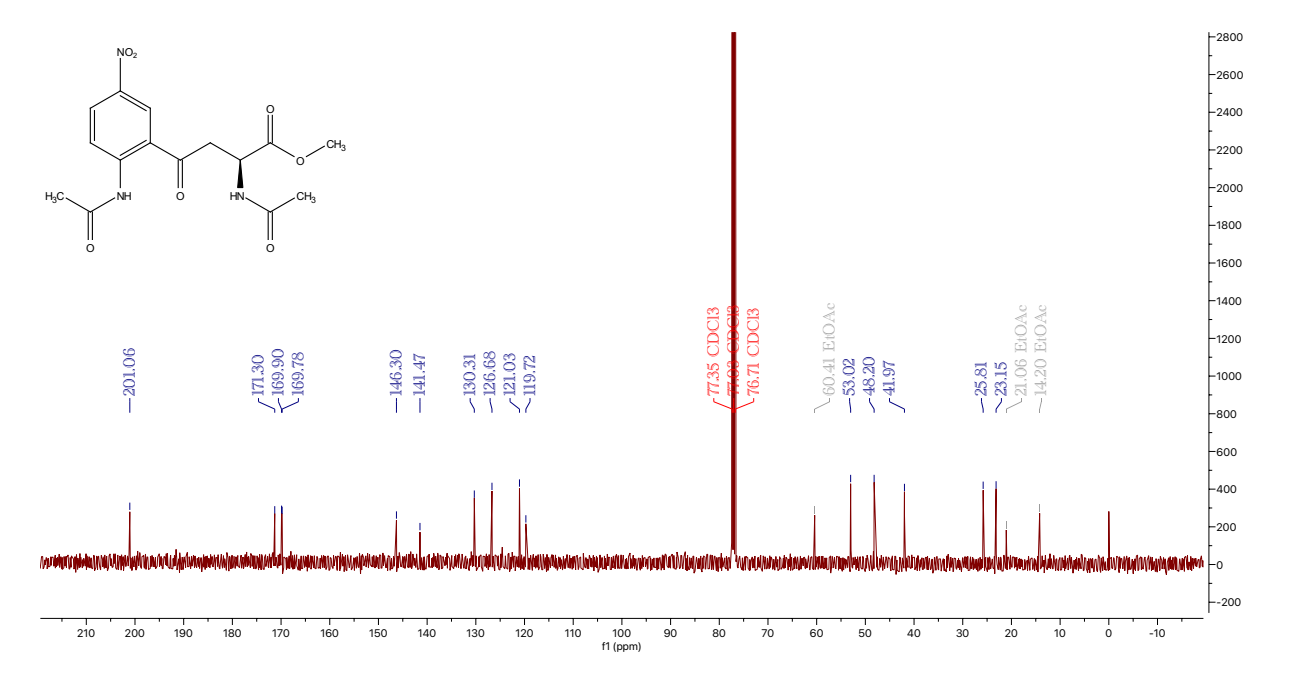
<sup>1</sup>H NMR for **28** 



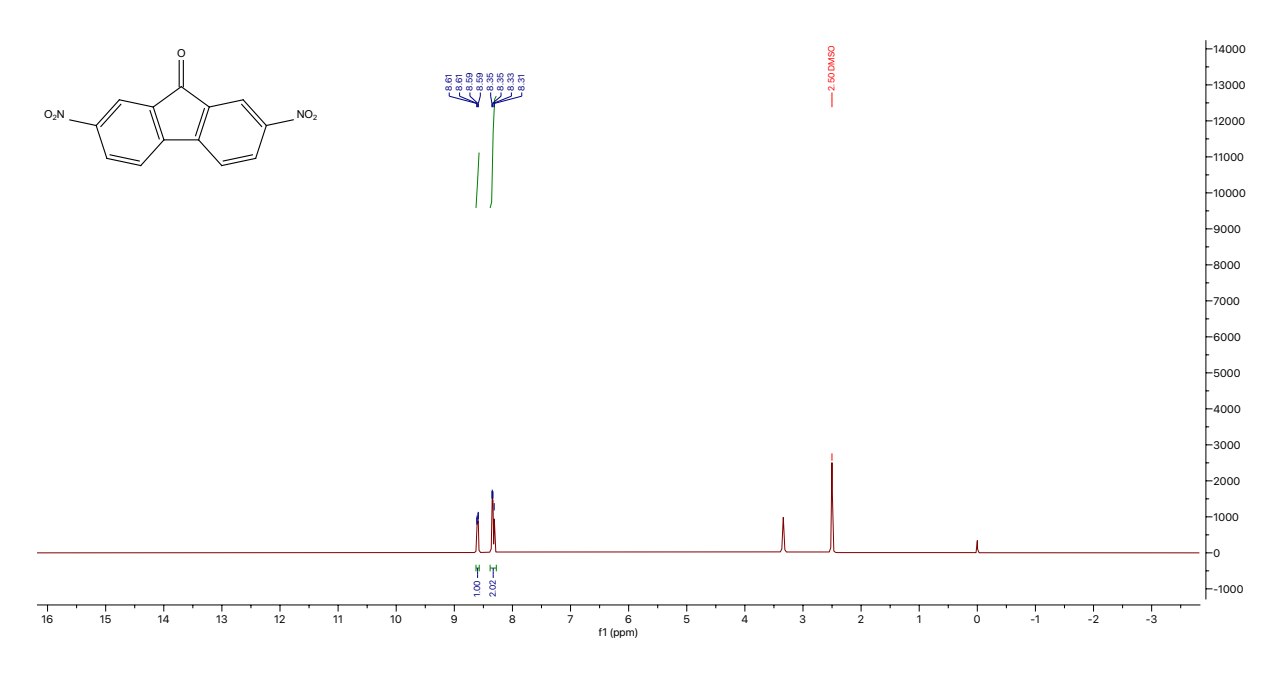


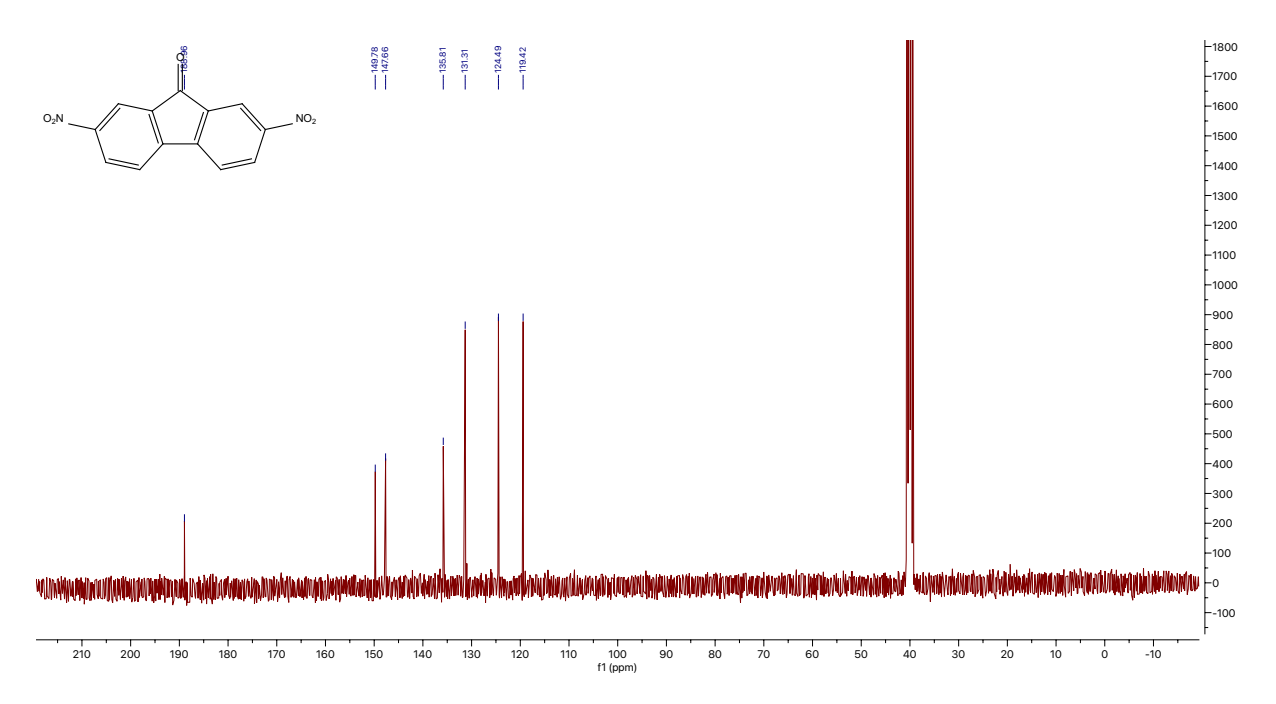
<sup>1</sup>H NMR for **29** 



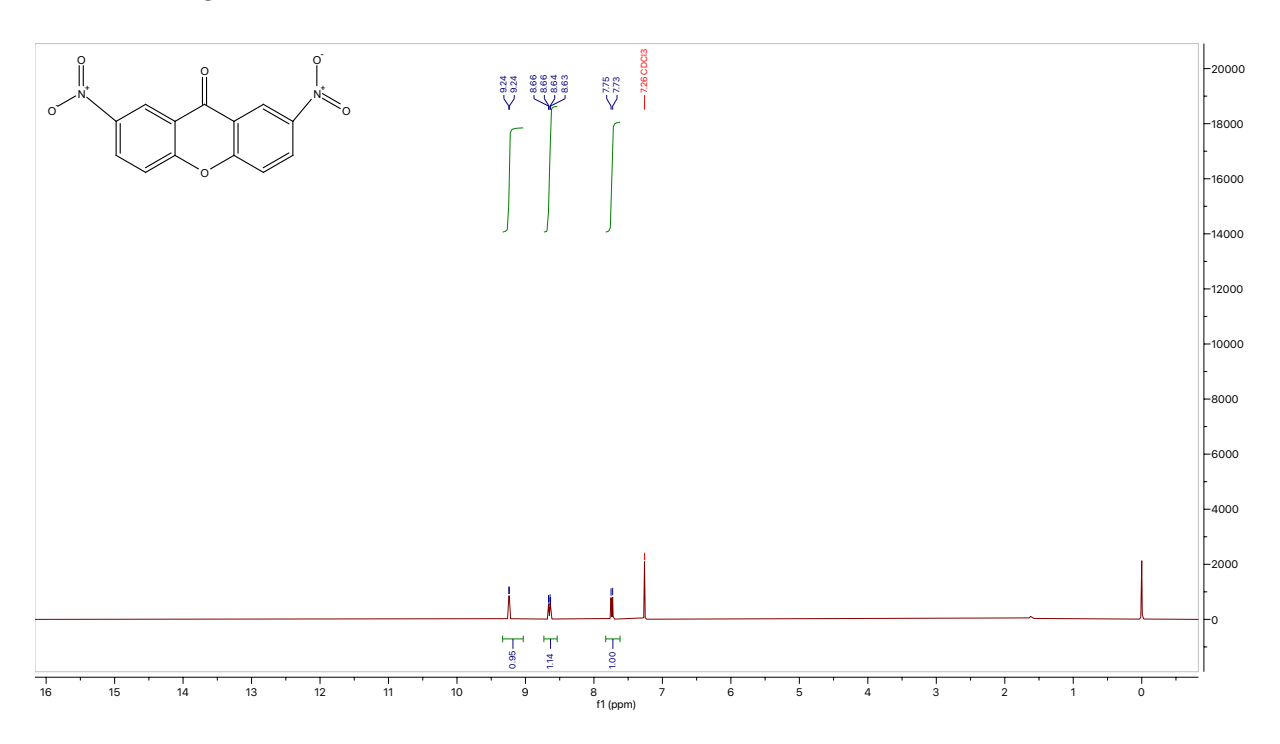


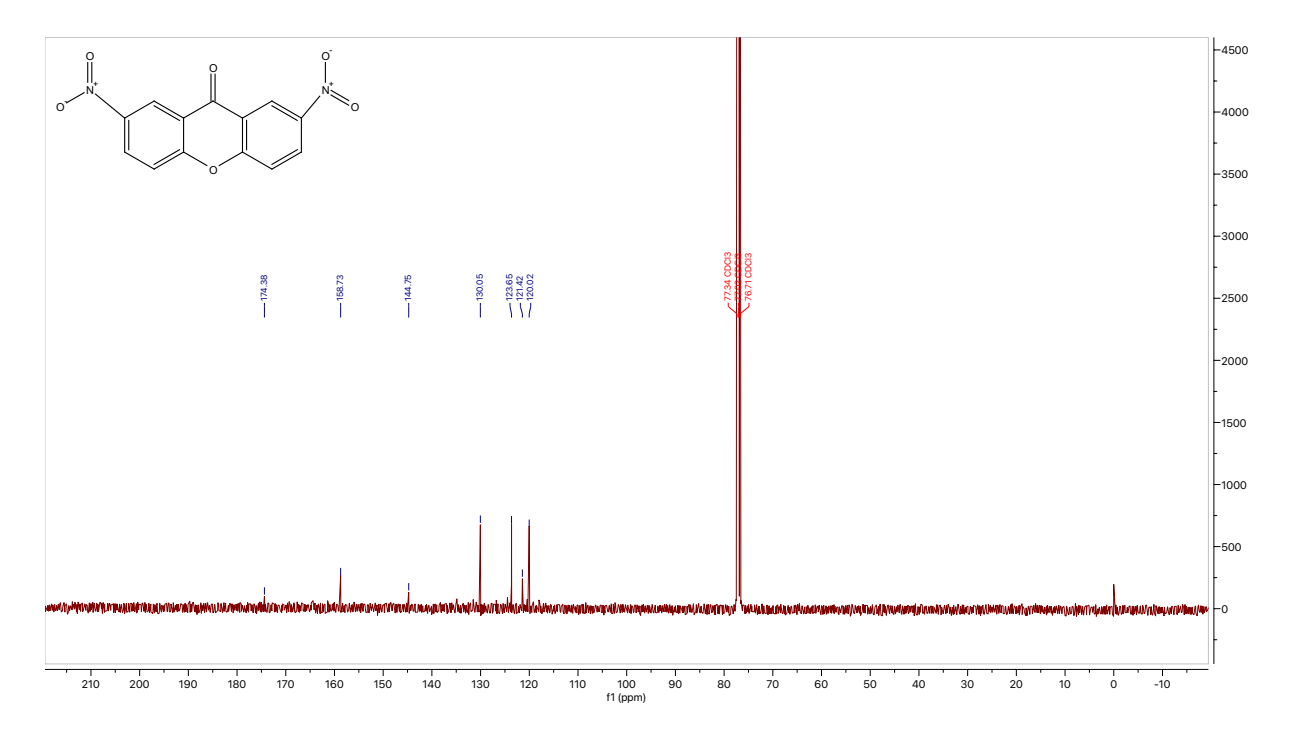
<sup>1</sup>H NMR for **30** 



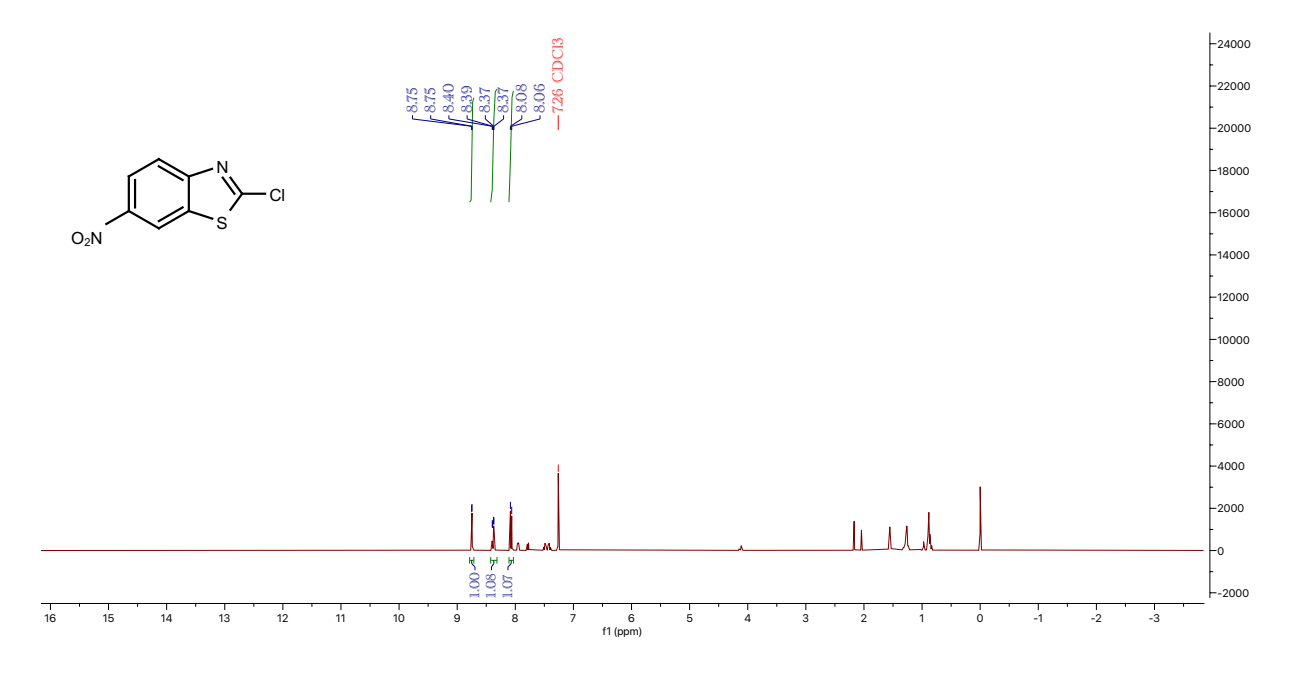


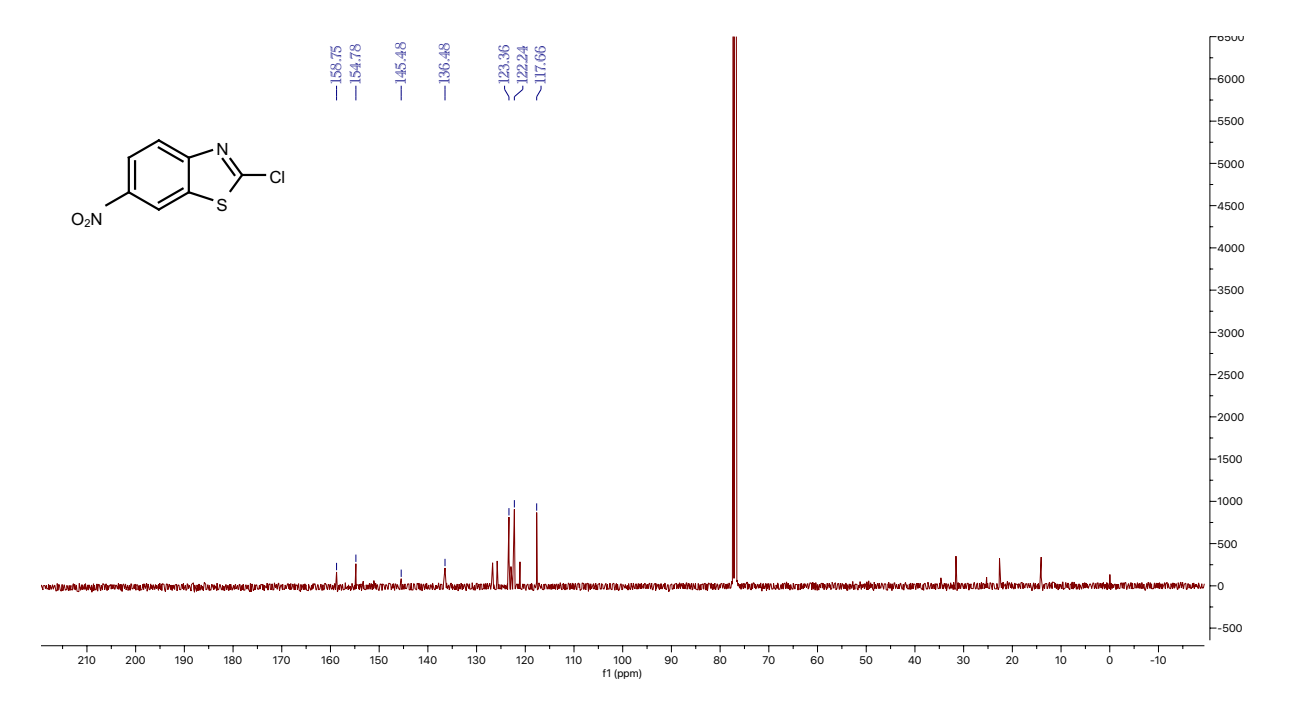
<sup>1</sup>H NMR for **31** 



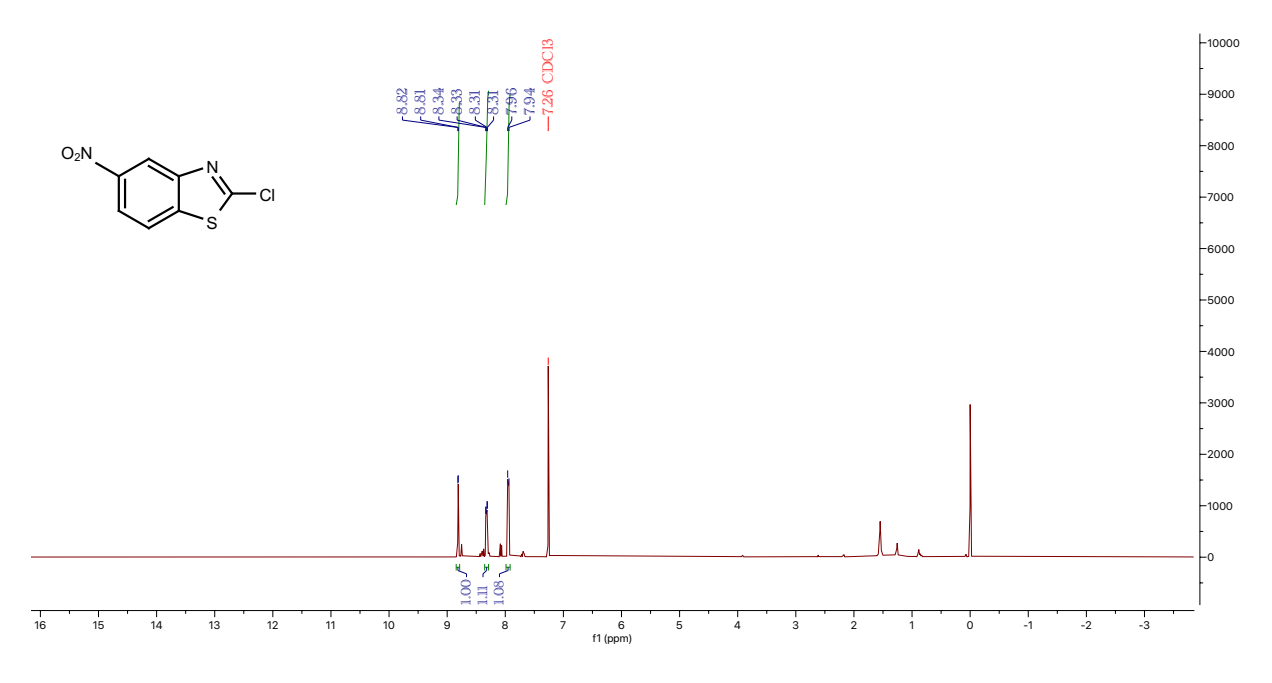


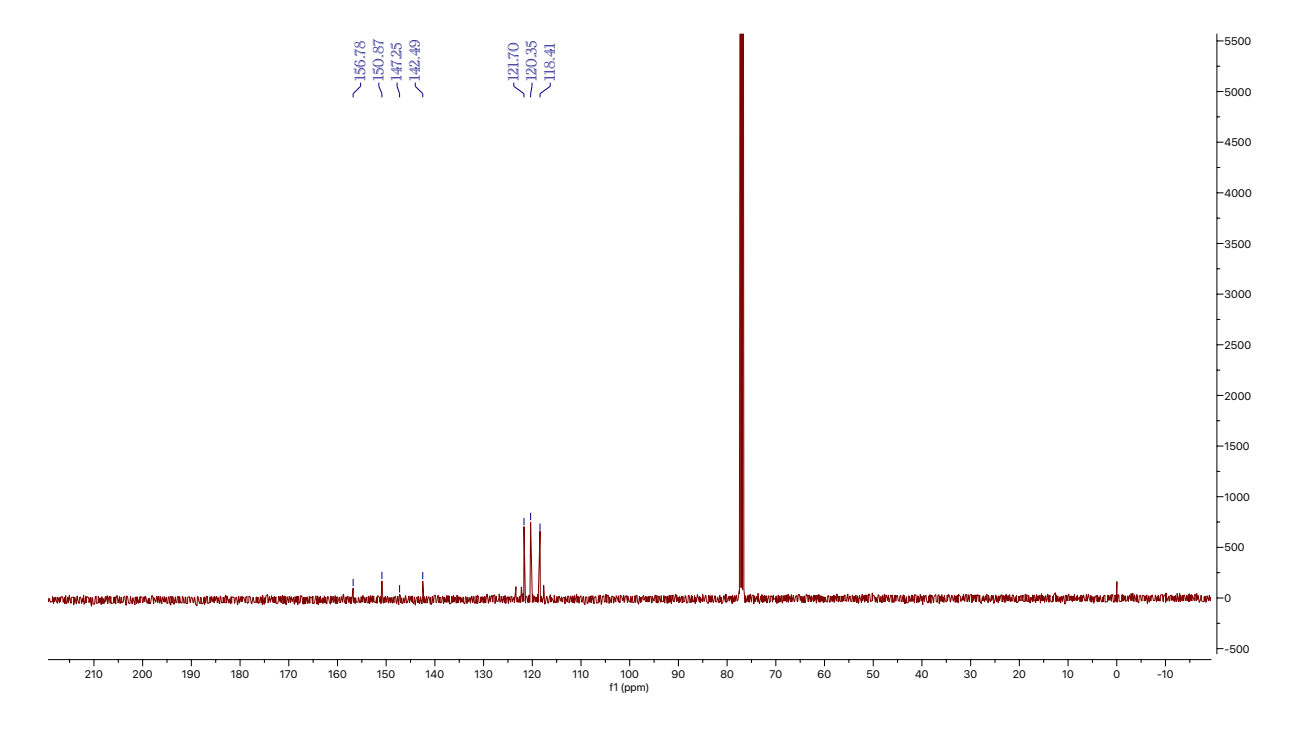
### <sup>1</sup>H NMR for **32a**



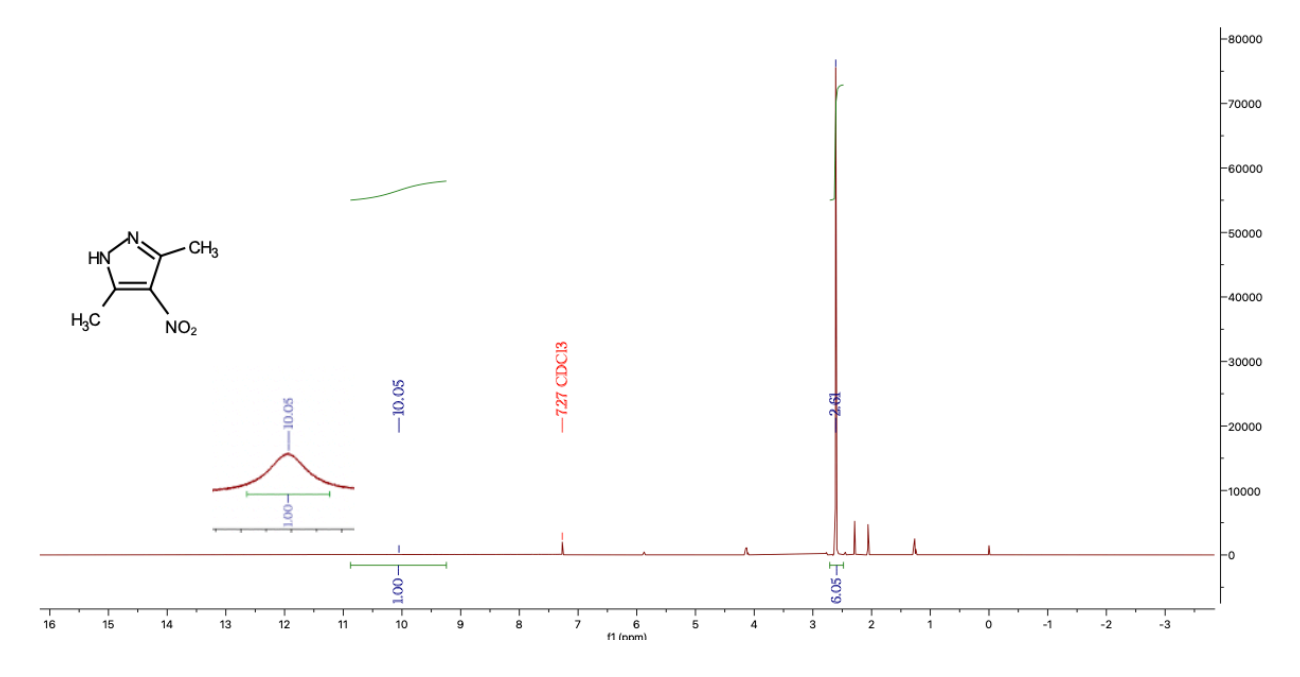


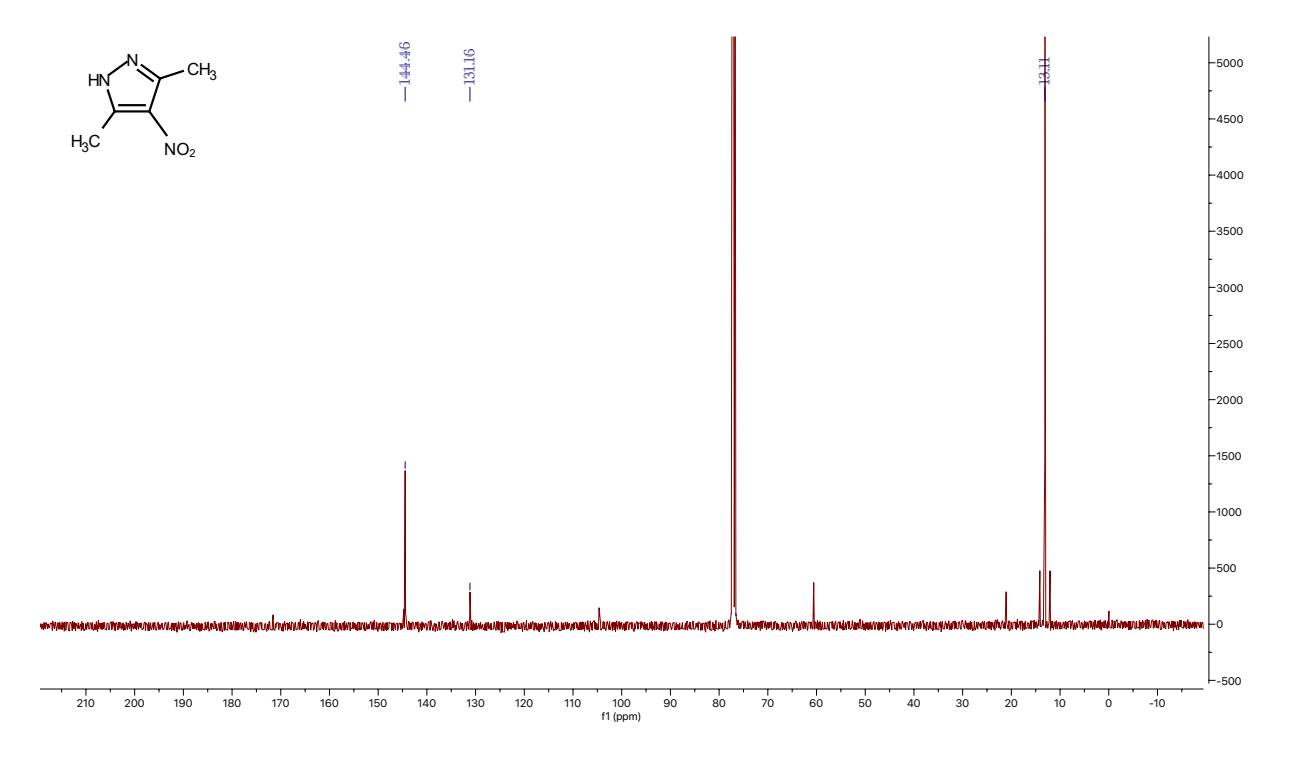
<sup>1</sup>H NMR for **32b** 



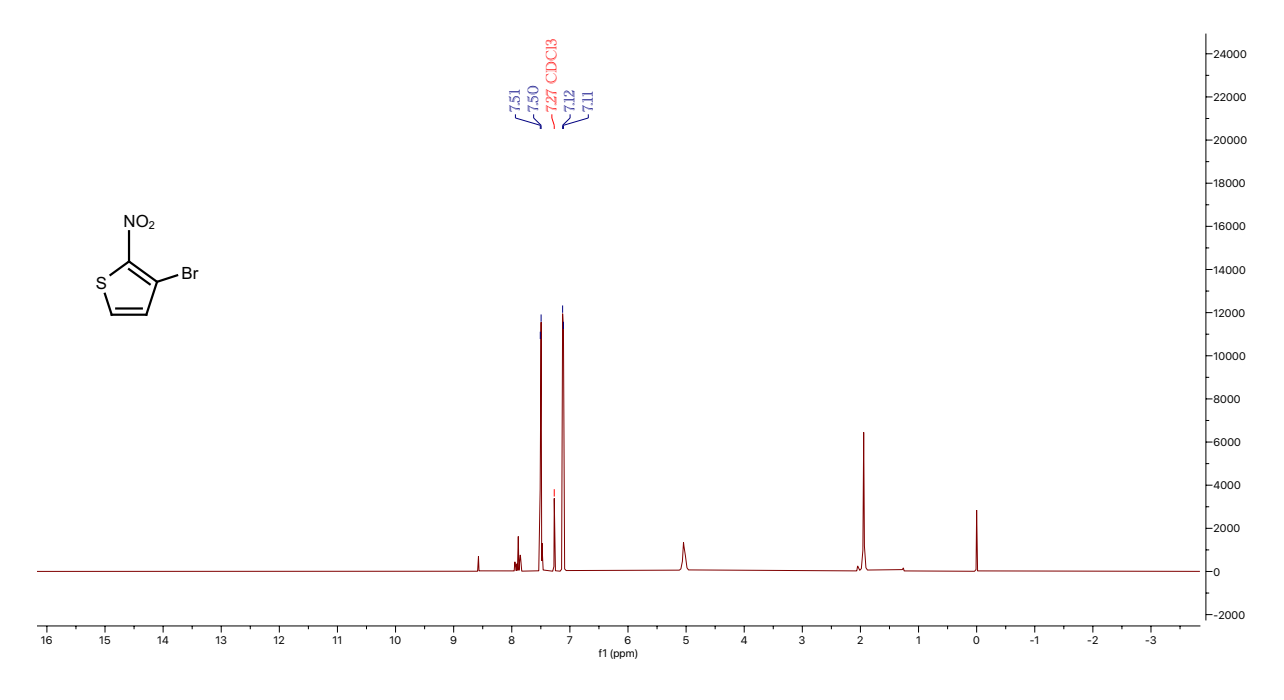


<sup>1</sup>H NMR for **33** 

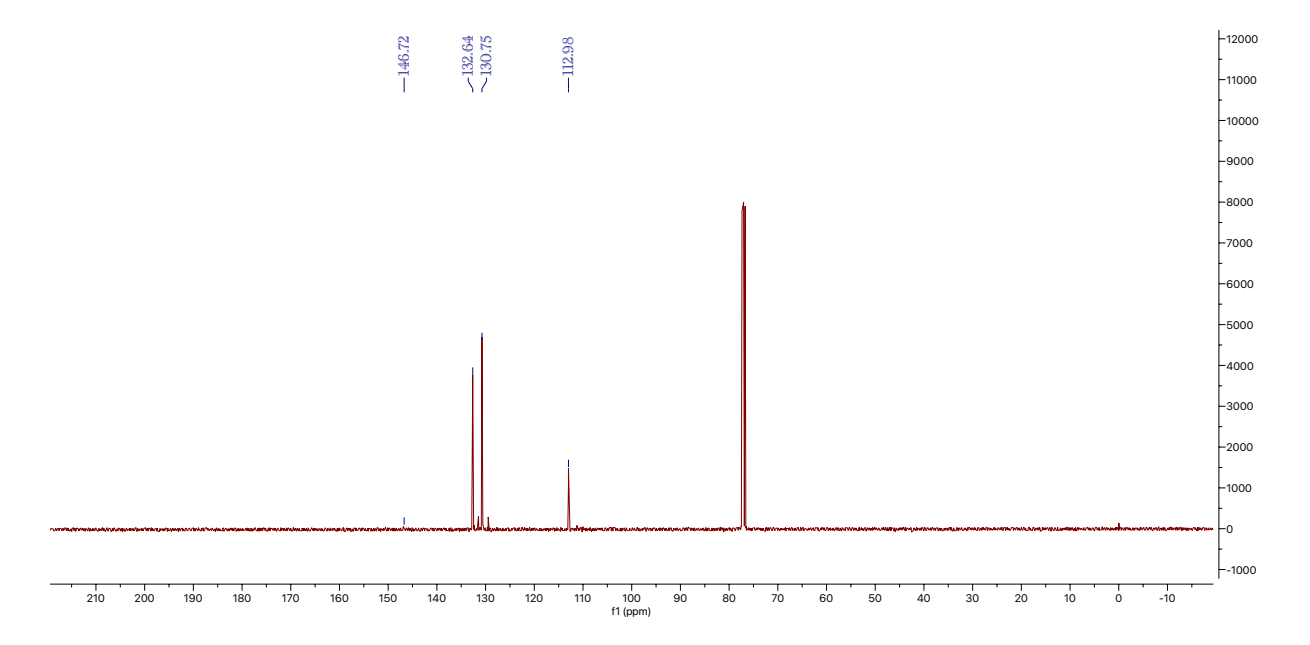




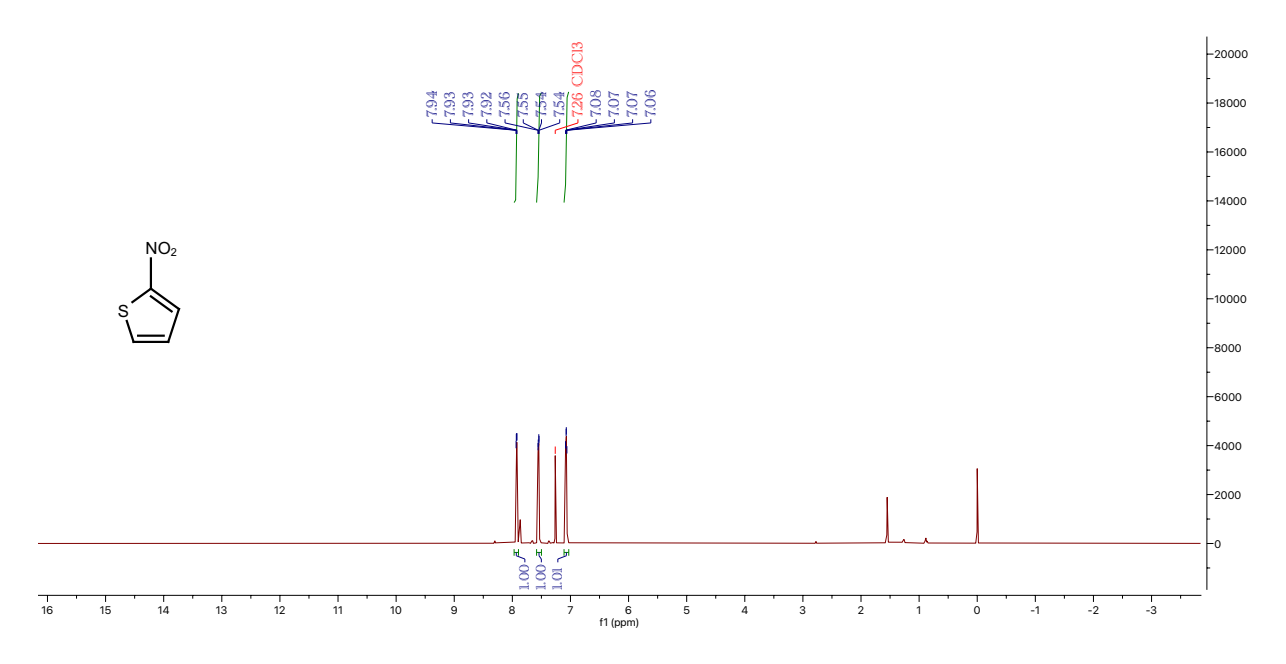
<sup>1</sup>H NMR for **34** 

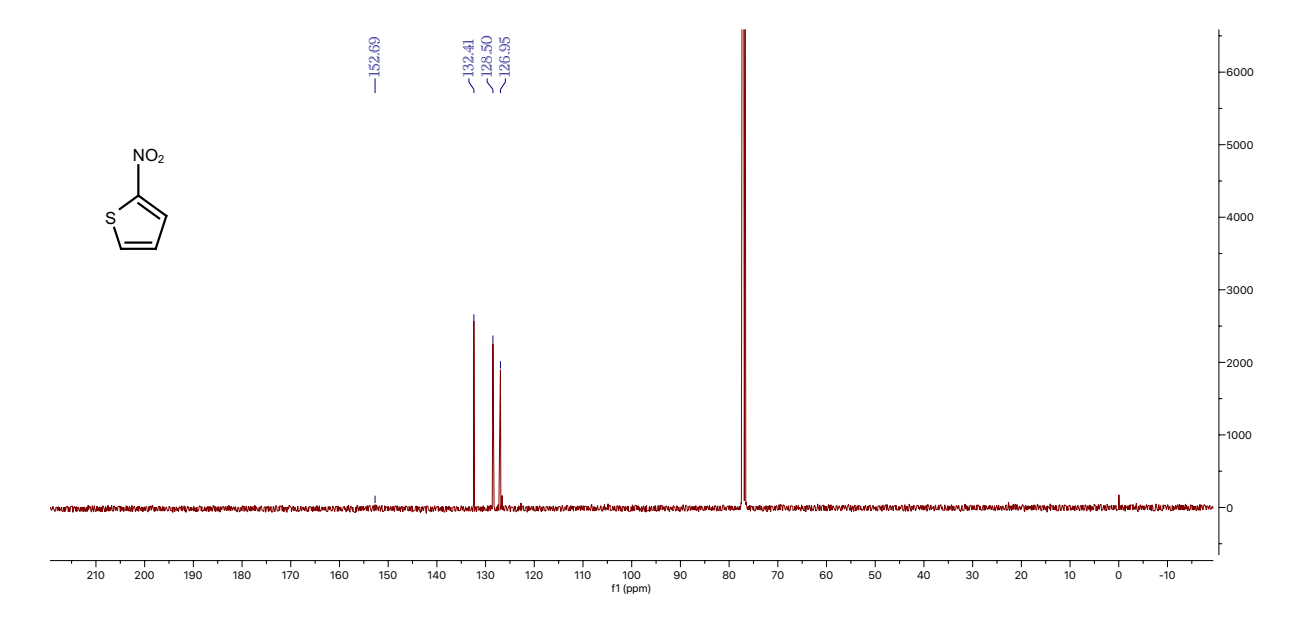


<sup>13</sup>C NMR for **34** 

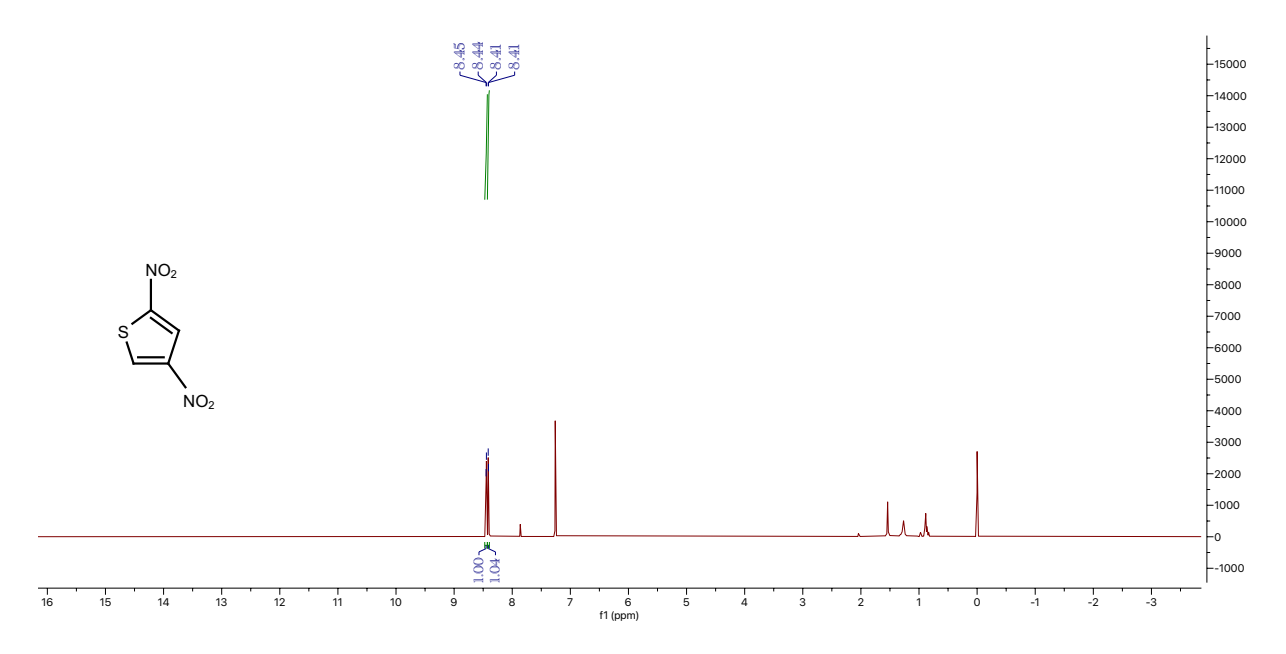


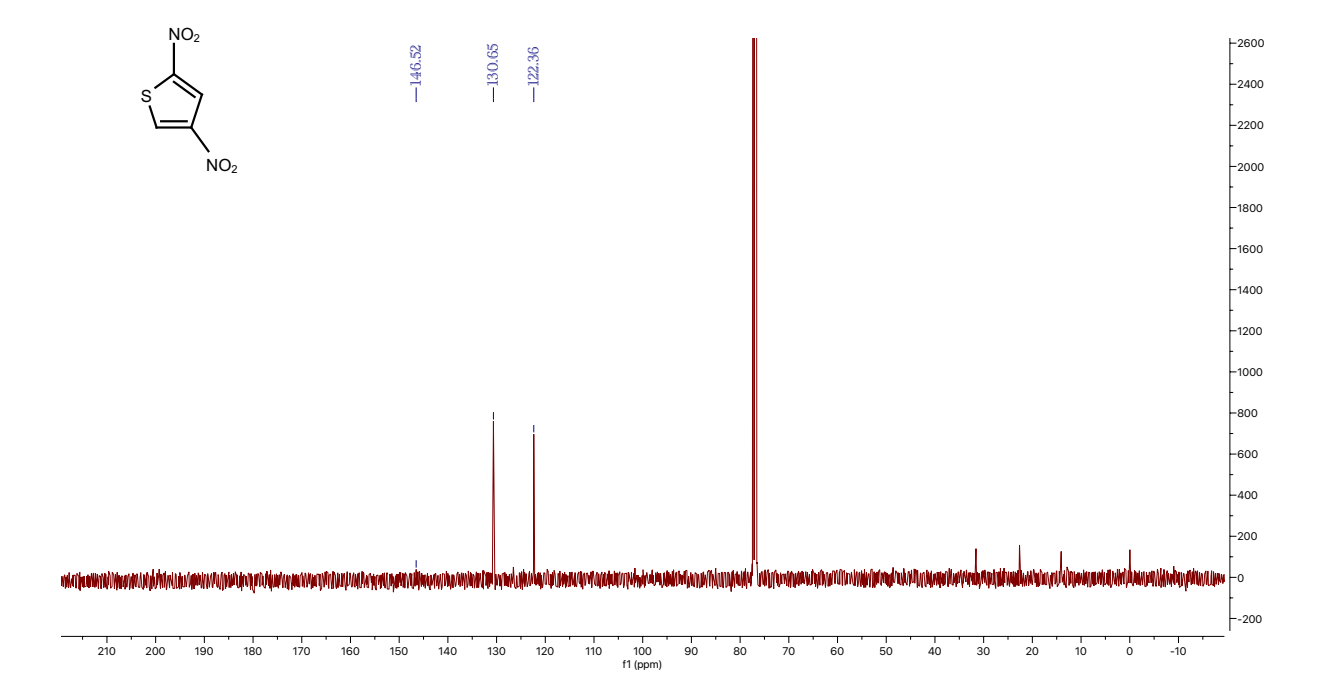
<sup>1</sup>H NMR for **35a** 



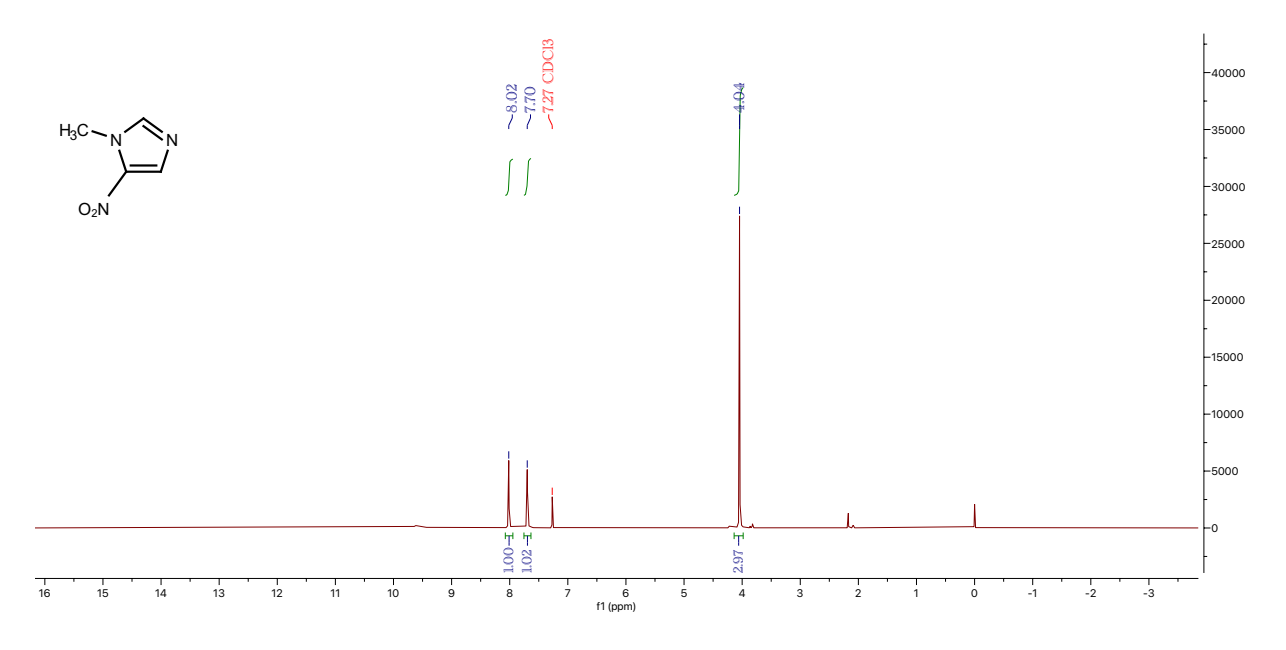


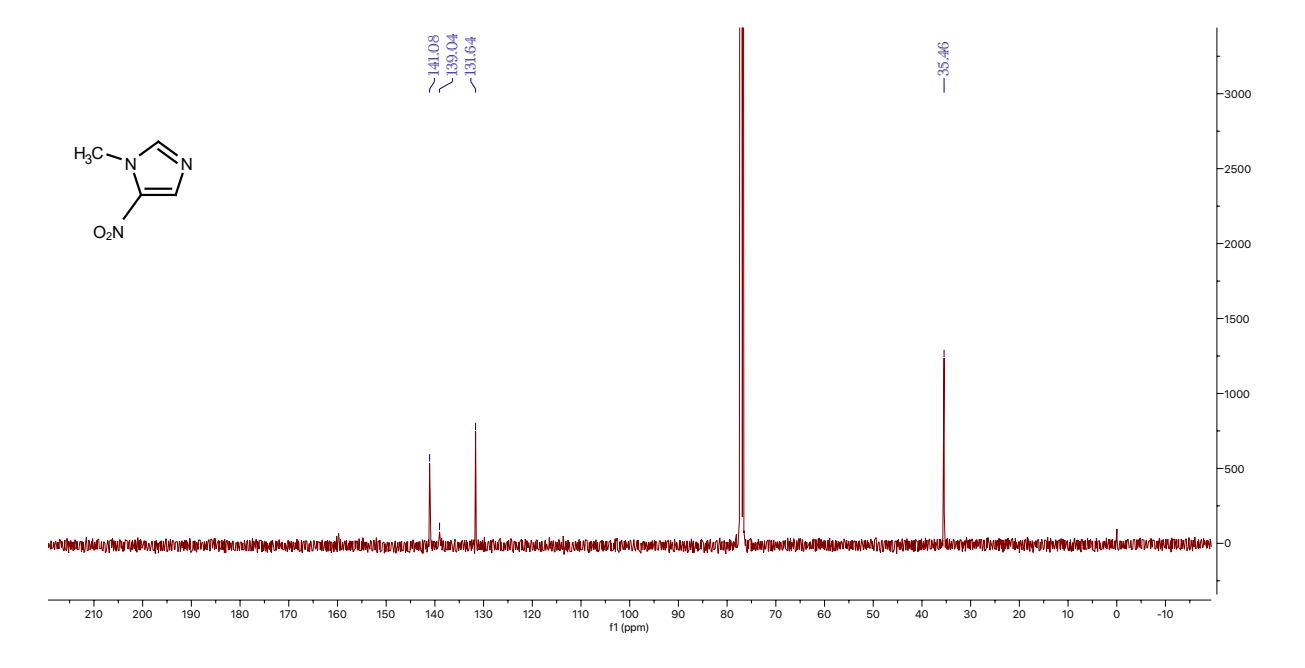
<sup>1</sup>H NMR for **35b** 





<sup>1</sup>H NMR for **36a** 





### <sup>1</sup>H NMR for **36b**

